THE STRING AXIVERSE AND COSMOLOGY

David J. E. Marsh
University College
Rudolf Peierls Centre for Theoretical Physics
Department of Physics

A thesis submitted in candidature for the degree of Doctor of Philosophy
Trinity Term 2012

THE STRING AXIVERSE AND COSMOLOGY

David J. E. Marsh
University College
Rudolf Peierls Centre for Theoretical Physics
Department of Physics

ABSTRACT

This thesis studies the cosmology of ultra-light scalar fields with masses in the range $10^{-33}\,\mathrm{eV} \lesssim m \lesssim 10^{-18}\,\mathrm{eV}$ and their effects on cosmology. The existence of such fields is motivated by the theoretical framework of the "String Axiverse". All types of string theory contain multiple axion fields associated with antisymmetric tensor fields compactified on closed cycles in the compact space. Since the masses of these fields scale exponentially with the volume of the cycle, it is possible for them to be naturally light. We study the effects of these fields as a component of the dark matter and show analytically and numerically that they cause a suppression of structure formation on cosmological scales set by the inverse mass. We show that it will be possible with future galaxy redshift and weak lensing surveys to detect an ultra-light field comprising of order a percent of the total dark matter. If such a field is allowed to couple to the geometry that provided its mass via a phenomenological scalar potential for the axion and modulus, then the expansion of the universe can be altered significantly. In particular, we find that it is possible to have multiple epochs of accelerated expansion over a large region of parameter space, and to have a flat universe with a big crunch in the distant future. Finally, we address the issue of isocurvature perturbations in axion cosmologies, and demonstrate that in the ultra-light case the power spectrum is effected. This may have implications for the conclusions made about fine tuning in the axiverse in relation to a potential detection of tensor modes in the CMB that are different to the case of a standard axion.

A thesis submitted in candidature for the degree of Doctor of Philosophy
University of Oxford
Trinity Term 2012

For Renée Hlozek, without whom I would be only half the scientist I am.

ACKNOWLEDGMENTS

When I started work on this thesis, I knew no cosmology, so first of all I would like to thank my supervisor Pedro Ferreira for teaching me, and for all the many meetings we had over three years full of support and inspiration. These thanks extend to everyone in our cosmology group, all who attend the Monday lunchtime meetings. Special thanks are due to Joe Zuntz, who put up with all my computing queries and idiocy: much of this thesis would have been impossible without his help.

Next I would like to thank all my collaborators: Ed Copeland, Dan Grin, Renée Hlozek, Edward Macaulay, Ewan Tarrant and Maxime Trebitsch. The three chapters in this thesis that relied on their work could not have happened without them.

I have the pleasure of acknowledging many inspiring conversations with my colleagues both here at Oxford and further afield. The first person to thank in such a regard is John March-Russell, who has inspired so much of my work and my thinking about physics. I also thank many Oxford Theory students and staff for chats over coffee, as well as formal teaching: Matt Bullimore, Matt McCullough, Francisco Pedro, Lukas Witkowski, Subir Sarkar, John Wheater, Rhys Davies and many others.

I spent many months during the final year of my DPhil in Princeton University, where the kind hospitality of David Spergel allowed me opportunity for hours of discussion with colleagues there.

All the Oxford skateboarding community deserve a huge thank you for keeping me sane through this DPhil: thanks to Leddy, Jon, Jono, and all at SS20 and OWP. The same thanks are due to friends far and wide for visiting me here: Ian, Heskey, Adam D, Adam S, Ben, Tomo, Beth, Becky, Hannah, Shaun, Claire, Jam, Martin, Rimmer, Andy, Orme, and Tom.

Thanks to all my family for love and support.

Finally, thanks most of all to Renée, for being the most amazing person I have ever met.

PUBLICATIONS

Chapter 2 is based on work published as a single author paper in *Physical Review* **D**83, 123526 (2011).

Chapter 3 is based on work published as *Physical Review* **D**86, 023508 (2012). It was authored with Ewan R. M. Tarrant, Edmund J. Copeland and Pedro G. Ferreira. The dynamical systems work in this Chapter, in the $\{x, y, z, r, s, t\}$ space, including the identification of fixed points was completed by ERMT. The numerical scan of this phase space was also performed by ERMT, based on a suggestion by me for the algorithm. I performed the analysis of the results. The discussion, and results on the potential as well as the setting of the work are all my own. The geometric descriptions of phase space and the fixed points are also my own, both in the $\{x, y, z, r, s, t\}$ space, and in $\{\dot{\phi}, \phi, \dot{\chi}, \chi, H\}$ space. The EDE descriptions, except for the CMB case, are my own. Figures are attributed where necessary.

Chapter 4 is based on work co-authored with Pedro G. Ferreira published as *Physical Review* **D**82, 103528 (2010).

Chapter 5 is based on work published as *Physical Review* **D**85, 103514 (2012). It was co-authored with Edward Macaulay, Maxime Trebitsch and Pedro G. Ferreira. The Fisher forecasts in this Chapter were performed by EM in the case of Galaxy Redshift Surveys, and by MT in the case of Weak Lensing Tomography. Aside from this, all the work in this Chapter is my own, including the modification of `CAMB` on which the forecasts are based. Figures are attributed where necessary.

Chapter 6 represents an ongoing project of as-yet unpublished work with Daniel Grin, Renée Hlozek and Pedro G. Ferreira. The modification of `CAMB` is my own. The detailed derivation of initial conditions, not shown but used in `CAMB` was made by DG. The MCMC analysis was performed by RH. Figures are attributed where necessary.

CONTENTS

1

INTRODUCTION

"The practice of bodhisattvas has emptiness as its realisation: when beginning students see emptiness, this is seeing emptiness, it is not real emptiness. Those who cultivate the Way and attain real emptiness do not see emptiness or non-emptiness; they have no views."

The fourth patriarch of Zen, in *Classics of Zen and Buddhism, T. Cleary*

PREFACE

Due to the extensive variety of the topics covered in this thesis, there will be no space for detailed derivations in this Introduction.

1.1 MODERN COSMOLOGY

Over the past two decades cosmology has become a precision science. This golden era of data-driven modern cosmology can be said to have begun with the COBE measurement of the cosmic microwave background black body spectrum and anisotropies [1–3], rapidly advanced in more recent years with surveys like WMAP [4, 5][1] and the SDSS surveys [7–10][2], and will reach culmination with the imminent release of the cosmological interpretation of the Planck data [13, 14]. In the greatest of

[1] The NASA legacy archive holds all COBE and WMAP data [6].
[2] The SDSS websites are [11, 12].

traditions, however, we will begin our story much earlier.

1.1.1 The Expanding Universe

With the dawn of the 20th century, came the dawn of relativity [15], soon followed by the general theory [16, 17], which for the first time gave physicists the playground in which they could ask questions about the very fabric of the universe. No longer was absolute space, as given to us by Newton [18] and Descartes [19], an inert and immutable background in which our island universe sat. The cosmological solution to Einstein's equations found independently by Friedmann and Lemaitre [20, 21] described an expanding universe. This dynamical state of affairs famously led Einstein to his 'biggest blunder': the introduction of a cosmological constant to tame the expansion and give a static and eternal universe [22]. The cosmological constant, Λ, this most curious of players on the cosmic stage, whose origin is tied up in some of the deepest questions of modern physics, will return to our discussion many times.

For the true believers, though, cosmic expansion held great fascination, especially after its empirical confirmation by Hubble's famous measurement of distances to galaxies outside our own, and by using the redshifts of these galaxies that were available to him inferring the linear relationship known as Hubble's law [23]. If the universe was expanding, then at some point that expansion must have had a beginning. As matter is squeezed into much larger densities, we know from the everyday experience of phase transitions that it does not remain as it was, and as the distances decrease ever further the quantum realm of Planck [24] is approached. The initial state of the universe must, therefore, have been very different from what we observe, out there, on the night sky. Lemaitre's 'primordial atom' [25], conceived against this backdrop of ideas, can be seen as the first modern scientific theory of creation, with the solid mathematics of General Relativity and the quantifiable observational evidence of Hubble to back it up. Einstein's blunder had been falsified, and cosmology entered the Popperian canon of true science [26, 27].

Nowadays, cosmologists have a wealth of data beyond that available to Hubble, and from it some of the most striking conclusions about the constituents of our universe, and perhaps even of other universes, have been drawn.

The point of departure to study relativistic cosmology is Einstein's equation:

$$G_{\mu\nu} = 8\pi G T_{\mu\nu} \,. \tag{1.1}$$

$G_{\mu\nu}$ is the Einstein tensor and is calculated from the geometry (see e.g. [28, 29]). In our case we begin with the Friedmann-Lemaitre-Robertson-Walker (FLRW) line element in physical time, t, with scale factor $a(t)$, for a spatially flat, homogeneous and isotropic universe (in units where the speed of light $c = 1$):

$$ds^2 = g_{\mu\nu} dx^\mu dx^\nu = -dt^2 + a(t)^2 (dx^2 + dy^2 + dz^2) \,, \tag{1.2}$$

where $g_{\mu\nu}$ is the metric[3]. It is common practice to normalise the scale factor value 'today' as $a_0 = 1$. Unless otherwise stated, we assume this convention always in this thesis. We will often find it useful to use the *redshift*, z, instead of the scale factor, defined by $a = 1/(1+z)$. As long as the scale factor is monotonic, it can be used as an alternative time co-ordinate.

The right hand side of Einstein's equation is specified by the matter content of the universe. In general the energy momentum tensor, $T_{\mu\nu}$, is found from the variation of the matter part of the action, $S_M = \int d^4x \sqrt{-g}\mathcal{L}$, where g is the determinant of the metric and $\mathcal{L}$ is the Lagrangian density[4], with respect to the metric and is given by:

$$T_{\mu\nu} = \frac{-2}{\sqrt{-g}} \frac{\delta S_M}{\delta g^{\mu\nu}} \,. \tag{1.3}$$

The energy momentum tensor for a homogeneous and isotropic perfect fluid of energy density ρ and pressure P is given, in units where $c = 1$, by:

$$T^\mu{}_\nu = \mathrm{diag}[-\rho, P, P, P] \,. \tag{1.4}$$

The time-time components of the Einstein equation, Eq. (1.1), give the Friedmann equation:

$$H^2 \equiv \left(\frac{\dot{a}}{a}\right)^2 = \frac{8\pi G}{3}\rho \,, \tag{1.5}$$

where H is the Hubble 'constant', and over dots denote derivatives with respect to time . This equation is the primary lens through which we see cosmology.

[3]Conventions for the relative sign of spatial versus temporal parts differ.
[4]Some authors include the measure, $\sqrt{-g}$, in the definition of $\mathcal{L}$.

The evolution of the energy density is fixed by the conservation equation $D^\mu T_{\mu\nu} = 0$, where D is the covariant derivative. Non-relativistic matter and radiation have their evolution specified in terms of a constant equation of state $w = P/\rho$ which is $w = 0$ for non-relativistic matter, $w = 1/3$ for radiation, and $w = -1$ for Λ:

$$\dot{\rho} + 3H(1+w)\rho = 0\,. \tag{1.6}$$

This has the solution for evolution of $\rho(a)$ given an input (though not necessarily initial) value $\rho_0 = \rho(a_0)$:

$$\rho(a) = \left(\frac{a_0}{a}\right)^{3(1+w)} \rho_0\,. \tag{1.7}$$

It is common practice to take the densities ρ_0 to be given by their values 'today'. For radiation $\rho_r \sim a^{-4}$, while for matter $\rho_m \sim a^{-3}$, and by definition ρ_Λ =const.. These evolutions are shown in Fig. 1.1. In Chapters 2 and 4 in particular we will see how these evolutions can differ when more exotic cosmic ingredients are included. As the universe expands, the scale factor increases and the energy density in matter and radiation is said to *redshift* away. Clearly from the solution of Eq. (1.5), given an initial condition of $H > 0$, i.e. an expanding universe, with only matter and radiation present, the expansion continues and monotonically decreases in speed as $H \to 0$ in the asymptotic future, while for a universe with a cosmological constant H asymptotes to the constant value $H_\infty = \sqrt{8\pi G\rho_\Lambda/3}$ where we have what is known as de Sitter (dS) space [30].

These scalings have an obvious physical interpretation. The energy density in matter is made up of a conserved number of particles. As the physical box size increases with a, the volume increases with a^3 and so the density goes down as a^{-3}. For radiation, there is the additional effect of gravitational redshift: wavelengths are stretched by the expansion and since $E \propto \omega \propto 1/\lambda$, the physical wavelength stretches by a factor of a and so the energy density scales with an extra factor of a^{-1} with the cosmic expansion. The cosmological constant does not dilute at all with the expansion: as space expands, there is more total energy density in the vacuum!

It is immediately obvious that for these standard cosmic ingredients the early history of the universe will be dominated by radiation, Gamow's 'hot big bang' [31, 32], there will be an intermediate period of matter domination, and a future cosmological

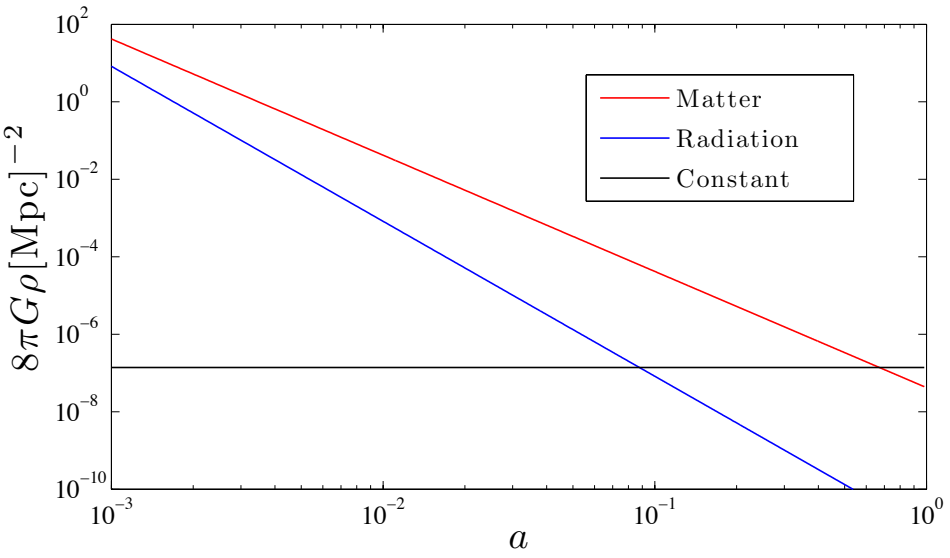

Figure 1.1 Evolution of the energy density, ρ, in radiation, r, matter, m, and cosmological constant, Λ, as a function of scale factor, a.

constant driven expansion. Measuring the Hubble rate at some time, say $H_0 \equiv H(a_0)$, gives a measurement of the total density at that time. If we have some reason to believe from independent measurements that various components of that energy density have fixed values, then the measurement of H_0 allows us to infer the relative density of the remaining pieces. It is common to express such statements in terms of the fraction of the total (critical, if the curvature is zero) density at a given time, $\Omega_i(a)$, in a component i:

$$\Omega_i(a) = \frac{8\pi G\rho_i(a)}{3H^2(a)}\,. \tag{1.8}$$

Taking values today $\Omega_i \equiv \Omega_i(a_0)$ and $H_0 = 100h\,\mathrm{km\,s^{-1}\,Mpc^{-1}}$, where h is the dimensionless Hubble parameter, we see that $\Omega_i h^2$ is proportional to the physical density ρ_i. Substituting into the Friedmann equation Eq. (1.5) we see that we always require $\sum_i \Omega_i = 1$.

It is not the subject of this thesis to discuss supernovae, and the so-called 'cosmic distance ladder' in any detail, but they play a significant historical role in the story of modern cosmology and deserve some short mention. In 1998 two independent teams of supernova cosmologists headed by Schmidt and Perlmutter [33, 34] set out to measure H_0 by measuring the distance to supernovae. The distance can be inferred by the brightness: the supernovae they sampled were what is known as

Type IA supernovae that are believed to have a fixed intrinsic brightness, therefore by comparing this to the measured brightness one can infer their distance. Next the redshift of the spectrum of light emitted by the supernova is measured. By combining the two measurements, one knows the 'distance-redshift relation', which in turn gives a measurement of Ω_m and Ω_Λ (see e.g. [29, 35] for more details). The value measured by [34], assuming a flat universe, was $\Omega_m = 0.28$, and therefore non-zero Ω_Λ (see [36] for a historical account of the status of Λ prior to this data: it was not so unexpected). Einstein's blunder had returned.

The important physical consequence of this measurement is that it implies that the expansion of the universe is *accelerating*, and has been since $z \approx 0.72$. This can be seen from the Friedmann acceleration, or Raychaudhuri [37], equation:

$$\frac{\ddot{a}}{a} = \dot{H} + H^2 = -\frac{4\pi G}{3}(\rho + 3P)\,, \tag{1.9}$$

which comes from the time derivative of Eq. (1.5) combined with Eq. (1.6). Accelerated expansion, $\ddot{a} > 0$, requires $\rho + 3P < 0$, i.e. total equation of state $w = \sum_i \Omega_i w_i < -1/3$. With only matter and a cosmological constant relevant at late times, accelerated expansion occurs for $\Omega_\Lambda \geq 1/3$.

1.1.2 *Precision Cosmological Observables*

Making cosmology into a precision science requires going beyond the simple isotropic and homogeneous picture provided by the Friedmann equation, and doing cosmological perturbation theory [38–40]. One constructs statistical distributions out of the perturbed quantities that depend sensitively on the dynamics of the cosmological fluids, measures these distributions and then infers the initial conditions on, and properties of, the fluids.

In this Introduction we will not delve in mathematical detail into these observables: more details on the relevant ones are given in the appropriate Chapters. We will simply give a broad survey of the two major arenas that this thesis focuses on, aiming to give historical and physical context to the major measurements and conclusions.

1.1.2.1 *Cosmic Microwave Background Anisotropies*

The cosmic microwave background (CMB) is the thermal relic of the hot big bang, first discovered in 1965 by Penzias and Wilson [41] as diffuse microwave radiation across the whole sky.

In the early universe, high temperatures imparted photons with enough thermal energy to ionise all the ordinary matter in the universe. Nuclei and electrons were free from each other, and these charged constituents were tightly coupled to the radiation via Thompson scattering. This primordial soup is known as the 'baryon-photon fluid'. The tightly-coupled photons could not move far without scattering off a charged particle, having a short mean-free-path. We say that the universe was opaque to photons, and the baryons and photons shared a common sound speed.

As the energy density of photons redshifted away and the universe cooled, the average thermal energy of photons dropped below the atomic binding energy. The Coulomb force between electrons and nucleons could now bring them together and bind them into neutral atoms that could not be smashed apart by the less energetic photons. Neutral particles do not scatter photons, and so now the radiation was free to propagate. The universe became transparent. From this time on, photons moved freely, no longer interacting and preserving a snapshot of the conditions during this decoupling epoch, approximately 300000 years after the Big Bang.

What we see as the CMB is comprised of these photons, that have travelled largely unimpeded to us from a surface a fixed distance away from us: 'the surface of last scattering'. The story of modern cosmology begins with the COBE satellite around 1991 [1], whose FIRAS instrument precisely measured the temperature of the CMB as 2.725 ± 0.002K, and showed it to be a perfect black body distribution.

However, we know from simply looking around us that the universe is not homogeneous: there are galaxies and clusters out there living in gravitational wells. The seeds of this inhomogeneity were in the initial conditions of the universe. Since the universe was opaque before the formation of the CMB, optical observation can see back only this far and thus it is here that we expect to see the remnants of the initial conditions, imprinted as anisotropies in temperature on the microwave sky. The COBE

DMR instrument measured these, and showed them to be tiny fluctuations, of order 1 part in 1×10^5.

Cosmologists express measurements of CMB anisotropies (for a review, see [42]) in terms a quantity C_ℓ^{XY} which is given by the correlation function of the expansion in Legendre polynomials of a field $X, Y = T, E, B$ associated to the CMB photons, where T is temperature, and E and B are polarisation modes [43]. For example, with temperature [29]:

$$T(\vec{x}, \hat{n}, \tau) = T(\tau)(1 + \Theta(\vec{x}, \hat{n}, \tau)) \,, \tag{1.10}$$

where $\vec{x}$ is position, $\hat{n}$ is a unit vector giving direction on the sky (we work in phase space, so $\hat{n}$ comes from the photon momentum, see [40]), τ is conformal time given from physical time in the line element by $a(\tau)d\tau = dt$, and Θ is the dimensionless perturbation about isotropy, $\frac{\delta T}{T} = \frac{1}{4}\frac{\delta \rho_\gamma}{\rho_\gamma}$ (note that there are also relativistic contributions from the gravitational potential and the Doppler shift, see [42]). We expand this in multipoles:

$$\Theta(\vec{x}, \hat{n}, \tau) = \sum_{\ell=1}^{\infty} \sum_{m=-\ell}^{\ell} a_{\ell m}(\vec{x}, \tau) Y_{\ell m}(\hat{n}) \,. \tag{1.11}$$

$Y_{\ell m}$ are the spherical harmonics, and ℓ, m are conjugate to the real space unit vector $\hat{n}$. The correlation function is then defined as:

$$\langle a_{\ell m} a^*_{\ell' m'} \rangle = \delta_{\ell \ell'} \delta_{m m'} C_\ell \,. \tag{1.12}$$

If we restore the units using the COBE T_{CMB}, the C_ℓ's have units of T^2 and are measured by taking the two-point correlation function of temperature in pixels across the sky. Theoretically, they are calculated by solving the hierarchy of Boltzmann equations for the perturbed expansion of the energy momentum tensor for the electromagnetic radiation coupled to baryons. Details of the Boltzmann hierarchy can be found in e.g. [40].

Practically, this system is always solved numerically. A starting point for the 'line of sight integration' approach is given in [46], which led to one of the first accurate codes for C_ℓ calculation, `CMBFAST` [47]. Approximations of this can be written quite simply in any programme capable of numerical integration, for example *Mathematica*,

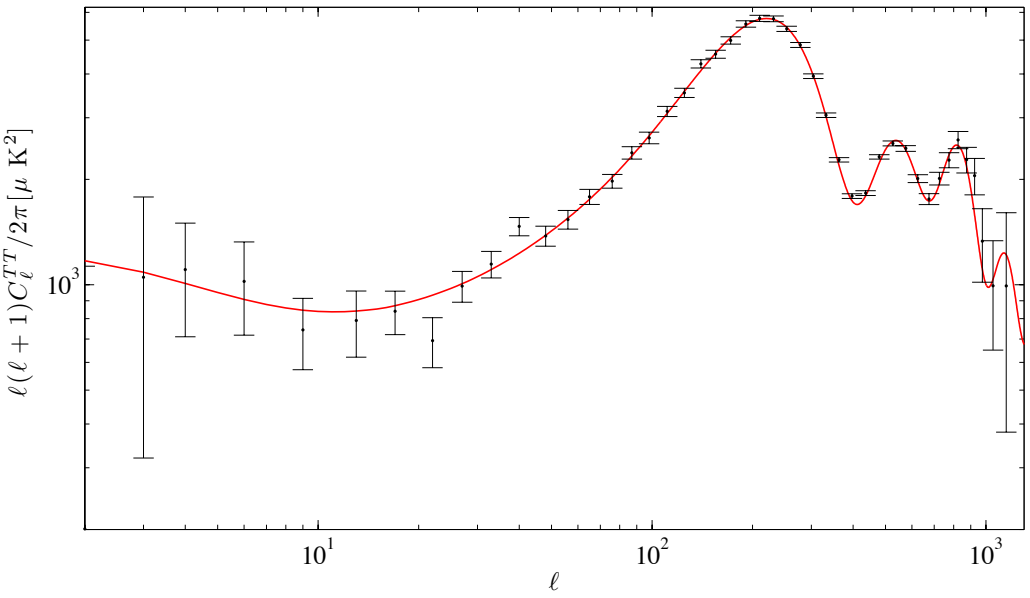

Figure 1.2 The cosmic microwave background anisotropies shown as the temperature auto-correlation power spectrum, C_ℓ^{TT} (see Eqs. (1.10,1.11,1.12)). The data is from the latest WMAP data release [44], and the theoretical curve is given by the best fit parameters to this data (see Section 1.2.1), calculated using `CAMB` [45].

or with basic `FORTRAN` and the integrator `dverk`. In this thesis we will always calculate C_ℓ's using the publicly available code `CAMB` by Lewis [45, 48, 49], modified to deal with various extended cosmological scenarios. We detail two such extensions in Chapters 5 and 6.

The primary feature in C_ℓ^{TT} is the *Baryon Acoustic Oscillations* (BAO) which arise from the sound speed in the baryon photon fluid and the release of photons from gravitational wells after decoupling. They manifest as a series of acoustic peaks in C_ℓ and reflect the angular size of this sound horizon. They were first convincingly detected in the CMB by TOCO [50], BOOMERANG [51], and MAXIMA [52]. The location of the first peak breaks the degeneracy in the supernovae measurements with curvature and establishes the flat universe to a high accuracy. We will assume flatness throughout this thesis, but mention on occasion where this assumption might need relaxing.

The modern state of the art for all sky CMB surveys is the NASA WMAP satellite [4] whose latest data release was in 2011 [5], which gave a measurement also of the polarisation spectra C_ℓ^{TE} and C_ℓ^{EE}, and a limit to the amplitude of the B-mode

generated by tensor perturbations (gravitational waves) and gravitational lensing. There also exist many accurate, small-scale, ground-based CMB telescopes that make measurements to larger ℓ, such as ACT [53] (cosmological parameters in [54]) and SPT [55] (spectra and parameters in [56]). In Fig. 1.2 we show the WMAP data for C_ℓ^{TT} and the theoretical model inferred from it. The cosmological parameters (see Section 1.2.1) can be inferred with astonishing accuracy from data like this. A common method to do this is via a Monte Carlo Markov Chain likelihood analysis, for example using the publicly available code `cosmomc` [57, 58], that determines the statistical best fit parameters and the errors on them. We will perform such an analysis in Chapter 6. The future of CMB observation is the ESA *Planck* satellite [13, 14], the cosmological data from which is expected to be available in early 2013. In Chapter 5 we will forecast, using a Fisher Matrix formalism (see e.g. [29, 59]), for the expected accuracy of Planck constraints on the cosmological parameters.

1.1.2.2 *Large Scale Structure*

The study of large scale structure (LSS) or the 'cosmic web' involves mapping the density field of matter, dark or luminous, in the universe. This can be done in a number of ways, but the simplest approach is a galaxy redshift survey (GRS), the benchmark surveys being the Sloan Digital Sky Survey (SDSS) [7], and prior to that 2dFGRS [60–63]. These surveys produced famous images of the LSS showing the cosmic web, and giant features in it such as 'the great wall' and 'the fingers of god', the observational equivalent of the astounding, computer generated 'Millenium Simulation' [64].

In this thesis, however, as with the CMB, what will concern us when it comes to LSS are not maps of the sky, but the matter correlation function, or rather its Fourier transform the *matter power spectrum*, $P(k,z)$, where z is the redshift of the objects. The power spectrum is defined from the matter overdensity, $\delta_m = \frac{\delta\rho_m}{\rho_m}$ by:

$$\langle \delta(k)\delta(k') \rangle = (2\pi)^3 P(k)\delta^3(k-k')\,, \tag{1.13}$$

where $\delta^3(x)$ is the Dirac delta distribution. Gravity acts to evolve the initial small

perturbations in the universe, the one part in 10^{-5} of COBE, into the structures we see today. These initial perturbations are also described by a power spectrum, the primordial power spectrum, $\mathcal{P}(k)$, which is often assumed to arise from inflation. Since we will always work in first order, linear perturbation theory in the overdensities, the different Fourier modes do not mix and the power spectrum today is a linear evolution of this primordial spectrum, given by a growth function, $D(z)$, and the mode evolution is given by a transfer function, $T(k)$. We can think of this as:

$$P(k,z) = \mathcal{P}(k) \times T^2(k) \times D^2(z)\,. \tag{1.14}$$

We will often calculate all of the matter power spectrum by numerically evolving $\delta(k,z)$ for each mode given a set of initial conditions, but the intuitive picture is worth bearing in mind. If the factorisation separating $T(k)$ and $D(z)$ is possible, which it is in ΛCDM (see e.g. [65]), then the growth rate, defined as the logarithmic derivative of the overdensity with respect to the scale factor, will be scale independent. The factorisation is possible because in ΛCDM in the post recombination universe there are no scales at play, only the growing mode.

We show the results of SDSS DR7 [66] for $P(k, z = 0)$ in Fig. 1.3 with the WMAP7 cosmology as the theory line. The CMB alone, under the assumption of flatness, gives parameters that fit LSS data remarkably well. LSS measurements in the future will include the ESA Euclid satellite [67, 68]. In Chapter 5 we make forecasts for the expected accuracy of a similar mission in measuring cosmological parameters.

There are two main features in the power spectrum. The BAO are imprinted in the baryons at decoupling when they are also imprinted in the CMB, and are gravitationally communicated to the rest of the matter. The BAO defines a preferred length scale in the correlation function, and thus the Fourier transform is a wave of a certain frequency. We will discuss BAO in some detail in Chapter 5. There is also the *turnover*, caused by different rates of growth in the density perturbations during matter and radiation dominated epochs.

The growth of modes is governed by the dynamical length scale in the problem: the Hubble scale, $1/H$. The physical length is given by a/k so a mode is of the Hubble scale when $k = aH$: modes with larger wavenumber k than this are in causal contact.

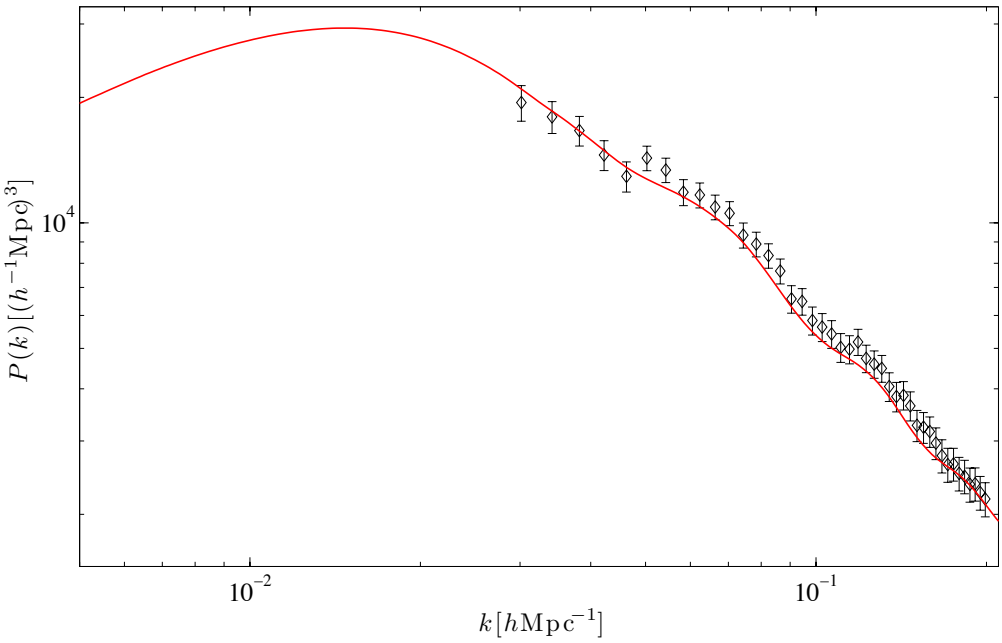

Figure 1.3 The matter power spectrum, $P(k)$ (see Eq. (1.13). The data is from SDSS [66], and the theoretical curve is given by the best fit parameters to the *WMAP data* (see Section 1.2.1 and [6]), calculated using `CAMB` [45]. Note that because of this, the fit is not perfect. The fitted parameters are altered slightly from their central values if additional LSS data is included, but there is remarkable agreement.

We refer to such modes as being 'inside the horizon' (this is the particle horizon, there are no event horizons: the Penrose diagram [69] of the FLRW universe with no cosmological constant is that of flat space). The evolution of any mode will depend on what the physics at play is when it enters the horizon. During the normal course of cosmic evolution, aH is shrinking and modes on larger scales (smaller k) are entering the horizon. This is not true in any pure dS phase of expansion dominated by a constant energy density. Such a phase will occur in our future if there really is a cosmological constant, and as we will discuss in Section 1.2.5, in the early universe this plays a very important role in the physics of inflation.

Since aH is shrinking during the matter and radiation epochs, the location of the turnover is given by the mode that entered the horizon at matter-radiation equality, $k_{\mathrm{eq}} = a_{\mathrm{eq}}H_{\mathrm{eq}}$, because this separates modes that entered the horizon during radiation domination from modes that entered the horizon during matter domination. Modes either side of this have seen different growth histories.

1.2 COSMIC INGREDIENTS AND PARAMETERS

1.2.1 *Observational State of Play*

Measurements in cosmology lead to constraints on sets of parameters. All current measurements can be fit by just six parameters of what is known as the *Concordance Model*. These are:

- A_s: the scalar amplitude. A dimensionless parameter which gives the square amplitude of primordial fluctuations.
- n_s: the spectral index. This is the exponent giving the 'tilt' of the inflationary power spectrum. It parameterises deviations from scale invariance.
- $\Omega_b h^2$: baryon density. A dimensionless number proportional to the physical density on baryons in the current epoch.
- $\Omega_c h^2$: cold dark matter (CDM) density in the current epoch. The CDM is assumed to be described by a perfect fluid with zero sound speed and equation of state $w = 0$.
- Ω_Λ: fraction of the critical density in the cosmological constant.
- τ: optical depth to reionisation. This tells us when the first astrophysical objects were formed that reionised the universe and ended the cosmic dark ages.

The constraints on these parameters given by the final, 7 year, data release of WMAP taken from [5] (WMAP7) are given in Table 1.1.

The temperature of the CMB as measured by COBE, which gives the density in electromagnetic radiation, is taken to be exactly fixed. Various other assumptions come with the use of these parameters, for example the following will be of concern to us:

- Flat universe. The concordance model assumes that there is zero curvature. In the CMB there is a large degeneracy between Ω_Λ and Ω_k, but inclusion of supernova or LSS BAO data break this degeneracy (see e.g. [70]) and agree on $\Omega_k = 0$, so the data can be fit without it. The knock on degeneracies caused by

Parameter	Central Value	Error
A_s	2.43×10^{-9}	0.11×10^{-9}
n_s	0.963	0.014
$\Omega_b h^2$	0.02258	$^{+0.00057}_{-0.00058}$
$\Omega_c h^2$	0.1109	0.0056
Ω_Λ	0.734	0.029
τ	0.088	0.015
$N_{\rm eff}$	> 2.7	95%C.L.
$\sum m_\nu$	$< 1.3\,{\rm eV}$	95%C.L.

Table 1.1 Constraints on the 6-parameter Concordance Model taken from WMAP7. For brevity with the extended models we only quote the constraints on the new parameters, but note that central values and errors on other parameters may change. The full results are at [6].

this assumption beyond the concordance model can be very important (see e.g. [71, 72]), but we will have little more to say about curvature in this thesis.

- Adiabatic initial conditions. This is an assumption based on the physics of inflation that holds in the simplest single field models and reheating scenarios.

- $N_{\rm eff} = 3.04$. The number of relativistic neutrino species. This assumes that all neutrinos are massless, and have a standard thermal and decoupling history. See Section **??**.

- The equations of motion are given from General Relativity and first order cosmological perturbation theory applied to the various species, with no decays between species.

We will investigate many of the above assumptions in detail throughout this thesis and will say no more about them here.

The single most striking thing about these parameters is that only two, $\Omega_b h^2$ and τ, bear any relation to the Standard Model of particle physics (we will discuss the problem of Λ in Section 1.2.4), and only one of the assumptions, that on $N_{\rm eff}$, is fixed by this.

1.2.2 *A whistle-stop tour of the Standard Model*

The Standard Model (SM) of particle physics[5] is a triumph of 20th century physics. It has its roots in Dirac's pioneering work [74], which led to the creation of QED and renormalization by Feynman, Schwinger, and Tomonaga [75–77], and unified by Dyson [78]. QED is the relativistic quantum field theory of the electromagnetic interaction with charged fermions. It is a gauge theory with abelian $U(1)$ symmetry and is self consistent. However, when the charge is renormalised and the so-called β-function for the running coupling is computed, it is found that there is a super-Planckian Landau pole where the coupling diverges.

As the 20th century progressed the rise and rise of gauge theory continued. The Higgs mechanism and boson [79–81] was added to its armoury which allows gauge theory to describe massive vector bosons as well as massive fermions in the context of the chiral weak force. Glashow, Salam and Weinberg [82–84] incorporated this fully into the electroweak theory where the non-abelian gauge group $SU(2)_L \times U(1)_Y$ is broken by the Higgs mechanism to $U(1)_{em}$ of QED. Its predictions of the Z_0 boson with the weak mixing angle, and the quark mixing of the Cabibo-Kobayashi-Maskawa matrix [85, 86], along with many other precision tests, were verified by experiments at CERN and other locations in the latter half of the 20th century.

The strong nuclear force that seemed so stubborn was brought into the fold by the quark model of Gell-Mann [87]. This model eventually grew into the fully fledged theory, QCD, which describes the interactions of quarks and gluons via an $SU(3)$ gauge theory [88]. In the 1970's 't Hooft and Veltman [89–91] proved that non-Abelian gauge theories were renormalizable and thus this was a consistent description of physics despite strong coupling at everyday energies because of the *asymptotic freedom* of QCD [92–95]. QCD behaves in the opposite way to QED, becoming weakly coupled at high energies. Thus one can calculate scattering cross sections involving quarks, and predictions for a machine like the LHC can be trusted.

Constructing the SM requires specifying the gauge group, $SU(3) \times SU(2) \times U(1)$, the matter content, quarks, leptons, and the Higgs field, and the representations that

[5] For the complete review of the status of the SM including all measured parameter values and precision tests, see the Particle Data Group [73].

the matter fields occupy in the gauge group, in every case either the fundamental or a singlet for the non-abelian groups. In specifying the matter content, the original model makes the neutrinos massless (left handed Dirac fields only). One then writes down every possible renormalizable interaction consistent with these specifications and gauge invariance, and the SM is complete.

The SM thus specified contains only 18 parameters, all of which have now been measured. The culmination of this came with the recent measurement of the Higgs mass $m_h \approx 125\,\text{GeV}$ [96].

The only stable particles in the standard model are the electrons (lightest charged particle), neutrinos (lightest hypercharged particle), the photon (massless gauge boson), and the proton (lightest particle with baryon number, strongly coupled bound state of quarks and gluons) [6]. Nuclear physics and the long life time of the neutron allow the formation of stable nuclei and atoms, leading to all the rich physics of both everyday life and the nuclear interactions that keep stars alight. The nuclei are formed in the hot big bang during Big Bang Nucleosynthesis (BBN) [32] (see e.g. [29, 97]), with heavier elements formed inside stars and supernovae by known nuclear processes. Aside from these few constituents, the standard model predicts no other cosmic ingredients: from the point of view of parameters we have T_{CMB}, $\Omega_b h^2$, τ, and N_{eff}.

The SM allows for, but does not predict, T_{CMB} or $\Omega_b h^2$. T_{CMB} is essentially a time from the epoch of nucleosynthesis, and predicting $\Omega_b h^2$ requires a theory for baryogenesis, which we will not discuss but note that the SM is incapable of providing. The two combined are a measure of the entropy per baryon. For a discussion of these topics, see e.g. [35]. τ and N_{eff}, on the other hand, should be essentially calculable from SM physics given appropriate astrophysical inputs about star formation, light element abundances, and neutrino decoupling.

[6] The proton is unstable non-perturbatively due to instanton effects that violate baryon number conservation, but the life time of the proton due to such processes is orders of magnitude longer than the age of the universe.

1.2.2.1 *Neutrinos*

The neutrino sector in the SM is uniquely specified, as we have said, by specifying the field content, since it does not allow for neutrino mass or mixing and hence there are no free parameters, but with measurements this field content is open to revision.

Observations of neutrino oscillations both from astrophysical sources and reactors are definitive evidence that neutrinos have (see e.g. [98]). Neutrinos can only be given Majorana masses in the SM, and at the expense of introducing non-renormalizable operators that introduce a large energy scale $\mathcal{O}(10^{14})$ GeV beyond which the SM is not valid. The parameters of the neutrino mixing matrix, the PMNS matrix [99, 100], have all now been measured, except for possible *CP* violation.

The unknowns in this sector are the absolute neutrino mass scale, parameterised in cosmology as $\sum m_\nu$, the sum of neutrino masses, whether the hierarchy is 'normal' or 'inverted' (two light or two heavy neutrinos), and whether the neutrinos are Dirac or Majorana particles. It is also possible to change $N_{\rm eff}$ by playing with the physics of BBN and neutrino decoupling within the SM (see e.g. [101]). Cosmology places constraints on $\sum m_\nu$ and $N_{\rm eff}$, which are both common secondary parameters in addition to the parameters of the concordance model. The WMAP7 constraints on these extended models are also given in Table 1.1. We will have much more to say about neutrinos and cosmology in Chapter 5.

1.2.2.2 *The Strong CP Problem*

Gauge and Lorentz invariance allow the inclusion of the 'topological' term:

$$S_\theta \propto \int d^4x \theta \mathrm{Tr}[\tilde{G}^{\mu\nu} G_{\mu\nu}]\,, \tag{1.15}$$

in the standard model action, where G is the gluon field strength tensor (*not* the Einstein tensor), and $\tilde{G}^{\mu\nu} = \epsilon^{\mu\nu\alpha\beta} G_{\alpha\beta}$ and ϵ is the totally antisymmetric 4-tensor. This is a topological term since in GR it does not require the measure $\sqrt{-g}$ in order to be diffeomorphism invariant, and thus does not depend on the geometry of space-time.

The antisymmetry of the tensors in this term mean that it violates time reversal, T, and parity, P, symmetry, and thus, since the term is *CPT* invariant, it must also violate

CP. It is a theorem that *CPT* is a necessary symmetry of a consistent, local, Lorentz-invariant quantum field theory, however *CP* is violated by the weak interactions due to the complex phase of the CKM matrix, and thus there is no symmetry forbidding inclusion of this term. The term is a total derivative so does not affect the classical equations of motion or appear perturbatively. However, contributions to this term are generated non-perturbatively by QCD, via instantons and the 'theta vacuum' (see e.g. [102]), and in the weak sector from the phase of the determinant of the quark mass matrix.

This term is problematic, since it generates an electric dipole moment for the neutron that depends on θ. The neutron electric dipole moment has not been detected, and current limits imply that $|\theta| \lesssim 10^{-10}$ [103, 104]. Because there are dynamical contributions to θ from two distinct parts of the SM this small value would require a fine tuning of two unrelated phenomena and is regarded as unnatural. Non-perturbative effects like this are relevant for QCD because the quark masses $m_u, m_d, m_s < \Lambda_{\rm QCD}$, where $\Lambda_{\rm QCD}$ is the scale at which QCD becomes non-perturbative.

There are two viable solution to this problem that extend the SM (they are Beyond the SM, or BSM): the Nelson-Barr solution [105, 106], which introduces a new discrete symmetry, and the Peccei-Quinn-Weinberg-Wilczek axion [107–109]. We will have much more to say about axions throughout this thesis, as they can play an important role in cosmology.

1.2.3 *Dark Matter: evidence and models*

There are many reasons to believe that there is a significant component of *Dark Matter* (DM) in the universe. The evidence that most concerns us comes from cosmology in the form of the parameter $\Omega_d h^2 \neq 0$. The cosmological observables discussed in Section 1.1.2 simply cannot be fit with models containing no DM. In terms of cosmological perturbation theory, DM is described by a perfect fluid of 'dust' with zero equation of state and zero sound speed. This type of dark matter is *cold* DM (CDM). When the dark matter is multi-component, we will use the subscript 'c' to distinguish the CDM piece.

From a particle physics point of view, DM must have a number of properties to

fulfil this role. It must be weakly interacting with the particles of the SM, or else it would not be dark, and it would not have the properties of a dust fluid. It must be stable on very long time scales. It must be produced in the early universe in large quantities. Finally, if the DM is produced by thermal freeze out, it must be heavy, $\gtrsim \mathcal{O}(\text{few})\,\text{MeV}$, or else the temperatures in the early universe would impart it with large velocities, making it relativistic on cosmologically relevant timescales and not being properly cold. The name given to such a particle is a 'WIMP', a weakly interacting massive particle.

Such a particle arises very naturally in supersymmetric extensions of the standard model, such as the minimally supersymmetric SM, the MSSM [110]. The lightest supersymmetric partner, or LSP, will be stable if the theory has a preserved R symmetry. R symmetry is a global symmetry, like baryon number in the standard model, under which different fields in the same supermultiplet (SM particles and their superpartners) have different charges. Noether's theorem [111] tells us that every global symmetry has an associated conserved charge, and thus decays where the number of SM particles relative to superpartners changes are forbidden. Thus the LSP is stable. R symmetry is useful in the MSSM for a completely different reason: it also forbids proton decay, which would otherwise occur and has not been observed [73]. For the LSP to be the DM it must be neutral, a singlet under $SU(3)$ and $U(1)_{\text{em}}$: a 'neutralino'. Weak scale thermal cross sections then make the production in the early universe via 'thermal freeze out' give a value for $\Omega_d h^2$ approximately consistent with observations (see e.g. [112]). The LSP mass is set by the supersymmetry (SUSY) breaking scale, which in the MSSM is set around a TeV in order to solve the hierarchy problem on the quantum corrections to the Higgs mass.

From BSM particle physics there are many, many, candidates for the CDM that differ from this standard WIMP in lesser or greater ways. These differences may affect their properties during inflation, during baryogenesis, or during BBN. These early time effects are of no concern to us in this thesis. As long as the dark matter is cold, we count it into Ω_c. Late time effects, such as possible decay, or couplings within the dark sector, while cosmologically relevant, are also beyond the scope of this thesis. Such effects occur, for example when the DM abundance is 'frozen in', rather than

frozen out, in the model of [113, 114]. What will concern us more is the DM mass, and the effect that reducing it has on the cosmological observables. If the DM is thermally produced, lowering the DM mass to around keV will make it warm DM, and even lower to around eV will make it hot DM. Massive neutrinos with masses around the limit given in Table 1.1 constitute such a hot component.

In cosmological perturbation theory, Hu presented the most general phenomenological parameterisation for the DM and its effects on LSS and the CMB [115]. In this formulation, the DM equation of state is free, and it is also free to have sound speed, entropy perturbations, and anisotropic stress. By focusing on the perturbed energy momentum tensor and it components, this treatment captures all possible evolution in the dark sector, but as Hu notes may be impractical to apply to some models, in particular some scalar field models.

A perturbed DM fluid with no anisotropic stress (and hence excluding neutrinos), in synchronous gauge (see Section 4.1) and in conformal time, to first order in cosmological perturbation theory is described by the following two evolution equations [40, 115]:

$$\dot{\delta} = -(1+w)\left(\theta + \frac{\dot{h}}{2}\right) - 3\mathcal{H}\left(\frac{\delta P}{\delta\rho} - w\right)\delta\,, \tag{1.16}$$

$$\dot{\theta} = -\mathcal{H}(1-3w)\theta - \frac{\dot{w}}{1+w}\theta + \frac{\delta P/\delta\rho}{1+w}k^2\delta\,. \tag{1.17}$$

Dots denote derivatives with respect to conformal time, $\mathcal{H} = \dot{a}/a = aH$, h is the synchronous gauge potential, and θ is related to the fluid velocity and comes from the perturbed energy momentum tensor as $(\rho + P)\theta = ik^j \delta T^0{}_j$. The fluid is specified by the equation of state, $w(\tau)$, and by the sound speed, $c_s^2 = \frac{\delta P}{\delta\rho}$. Hu breaks this sound speed up into an adiabatic piece, $c_g^2 = \frac{\dot{p}}{\dot{\rho}}$, and a piece due to entropy:

$$P\Gamma = \delta P - c_g^2 \delta\rho\,. \tag{1.18}$$

We will make use of this formalism to describe axions in Chapter 6, and the intuition it provides will be useful throughout this thesis.

From the point of view of non-linear structure formation and cosmological phenomenology, dark matter self-interactions [116] and ingredients like 'Fuzzy Cold Dark Matter' (FCDM) [117] have been proposed as resolutions to the problems of cuspy

dark matter halos, the large predicted but unobserved numbers of dwarf galaxies in the standard CDM model (the well known 'missing satellites' problem), and finally as a mechanism to produce 'caustic rings' [118]. This has led some to general consideration of Bose-Einstein-Condensate (BEC) dark matter (see, for example, [119–121], and in the case of axions [122, 123]). Indeed, the numerical simulation of [124] showed that the presence of such an ultra-light scalar condensate indeed reduces the number of dwarf galaxies, but in fact does very little to the cuspy density profile. However there are also many unaccounted for factors in standard galaxy formation models with CDM that may affect the formation of cusps and dwarf galaxies, such as baryon physics and supernova feedback (see, for example, [125] and references therein).

Scalar fields with masses in the range $10^{-33}\,\mathrm{eV} < m < 10^{-22}\,\mathrm{eV}$ would constitute an FCDM component. The Compton wavelength of the particles associated to ultra-light scalar fields, in natural units, $\lambda_c = 1/m$, is of the size of galaxies or clusters of galaxies, an so the uncertainty principle prevents localisation of the particles on any smaller scale. The large phase space density of such ultra-light scalar fields causes them to form BECs (see [122] and references therein) and allows them to be treated as classical fields in a cosmological setting. This could lead to many interesting, and potentially observable astrophysical phenomena, such as formation of vortices in the condensate [119, 126], and black hole super radiance [104, 127, 128].

1.2.4 Λ *and Dark Energy*

The evidence for a non-zero cosmological constant comes from the necessity of the cosmological parameter $\Omega_\Lambda \neq 0$ in our Table 1.1. One should note that WMAP alone does not pin this down, due to a large degeneracy with curvature, expressed as curvature energy density, Ω_k. Until recently it was necessary to include supernova and/or BAO distance measures to break this degeneracy and assert the flat, accelerating universe that our parameters show (for a description, see e.g. [70]), however ACT [129] recently used CMB lensing to detect Ω_Λ using the CMB alone. The value $\Omega_\Lambda = 0.734$ implies that $\sim 73\%$ of the energy density of the universe at the current epoch is in the cosmological constant, or a time varying component with similar effects on the acceleration of the universe dubbed *Dark Energy* (DE). However, as we

have already mentioned, Einstein was bothered by Λ, and the size of Λ is a theoretical problem much older than precision cosmology. The classic review of Weinberg [36] covers all of the essence of the problem, which has changed rather little since 1989. Our discussion below follows Weinberg.

The cosmological constant is a free parameter in Einstein's equations, and we have no reason to expect it to have any particular value at all. Here, we take the purely gravitational contribution to be given by Λ. However, in a quantum field theory like the SM, there are dynamical contributions. In the vacuum, the energy momentum tensor takes the form:

$$\langle T_{\mu\nu} \rangle = -\langle \rho \rangle g_{\mu\nu} \,, \tag{1.19}$$

so that we introduce:

$$\begin{aligned} \Lambda_{\text{eff}} &= \Lambda + 8\pi G \langle \rho \rangle \,, \\ \rho_\Lambda &= \frac{\Lambda_{\text{eff}}}{8\pi G} \,. \end{aligned} \tag{1.20}$$

In a flat universe with all the energy density in the cosmological constant, which is close enough to observation to allow us to estimate H_0:

$$H_0^2 \approx \frac{8\pi G}{3} \rho_\Lambda \,. \tag{1.21}$$

Rearranging:

$$\rho_\Lambda \approx \left(\frac{H_0}{M_{pl}} \right)^2 M_{pl}^4 \,, \tag{1.22}$$

where $M_{pl} = 1/\sqrt{8\pi G} \approx 10^{18}\,\text{GeV}$ is the reduced Planck mass. In natural units where $\hbar = c = 1$, $H_0 = 100h\,\text{km}\,\text{s}^{-1}\,\text{Mpc}^{-1} \approx 10^{-33}\,\text{eV}$, so that:

$$\rho_\Lambda \sim 10^{-120} M_{pl}^4 \,. \tag{1.23}$$

What do we expect from quantum field theory? There exists the zero point energy, demonstrated as physical by the Casimir effect [130, 131]. We can calculate the zero point energy of a field of mass m in a theory with cutoff $\lambda_c \gg m$, it is:

$$\langle \rho \rangle \simeq \frac{\lambda_c^4}{16\pi^2} \,. \tag{1.24}$$

If we are optimistic and believe in GR plus the SM up to the Planck scale then $\lambda_c = M_{pl}$ and we see that that the observed value of ρ_Λ would require a tuning for cancellation between the gravitational and zero point contributions to 118 decimal places (not the famous 120, due to the factor of $16\pi^2$).

The problem is exacerbated by the contribution to vacuum energy from the Higgs potential, which means that the cancellation also involves the weak scale and will change at the electroweak phase transition when the Higgs acquires a vacuum expectation value (vev). Furthermore, while SUSY makes the scalar potential, and zero point energies zero, the zero point energies must be corrected at the SUSY breaking scale (since nature is manifestly not supersymmetric), and in supergravity the scalar potential is negative definite.

However, the observed in Planck units, $\rho_\Lambda \sim 10^{-120}$ is not so surprising given that we actually have observed it, i.e. given the *anthropic principle*. The 'Weinberg window' [132] sets $|\rho_\Lambda| \lesssim 10^{-120}$: if $\rho_\Lambda \gtrsim 10^{-120}$ then accelerated dS expansion sets in before any bound structures can form and no life-as-we-know-it-Jim could exist to make an observation, while if $\rho_\Lambda \lesssim -10^{-120}$ then the universe would expand and then collapse to a singularity again, also before any bound structures could form. The simple fact of our observation gives the correct order of magnitude for ρ_Λ. The modern realisation of this anthropic selection is given by Coleman-De Luccia [133] tunnelling through the vast landscape of false vacua in the scalar potentials of string theory during eternal inflation in the model of Bousso and Polchinski [134] (and earlier discussed by e.g. [135]).

Finally, there are other 'coincidences' that can be seen to exacerbate the cosmological constant problem, for example why does the measured value of $h \approx 71$ give $\Omega_\Lambda \approx \Omega_m$ in the current epoch, i.e. why do we live close to the matter-Λ transition? For two more modern perspectives on cosmic coincidences see [136, 137].

A huge amount of research in modern cosmology goes into models for the 73% of DE that treat it other than as a cosmological constant, for example modified gravity [138] and quintessence [139–142]. Many of these models alter the equation of state, $w(z)$, of DE, an effect degenerate with neutrino masses at some scales. In particular, models where there is a component of dark energy with effects at high redshift

(early dark energy, EDE) are known to share many degeneracies in their effects on cosmological observables with extra relativistic energy density, massive neutrinos, and other forms of hot dark matter or any other structure-suppressing cosmological ingredients (see, for example, [143–145]). The potential degeneracies can, however, be broken by the use of multiple observables [145]. We note that any potential detection of an exotic component like EDE can only be truly qualified if all other aspects of cosmology with potentially similar effects are well understood. Finally, massive neutrinos are a key ingredient, along with a modified inflationary period, in allowing the model of [146] to fit the data and analyses of [129, 147] without the inclusion of a DE sector (i.e. $\Omega_\Lambda = 0$), so that the future success or failure of this non-standard model, too, must hinge on thorough understanding of the structure suppressing DM species.

1.2.5 Inflation: the bare essentials

Inflation will feature only in passing in this thesis. Since we will not be concerned with specific models, we survey here only some motivation for this bizarre phase in cosmic history and the general features that the most minimal models lead to in relation to the concordance model and the string theory landscape. There is a vast literature on inflation, with many excellent review articles. A textbook starting point for the interested reader is [148].

Inflation is a period of quasi-dS expansion in the very early universe similar to the current epoch of Λ dominated expansion. It was introduced in the early 1980's [149–151] to solve , among other things, the *horizon problem*: in the CMB we observe a uniform temperature of the CMB across the whole sky and large scale correlation between modes $k < (aH)_{ls}$, so that their physical size is greater than the horizon size at last scattering and they should not have been in causal contact at CMB formation. In Section 1.1.2.2 we discussed that during normal cosmic evolution aH shrinks and modes not previously in causal contact enter the horizon and come into causal contact. However, during a quasi-dS phase of expansion, aH *grows* since $a \sim e^{Ht}$ and H remains fixed. Therefore during such a phase modes are initially in causal contact and then the exponential expansion pushes them out of the horizon and out of causal

contact. During inflation the large scale modes of the CMB were in causal contact and were thermalised, they were then pushed out of causal contact and remained so at CMB formation.

Models of 'new inflation' [150] realise the onset and end of this expansion phase via the slow rolling of a scalar field in its potential. As well as solving the horizon problem, this has a major observational consequence for our parameters. The quantum fluctuations of a field in dS space produce the primordial power spectrum, $\mathcal{P}(k)$, as near to scale invariant with the amplitude A_s and *spectral index* n_s:

$$\frac{k^3}{2\pi^2}\mathcal{P}(k) = A_s \left(\frac{k}{k_0}\right)^{n_s-1}, \tag{1.25}$$

where k_0 is a 'pivot scale' taken to be $k_0 = 0.002\,\mathrm{Mpc}^{-1}$ in the WMAP analyses. Both A_s and n_s are specified by the inflationary potential. The observed values of these parameters preclude the *inflaton* field from being the Higgs field of the SM, and so more new physics is necessary to explain inflation.

Three other additional predictions of single-field slow roll inflation are *flatness*, as curvature is diluted by the rapid expansion and as we have seen is already a verified prediction to a high degree of accuracy; *adiabatic* fluctuations in the CMB, which are assumed in the concordance model; and the existence of primordial tensor fluctuations in the CMB[7], with a tensor to scalar ratio, r, specified by the inflationary potential. We will have much more to say about these predictions in Chapter 6.

Finally, inflation has an important implication for the cosmological constant problem and the string theory landscape that we have already touched on in Section 1.2.4: *eternal inflation* [152, 153].We will not go into the technical details here, but there is an intuitive explanation (for a pedagogical introduction, see e.g. [154]). Inflation ends when the inflaton is no longer slowly rolling, or in the context of old inflation [155], when the false vacuum decays (a phase of old-type inflation is always believed to necessarily precede slow roll). The end of inflation must happen causally, i.e. not over all of space at once. Once a region stops inflating, the bubble wall moves at the speed of light and swallows up space around it. However, the space that has not decayed and is therefore still inflating between the bubbles is expanding super-luminally. As long

[7]Tensor fluctuations are also generated by gravitational lensing as CMB photons pass from the surface of last scattering to us.

as bubble nucleation happens in some sense slower than the inflationary expansion then there will always be an inflating region that survives to parent new and different vacua. In the context of the landscape, the decays happen in all directions and populate the different vacua with different low-energy physics, and different Λ (see [36]). Decays cascade to the stable true vacuum, if one exists, or else terminate in vacua with negative cosmological constant that collapse to form big crunch singularities.

1.3 THE AXIVERSE

With so many competing theories of the 'missing' cosmological components, either phenomenological or theoretical, competing for dominance while we wait for more complete evidence and theories, one would like to find a framework in which to speak about them that satisfies a number of criteria:

- *Distinct*: The framework should contain observational features that allow it to be distinguished from other models, using one or more observables.
- *HEP foundations*: The framework should have clear ties to high energy physics (HEP), so that one can consistently apply logic that links late time cosmology to early time cosmology, and potentially other areas in HEP such as SUSY and other fine tuning, and quantum gravity.
- *Theoretical generality*: One would like the framework to be general enough that one does not have to build specific models to study on a case by case basis in order to find out what the cosmology is.
- *Theoretical specificity*: Despite this, one does not want to be so general that the framework cannot be falsified, or have evidence stack up against it. As such, it should be discussed within a specific theoretical context.

String theory [156, 157] is the most complete theory of HEP and quantum gravity, however it has often been criticised as being untestable [158]. There is so much freedom within string theory once it is reduced from its natural 10 or 11 dimensions to the 4 we observe by the process of *compactification* and *moduli stabilisation* [159]

that finding its salient features in any given situation becomes almost impossible. For example, the Bousso-Polchinski method [134] for generating an acceptably small cosmological constant within string theory leads to the famous 10^{500} string vacua and the so-called *landscape* of string theory. However, as argued for example by [160], there is at least one absolutely general feature of string theory: a profusion of scalar fields.

In particular, for reasons we will argue below, a particularly interesting set of such (pseudo-) scalars are *axions*. It was in this spirit of searching for 'model independent' features of string theory that have astrophysical and cosmological implications that the authors of [104] took a positive view of the landscape and proposed the existence of the *String Axiverse*, after which this thesis is titled, and will constitute our framework. They quoted Leibniz:

> The Principle of Plenitude: *"This best of all possible worlds will contain all possibilities, with our finite experience of eternity giving no reason to dispute nature's perfection."*
>
> Gottfried Leibniz (1646-1716), in *Theodicee*

1.3.1 Axions

We have already discussed the strong *CP* problem and its possible resolution via the introduction of an additional particle: the (QCD) *axion* [107–109, 135, 161–177]. We have already briefly discussed how axions can play a cosmological role as DM: for reviews of axion cosmology, see [118, 178]. In this axion solution the problematic *CP* violating parameter θ occurring in the SM action is made dynamical as the Goldstone boson of a spontaneously broken global $U(1)$ symmetry, called a Peccei-Quinn or *PQ symmetry*, and driven to its *CP* conserving value by a potential induced non-perturbatively by QCD instantons[8] [180]. The quantum of excitation of θ is then the axion. The global symmetry is broken at the scale f_a, whilst the non-perturbative physics giving the axion its potential switches on at a scale μ (in QCD $\mu = \Lambda_{\rm QCD}$). This makes the axion a pseudo-Nambu-Goldstone boson (PNGB). Ultra-light axions

[8] We will not have time or space here to discuss such non-perturbative physics, but direct the reader to the books [102, 179].

and other PNGB's motivated in high energy physics, such as in [181, 182] have been studied as resolutions to the cosmological constant problem ever since it has existed [132].

Depending upon their mass, axions can constitute the full range of dark matter 'temperatures', from cold through warm to hot: a true feast for Goldilocks. A model dependent coupling to photons can make them not really dark at all, and constraints can be derived on this from dimming of supernovae [183]. Hot, thermal axions can contribute to $N_{\rm eff}$, but their weak couplings make this contribution fractional [175]. For our purposes, the standard QCD axion will be considered part of $N_{\rm eff}$ or Ω_c appropriately.

QCD axions in the mass range $0.7\,{\rm eV} \lesssim m_a \lesssim 300\,{\rm keV}$ are excluded by cosmology for a variety of reasons [175, 177, 184]. Sub eV mass axions contribute as HDM, and their mass is limited by constraints on $N_{\rm eff}$: in exact analogy to neutrinos, they cannot be too heavy. Heavier axions, which are too heavy to be HDM, if they couple to photons, are restricted by their decays/inverse decays via effects on BBN, CMB distortions, and concordance between BBN and CMB determined values of the baryon to photon ratio. In addition, in this scenario, early axion decays to photons dilute the effective number of neutrino species, creating more tension with the large measured values of $N_{\rm eff}$ discussed in Section **??**.

Goldilocks properties of axions are abundant as they make multiple changes in their apparent dark matter 'temperature' as one moves through their possible mass spectrum. One normally considers heavy WIMPs with GeV masses as cold dark matter (CDM), and light neutrino-like particles with eV masses as HDM, and axions can indeed populate these masses and temperatures in the same way. However, when they are non-thermally produced, very light axions with $m \lesssim 1\mu\,{\rm eV}$ once again constitute CDM, and the types of limits given above from couplings to photons cease to apply [178] (it is, in fact, possible for the QCD axion to be this light, or lighter [104]). As we will see through the course of this thesis, another transition occurs when these light CDM-like axions become lighter still and their quantum properties cause them to behave like HDM in the LSS. This range of behaviour has to do with competition between various physical processes which come in and out of dominance

as coupling properties and relic density contributions of axions vary with mass and cosmic evolution. We do not know the fundamental model and parameters that would exactly determine axion behaviour. Names can also deceive us: as we will see, the QCD axion is not the only axion relevant for cosmology, and not all axions behave in the same way.

1.3.2 *String Axions*

We saw above that cosmologists often invoke the existence of light scalar fields in the late universe as DM and DE components, for example in theories of quintessence, coupled quintessence (e.g. [185]), chameleons [186, 187], unified dark matter, FCDM, and Bose-Einstein condensates. From a particle physics/string theory point of view these ingredients come up against two main problems: fifth-force constraints, and cosmologically light masses, which are not unrelated[9].

For a (coherent) scalar field to be cosmologically distinct from CDM, or to play a quintessence like role, it must be very light: $10^{-33}\,\mathrm{eV} \lesssim m_\phi \lesssim 10^{-18}\,\mathrm{eV}$. Gauge invariance and Lorentz invariance then allow this scalar to multiply terms in the Lagrangian of the standard model fields, leading to problematic long range 'fifth forces'. Unless a symmetry forbids them, these couplings should be universal and cannot be restricted ad hoc to the dark sector alone. If the field is to have an origin in new physics beyond the standard model then its lightness and stability also become hard to explain without introducing additional hierarchy problems. For this reason, scalars in the late universe are considered generally problematic in models of particle physics; keeping them under control is part of the *cosmological moduli problem* in string theory [191].

There is, however, at least one generic source of light scalars coming from high energy physics that evades the problems highlighted above: the String Axiverse ([104] gives a more detailed version of the following argument). We would like string theory to furnish us with the QCD axion and its solution to the strong *CP* problem. All types of string theory and M-theory contain multiple axion fields [192, 193] that are Kaluza-Klein zero modes of antisymmetric tensor (form) fields analogous to the Maxwell

[9] Addressing these issues for chameleons and string moduli has been looked at in e.g. [188–190].

tensor, $F_{\mu\nu}$. These terms appear when the form fields are compactified on closed cycles in the compact space, with 3-forms being compactified on closed 3-cycles, 2 forms on closed 2-cycles etc. The number of axions arising due to the existence of a given form field is given by the number of closed cycles of the corresponding order; the relevant fields, however, depend on which string theory on is working in: Type I, Type IIA, Type IIB or the Heterotic theories. Generic string theory compactifications capable of realising realistic theories of high energy physics can have highly complicated topologies known as Calabi-Yau manifolds [194], containing many hundreds of closed cycles of different orders, and thus give rise to *many axions*. For example, the simplest Calabi-Yau is the six-torus, which possesses 15 different two-cycles, and the same number of four-cycles. In the landscape, the number of such cycles can reach of order 10^5 [159].

The underlying symmetries require axions to possess a shift symmetry, $\theta \to \theta + 2\pi$, and so their potential must be periodic. The low energy four dimensional Lagrangian for an axion, θ, with periodic potential $U(\theta)$ is:

$$\mathcal{L} = -\frac{f_a^2}{2}(\partial\theta)^2 - \Lambda_a^4 U(\theta)\,. \tag{1.26}$$

The two scales in this Largrangian, the decay constant f_a, and potential energy scale Λ_a, are both determined separately for each axion by their dependence upon the action, S, of the non-perturbative physics on the corresponding cycle:

$$\begin{aligned} f_a &\sim \frac{M_{pl}}{S}\,, \\ \Lambda_a^4 &= \mu^4 e^{-S}\,. \end{aligned} \tag{1.27}$$

Here M_{pl} is the (reduced) Planck mass and μ sets the scale of non-perturbative physics, for example the QCD scale or, in string theory, the geometric mean of the SUSY breaking scale, $M_{\rm SUSY}$ and the Planck scale, $\sqrt{M_{pl}M_{\rm SUSY}}$.

The potential $U(\theta)$ is, just like in the QCD case, generated non-perturbatively. In string theory there are many sources of non-perturbative physics, as well as gauge theory instantons, for example worldsheet instantons and Euclidean D-branes wrapping the cycle [104]. The temperature dependence of these effects cannot be

predicted model-independently, and in this thesis we will always take them to have their fixed zero-temperature values at all epochs of interest. The string axion that solves the strong *CP* problem is the axion whose potential comes dominantly from QCD instantons.

Bringing the kinetic term into canonical form we define the field $\phi = f_a\theta$, with Lagrangian:

$$\mathcal{L} = -\frac{1}{2}(\partial\phi)^2 - V(\phi)\,, \tag{1.28}$$

where $V(\phi)$ is again a periodic potential. Expanding the potential in powers of ϕ/f_a, all the couplings of the field ϕ come suppressed by the scale f_a, and from the quadratic term we find that the mass is given by:

$$m_a^2 = \frac{\Lambda_a^4}{f_a^2}\,. \tag{1.29}$$

Solving the strong *CP* problem requires $S \gtrsim 200$ [104, 193], giving rise to stringy values of $f_a \approx 10^{16}\,\text{GeV}$, and this should be roughly constant for all these axions. The exact value of S, however, scales with the area/volume of the corresponding cycle (itself set by the scalar modulus partner of the axion), so that small variations in the area lead to exponential variations in the scale of the potential, and thus the axion mass.

It should be noted that in the axiverse scenario the lightest axions are *not* the standard QCD axion, however they do owe their existence to it. Hundreds of cycles of varying sizes lead us to expect the appearance of at least some extremely light axions, given the following scenario. Axions generically get their masses lifted to high values at tree level, however the required lightness of the QCD axion necessary to solve the strong *CP* problem, therefore necessarily avoiding such liftings of the mass, implies that other axions too may survive as light and stable. If string theory solves the strong *CP* problem by giving us the QCD axion, then the axiverse appears as a natural source of light scalars for cosmology. Some authors have been able to propose realisations of this scenario [195–197], although the axiverse paradigm is expected to be much more general than these specific constructions.

The axion shift symmetry also enforces that couplings to fermions appear derivatively as $\partial_\mu\phi\bar{\psi}\gamma^\mu\psi$, leading to factors of momentum at axion-fermion vertices. At

low momentum this suppresses long range forces on fermions by factors of k/f_a and string axions avoid fifth force constraints. In fact all axion couplings, including self couplings in the scalar potential, couplings to gauge fields like the photon due to higher dimensional operators, and topological couplings like the original $\theta\tilde{G}_{\mu\nu}G^{\mu\nu}$, come suppressed by this high scale.

For the most part in this thesis, because of the weak couplings caused by the high scale f_a, we will choose to work simply with the quadratic part of the potential, and largely ignore the effects of anharmonicities. Therefore for cosmological purposes we will consider these axions to be completely decoupled, non-interacting massive scalar fields with potential:

$$V(\phi) = \frac{1}{2}m_a^2\phi^2\,. \tag{1.30}$$

Thus these axions are completely described by their mass, which we take to be a free parameter. We will consider dark matter axions with masses as low as $m \sim 10^{-32}\,\mathrm{eV}$ in the presence of additional CDM, neutrinos and a cosmological constant. Axion masses go as low as $m \lesssim 10^{-33}\,\mathrm{eV}$, at which point the axion behaves as quintessence, as in the scenario of [198] described earlier.

The equation of motion for a homogeneous axion field in an expanding universe is found from the variation of the action. In physical time, where dots denote derivatives with respect to time, it is:

$$\ddot{\phi} + 3H\dot{\phi} + m^2\phi = 0\,. \tag{1.31}$$

Production of cosmological axions proceeds by the vacuum realignment mechanism. When the PQ symmetry is broken at the scale f_a the axion acquires a vacuum expectation value, θ_i, uncorrelated across different causal horizons. However provided inflation occurs after symmetry breaking, and with a reheat temperature $T \lesssim f_a$, then the field is homogenised over our entire causal volume. Large f_a suppresses other axion couplings and makes thermal production negligible: this is the scenario we will always consider in this thesis. Once the mass overcomes the Hubble drag in Eq. (1.31) the field begins to roll towards the minimum of the potential, in exact analogy to the minimum of the instanton potential restoring *CP* invariance in the Peccei-Quinn mechanism for the QCD axion. Coherent oscillations about this minimum lead to the

production of the weakly coupled axion-like particles (ALPs). [178, 199, 200]

If ALPs exist in the high energy completion of the standard model of particle physics, and are stable on cosmological time scales, then regardless of the specifics of the model Tegmark et al have argued [201] that on general statistical grounds we indeed expect a scenario where they make up an order one fraction of the DM, alongside the standard WIMP candidate of the LSP. Some interesting features of the cosmology of string axions and their relation to inflation, the production of gravitational waves and isocurvature perturbations were explored in [174, 199, 200]. The objections of Mack and Steinhardt [202, 203] arise when we consider a population of light fields in the context of inflation. The problem with these objections is that they make some assumptions about what we mean by 'fine tuning' of fundamental physical theories, which is also related to the problem of finding a measure on the landscape of string theory and inflation models (see, for example, [204]), the so-called 'Goldilocks Problem'. Addressing these arguments in any detail is beyond the scope of this thesis although we begin a discussion in Chapter 6. We consider the issue sufficiently unresolved, and ultra-light scalar fields to be sufficiently well motivated as DM candidates otherwise, to press on regardless in search of phenomenology.

In the context of generalized dark matter [115] we can see the effect of the Compton scale of these fields through the fluid dynamics of the classical field. Once oscillations have set in and been averaged, the sound speed, $c_s^2 = \delta P/\delta\rho$ of a field with momentum k and mass m at a time where the scale factor of the FLRW metric is a is given by:

$$\begin{aligned} c_s^2 &= \frac{k^2}{4m^2a^2}; \quad k < 2ma\,, \\ c_s^2 &= 1; \quad k > 2ma\,. \end{aligned} \tag{1.32}$$

We will derive this result in Chapter 4. On large scales the pressure becomes negligible, the sound speed goes to zero and the field behaves as ordinary dust CDM and will collapse under gravity to form structure. However on small scales, set by λ_c, the sound speed becomes relativistic, suppressing the formation of structure. This observation is our main point of departure to consider the effect of ultra-light scalar fields on the matter power spectrum in Chapter 4. Ultra-light scalar fields are known to share

qualitative features and many degeneracies in their effects on cosmology with massive neutrinos and thus with many other cosmic ingredients [205]. It is the aim of Chapter 5 to explore the effects of ultra-light string axions on the CMB and LSS, and thus these degeneracies, in detail.

1.3.3 Moduli

Recently a specific construction in string theory realising the axiverse of [104] was given [195, 196]. The authors of [195, 196] suggested that non-thermal processes are particularly important for the cosmology of such a model. In this thesis, in Chapters 2 and 3, we will study a simple extension of the axiverse that includes further non-thermal processes that couple the axion fluid and greatly enrich the phenomenology of axion DM in a way analogous to the enrichment of DE phenomenology arrived at through the study of coupled quintessence [185]. In this framework the behaviour of the axion DM component is no longer a simple transition in w (c.f. Chapters 2 and 4), and one hopes to look for novel features in the late time expansion history of the universe, as has been done fruitfully in many works on DE (see, for example, [144, 206]).

Moduli are scalar fields in string theory that control the size and shape of the compact manifold. These fields must be given stabilising potentials so that their cosmological effects can be controlled. A typical potential for moduli stabilisation in the LARGE volume scenario [207] for a modulus χ is of the parametric form:

$$V_{mod}(\chi) = Be^{-2C\chi} - De^{-C\chi}\,, \tag{1.33}$$

where B, D and C are for our purposes free parameters, with the only restriction that for a stabilising minimum we have $2B > D$. The typical scales of these parameters will be discussed shortly. We will also add the cosmological constant as ρ_Λ, thus allowing for a late time de-Sitter expansion and acceptable phenomenology. This is a prescription necessary in most all moduli stabilisation, since the supersymmetric vacuum is always of negative energy in supergravity (anti-de Sitter, or AdS).

In the LARGE volume scenario, the lightest modulus is the volume modulus, which like the dilaton controls the overall scale of couplings in the model, but we

might expect the presence of *many light moduli*. There are moduli corresponding to each closed cycle in the compact space, and as such there is a modulus for each axion. In particular there will be a modulus controlling the area of a cycle and as such:

$$S \sim \chi \,. \tag{1.34}$$

The modulus mass scale that leads to rolling in the potential is often tied to the axion mass, so that the presence of cosmologically rolling axions suggests the presence of *cosmologically rolling moduli*. In this way we extend the axiverse.

The displacement of moduli from their stabilised values (vacuum destabilisation) by astrophysical processes is not a new idea: it has been exploited before in chameleon models (where destabilisation is attained via coupling to density) and other similar scenarios (see, for example [186, 187, 189, 208]). The variant on the scenario that is proposed here is as follows. The lightest axions and moduli have masses below the Hubble scale and are stabilised by Hubble friction, contributing to an effective cosmological constant. The heaviest moduli are stabilised by potentials of the form Eq. 1.33, which includes the moduli for standard model couplings[10]. There are then cosmological axions that roll in their potentials at late time and contribute to the dark matter density and perturbations in a distinct way from standard CDM. As such, *some* moduli *may* also roll in their potentials on cosmological time scales, which will lead to a rolling of the scale of the axion potential and consequently a *rolling of the axion mass*. It is this feature of coupling that we hope to exploit in looking for novel features in the cosmological expansion rate and equation of state in the dark sector. It is worth stressing again that cosmologically rolling moduli are not general, but we explore the phenomenology of allowing such a scenario for some of the moduli.

In this model, which will be explored in Chapters 2 and 3, we are working in the optimistic philosophy of the authors of [104] to use the vastness of the string landscape to look for general properties exploitable for cosmological phenomenology, i.e. realistic string compactifications and scenarios for the moduli are complicated and varied but do have some general and model independent features [209]. In the literature there has been a long standing link between string theory and inflation

[10] We will not investigate any evolution of the couplings with cosmic scale. The possibility and implication of such effects in this model are discussed briefly in Chapter 3.

physics (see [210] and references therein, and the reviews [211, 212]). In particular it was the aim of [210] to connect inflationary observables to topological properties of the compact space; this is analogous to 'cohomologies from cosmology' in [104]. However in the simplest axiverse scenario for dark matter axions there are two parameters per axion that can be constrained using cosmology: the axion mass, m_a, and the axion fraction, $f_{ax} = \Omega_a/\Omega_m$. The fraction f_{ax} is determined by the initial misalignment angle and tells us nothing about the compact space or vacuum, so any cosmological bounds based on the expansion rate or formation of structure can only limit the contribution from a given axion or number of axions of given masses rather than place definite constraints on the number and size of closed cycles that determine the masses. There could be many light axions of many masses but if their contribution to the energy density is too small then we will not observe them[11]. An observation of the effects of a number of axions, modulo a prior on the potential and degree of fine tuning, may also hope to place bounds on their common axion decay constant, f_a. Assumptions about inflation can also bound f_a, as discussed in [199–203], and vice versa an assumed ultra-light axion bounds H_I, the Hubble scale during inflation, from considerations of isocurvature perturbations, as discussed in e.g. [174], and in Chapter 6.

Considering axions and moduli in the landscape and whether they survive to be observed is closely linked to the question of SUSY breaking, and is discussed in [215]. We will discuss it no further here, except to stress again that issues of naturalness and fine tuning *within* the landscape will not concern us here: we simply motivate a theoretically plausible, phenomenolgically viable, and observationally testable scenario.

Extending the axiverse scenario as proposed here gives much greater scope for direct connections between late time cosmology and BSM/string physics, akin to those already fruitfully explored in inflationary physics, but distinct from those connections already explored in tackling the DM problem in the context of the MSSM and its progeny, or in directly addressing the cosmological constant problem.

[11] The existence of an axion field coupling to standard model fields can be constrained in many other ways: for example, by light shining through a wall experiments (for a recent review, see [213]), and astrophysical processes such as those explored in [127, 128, 183, 214]

However, as phenomenologists we must be careful about any statements we make about fundamental physics based on any results obtained using our models. In a parameterised phenomenological model such as the one proposed here, the parameters should be taken as just that: it is only in the context of a full string model such as those in [193, 195, 210, 216] (with all the assumptions that go into constructing such a model) that the parameters take on their physical high energy physics meanings.

With all the complications that come from facing up to real observations, to the moduli problem and inflation, we will find in this thesis that even the simple framework of the axiverse with its light scalar addition to cosmology will make us face up to many varied problems. We might be more inclined to agree with Candide than Leibniz:

> Pangloss sometimes said to Candide:
>
> *"There is a concatenation of events in this best of all possible worlds: for if you had not been kicked out of a magnificent castle for love of Miss Cunégonde–if you had not come under the Inquisition–if you had not walked over America–if you had not stabbed the Baron–if you had not lost all your sheep from the fine country of El Dorado– why, then, you would not be here, eating preserved citrons and pistachio-nuts."*
>
> *"All that is very well,"* answered Candide, *"but let us cultivate our garden."*
>
> Voltaire (1694-1778), *Candide*

2

MODULI AND DARK ENERGY

"The failure of the Zen path comes from [people]... just following popular fads and current customs, content to sink themselves in the domain of intellectual knowledge and verbiage, not knowing how to return."

Ch'ih-chueh (fl. ca. 1208 – 1255), in *Classics of Zen and Buddhism, T. Cleary*

PREFACE

This chapter follows up on the axiverse idea by making the action, S, that controls the axion mass directly proportional to a modulus field, which itself has a stabilising potential. We then study the Dark Energy cosmology that emerges when we parameterise this potential. It is based on the work in Ref. [217]

2.1 THE MODEL: COUPLED AXIONS IN THE DARK SECTOR

2.1.1 *Equations of Motion*

As with everything in string theory, our low energy 'constants', such as m_a, are not really constant at all, but depend upon moduli. In this case the modulus of interest is the one controlling the area of the cycle giving us our axion. The action of non-perturbative physics on this cycle, S, depends on this area, and so we can choose to identify $S = \tilde{C}\chi$ for some modulus field χ, and coupling $\tilde{C}$. Eq. (1.27) then implies

that *axions and moduli are coupled*.

This modulus must be stabilised non-perturbatively [218]. Typical potentials are sums of exponentials (see, for example, [189, 195, 216, 219, 220])[1].

The coupled axion-modulus Lagrangian takes the following form:

$$\begin{aligned} \mathcal{L} &= \frac{1}{2}(\partial\phi)^2 + \frac{1}{2}(\partial\chi)^2 - V(\phi,\chi)\,, \\ V(\phi,\chi) &= Be^{-2C\chi} - De^{-C\chi} + \frac{1}{2}e^{-\tilde{C}\chi}M^2\phi^2\,, \end{aligned} \tag{2.1}$$

where ϕ is the axion, χ is the modulus, B, D are dimension four parameters for the modulus potential, C is related to the overall volume of the compact space in string units, $\tilde{C}$ is related to the instanton action, $M^2 = \mu^4/f_a^2$ and we make the simplifying assumption to work with only the mass term for the axion. In the interests of economy of parameters we will often take $\tilde{C} = C$. Also, when $C \neq \tilde{C}$ the problem of minimising the potential becomes much less tractable generically, and for specific values of C, $\tilde{C}$ many minima appear (e.g. 19 minima with $C = 10$, $\tilde{C} = 1$), which is related to the emergence of the landscape in string theory and the analysis of which is beyond the scope of this work.

In this Chapter we will only be concerned with the homogeneous background fields, so will use the notation $\phi \equiv \phi_0 = \phi_0(\tau)$, where τ is conformal time, and similarly for the modulus.

The energy momentum tensor and equations of motion for the coupled system follow in the usual way from the Lagrangian. For a homogeneous FLRW metric, with scale factor a, in conformal time:

$$\begin{aligned} \ddot{\phi} + 2\mathcal{H}\dot{\phi} + M^2a^2e^{-C\chi}\phi &= 0\,, \\ \ddot{\chi} + 2\mathcal{H}\dot{\chi} - Ca^2(2Be^{-2C\chi} - De^{-C\chi}) &= \frac{1}{2}CM^2a^2e^{-C\chi}\phi^2\,, \end{aligned} \tag{2.2}$$

[1] (i) The general form of the potential we study fits into the class of models of 'Generalized Assisted Inflation' [221–223], though we mainly emphasise its use for quintessence, rather than inflationary, purposes. (ii) At large values of χ, loop effects will eventually cause the potential to rise again, as in [220, 224]. We do not consider such contributions. Our conclusions only depend on having a sufficiently long, flat region of the potential before these effects kick in, but we do not compute the scales of parameters necessary for this.

where over dots denote derivatives with respect to conformal time, and $\mathcal{H} = \dot{a}/a$. The energy momentum tensor for the combined axion-modulus system has the form of a perfect fluid with energy density ρ and pressure P: $T^0{}_0 = -\rho$, $T^i{}_j = P\delta^i{}_j$. This gives:

$$\begin{aligned} \rho &= \frac{a^{-2}}{2}(\dot{\phi}^2 + \dot{\chi}^2) + V(\phi, \chi)\,, \\ P &= \frac{a^{-2}}{2}(\dot{\phi}^2 + \dot{\chi}^2) - V(\phi, \chi)\,. \end{aligned} \tag{2.3}$$

Due to the coupling, only these combined quantities obey the conservation equation $\dot{\rho} = -3\mathcal{H}(\rho + P)$.

The form of the potential suggests a natural splitting of this into components due to the axion, subscript ϕ, and modulus, subscript χ:

$$\begin{aligned} \rho_\phi &= \frac{a^{-2}}{2}\dot{\phi}^2 + \frac{1}{2}e^{-\tilde{C}\chi}M^2\phi^2\,, \\ P_\phi &= \frac{a^{-2}}{2}\dot{\phi}^2 - \frac{1}{2}e^{-\tilde{C}\chi}M^2\phi^2\,, \\ \rho_\chi &= \frac{a^{-2}}{2}\dot{\chi}^2 + Be^{-2C\chi} - De^{-C\chi}\,, \\ P_\chi &= \frac{a^{-2}}{2}\dot{\chi}^2 - Be^{-2C\chi} + De^{-C\chi}\,, \end{aligned} \tag{2.4}$$

though in certain cases this distinction should be looked at more carefully [225].

With these definitions we will investigate the scalings of the energy density for axion and modulus components, and also the combined system. It is not only the scaling of the energy density that effects the cosmological expansion history: we will also investigate the pressure through the equation of state, given by: $w_i = P_i/\rho_i$ for components $i = ax, mod, ax + mod, tot$, which will effect the expansion rate in the usual way [29, 35].

The Friedmann equation, Eq (1.5), in conformal time is:

$$\mathcal{H}^2 = \frac{8\pi G}{3}a^2\rho\,. \tag{2.5}$$

In addition to the axion-modulus system of Eq. (2.3) we will consider components of the energy density coming from radiation, ρ_γ, CDM, ρ_c, and a cosmological constant,

ρ_Λ, all of which will redshift in the usual way. This completes the description of the system.

2.1.2 *The Scales of Parameters*

This model is to be understood phenomenologically, and thus all the parameters will be taken as free when searching for interesting cosmological features, however it will be useful to have some idea of the natural scales in relation to the units used in numerical solution of the equations. Firstly, we scale the reduced Planck mass, $8\pi G = \frac{1}{M_{pl}^2}$, out of the Friedmann equation by rescaling the fields to be in Planck units: $\phi \to \phi/M_{pl}$, $\chi \to \chi/M_{pl}$, and absorbing factors of M_{pl}^2 into B, D and the densities of the standard ΛCDM components. Next we change time variables to work in units of H_0: $\tau \to H_0\tau$. This can be divided through the equations of motion and absorbed into the parameters and densities, so that the densities are now: $\rho \to \rho/(H_0^2 M_{pl}^2)$, and $\rho_i(a)/3 = \Omega_i(a)$. Finally we express all the parameters in the potential in Planck units (natural for a string inspired model) as $X \to M_{pl}^x X$, with X the parameter and x its mass dimension. Thus, finally we have:

$$
\begin{aligned}
B &\to \left(\frac{M_{pl}^2}{H_0^2}\right) B\,, \\
D &\to \left(\frac{M_{pl}^2}{H_0^2}\right) D\,, \\
M^2 &\to \left(\frac{M_{pl}^2}{f_a^2}\right)\left(\frac{M_{pl}^2}{H_0^2}\right) \bar{M}^2\,, \\
\bar{M} &= \sqrt{\frac{M_{SUSY}}{M_{pl}}}\,,
\end{aligned}
$$

All the parameters on the left hand side are now dimensionless, and it is these that will be used when quoting results.

Using $M_{pl}^2/H_0^2 \sim 10^{120}$, $f_a \sim 10^{16}\,\mathrm{GeV}$, and Planck scale SUSY to give an upper bound on $\bar{M} = 1$, gives an idea for the approximately natural scales of all the

parameters[2]:

$$B \sim 10^{120},$$
$$D \sim 10^{120},$$
$$M \lesssim 10^{62}.$$

For the fields, a large value of $\phi > 1$ will be transplanckian, and any value $\phi > \pi(f_a/M_{pl})$ will represent a departure from the periodic nature of the axion, whereas χ is an area/volume, so a large value in Planck units is not problematic, and is in fact what one expects in a LARGE volume scenario for moduli stabilisation. The initial conditions on the fields are free parameters in the model: χ representing an initial 'position in the landscape', and ϕ being selected by spontaneous symmetry breaking. We will discuss an early universe scenario for setting these in Chapter 3. The flatness condition fixes the density in the axion-modulus system. Choosing the densities in Λ and standard CDM to be close to their observed values allows the axion-modulus system to be set as sub-dominant. Thus for now we ignore the question of fixing the initial conditions so as to obtain H_0 at its observed value, since the subdominant components will not cause much variation away from this ($H_0 = 1$ in our units).

We expect the dimensionless parameters C and $\tilde{C}$ to both be $\mathcal{O}(1)$.

2.1.3 *Comments*

At this stage some comments on the system of equations in relation to other models in the literature will be useful. A brief comparison will be made to three models: [225–227], stating the main similarities and differences. The take-home message, though, will be that these models, whilst interesting, are connected to very different sources of new physics. They are for the most part motivated by scalar-tensor theories modifying the gravity sector to build DE models, whilst the model presented here is firmly cast in the context of strings, and the landscape, with dark matter candidates

[2] TeV scale SUSY is more phenomenologically attractive from a particle physics viewpoint in resolution of the hierarchy problem.

and modifications to the dark energy sector a by-product, the effects of which can be investigated phenomenologically.

In [226] the scalar field analogous to our modulus is coupled non-minimally to gravity via the term $\phi^2 R$, and has its own scalar potential. The field is also used to Higgs the Dirac dark matter particle via a Yukawa coupling $f(\phi)\bar{\psi}\psi$, thus introducing a ϕ-dependent mass to the dark matter. However no explanation for this coupling is given in terms of fundamental particle physics (general couplings of this form can, however, be constructed in scalar-tensor theories by transforming between the Jordan and Einstein frames: see for example [228]). Assuming they have a standard neutralino dark matter particle, then the scalar field will be a Higgs of some supersymmetric extension to the Standard Model and one may worry about effects both on the freeze-out mechanism for the neutralino, or on other effects where the true Higgs rolls and causes mass changes in the Standard Model particles. This model building issue aside, the authors go on to explore the effects of different potentials and coupling terms that allow matching to the standard cosmology.

There are some important distinctions between the model of [226] and the one presented here, the first being that the axion-modulus model makes no change in the gravity sector, and as such the FLRW equations take their standard form, though [226] can be brought into standard form via a conformal transformation: this is the usual degeneracy of Modified Gravity theories to scalar field theories of DE (again, see [228]). Secondly, the DM sector in [226] is, apart from the coupling, assumed standard, whereas the axiverse model is motivated by non-standard DM components. Finally, many scalar potentials and couplings are explored in [226] within a general framework, whereas in the axion-modulus model the forms are essentially fixed via the motivation in string theory.

Coupling axions and moduli bears much similarity to "axion-dilaton cosmology" [227, 229]. In these models the axion has no potential of its own but is coupled in its kinetic term to the dilaton after a conformal transformation renders the gravity sector standard: $\mathcal{L} \subset -\frac{1}{2}e^{\mu\sigma}(\partial\chi)^2$, where σ is the dilaton, and χ the axion. The dilaton potential is then also exponential $\Lambda e^{-\lambda\sigma}$, appearing on the cosmological constant term after the conformal transformation. This model is then entirely specified by two

free parameters. The dynamics in the scalar field sector consists of the existence of attractors bringing the equation of state periodically into accelerating phases, with possibly observable consequences as explored in [206]. The highly constrained axion-dilaton model should serve as a useful heuristic guide when thinking about the coupled scalar field dynamics of the axion-modulus model, the important differences being that this axion-modulus model has an axion mass term with a coupling on it, but standard kinetic term. The potential for the modulus has a finite-field, negative energy potential minimum, in contrast to the dilaton, which in the axion-dilaton model is not stabilised. We will expect this to make quantitative and qualitative changes to the equation of state evolution.

Finally, the model of [225] bears the most resemblance to the axion-modulus model with the mapping of axion ϕ to "geon" χ, and modulus χ to "cosmon" φ, the only important difference being that the modulus potential has a minimum, whilst the cosmon potential does not represent a stabilised dilaton. The analysis of [225] will accordingly be very useful for helping us understand the axion-modulus system. However, we choose to include a standard cosmological constant as well as the scalar fields. In the axion-modulus model this is necessary unless the axion can provide all of the dark energy, which is impossible without invoking some monodromy to allow large field values [230]. We also choose to include a standard DM component in addition to the scalar fields: Chapter 4 shows that ultra-light scalar fields rolling on the time scales of interest here and in [225] suppress structure formation according to their fraction and hence, just like massive neutrinos, they cannot make up all of the dark matter [205], as is assumed in [225].

This concludes the discussion of the model.

2.2 RESULTS

2.2.1 *Example Cosmology 1*

This first example is concerned with parameter values close to those considered natural in Section 2.1. The evolution of the various components of the density, ρ, obtained

from numerically integrating the equations of motion are plotted as a function of scale factor, a, in Figure 2.1, with the associated Ω's plotted in Figure 2.2. The parameter values used are:

$$\begin{aligned} M &= 10^{62}\,, \\ B &= 10^{120}\,, \\ D &= 10^{119}\,, \\ C &= \tilde{C} = 10\,, \\ \phi_i &= 1\,, \\ \chi_i &= 25\,, \\ \Omega_\Lambda &= 0.7\,, \\ \Omega_c &= 0.2\,, \\ \Omega_\gamma &= 8\times 10^{-5}\,, \end{aligned} \tag{2.6}$$

In Figure 2.1 there are a number of qualitative features worthy of comment. Firstly, the logarithmic scale prevents us from showing the small negative energy density associated to the modulus at early and late times, we only see it emerge onto the plot between scale factors $10^{-6} \lesssim a \lesssim 10^{-1}$ as it enters an attractor scaling solution. During this time the modulus is displaced from its initial value and its equation of state becomes kinetic dominated, $w = 1$, the additional energy density being kinetic, as demonstrated in Figure 2.3. This transit causes a corresponding evolution of the axion mass, as demonstrated in Figure 2.6. It also induces a tracking behaviour in the axion density whilst the modulus is rolling. The axion field then begins its usual oscillatory behaviour and the axion behaves as dark matter for $a \gtrsim 10^{-1}$. The final cosmology today at $a = 1$ has a negligible negative component of energy density in the frozen modulus, whilst an ultra-light dark matter axion makes up a fraction of the critical density of order that in radiation (note this gives $\Omega_\Lambda > 0.7$ input value).

The axion equation of state, w_{ax}, and the axion-modulus equation of state, w_{ax+mod}, are shown in Figure 2.4. The axion equation of state differs from the usual case of a quick transition between $w = -1$, and oscillations averaging to $w = 0$. Once the

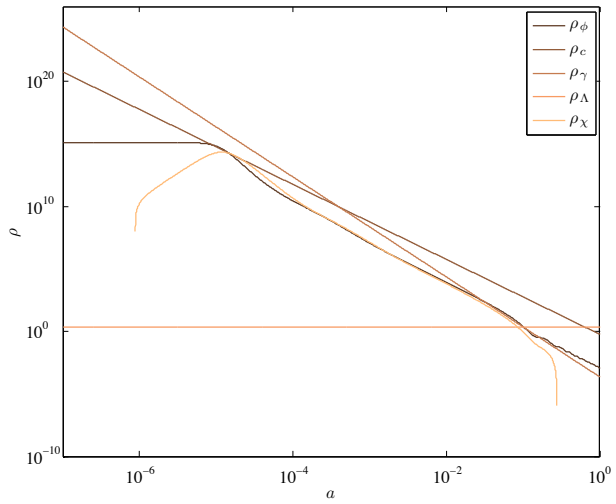

Figure 2.1 Densities as a function of scale factor for the parameters of Equation 2.6. Notice the tracking dynamics of the axion-modulus system between $10^{-6} \lesssim a \lesssim 10^{-1}$, when the modulus gains positive energy density, and the end of this tracking at $a \gtrsim 10^{-1}$ caused when the axion field begins oscillations and the axion density makes its standard transition to matter-like behaviour.

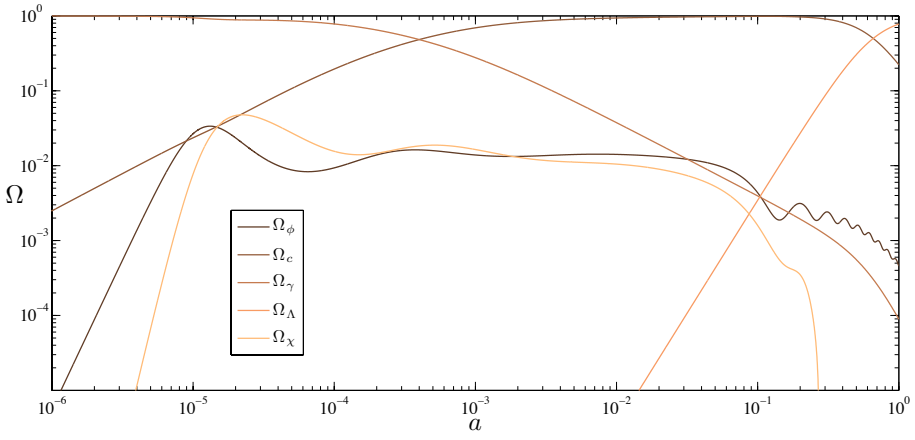

Figure 2.2 Fraction of the critical density, Ω, as a function of scale factor for the parameters of Equation 2.6.

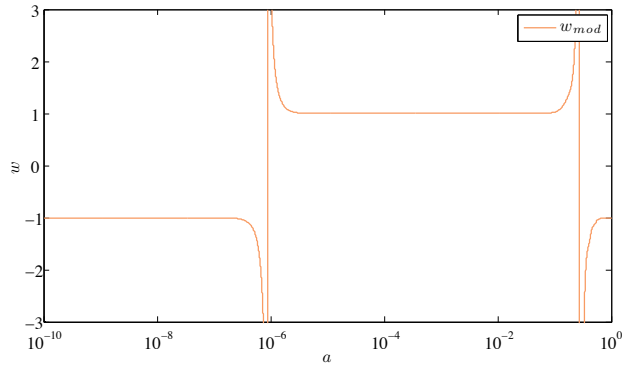

Figure 2.3 Evolution of the modulus equation of state w as a function of scale factor for the parameters of Equation 2.6.

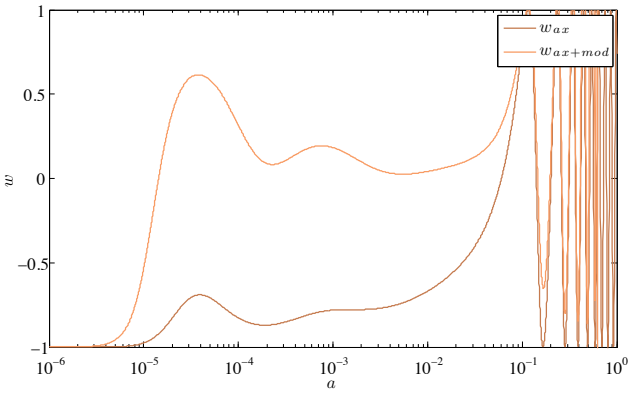

Figure 2.4 Evolution of the axion and combined axion-modulus equation of state w as a function of scale factor for the parameters of Equation 2.6. Notice the tracking behaviour of the combined equation of state, and the end of this when axion field oscillations cause oscillations in the pressure, averaging to zero.

axion field begins oscillations it causes the equation of state to oscillate and the axion pressure averages to zero, i.e. the axion behaves as pressureless dark matter. It is in the combined equation of state that we see tracking behaviour as w tries to follow the equation of state of the dominant component (in this case matter with $w = 0$), before the axion oscillations begin. The oscillations are the cosmic trigger event that destroys tracking and restabilises the modulus (in this context, stabilisation is defined by $w_{mod} \to -1$).

The resulting behaviour of the total equation of state for all fluids is plotted in Figure 2.5, where we see that it develops a kink around scale factor $a \simeq 10^{-5}$ away from its usual ΛCDM evolution through matter-radiation equality, caused by the presence of a significant component of the fractional density in the axion-modulus system at

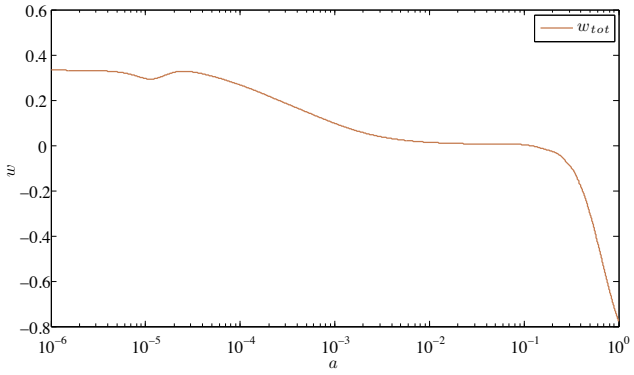

Figure 2.5 Evolution of the total equation of state w as a function of scale factor for the parameters of Equation 2.6. Note the appearance of a feature around $a \simeq 10^{-5}$ that departs from the standard smooth ΛCDM evolution. Compare this to Figure 2.2, where an overshoot as the axion-modulus system enters its tracking solution causes a significant contribution to the critical density at this scale factor.

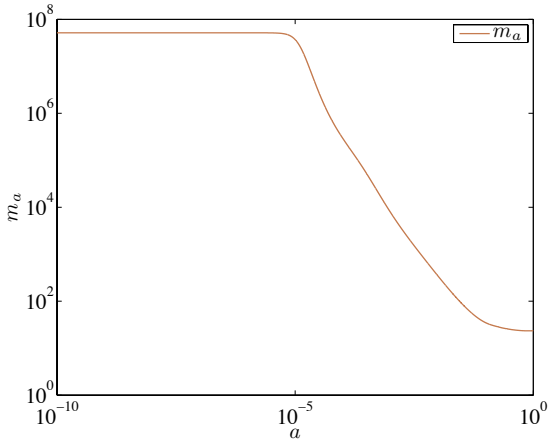

Figure 2.6 Evolution of the axion mass as a function of scale factor for the parameters of Equation 2.6. Compare this to Figure 2.3: the rolling occurs whilst $w_{mod} = 1$ and the modulus has kinetic energy.

this time, as demonstrated in Figure 2.2. This is EDE-like behaviour, although the equation of state is not dragged low enough to cause an early period of accelerated expansion. In Chapter 3 we will see that this is impossible in the radiation dominated era.

Having identified the main features of cosmology in this example, we now turn to briefly assess the dependency of these features on the parameters. A full description of the system in this way will require analysing it as a dynamical system in the phase plane and then identifying the fixed points [185, 231], which we carry out in Chapter 3.

Decreasing the axion initial value, ϕ_i, can cause a significant change in the modulus

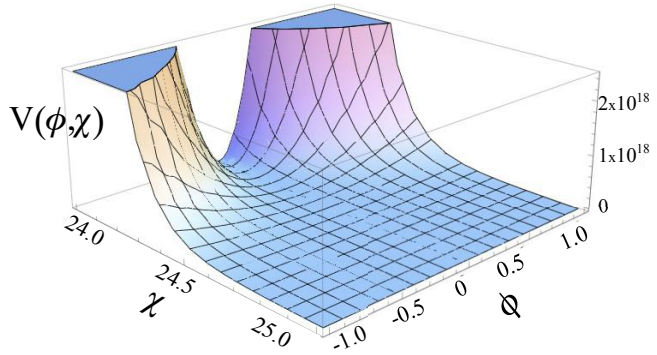

Figure 2.7 The potential $V(\phi, \chi)$ of Equation 2.1, plotted for χ in the range $\{24, 25\}$, ϕ in the range $\{-1, 1\}$, for the parameters of Equation 2.6.

behaviour. With $C = \tilde{C}$ the condition for the modulus to have a finite real minimum is given by:

$$2D > M^2\phi^2 \,. \tag{2.7}$$

For the values used in Equation 2.6 this can only occur as the axion decays, and the $\phi = 0$ minimum is at $\chi = 0.3$. Now, the dependence on axion initial condition can be most easily seen by plotting the potential $V(\phi, \chi)$. In Figure 2.7 the potential is plotted for ϕ in the range $\{-1, 1\}$, whilst in Figure 2.8 it is plotted with ϕ in the range $\{-0.01, 0.01\}$. We see that, for small amplitude axion oscillations the exponential descent into the modulus minimum for $\phi = 0$ shows up strongly, whereas this feature is hidden on the same scale when the oscillations of the axion have a larger amplitude. We can similarly remove the axion from the potential energy density almost entirely by increasing $\tilde{C}$ by an order of magnitude, making the axion effectively massless and allowing the modulus to rapidly reach its minimum.

Thus it is the axion oscillations which here stabilise the modulus away from its true minimum (as is visible comparing Figures 2.1 and 2.3). If the modulus falls into this minimum then a large negative potential is generated causing the universe to collapse [232]. That this occurs prior to $a = 1$ for a small axion initial field value corresponding to reasonable initial misalignment $\theta_i = 1$ (not shown) rules out these particular parameters, and will require tuning in these models to avoid it. This decay and collapse may occur in the future as the amplitude of axion oscillations decays [233] for any model that looks viable today, and the parameters can then be used to estimate the lifetime of the universe [234]. The analysis of a collapsing universe in

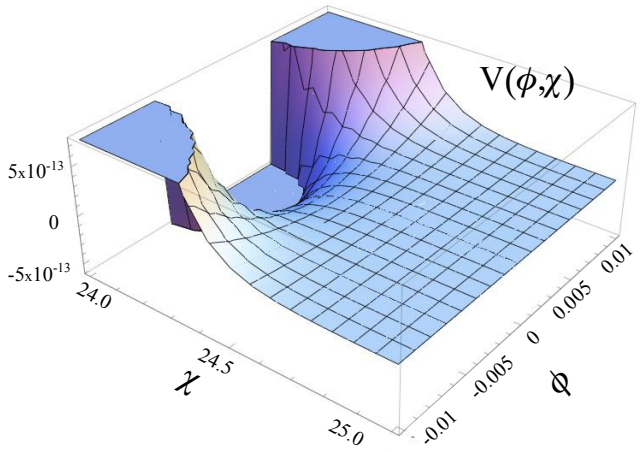

Figure 2.8 The potential $V(\phi, \chi)$ of Equation 2.1, plotted for χ in the range $\{24, 25\}$, ϕ in the range $\{-0.01, 0.01\}$, for the parameters of Equation 2.6.

this model is done in Chapter 3. Some further comments on entry into a collapsing phase will be made in Section 2.2.2.

Even a sight decrease in $\tilde{C}$ to 8 or 9 also has a dramatic effect on the potential, allowing for the appearance of new minima as the axion field oscillates about zero, and the M^2 and D terms in the potential play off against one another. These new minima are sharp and highly localised in field space. Entry into them occurs as the modulus grows through its tracking solution and axion oscillations decay. Even a brief dip through such a minimum leads to a turn around in scale factor evolution as the total energy density goes to zero, which the Friedmann equation alone is incapable of dealing with. We discuss this in more detail in Chapter 3

2.2.2 *Example Cosmology 2*

The purpose of this example is to demonstrate the large freedom in choosing values for parameters in these models by producing a similar and viable cosmology to that presented in Section 2.2.1, but with parameters many orders of magnitude different. This also shows that we expect many degeneracies in the parameters, with only the

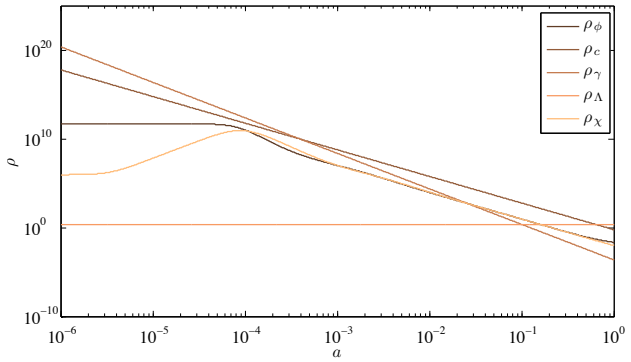

Figure 2.9 Densities as a function of scale factor for the parameters of Equation 2.8.

ratios of some being relevant. Specifically, the parameters in this example are:

$$\begin{aligned} M &= 10^3\,, \\ B &= 10^6\,, \\ D &= 10^5\,, \\ C &= \tilde{C} = 10 \\ \phi_i &= 10^3\,, \\ \chi_i &= 10^{-5} \\ \Omega_\Lambda &= 0.7\,, \\ \Omega_c &= 0.2\,, \\ \Omega_\gamma &= 8\times 10^{-5}\,. \end{aligned} \tag{2.8}$$

The evolution of the densities, Ω's, equations of state, axion mass, and the axion field, are shown in Figures 2.9, 2.10, 2.11, 2.12, 2.13, 2.14 and 2.15.

This example shows best the possibility of the axion-modulus system to display tracking EDE behaviour. The densities of both fields are always positive and show a scaling with the dominant component of energy density. Whilst the modulus equation of state is kinetic dominated once rolling begins, $w = 1$, the axion equation of state remains always potential dominated, $w = -1$, and the axion slowly rolls, never beginning oscillations as the mass is exponentially damped below the Hubble scale (see Figures 2.14, 2.15). Tracking for the combined system thus persists into the present

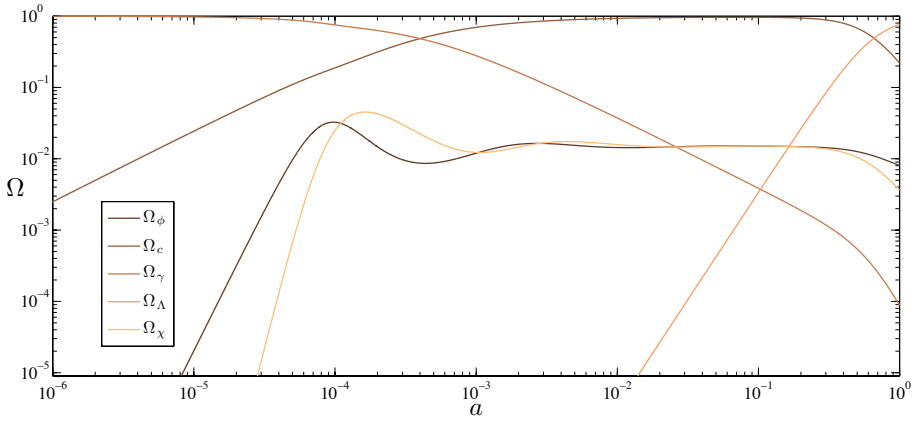

Figure 2.10 Fraction of the critical density, Ω, as a function of scale factor for the parameters of Equation 2.8.

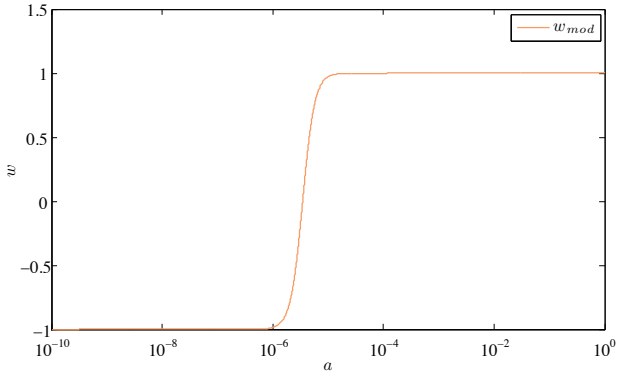

Figure 2.11 Evolution of the modulus equation of state w as a function of scale factor for the parameters of Equation 2.8.

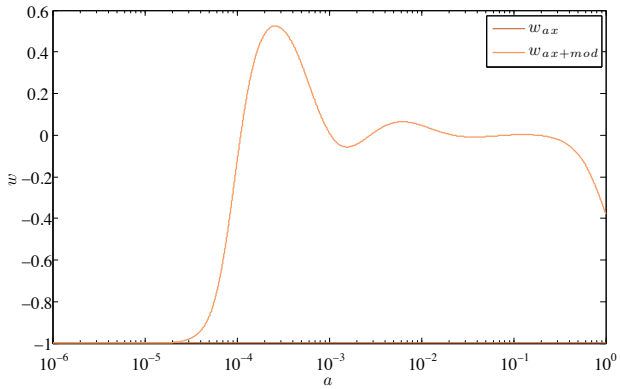

Figure 2.12 Evolution of the axion and combined axion-modulus equation of state w as a function of scale factor for the parameters of Equation 2.8. Note that the axion remains always slowly rolling with $w \approx -1$.

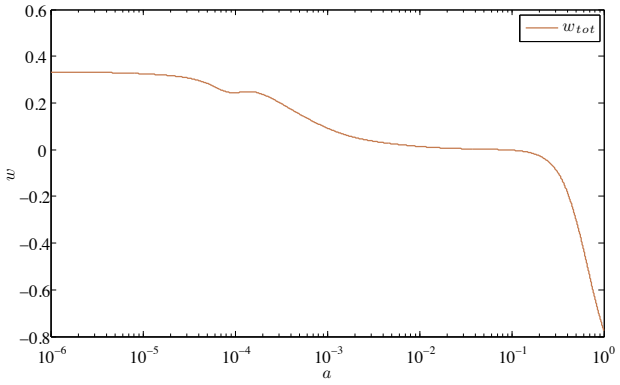

Figure 2.13 Evolution of the total equation of state w as a function of scale factor for the parameters of Equation 2.8.

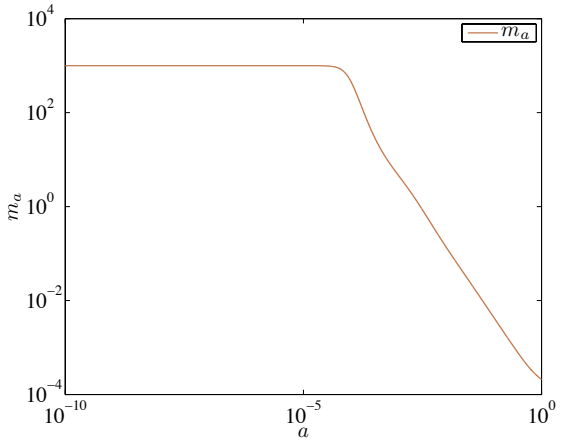

Figure 2.14 Evolution of the axion mass as a function of scale factor for the parameters of Equation 2.8.

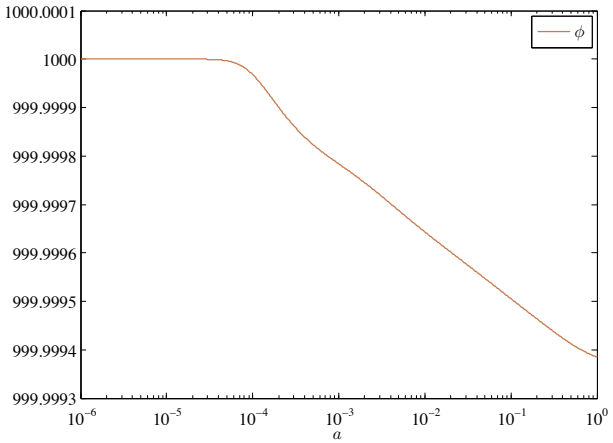

Figure 2.15 Evolution of the axion field as a function of scale factor for the parameters of Equation 2.8.

epoch, and should persist for a vast amount of time, being absent the trigger event of axion oscillations to end it and relying on the axion slow roll. In this case, the splitting of the energy density between the two components as done in Equation 2.4 is not really so clear (there is not an oscillating DM term) and it makes sense to speak more in terms of the combined axion-modulus system as a quintessence fluid.

In this example the equation of state for the axion-modulus system (see Figure 2.12) has a novel shape, with no oscillations, varying through behaviour like a cosmological constant, radiation, matter, and quintessence as it begins rolling and goes through its various scaling stages. The total equation of state (Figure 2.13) is again marginally perturbed by the presence of a significant axion-modulus component near equality, and the final fractional density in the axion-modulus system is $\Omega_{ax+mod} \simeq 0.01$. Compare to the previous example: the fractional density in the axion-modulus system is approximately the same at early times due to the scaling solution (at fixed coupling C, see Chapter 3), but makes a significant contribution at the slightly later time of $a \sim 10^{-4}$, and correspondingly alters the total equation of state at this time. This demonstrates that there is control in the parameters over features in the total equation of state. In this example the scaling solution persists to the present day, since no axion oscillations occur, and hence the late time density in the axion-modulus system is larger than in the previous example.

Reducing the initial field value for the axion in this example only changes the Ω's slightly, as one would expect when tracking is present, but moves the scale of the kink in w_{tot} to yet later times (not shown). Increasing M undoes this change, as we expect since for slowly varying ϕ it is the χ dependence of the potential that counts, and $M^2\phi^2$ is just a multiplicative factor in the exponential χ potential, like B and D. It is the $M^2\phi^2$ term that is dominant for the parameters in question and as such the example is similar to the well studied case of a single scalar modulus field with an exponential potential.

Further variations now cause qualitative changes in the cosmology, which are demonstrated in Figures 2.16 and 2.17. A higher mass $M = 10^8$, and lower misalignment angle $\theta_i = 1$ ($\phi_i = 10^{-2}$) destroys the axion tracker and the axion behaves as standard, oscillating and making up a subleading fraction of dark matter, with the

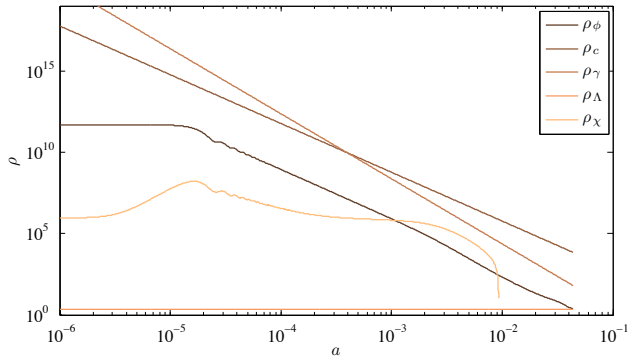

Figure 2.16 Densities as a function of scale factor for the parameters of Equation 2.8 but with the change $M \to 10^8$, $\phi_i \to 10^{-2}$. Notice that the axion field behaves completely as standard [205, 233]. The modulus begins at positive Λ like behaviour, before a fall into a negative potential dominated phase, signalling the onset of cosmological collapse.

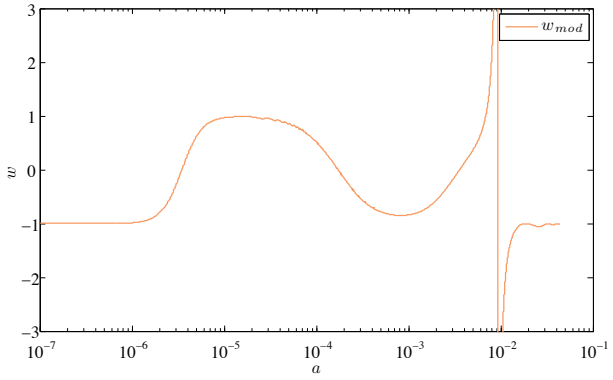

Figure 2.17 Evolution of the modulus equation of state w as a function of scale factor for the parameters of Equation 2.8, but with the change $M \to 10^8$, $\phi_i \to 10^{-2}$. The tracking solution is never quite found, as the equation of state makes a slow oscillation. When the modulus settles into its true negative potential minimum we see a spike in the equation of state at $a \approx 10^{-2}$, as $H \to 0$.

modulus potential dominated by the axion mass term and thus contributing a positive energy density. However, at later times the modulus falls into and bounces from its own potential minimum, eventually driving the energy density to zero and causing rapid entry into a phase of cosmic contraction [232, 234]. During this evolution the modulus equation of state makes a slow oscillation as the field moves around in its potential and settles in the true minimum.

We note again that contraction cannot be properly analysed in the framework presented here, since the Friedmann equation alone does not allow for it. The framework to use is the Friedmann acceleration (or Raychaudhuri) equation for $\ddot{a}$

[234]. We carry out this analysis in Chapter 3.

2.3 CONCLUSIONS

In this Chapter a model has been proposed that introduces a coupling between axions and moduli in the string axiverse. The coupling is motivated by the observation that the mechanism causing axion masses to distribute on a logarithmic scale, and thus for some to exist with masses in the range $10^{-33}\,\mathrm{eV} \lesssim m_a \lesssim 10^{-18}\,\mathrm{eV}$ where their cosmological dynamics can produce interesting phenomenology, is due to an exponential dependence of the mass on the size of cycles in the compact space. The sizes of these cycles are controlled by scalar fields called moduli, which are themselves dynamical. Moduli stabilisation is an important problem in string theory. We investigate the possibility that if there are light axions that roll in their potentials on timescales of cosmological interest then some moduli may also roll in their potentials, given by a general form for stabilisation, and that this vacuum destabilisation can be affected in turn by the presence of the axions.

We then explore the consequences of having one cosmologically relevant axion and allowing its counterpart modulus to also roll. The resulting system, in terms of the background expansion of the universe, is a simple one of two coupled scalar fields with a scalar potential containing a number of free parameters, decoupled from the other cosmic fluids. The potential causes the fields to have scaling solutions where the energy density tracks that of the dominant component. This destabilises the modulus, and the resulting evolution causes an evolution of the axion mass, altering the dynamics from the most simple case of a single decoupled axion.

The axion-modulus system has a number of different phases in its evolution, of which we have identified some which may be of phenomenological interest. A common feature is that when tracking begins, the fraction of the total energy density in the axion-modulus system rises to an appreciable level and causes a non-standard evolution in the total equation of state in a manner similar to models of Early Dark Energy. In the examples considered in this Chapter this resulted in a decrease of the equation of state by $\mathcal{O}(10\%)$ around the epoch of equality.

The fate of the axion-modulus system, and consequently the fate of cosmic expansion, then depends on the rate of decay of the axion mass and the amplitude of axion oscillations. If the axion oscillates and the amplitude of its oscillations decrease below some critical value then the modulus falls into its globally stabilising minimum at negative potential, which if this potential comes to dominate the energy density will signal the onset of an epoch of cosmic collapse. If the dynamical axion mass can be sufficiently damped by the modulus evolution then oscillations cannot begin and the tracking solution remains stable for longer.

There is also the possibility that a modulus that looks to have been stabilised by Hubble friction at early times might be destabilised when its counterpart axion begins to roll at late times, and that this vacuum destabilisation may be observable indirectly through its effects on couplings of both gravity and the standard model, though the viability of this scenario in a realistic model requires much further attention.

We have shown that these phenomena might be expected as fairly generic since they are exhibited for values of the parameters spanning many orders of magnitude. We also note that in a scenario such as the string axiverse, where there is a plethora of light fields at the phenomenologists disposal then it is possible to create cosmologies where phenomena like those described here may occur at multiple different epochs in the history and future of the universe, both by having multiple fields or by the two field dynamics spiralling towards some attractor and periodically entering and exiting different regions in phase space.

In the interests of simplicity no attempt was made to describe a universe where a significant and controllable fraction of the dark sector energy density is contributed by the axion-modulus system, except in the case where rapid decay of the modulus leads to cosmological collapse. This question of initial conditions will be the subject of a future work.

Chapter 3 will focus on delineating the regions of parameter space which give rise to the phenomena described in this Chapter and thus provide the tools to both construct desirable models for cosmological phenomenology, and also to place limits on the possible values of parameters in any model of this type, which will be severely limited by the possibility of cosmological collapse.

The coupling induces a tracking of energy densities in the axion-modulus system, which, just as it does for quintessence, may be fruitfully used to address problems of fine tuning, which are of a major concern for high f_a axions. The tracking dynamics may also allow a modulus which appears naively to be stabilised in some negative energy density AdS minimum to in fact hide this energy density with large field values and along with the cosmological constant lead to late time dS expansion, which may contribute in some way to the solution of the cosmological constant problem in the string theory landscape.

This simple extension of the axiverse has a rich structure and suggests models which we hope may be of use to both cosmologists and string theorists, and displays features which may, when fully investigated, be measured and constrained by cosmological experiments, particularly once the perturbations have been analysed to allow computation of effects on the CMB and matter power spectrum.

3

AXIONS AND MODULI AS A DYNAMICAL SYSTEM

"The body is basically not different from the reflection. You cannot have one without the other: If you try to keep one and get rid of the other, you'll be forever estranged from the truth."

Pao-chih, in *Classics of Zen and Buddhism, T. Cleary*

PREFACE

This Chapter takes the model of Chapter 2 and further develops its study. We present more context, and a more systematic analysis of the potential and the dynamics. This work is based on Ref. [235]. A table of symbols defined in this Chapter is given in Table 3.1 for reference.

3.1 THE MODEL

3.1.1 Formalism

We begin by restating the modulus potential of Chapter 2 in the following form:

$$V(\phi,\chi) = Be^{-2C\chi} - De^{-C\chi} + \frac{1}{2}M^2e^{-C\chi}\phi^2 + \rho_\Lambda\,, \tag{3.1}$$

where ρ_Λ is the cosmological constant, added *arbitrarily* in this model so that whatever value the potential takes today can be made consistent with observations. We also

Symbol	Meaning	Ref. Eq.
f_a	axion decay constant	(1.26)
Λ_a	axion potential energy scale	(1.26)
μ	energy scale of non–perturbative physics for axion potential	(1.27)
B, D	modulus potential parameters	(3.1)
ρ_Λ	cosmological constant energy density	(3.1)
Λ	value of the true vacuum energy	(3.21)
ϕ	axion field	(1.28)
χ	modulus field	(3.1)
C	axion–modulus coupling constant	(3.1)
$\gamma_{\rm b}$	baryotropic fluid equation of state	(3.3)
x, y, z, r, s, t	autonomous system variables	(3.16)
$N_{\rm efd}$	number of e–folds from beginning of model evolution until end of fluid domination	–
$\mathcal{N}_{ae}$	number of periods of accelerated expansion	–
Ω_e	early dark energy (EDE) density	(3.35)
M	$= \mu^2/f_a$ (axion mass scale)	(3.1)
β	$= \sqrt{3M^2/D}$	(3.9)
$\tilde{\phi}$	$= \sqrt{6}/\beta$ (critical value of ϕ above which modulus is destabilised)	(3.10)
ω	$= \sqrt{B/D}$	(3.8)
ζ	$= B\rho_\Lambda/D^2 = t^2z^2/r^4$ (vacuum constraint). $\zeta > (<) 1/4$ gives dS (AdS)	(3.20)

Table 3.1 Symbols used in this Chapter.

have $M^2 = \mu^4/f_a^2$, and in this Chapter always take $\tilde{C} = C$ for simplicity. The total Lagrangian is then of the form:

$$\mathcal{L} = \frac{1}{2}(\partial\phi)^2 + \frac{1}{2}(\partial\chi)^2 - V(\phi,\chi)\,. \tag{3.2}$$

There is one important caveat to this picture: by taking f_a fixed we are implicitly assuming small modulus variations. This greatly simplifies our system, since if we allowed for the variation of $f_a(\chi)$ this would change the canonical normalisation of the axion kinetic terms. This effect could introduce new phenomenology in extreme trajectories with large $\Delta\chi/\chi$, for example the possibility of chaotic behaviour, but we defer study of this to a future work[1]. We make some comments on the effect on the potential in Section 3.4.

We assume that the axion and modulus fields evolve in a spatially flat FLRW background containing the bare cosmological constant, ρ_Λ, and a single fluid with baryotropic equation of state $P_{\rm b} = (\gamma_{\rm b} - 1)\rho_{\rm b}$, where $\gamma_{\rm b}$ is a constant, $0 \leq \gamma_{\rm b} \leq 2$. For radiation $\gamma_{\rm b} = 4/3$ or for dust CDM $\gamma_{\rm b} = 1$. In standard cosmic time, with dots

[1] We thank John March-Russell for pointing this fact out to us.

denoting derivatives with respect to this, the evolution equations are:

$$\begin{aligned}
\ddot{\phi} &= -3H\dot{\phi} - \frac{\partial V}{\partial \phi}\,, \\
\ddot{\chi} &= -3H\dot{\chi} - \frac{\partial V}{\partial \chi}\,, \\
\dot{\rho}_{\rm b} &= -3H\rho_{\rm b}\gamma_{\rm b}\,, \\
\dot{H} &= -\frac{1}{2}[\rho_{\rm b}\gamma_{\rm b} + \dot{\phi}^2 + \dot{\chi}^2]\,.
\end{aligned} \tag{3.3}$$

These are subject to the Friedmann constraint

$$3H^2 = \rho_b + \rho_\Lambda + \rho_\phi + \rho_\chi\,, \tag{3.4}$$

where we have assumed that we can define the following distinct densities and pressures:

$$\begin{aligned}
\rho_\phi &= \frac{1}{2}\dot{\phi}^2 + U(\phi,\chi)\,, \\
P_\phi &= \frac{1}{2}\dot{\phi}^2 - U(\phi,\chi)\,, \\
\rho_\chi &= \frac{1}{2}\dot{\chi}^2 + V_B(\chi) - V_D(\chi)\,, \\
P_\chi &= \frac{1}{2}\dot{\chi}^2 - V_B(\chi) + V_D(\chi)\,.
\end{aligned} \tag{3.5}$$

by splitting the potential as:

$$V(\phi,\chi) = V_B(\chi) - V_D(\chi) + U(\phi,\chi) + \rho_\Lambda\,, \tag{3.6}$$

where

$$\begin{aligned}
V_B(\chi) &= Be^{-2C\chi}\,, \\
V_D(\chi) &= De^{-C\chi}\,, \\
U(\phi,\chi) &= \frac{1}{2}e^{-C\chi}M^2\phi^2\,.
\end{aligned} \tag{3.7}$$

We note that the split in these cases between dark matter and dark energy is somewhat arbitrary [236]. When scalar fields begin oscillating, they redshift and cluster as dark matter, with an individual equation of state $w_{\phi\chi} \to 0$, but the modulus term also has a vev, behaving as a cosmological constant. We will see later that there is also the possibility that either or neither field oscillates; this and the inclusion of

ρ_Λ muddies the waters further. Also, it is completely arbitrary in the presence of coupling to place $U(\phi, \chi)$ in ρ_ϕ.

In the axiverse as presented in [104] all moduli were assumed to be absolutely stabilised. The different sizes at which they were stabilised led to the different masses for the axions. Some were stabilised at larger values than others in order to make some axions light, but the differences are not hierarchical. Assuming absolute stability implied that the moduli were heavy, and lived in their global minimum. The axiverse has been concretely realised in the moduli stabilisation scheme of [195]. In the scheme of [220], moduli were stabilised at hierarchically different values, which allowed some moduli to remain very light. In this picture the axion phenomenology is not considered, and they are set to their vacuum values at zero. This is perfectly well justified even for light axions if all we are concerned with is the existence of a stable minimum for the moduli and in calculating their masses at this minimum, but if the axion evolution is our focus, then their possible effects on the moduli cannot be ignored. In both [195] and [220] only a handful of fields were considered, not the hundreds motivated in the axiverse. Here we take inspiration from the success of these models, and apply to it the spirit of optimism of the axiverse to look for phenomenology in a larger arena of possibilities.

3.1.2 Cosmic Overview

Here we give an overview of a scenario that may lead to the realisation of the initial conditions appropriate to our model, and the picture of cosmic history that emerges.

We will assume that the universe begins in an eternally inflating dS false vacuum. This vacuum decays via tunnelling and bubble nucleation [133] into the standard phase of slow-roll inflation required to generate the primordial power spectrum. It must also be assumed that initial conditions on the axion and modulus fields are laid down *prior* to inflation. After slow-roll inflation ends, the inflaton decays and reheats the universe. We will consider the toy model of a post-inflation universe consisting only of matter, radiation, and the axion and modulus field condensates contributing a dark sector energy density as described in Chapter 2.

In Chapter 2, example cosmology 1, initial conditions were such that the modulus

began at a large value, χ_i and the axion mass $m_a = M^2 e^{-C\chi}$ was cosmologically light, $m_a = \mathcal{O}(1 - 10^{10})H_0$. This modulus initial condition was *not* at the local minimum of the potential, $\langle\chi\rangle(\phi)$. The axion initial condition, ϕ_i is set at the Peccei-Quinn (PQ) phase transition by spontaneous symmetry breaking [107, 112]. There are two logical possibilities for modulus evolution: there is a local modulus minimum at ϕ_i, or there is not. If there is a minimum, and the modulus is sufficiently heavy to overcome Hubble friction, it will, like the inflaton before it, roll to the *local* minimum, while the light axion frozen at ϕ_i prevents it from reaching the global minimum. If there is no local minimum, then the modulus will roll to yet larger values until stopped by Hubble friction, only decaying to a local minimum once one exists (see e.g. [237])[2]. Under these conditions, although the modulus and axion masses at the global minimum could be large (e.g. SUSY/string/Planck scale), interactions instead freeze the modulus either in its local minimum, or at $\chi > \chi_i$. In both cases, the modulus *must* evolve with the axion.

For these initial conditions to be possible the only requirement is that the PQ phase transition and the switching on of the appropriate instanton effects, which create the axion condensate and form the coupled potential, happen *before the modulus finds its minimum*. Certainly, during slow-roll inflation there are scalar fields yet to find their minima: the inflaton itself is one such field. It is not unreasonable to assume that there are other moduli present that also exist away from their minima. Indeed, this is the case in any model of multi–field inflation and is the string interpretation of any quintessence model. This is also the expectation for the post-inflation, pre-hot-big-bang phase in string cosmology, where the post-inflation universe is dominated by the yet-to-decay, matter-like moduli [135, 195, 240].

The requirement that inflation occurs after the PQ phase transition, and that the reheat temperature does not restore the PQ symmetry, is generic to almost all models with axions as it is required to avoid a cosmological abundance of disastrous domain walls and the like [112]. In addition, string axion models require a low energy scale of inflation [104], in part to avoid overproduction of axion isocurvature perturbations.

[2]These considerations are basically a statement of the Brustein-Steinhardt problem [238] for this model. Related issues in inflation are discussed in [239].

After the radiation and matter dominated phases end, the next stage in the evolution of the universe again has a number of possibilities depending on the axion and modulus fields. The additional cosmological constant in the potential, ρ_Λ, can be regarded as the usual left over contribution to the vacuum energy. It has contributions which reduce it over time after spontaneous symmetry breaking (e.g. at the electroweak transition), positive contributions from dS stabilised moduli and vacuum fluctuations of quantum fields, and negative contributions from AdS stabilised moduli (see e.g. [241]). The value of this constant relative to the potential minimum in the axion and modulus fields determines the fate of the universe.

If the axion and modulus fields are heavy and their field values are small, such that they are oscillating about, or slowly rolling into, their global minimum during the present epoch, then the scenario will be much like any other quintessence or axion dark matter scenario. The value of the total cosmological constant in the bottom the potential must be small, and of the correct magnitude to account for the observed accelerated expansion of the universe. However, if the fields are light enough and their initial values large enough that they are on the plateau of the potential, then the phenomenology can be quite different. Here, the potential energy of the axion and modulus are a small contribution, and the current accelerated expansion will be driven almost entirely by ρ_Λ, as was the case in Chapter 2.

However, as also described in Chapter 2, the axion-modulus system is only quasi-stable: eventually axion oscillations will decay and the modulus will find the global minimum. Depending on the initial conditions and the parameters in the potential it is possible to arrange for an acceptable cosmology where the vacuum energy at the global minimum is either positive, negative, or indeed zero. If the vacuum energy is negative then the decay of the modulus will trigger rapid cosmological collapse, rather than life in a stable AdS state [133, 242, 243]. In the case where it is positive, then a scenario such as explored in [244] will ensue.

3.2 AXION-MODULUS DYNAMICS AND THE COUPLED POTENTIAL

Before we begin our detailed dynamical systems analysis in Section 3.3, we aim to give here some basic intuition about the types of phenomena possible in a cosmology with coupled scalar fields and an arbitrary vacuum energy. In particular, we give examples of phenomena not explored previously in Chapter 2. The examples use arbitrary values of the parameters and are for illustration only.

3.2.1 Local Minima, the Adiabatic Trajectory, and an Effective Potential

The form of the potential is such that there is just one minimum, when the axion is at zero. However, for light axions, most of cosmic history [3] is spent away from this global minimum. The form of the coupling between axion and modulus then means that the moduli, too, will live away from their global minimum and consequently *moduli must evolve during the course of cosmic history*.

We find that the local minimum in the modulus direction as a function of the axion background is:

$$\langle\chi\rangle(\phi) = -\frac{1}{C}\ln\left[\frac{1}{2\omega^2}\left(1-\frac{\beta^2}{6}\phi^2\right)\right], \tag{3.8}$$

where

$$\beta = \sqrt{\frac{3M^2}{D}}. \tag{3.9}$$

and $\omega^2 = B/D$. We plot this trajectory on the potential surface in Fig. 3.1.

The existence of the global minimum at positive modulus translates into the bound: $\omega > \frac{1}{\sqrt{2}}$. We also find that there is no local modulus minimum for large axion field values:

$$\phi > \frac{\sqrt{6}}{\beta} \equiv \tilde{\phi} \quad \Rightarrow \text{no modulus minimum}. \tag{3.10}$$

That is to say: *for large axion field values, the corresponding modulus will become destabilised*[4]. The disappearance of the minimum at large axion field values is precisely the appearance of the 'valley walls' in the potential, as described in Chapter 2, Figs. 2.7 and 2.8. This condition was expressed in Chapter 2 in Eq. (2.7).

[3] When viewed in redshift space, where we have cosmic coincidence for things occurring within $z = 1$ of us, which is of order billions of years. The coincidence problem is in fact much more of a problem *forwards* in time: why are we not Boltzmann brains in thermal de-Sitter space?

[4] The same is true when the variation of f_a with χ is taken into account, but the condition must be found numerically.

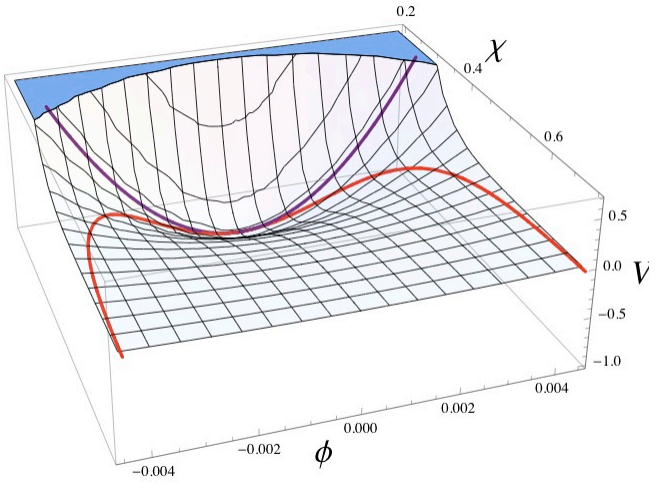

Figure 3.1 The potential of Eq. (3.1) near the global minimum, for arbitrary parameters. In red, the adiabatic trajectory: the modulus minimum as a function of ϕ (Eq. (3.8)). When ϕ takes large values (defined by Eq. (3.10)), the minimum at finite χ is destroyed. In purple, the naive trajectory: the axion potential at fixed $\chi = \langle\chi\rangle(0)$. For a heavy modulus the adiabatic trajectory will be followed, which is shallower near the minimum than the naive trajectory.

When the axion has a periodic potential, canonically of the form $U(\theta) = 1 - \cos(\theta)$, then the axion has a maximum field value at $\theta = \pi$. Such a periodic field can spoil the local modulus minimum with $\theta < \pi$ when:

$$\frac{\mu^4}{D} > \frac{1}{2}. \tag{3.11}$$

If the axion initial conditions are such that field values are large then the corresponding modulus has no potential minimum in the early universe. If the axion undergoes monodromy [230, 244, 245] the shift symmetry is broken and large field values are natural. For smaller axion field values this condition can still be satisfied for sufficiently large β^2, or if the bound of Eq. (3.11) is satisfied.

Eqs. (3.10, 3.11) show that if the natural scales in the axion potential (either M^2 or μ^4) arising from non-perturbative physics, are of the same order or slightly larger than the natural scales in the modulus potential (in this case D), which are also non-perturbative, then destabilisation can occur even for small field values. Whether or not this mild hierarchy of scales occurs in actual models of moduli stabilisation is not the subject of this work, but we see no *a priori* reason why it should not be possible.

In the rest of this section we will be concerned with situations where a local minimum for χ *does* exist. In this case where there is a local modulus minimum, there is still interesting physics caused by the axion background. If the modulus begins life at its local minimum in the frozen axion background then the fractional change in the modulus field during axion evolution from $\phi = \phi_i$ to $\phi = 0$ is:

$$\frac{\Delta\chi}{\langle\chi\rangle(0)} = \frac{|\Delta f_a|}{f_{a,i}} = \frac{\ln\left(1 - \left(\frac{\phi_i}{\tilde{\phi}}\right)^2\right)}{\ln\left(\frac{1}{2\omega^2}\right)}\,. \tag{3.12}$$

This ratio blows up when $\phi_i = \tilde{\phi}$, where the modulus is destabilised and the local minimum is at $f_{a,i} = 0$. However, it remains $\mathcal{O}(1)$ for $\phi < \tilde{\phi}\sqrt{1 - \frac{1}{2\omega^2}}$. As we will see, ω does not appear in our dynamical system analysis and so can be picked arbitrarily large (corresponding to stabilising the modulus at larger and larger values) and these results can be made insensitive to the approximation that f_a is fixed. For the consistency of our assumption that PQ symmetry is broken before inflation, we must have f_a larger than the inflationary energy scale, and it must remain large enough that the symmetry is never restored. Two comments are in order here. Firstly, the modulus will never roll out to truly infinite values because of Hubble friction. Secondly, however, we may in general expect trajectories that go from a destabilised region on the plateau of the potential into the global minimum to require some fine tuning in order not to break our assumption of fixed f_a. We will comment more on this later.

The ratio of modulus mass at the start and end of this trajectory is:

$$\frac{m_\chi(\langle\chi\rangle(\phi_i))}{m_\chi(\langle\chi\rangle(0))} = 1 - \left(\frac{\phi_i}{\tilde{\phi}}\right)^2\,. \tag{3.13}$$

This ratio can become small as the bound of Eq. (3.10) becomes saturated. When this bound is saturated, or nearly saturated, and if other corrections to the modulus mass are small[5], then an effective field theory obtained by integrating out the modulus based on its mass at the global minimum may fail. The potential is anharmonic, and so if the modulus is displaced far from its local minimum the mass will not be given by this formula.

[5]For example, suitable decoupling occurs in the scenario of [220].

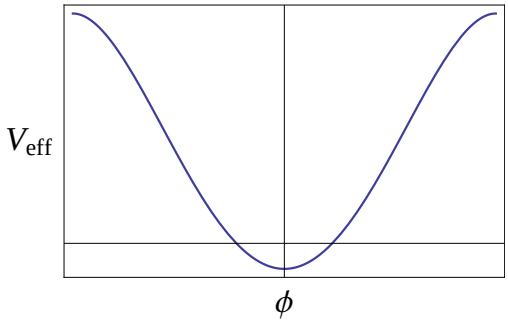

Figure 3.2 Sketch of the potential of Eq. (3.14), the effective potential for the axion when the modulus remains always in the adiabatic trajectory of Eq. 3.8.

The ratio of Eq. (3.13) occurs also for the axion mass along this trajectory, implying that in such a situation the fields cannot change their relative masses during the course of their evolution. If the modulus is heavier at the global minimum, it will also be heavier in any local minimum. This allows for consistency of the assumption above: if the modulus minimises first it should be a good approximation in this case to consider the trajectory as being $\langle\chi\rangle(\phi)$. We will call this trajectory the *adiabatic trajectory*, i.e. the one that the modulus follows if it is always heavy enough to return to equilibrium sufficiently quickly as the axion rolls.

We can obtain an effective potential for the axion that approximates the full effective field theory description by substituting the adiabatic trajectory for the modulus back into the potential of Eq. (3.1):

$$V_{\rm eff}(\phi) = \frac{1}{2\omega^2}(1-\frac{\beta^2}{6}\phi^2)\left[\frac{B}{2\omega^2}(1-\frac{\beta^2}{6}\phi^2) - D + \frac{M^2}{2}\phi^2\right] + \rho_\Lambda\,. \tag{3.14}$$

This potential differs from the harmonic potential by becoming flat as $\phi \to \tilde{\phi}$. Beyond $\phi = \tilde{\phi}$ it should not be used. The potential is sketched in Fig. 3.2.

During this evolution the fields follow a *curved* trajectory in field space, just like in multi-field inflation, with the axion and modulus both always moving to smaller values and becoming heavier. Therefore the normal course of cosmic evolution will not endanger late time stability (if the minimum has positive cosmological constant, see later). However, as the bound of Eq. (3.10) becomes saturated we should see that axions and moduli undergo significant evolution in their masses while moving

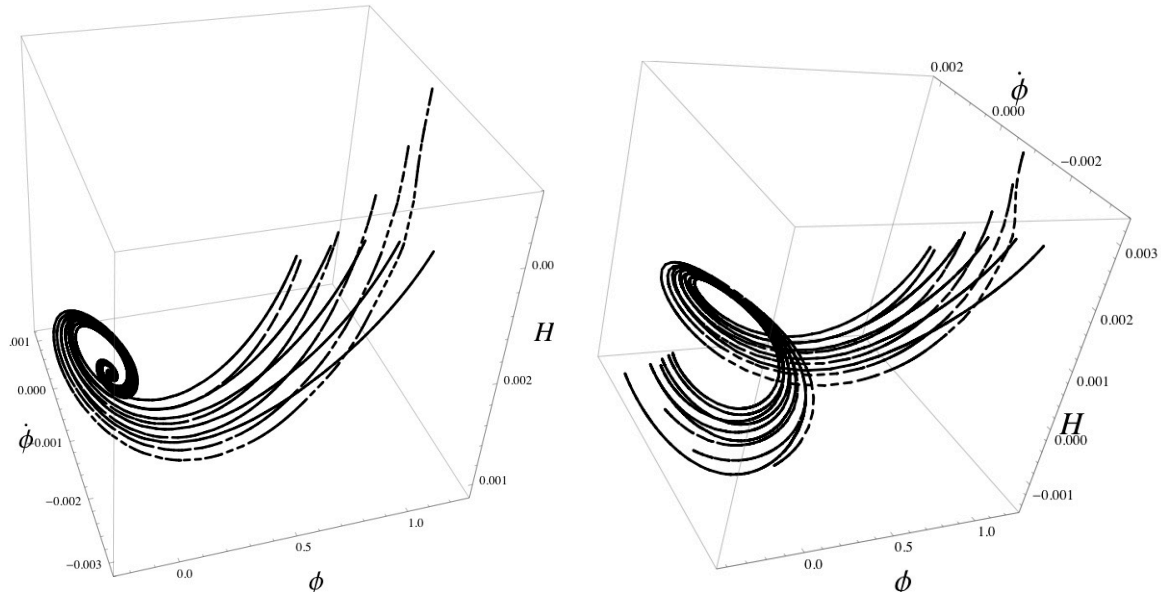

Figure 3.3 Phase space topology in $\{\phi, \dot{\phi}, H\}$. *Left panel*: $\Lambda > 0$, with evolution to a minimum H. *Right Panel*: $\Lambda < 0$, trajectories spiral through $H = 0$ and the universe collapses. Dashed lines are for evolution in the full potential, and solid lines in the adiabatic potential, where the modulus remains always in its local minimum. Different trajectories correspond to different initial conditions on $\phi < \tilde{\phi}$.

towards the global minimum. If the axion is light in the current epoch then this evolution will still be occurring.

Again drawing the analogy to multi-field inflation, even if the evolution in the modulus direction is slight, a tight turn in the field space trajectory may lead to observable features in the axion power spectrum [246, 247]. Such tight turns do not appear possible in the potential we study, and we also will not be considering the effect of inhomogeneous perturbations.

We finally note here that if the amplitude of axion oscillations were allowed to grow, such as in the scenario explored in [248] where axion oscillations are amplified by the Penrose process near a black hole, then this may also lead to novel effects on the modulus sector and the vacuum energy (see also [189] on moduli induced vacuum destabilisation in other astrophysical and cosmological processes).

3.2.2 *Dynamics in Phase Space and the Equation of State*

The value of the vacuum energy (which should not be confused with the scale of the potential), $\Lambda = V(0, \langle\chi\rangle)$, which includes the ρ_Λ contribution, is a free parameter

in our model. Its sign controls the topology of phase space [232]. We show this effect in our model in Fig. 3.3, where we plot trajectories in $\{\phi, \dot{\phi}, H\}$ phase space obtained by numerically solving the equations of motion (Eqs. (3.3)). With $\Lambda > 0$ the trajectories are confined to the expanding branch, $H > 0$ (or if $H_i < 0$, the contracting branch), and the phase space is disconnected. With $\Lambda < 0$ it is possible for the total energy density to go to zero, and so $H \to 0$ connecting the expanding and contracting branches and making phase space connected.

When $H = 0$ the evolution of the scale factor turns over, such that with $\Lambda < 0$ the universe expands and then contracts to a big crunch despite, in these cases, having zero curvature (see e.g. [249] and references therein). We plot the evolution of the scale factor for $\Lambda < 0$ in Fig. 3.4.

The trajectories of Fig. 3.3 all begin at the local modulus minimum, $\langle\chi\rangle(\phi_i)$, with stationary fields in a fluid dominated universe, and ϕ_i takes various values between 0 and $\tilde{\phi}$. We begin at time $t = 0$ during matter domination, and normalise to $a = 1$ at this time; we look at the evolution towards the DE universe of today. We have shown trajectories given by evolution in the full potential (dashed lines), and in the effective potential (solid lines). Those trajectories with large initial axion field values in the full potential depart from the evolution in the effective potential. This is because at large axion values the modulus is light and the adiabatic assumption is no longer good enough. The scale factor evolution for $\Lambda < 0$ is shown in Fig. 3.4 and a clear difference is visible between evolution in the two potentials, with the maximum size of the universe being larger when the full potential is used.

We investigate the accuracy of the adiabatic approximation for $\Lambda > 0$ in Fig. 3.5, where we give $\Delta\chi/\chi(t) = 1 - \langle\chi\rangle(\phi)/\chi$ in percent. We see that at early times the trajectories with large initial ϕ depart by as much as 25% from the adiabatic trajectory. All trajectories undergo damped oscillations about the adiabatic trajectory as the modulus mass increases over time.

We conclude this section by commenting on the effect of the combined axion-modulus oscillations about the minimum on the DE equation of state. With $\Lambda > 0$ and at least one light field (conservatively, an axion of the axiverse), the fields at or close to their initial values can come to dominate the energy density as DE, yet still

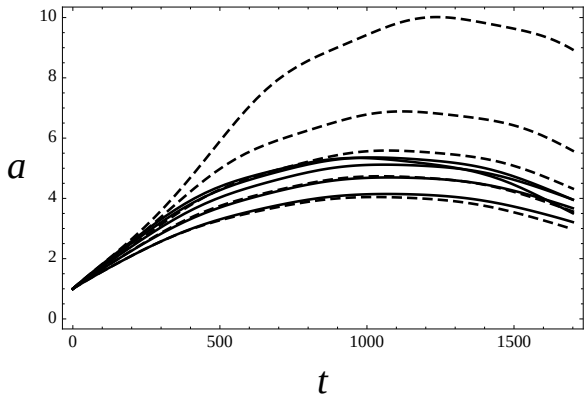

Figure 3.4 The evolution of the scale factor for $\Lambda < 0$, showing a turn over and collapse of the universe despite there being zero curvature. Again, dotted lines are for evolution in the full potential, while solid lines are in the adiabatic effective potential. Bottom to top corresponds to increasing $\phi_i \to \tilde{\phi}$. At large ϕ_i the universe reaches a larger size when the full potential is used.

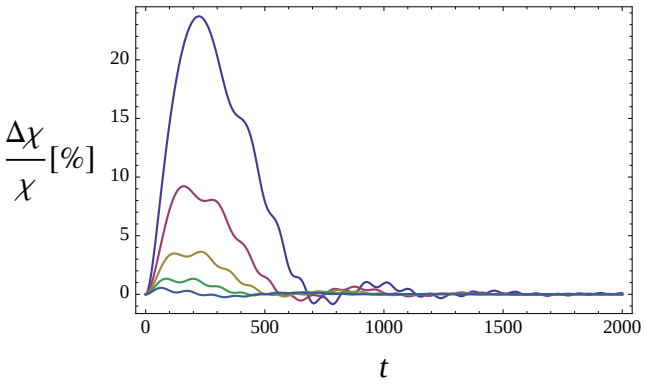

Figure 3.5 Comparing modulus evolution for motion in the full potential versus motion in the adiabatic effective potential with $\Lambda > 0$. The modulus always begins in the local minimum. Lines from bottom (light blue) to top (dark blue) represent increasingly large axion initial field values, $\phi_i/\tilde{\phi} \to 1$. The modulus departs by up to 25% from the adiabatic trajectory when the initial value of the axion field is large.

be evolving towards, and oscillating about, the true vacuum at late times. We show the effect of this on the equation of state $w_{\phi\chi\Lambda} = (\rho_\phi + \rho_\chi + \rho_\Lambda)/(P_\phi + P_\chi - \rho_\Lambda)$ in Fig. 3.6, for the trajectories of Fig. 3.3 (left panel), again comparing the cases of the effective potential and the full potential.

In this evolution, the dark energy axion-modulus fluid is already dominating the energy density at early times, $t \sim 100$, with $w \approx -1$ (which could define 'today', if we wish). However, w is rising as the fields move towards the minimum leading to large departures from $w = -1$. For large axion initial values in the full potential this

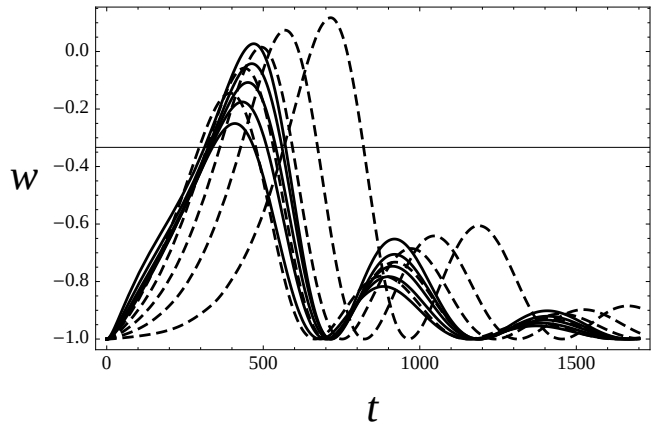

Figure 3.6 The DE equation of state for $\Lambda > 0$. Dotted lines are for motion in the full potential, solid lines for motion in the adiabatic effective potential. Left to right lines have increasing $\phi_i \to \tilde{\phi}$. DE has come to dominate the energy density around $t = 100$, but later both the DE and total equation of state go back above $w = -1/3$ (horizontal line), temporarily halting accelerated expansion. In the most extreme case of large ϕ_i in the full potential this can happen even when the equation of state today is very flat and close to $w = -1$. The late time expansion is asymptotically dS as the fields relax into the minimum.

motion is delayed and w remains flatter for longer. In all cases, as oscillations begin w rises so much as to halt accelerated expansion altogether for a short time ($w > -1/3$). The positive value of Λ in the true vacuum means that at late times w will relax to exactly -1 and that w is bounded to $-1 \leq w \leq 1$. This bound does not hold for a negative potential [250], indeed $|w_\chi| > 1$ was observed for this potential in Chapter 2.

3.3 DYNAMICAL SYSTEMS ANALYSIS

To delineate the regions of parameter space that may give rise to acceptable and interesting cosmological phenomenology we perform a dynamical systems analysis by transforming the coupled axion–modulus system into autonomous form, where there is no explicit dependence on the independent variable, in this case the scale factor. The axion and modulus fields and the perfect baryotropic fluid evolve according to Eqs. (3.3), subject to the Friedmann constraint Eq. (3.4).

3.3.1 Autonomous System

Following [231] we make the change of variables:

$$\begin{aligned} x &\equiv \frac{\dot{\phi}}{\sqrt{6}H}, & y &\equiv \frac{\dot{\chi}}{\sqrt{6}H}, \\ z &\equiv \frac{1}{H}\sqrt{\frac{V_B}{3}}, & r &\equiv \frac{1}{H}\sqrt{\frac{V_D}{3}}, \\ s &\equiv \frac{1}{H}\sqrt{\frac{U}{3}}, & t &\equiv \frac{1}{H}\sqrt{\frac{\rho_\Lambda}{3}}. \end{aligned} \tag{3.15}$$

The evolution Eqs. (3.3) can then be transformed into autonomous form $\mathbf{X}' = \mathbf{f}(\mathbf{X})$, where $\mathbf{X}$ is the column vector of compact variables and $\mathbf{f}(\mathbf{X})$ is the corresponding column vector constituting the autonomous system equations:

$$\begin{aligned} x' &= -\left[\frac{H'}{H} + 3\right] x - \beta r s\,, \\ y' &= -\left[\frac{H'}{H} + 3\right] y - \sqrt{\frac{3}{2}} C[r^2 - s^2 - 2z^2]\,, \\ z' &= -\left[\frac{H'}{H} + \sqrt{6}Cy\right] z\,, \\ r' &= -\left[\frac{H'}{H} + \sqrt{\frac{3}{2}}Cy\right] r\,, \\ s' &= -\left[\frac{H'}{H} + \sqrt{\frac{3}{2}}Cy\right] s + \beta x r\,, \\ t' &= -\frac{H'}{H} t\,, \end{aligned} \tag{3.16}$$

with

$$\frac{H'}{H} = -\frac{3}{2}\gamma_b(1 - x^2 - s^2 - y^2 - z^2 + r^2 - t^2) - 3x^2 - 3y^2\,, \tag{3.17}$$

where β was defined in Eq. (3.9).

Here, a prime denotes differentiation with respect to the number of e–foldings $N \equiv \ln(a)$. The dimensionless density parameters $\Omega_i \equiv \rho_i/3H^2$ of the cosmic components i can be expressed as

$$\Omega_\phi = x^2 + s^2\,, \quad \Omega_\chi = y^2 + z^2 - r^2\,, \quad \Omega_\Lambda = t^2\,, \tag{3.18}$$

and furthermore, flatness imposes

$$\Omega_\mathrm{b} = 1 - (x^2 + s^2 + y^2 + z^2 - r^2 + t^2)\,. \tag{3.19}$$

At this point some comments on the system (3.16) are in order. Notice that due to the negative contribution from V_D in the modulus potential, trajectories are not confined to the unit hypersphere in the full phase space. The set of phase space variables $\{x, y, z, r, s, t\}$ is of one dimension more than the actual $\{\phi, \dot{\phi}, \chi, \dot{\chi}, H\}$ degrees of freedom. This is because there is a relation that exists between the phase space variables, which provides an additional constraint and defines a surface on which the motion takes place, just like the Friedmann constraint gives the topology of phase space in [232]. The constraint is:

$$\frac{t^2 z^2}{r^4} = \frac{B\rho_\Lambda}{D^2} \equiv \zeta \,, \tag{3.20}$$

which is a simple consequence of the definitions of the variables and the form of the potential. Trajectories are confined to live on this plane, defined by the choice of initial conditions. There is a simple interpretation of this that will help us visualise phase space: Choosing ζ corresponds to a choice of sign for the vacuum energy, including the bare cosmological constant. Combining Eqs. (3.1) and (3.8) and $\phi = 0$ to get the vacuum energy $\langle V \rangle = \Lambda$:

$$\Lambda = \frac{D^2}{B}\left(\zeta - \frac{1}{4}\right) . \tag{3.21}$$

The Minkowski vacuum is given by $\zeta = \frac{1}{4}$, whilst $\zeta < \frac{1}{4}$ is an AdS vacuum, and $\zeta > \frac{1}{4}$ is a dS vacuum (we show the planes for three values of ζ in Fig. 3.7, which we will discuss in more detail later), but we note that ζ does not set the scale of the vacuum energy. This would be fixed observationally *if* we were to want the vacuum to give us the correct H_0, but this is not necessary: $\langle V \rangle$ can be much less than this, but not greater.

Furthermore, this geometrical picture of surfaces in the $\{z, r, t\}$ subspace can give another view on the boundedness of trajectories and topology of phase space discussed in Section 3.2 and shown in Fig. 3.3. The requirement of a flat universe imposes the constraint:

$$x^2 + y^2 + s^2 + z^2 - r^2 + t^2 \leq 1 \,. \tag{3.22}$$

Clearly, the location of the hypersurface defined by saturation of the bound moves as the variables evolve, however we can picture its effect in the limit of heading to

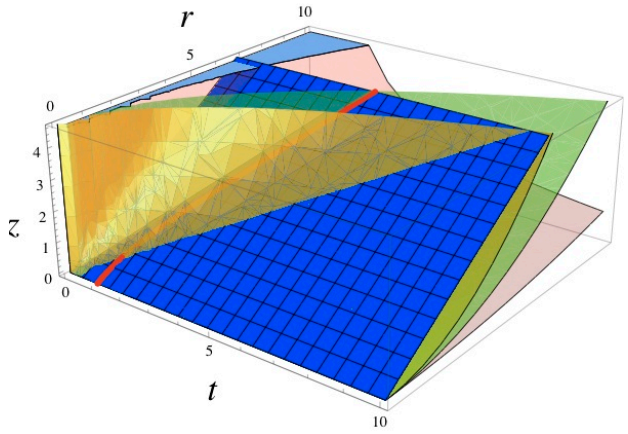

Figure 3.7 Dynamical constraint surfaces in the $\{z, r, t\}$ subspace. The flat meshed (blue), surface corresponds to the $\mathcal{Z}$ plane, which is the minimum of the potential. The foremost curved (yellow) surface is the constraint for a dS vacuum with $\zeta > 1/4$. Next behind it is the Minkowski plane (green) with $\zeta = 1/4$. Finally, the rearmost curved surface (red) is the constraint for an AdS vacuum with $\zeta < 1/4$. The bold (red) line on the $\mathcal{Z}$ surface corresponds to the critical line **M**. We see that **M** crosses only dS planes and asymptotes to the Minkowski plane at co–ordinate infinity, while the minimum surface crosses all ζ planes on a line. The non-crossing of fixed line **M** with surfaces of $\zeta < 1/4$ is another geometric illustration of the instability of a negative potential to collapse.

the vacuum: $x = y = s = 0$. Now there is an additional surface that intersects those of Fig. 3.7. If one were to plot it, one would see that it intersects dS surfaces, with $\zeta > 1/4$, making an arc below which trajectories are confined, unable to reach co–ordinate infinity. For AdS surfaces, with $\zeta < 1/4$, the surface funnels outwards, restricting trajectories to a region of their ζ surface, but not confining them to finite values. This is another manifestation of our choice of dynamical system variables: for a negative vacuum energy it is possible for $H \to 0$, where the co-ordinates diverge and trajectories on the potential become unconfined.

The plane defined by $\zeta = \frac{1}{4}$, which we will call the Minkowski plane, therefore divides the phase space into three: above the Minkowski plane, phase space is bounded, and the collapsing and expanding universe branches ($z, r, s, t < 0$ and $z, r, s, t > 0$ respectively) are separated; on the Minkowski plane the asymptotic future lies at infinity, where $H = 0$; below the Minkowski plane, phase space is connected and there are trajectories through infinity that join the expanding and contracting branches. When the transition is made from expansion to contraction and H changes

sign, all six variables, x, y, z, r, s, t also change sign, so that the contracting branch is the opposite, negative octant of the $\{z, r, t\}$ space shown in Fig. 3.7.

Choosing to work with a phase space of one higher dimension is useful for our analysis of fixed points, since it allows us to see what happens when one or more of these variables can be approximated as vanishing relative to the others, for example z and r vanish as the modulus goes to large values, and t vanishes in the early universe.

When $H = 0$ our variables diverge and so the system (3.16) cannot be evolved through the transition between expanding (H^+) and contracting (H^-) universes. It is actually possible to construct a set of compact variables which remain finite at $H = 0$:

$$\begin{aligned} x_Q &\equiv \frac{\dot{\phi}}{\sqrt{2}Q}\,, & y_Q &\equiv \frac{\dot{\chi}}{\sqrt{2}Q}\,, \\ z_Q &\equiv \frac{\sqrt{V_B}}{Q}\,, & s_Q &\equiv \frac{\sqrt{U}}{Q}\,, \\ t_Q &\equiv \frac{\sqrt{\rho_\Lambda}}{Q}\,, \end{aligned} \tag{3.23}$$

where

$$Q \equiv \sqrt{3H^2 + V_D}\,. \tag{3.24}$$

These variables are similar to those defined in [251]. Since V_D is positive definite, Q always remains well defined. Defining a new independent variable $(') = \frac{1}{Q}\frac{\mathrm{d}}{\mathrm{d}t}$ one can transform the evolution Eqns. (3.3) and (3.4) into autonomous form. This alternative autonomous system is given in Appendix B of [235]. These compact variables, $\mathbf{X_Q}$, are related to our original compact variables $\mathbf{X}$ (Eqs. (3.15)) by

$$\mathbf{X} = \mathbf{X_Q}\hat{r}\,, \qquad \hat{r} = \sqrt{1 + r^2}\,, \tag{3.25}$$

where r was defined in Eqs. (3.15). We have kept our variables finite at $H = 0$, at the expense of losing the intuitive description of the division of phase space provided by the vacuum constraint Eq. (3.20), since the $\mathbf{X_Q}$ system has the minimally required dimensionality. For this reason we content ourselves with describing the axion–modulus system in terms of the variables of Eqs. (3.15), and do not study the transition at $H = 0$ explicitly. We will occasionally make use of the $\mathbf{X_Q}$ variables to numerically show the evolution of phase space trajectories.

3.3.2 *Fixed Points*

	x_c	y_c	z_c	r_c	s_c	t_c	Existence
A	0	0	0	0	0	0	all β, C, γ_b
B	0	0	0	0	0	± 1	all β, C, γ_b
C	$\pm\sqrt{1-y^2}$	$\pm y$	0	0	0	0	$-1 \leq y \leq 1$
D	0	$\sqrt{\frac{2}{3}}C$	$\pm\sqrt{1-\frac{2}{3}C^2}$	0	0	0	$C \leq \sqrt{\frac{3}{2}}$
E	0	$\sqrt{\frac{3}{8}}\frac{\gamma_b}{C}$	$\pm\frac{1}{4C}\sqrt{6\gamma_b(2-\gamma_b)}$	0	0	0	$\gamma_b \leq 2$
F	0	$\frac{C}{\sqrt{6}}$	0	0	$\pm\sqrt{1-\frac{C^2}{6}}$	0	$C \leq \sqrt{6}$
G	0	$\sqrt{\frac{3}{2}}\frac{\gamma_b}{C}$	0	0	$\pm\frac{1}{2C}\sqrt{6\gamma_b(2-\gamma_b)}$	0	$\gamma_b \leq 2$
I	0	$\frac{C}{\sqrt{6}}$	0	$\pm\sqrt{\frac{C^2}{6}-1}$	0	0	$C \geq \sqrt{6}$
M	0	0	$\pm z$	$\pm\sqrt{2}z$	0	$\pm\sqrt{z^2+1}$	all β, C, γ_b

Table 3.2 The fixed points of the system (3.16) and the conditions for their existence. Rather than having an isolated fixed point, **M** is formed of a continuous line of fixed points, called a critical line. This critical line intersects the ζ plane at a unique point $z = z_M$ given by Eq. (3.27).

The fixed (critical) points $\mathbf{X_c}$ of the autonomous system (3.16) are extracted by satisfying $\mathbf{X}' = \mathbf{0}$ and are listed, along with their conditions for existence, in Table (3.2). As mentioned earlier, the positive (negative) roots in the $\{z, r, s, t\}$ subspace correspond to expanding (contracting) universes. In total there are thirteen fixed points, four of which are imaginary and so are not physical and are not listed in Table (3.2). The energy densities Ω_i, the effective scalar field equation of state, $w_{\text{eff}} = (P_\phi + P_\chi)/(\rho_\phi + \rho_\chi)$ and conditions for acceleration and stability of these fixed points are given in Table (3.3). A fixed point corresponds to an accelerating solution if

$$(1 - x_c^2 - y_c^2 - s_c^2 - z_c^2 + r_c^2 - t_c^2)\gamma_b + 2x_c^2 + 2y_c^2 < \frac{2}{3}\,. \tag{3.26}$$

The stability of the fixed points may be determined by expanding about them, setting $\mathbf{X} = \mathbf{X_c} + \delta\mathbf{X}$, with $\delta\mathbf{X}$ the perturbations of the compact variables defined by Eqs. (3.15) considered as a column vector. To first order, the perturbations satisfy $\delta\mathbf{X}' = \mathbf{W}\cdot\delta\mathbf{X}$, where the matrix $\mathbf{W}$ contains the coefficients of the perturbation equations. The stability of the fixed points thus depends upon the nature of the eigenvalues of the matrix $\mathbf{W}$. The full stability analysis is somewhat cumbersome and may be

found in Appendix A of [235], the analysis there was carried out by Ewan Tarrant. Here, we give a general summary of the fixed points and their stability, focussing on the intuitive physics that the dynamical systems approach provides.

	Ω_ϕ	Ω_χ	Ω_Λ	Ω_b	$\ddot{a} > 0$?	w_{eff}	Stability
A	0	0	0	1	never	0	unstable
B	0	0	1	0	always	-1	marginally stable
C	$1-y^2$	y^2	0	0	never	1	unstable
D	0	1	0	0	$C < \sqrt{\frac{1}{2}}$	$-1+\frac{4}{3}C^2$	unstable
E	0	$\frac{3}{4}\frac{\gamma_b}{C^2}$	0	$1-\frac{3}{4}\frac{\gamma_b}{C^2}$	never	$\frac{3}{4}\frac{\gamma_b(\gamma_b-1)}{C^2}$	unstable
F	$1-\frac{C^2}{6}$	$\frac{C^2}{6}$	0	0	$C < \sqrt{2}$	$-1+\frac{1}{3}C^2$	unstable
G	$\frac{3}{2}\frac{\gamma_b(2-\gamma_b)}{C^2}$	$\frac{3}{2}\frac{\gamma_b^2}{C^2}$	0	$1-\frac{3\gamma_b}{C^2}$	never	$\frac{3\gamma_b(\gamma_b-1)}{C^2}$	unstable
I	0	1	0	0	$C < \sqrt{2}$	$-1+\frac{1}{3}C^2$	unstable
M	0	$-z^2$	z^2+1	0	always	-1	stable

Table 3.3 Properties of the fixed points given in Table (3.2) for an expanding universe. For **M**, the contribution from ρ_Λ has been included in w_{eff}.

Of the nine fixed points listed in Table (3.2), there are two trivial solutions: Fixed point **A** corresponds to the fluid dominated point where the kinetic and potential components of the axion and modulus fields are negligible, whilst fixed point **B** represents the ρ_Λ dominated solution. Point **A** is unstable in both expanding and contracting universes. Recall the ultimate fate of the universe is determined by the value of ζ. In the presence of a dS vacuum ($\zeta > 1/4$) the stability analysis reveals that fixed point **B** is associated with three *zero* eigenvalues in the $\{z, r, s\}$ subspace, whilst the remaining directions are stable. We say that this is a *marginally stable* solution in the sense that there is no instability growing exponentially, although it could be unstable to higher orders in the perturbation. To obtain the strict stability of this solution we would have to go beyond linear order in perturbation theory, which we do not pursue as numerical integration of the autonomous system confirms that this point is ultimately unstable: the asymptotic future in the presence of a dS vacuum is the stable fixed point **M**, the global axion–modulus potential minimum, which has a larger basin of attraction.

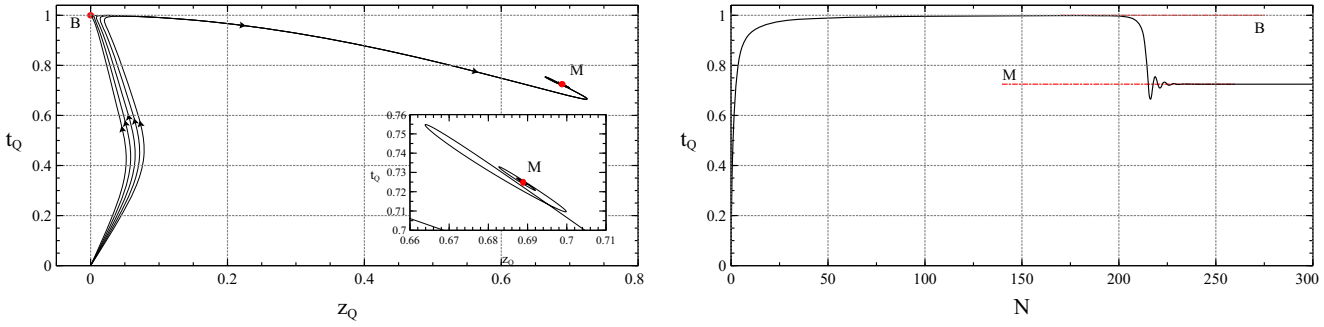

Figure 3.8 The evolution of phase space trajectories in the presence of a dS vacuum ($\zeta = 0.276$) obtained by integrating Eqs. (3.25). We set $C = 1$, $\gamma_b = 1$ and $\beta = 1.87$. The compact variables z_Q and t_Q are related to z and t through Eq. (3.25). *Left panel:* The temporary trapping of the z_Q and t_Q trajectories in fixed point **B** before the modulus begins to roll, finding its minimum at fixed point **M**. Saturation of the bound $C \leq \sqrt{\frac{3}{2}\left(\zeta - \frac{1}{4}\right)}$ (see Ref. [235] for more details), results in late–time modulus oscillations, which are seen in the figure as trajectories spiralling into **M**. *Right panel:* t_Q as a function of N, the number of e–foldings. Figure made by Ewan Tarrant.

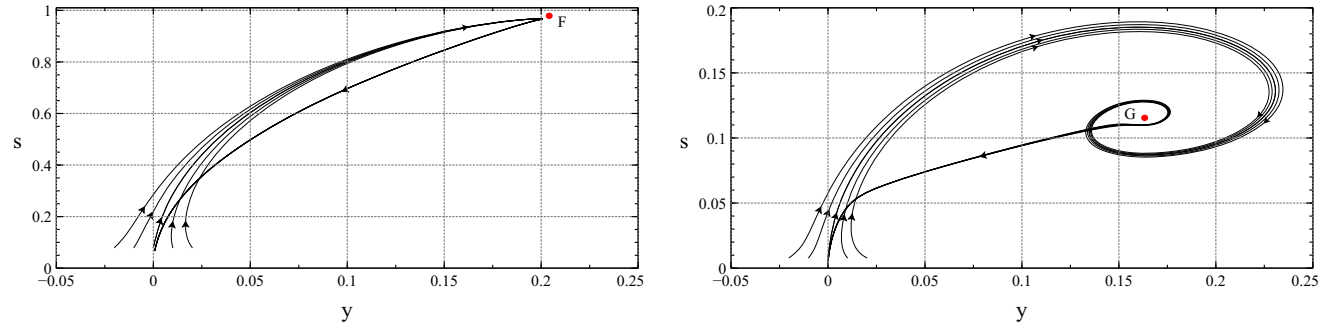

Figure 3.9 The evolution of phase space trajectories in the presence of a dS vacuum obtained by integrating Eqs. (3.16). *Left Panel*: Trajectories repelled from the unstable fixed point **F** and heading for the global potential minimum at **M**. We set $\zeta = 1.0$, $C = 0.5$, $\gamma_b = 4/3$ and $\beta = 1.732$. *Right Panel*: Trajectories spiralling into the unstable fixed point **G**, before the modulus finds the global potential minimum at **M**. We set $\zeta = 1.0$, $C = 10.0$, $\gamma_b = 4/3$ and $\beta = 10.0$. Figure made by Ewan Tarrant.

The existence of point **B** demonstrates the ability of a bare cosmological constant to overdamp modulus motion for the modulus beginning life high up on the plateau of its potential, shielding us from the true vacuum and seeing only the larger ρ_Λ. In Fig. 3.8 we show this temporary 'trapping' in fixed point **B** by plotting trajectories in the $\{z_Q, t_Q\}$ subspace. Whilst such a trapping may last for hundreds or even thousands of e–foldings, the modulus will eventually slowly roll and relax into its minimum; if this sufficiently reduces the Hubble friction then the fields will also oscillate.

Rather than having an isolated fixed point, point **M** is formed of a continuous line of fixed points, known as an *equilibrium manifold*, which we call a *critical line*. The emergence of this critical line is due to the fact that we are working in one dimension more than is required. In one dimension less, the line would degenerate to a unique point, which is given by the intersection of **M** with the ζ–plane,

$$z_M = \pm \frac{1}{\sqrt{4\zeta - 1}}\,, \tag{3.27}$$

which clearly only exists for $\zeta > \frac{1}{4}$. That is to say, the absolute potential minimum defined by the stable fixed point **M** is only a fixed point in the presence of a dS vacuum and corresponds to the asymptotic future. If $\zeta < \frac{1}{4}$ the global minimum is not a fixed point, and the asymptotic future is cosmic doomsday in a Big Crunch as will be discussed below. The global minimum is expressed in terms of the autonomous system variables by substituting $z = z_M$ in **M**. We finally note that the line **M** can equally be derived as the intersection of the minimum surface with the saturation of the flatness constraint in the potential dominated regime, $z^2 - r^2 + t^2 = 1$. Fig. 3.8 shows an example of late–time modulus oscillations as the trajectories spiral into the point z_M.

There is another plane which is of interest in the $\{z, r, t\}$ subspace, which defines the minimum of the potential itself at $\langle\chi\rangle$. At $\langle\chi\rangle$, $r = \sqrt{2}z$, which defines the plane, and the critical line **M** lives here. This plane, which we will call $\mathcal{Z}$, crosses the ζ plane on a line. Trajectories along this line are those living in the minimum and leading to the asymptotic future, either at the crossing point of **M** in a dS vacuum, or ultimately leading to collapse in an AdS vacuum. Trajectories crossing this line are modulus passages through, or oscillations about, the minimum. Trajectories in the full 6–d space, however, never cross each other: these are oscillations and static passages along the $\mathcal{Z}$–ζ crossing and are separated in the y–direction. These surfaces are shown in the expanding octant of the $\{z, r, t\}$ plot in Fig. 3.7, where we see the crossing of $\mathcal{Z}$ along a line in the dS, Minkowski and AdS example ζ planes, **M** lying in the $\mathcal{Z}$ plane, and crossing the dS plane at a point.

Fixed point **C** is the second critical line of the system, corresponding to an axion–modulus kinetic dominated (stiff fluid) solution. This critical line is the unit circle

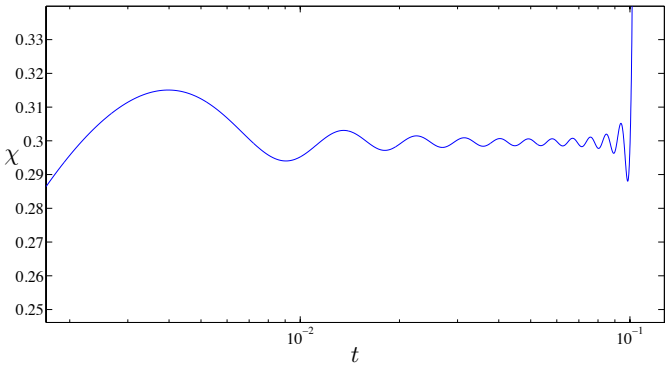

Figure 3.10 Evolution of the modulus field in a collapsing universe. As $a \to 0$ at $t \sim 10^{-1}$ the kinetic energy grows and dominates in fixed point **C** and the field value diverges. Since this would happen to *all* scalar fields and hence all moduli, this signals decompactification near a crunch. In this example plot the units and parameter values are all arbitrary.

$x_c^2 + y_c^2 = 1$ and is a symmetry of the autonomous system with $z_c = r_c = s_c = t_c = 0$. This is the usual enhancement of symmetry for massless scalar fields. In an expanding universe (where stability is ensured by negative eigenvalues of **W**), this point is always unstable. For a collapsing universe, a fixed point is stable if the eigenvalues of **W** are *positive*. This is because the 'time' variable $N \equiv \ln(a)$ of the autonomous system becomes a decreasing function of time. Hence, critical line **C** is stable in a collapsing universe and corresponds to the asymptotic future of any model with an AdS vacuum. This is consistent with the pre–big bang cosmology [252, 253] late time attractor solutions. The particular fixed point along **C** that the system will finally evolve to will depend upon the initial conditions of the system. Similarly to the phase space dynamics in the presence of a dS vacuum, the only possibility to save us from this Big Crunch cosmic doomsday is a temporary trapping in fixed point **B**. This situation was seen in the examples of Chapter 2 whenever ρ_Λ domination sets in before collapse and is achieved for large initial modulus values. This period of dS inflation would only be temporary however and the modulus will quickly relax into its AdS vacuum signalling cosmological collapse and leading to eventual decompactification as described in [254]. This is demonstrated in the example plot of Fig. 3.10: the growing kinetic energy of the modulus as $a \to 0$ drives it to large values.

All other fixed points are unstable in the presence of an AdS or dS vacuum. Points **D** and **E** correspond to 'dynamical modulus stabilisation' (slow roll and tracking) at

small modulus values ($z \neq 0$, $r = 0$), while **I** corresponds to dynamical stabilisation at large field values ($z = 0$, $r \neq 0$). This is of course only a meta–stability anyway, since these fixed points are unstable. Point **E** is also a scaling solution, on which the axion energy density vanishes ($\rho_\phi = 0$) and the modulus energy density scales with the dominant background fluid:

$$\rho_\chi = \frac{9H_i^2}{4C^2}\gamma_\mathrm{b}\left(\frac{a}{a_i}\right)^{-3\gamma_\mathrm{b}}, \quad w_\chi = \frac{3}{4}\frac{\gamma_\mathrm{b}(\gamma_\mathrm{b}-1)}{C^2}. \tag{3.28}$$

Hence, the modulus tracks the dominant background fluid and $\rho_\chi/\rho_\mathrm{b}$ remains constant.

Fixed point **F** represents a solution dominated by the modulus kinetic energy and the potential energy of the axion. On this solution, their relative energy densities and effective equation of state remains fixed:

$$\frac{\rho_\phi}{\rho_\chi} = \frac{6}{C^2} - 1, \quad w_\mathrm{eff} = \frac{1}{3}C^2 - 1. \tag{3.29}$$

The repulsive nature of fixed point **F** is illustrated in the left panel of Fig. 3.9.

The only fixed point which admits a non–vanishing background fluid density with a sizeable contribution from both axion and modulus is **G**. Here, the modulus energy density is dominated by its kinetic contribution, whilst the axion remains frozen, its motion suppressed by Hubble friction. Both the axion and modulus track the evolution of the dominant background fluid

$$\begin{aligned}\rho_\phi &= \frac{9H_i^2}{2C^2}\gamma_\mathrm{b}(2-\gamma_\mathrm{b})\left(\frac{a}{a_i}\right)^{-3\gamma_\mathrm{b}}, \\ \rho_\chi &= \frac{9H_i^2}{2C^2}\gamma_\mathrm{b}^2\left(\frac{a}{a_i}\right)^{-3\gamma_\mathrm{b}},\end{aligned} \tag{3.30}$$

whilst giving a background density $\Omega_\mathrm{b} = 1 - 3\gamma_b/C^2$. This dynamical attractor is precisely the axion and modulus tracking behaviour that was described in Chapter 2. It is in the combined equation of state

$$w_\mathrm{eff} = \frac{3\gamma_\mathrm{b}(\gamma_\mathrm{b}-1)}{C^2}, \tag{3.31}$$

(rather than the individual equations of state) that we see tracking as w_eff tries to follow the equation of state of the dominant component. Tracking is finally destroyed as axion oscillations begin. We show evolution into this fixed point in the right panel of Fig. 3.9.

Additional Comments on Fixed Point **G**

As a particularly interesting fixed point, we choose to discuss some additional phenomenology relating to fixed point **G**. Firstly we discuss accessibility of the fixed point. Even in the unbounded co-ordinates of an AdS minimum, approximate trapping in **G** requires variables other than $\{y, s\}$ to be approximately zero, and so flatness bounds us with $y^2 + s^2 < 1$, which defines a circle. This in turn imposes a constraint on C as a function of γ_b for **G** to be within this region:

$$C > \sqrt{3\gamma_b}; \quad \text{physically accessible } \mathbf{G}. \tag{3.32}$$

An interesting phenomenon when entering fixed points in a multi-field model is the possibility of multiple periods of accelerated expansion [227]. When projected down to the $\{y, s\}$ subspace the condition for $w < -1/3$ in an expanding universe becomes $s > \sqrt{(\frac{2-\gamma_b}{\gamma_b})(y^2 + \frac{\gamma_b - 2/3}{2-\gamma_b})}$.

A temporary trapping in point **B**, where there is a larger value of cosmological constant than in the true vacuum, could lead to a single period of accelerated expansion during an otherwise fluid dominated era. In such a case, the axion and modulus fields would pick up large additional isocurvature fluctuations from this brief period of inflation. This period would end when the fields move towards their vacuum, and as such the global minimum would have to be dS in order for this to be possible in our own universe.

The situation for **G** in this regard is more interesting. In a matter background, $\gamma_b = 1$, this is pictured in Fig. 3.11. Here we see that it is possible to have both a flat universe and $w < -1/3$ in a $\{y, s\}$ dominated phase. Trajectories in the $\{y, s\}$ subspace will spiral into **G** if the eigenvalues of the stability matrix **W** (that point in the $\{y, s\}$ directions) have an imaginary part. The stability analysis (see again Appendix A of [235]) reveals that this is the case if:

$$C^3 - 8C^2 + 24 > 0\,. \tag{3.33}$$

For the parameter space of interest, $C > 0$, this bound is satisfied for $C < 2$ and $C > 3 + \sqrt{21} \approx 7.6$. For any C between these two values, the eigenvalues are real and trajectories will not spiral into **G** but move in straight lines, and so cannot

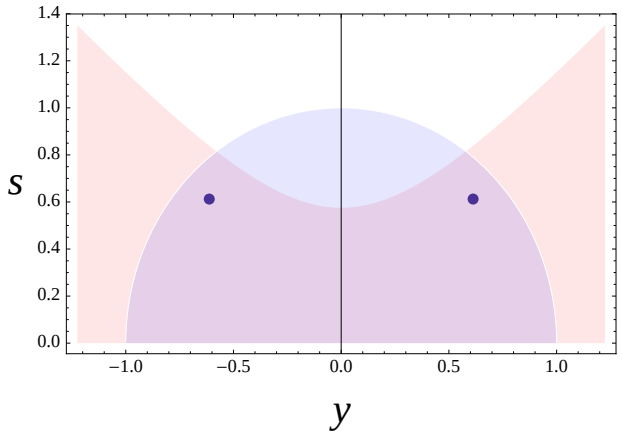

Figure 3.11 Constraints relevant to trajectories approaching the quasi-stable fixed point **G** with a background matter fluid, $\gamma_b = 1$. The blue shaded region under the semi-circle is the region allowed by the Friedmann constraint. The hyperbola bounds accelerated expansion, with the red shaded region having $w > -1/3$. The two points represent fixed point **G** for $s > 0$. For $C > \sqrt{3}$ these lie inside the allowed region. We conclude that it is possible for trajectories approaching **G** to cross the $w = -1/3$ divide if they spiral as they do so, possibly leading to multiple epochs of accelerated expansion.

cross $w < -1/3$. When Eq. (3.33) is satisfied however, the trajectories in $\{y, s\}$ can spiral toward **G**, having the possibility of crossing the $w < -1/3$ bound, perhaps multiple times. So, *trajectories approaching this fixed point can lead to multiple periods of accelerated expansion*. This phenomenon is extremely tightly constrained: such an epoch of acceleration must be less than 0.05 *e*–folds long [206]. This phenomenon is possible with both matter and radiation background fluids, however for a radiation background the accelerated region in $\{y, s\}$ space is smaller.

3.3.3 *Scanning Parameter Space*

Since the system of Eqs. (3.16) are first order and autonomous, they are very quick to integrate numerically. We exploit this nice property by performing a 'scan' of the model parameter space around regions of interest, selecting particular scenarios to investigate more systematically. We use our scans to further our qualitative understanding of the phenomenology of the model and to locate and single out specific novel features.

The autonomous system has eight different parameters which determine the subsequent motion of any given trajectory in phase space: six initial conditions,

$\{x_i, y_i, z_i, r_i, s_i, t_i\}$ and two parameters, $\{C, \beta\}$. To ensure that this rather large parameter space is sampled in a uniform and efficient way, we use the method outlined in Appendix C of [235], a method conceived by myself, but developed and implemented by Ewan Tarrant.

We briefly describe this process for initial conditions chosen to be close to fixed point **A**, i.e. beginning in the fluid dominated phase with a non–vanishing background fluid density, $\Omega_{\rm b}(\text{initial})$. It is trivially generalised to the case of any other fixed point. For **A**, with only some loss of generality, we make the simplifying assumption that the axion and modulus fields begin frozen, $x_i = y_i = 0$. Then, using the Friedmann constraint, Eq. (3.19), and the vacuum constraint, Eq. (3.20), we have

$$s_i^2 = p - \zeta \frac{r_i^4}{z_i^2} + r_i^2 - z_i^2 \,, \tag{3.34}$$

initially. Here, $p = 1 - \Omega_{\rm b}(\text{initial})$. For a choice of ζ, the initial conditions are constrained to lie on this three–dimensional manifold, which we will call $\mathcal{M}$. Scanning the initial conditions of the system then reduces to varying two initial conditions evenly over $\mathcal{M}$ with the third constrained by the equation for $\mathcal{M}$. We choose to vary z_i and r_i, whilst still being free to independently vary $\{C, \beta\}$. Since $\mathcal{M}$ has non–constant curvature, it is not trivial to sample it in a uniform way and so we use a statistical sampling method which is also presented in Appendix C of [235]. Choosing a value of $p \approx 0.01$ ($\Omega_{\rm b}(\text{initial}) \approx 0.99$) is our definition of 'near' to fixed point **A**.

We now begin to discuss the results and findings of our numerical analysis. Our ability to perform scans of this kind has many possible applications for investigating the cosmological phenomenology of our model. Here we choose to simply show some examples that illustrate the capabilities of our technique. All models we present have a dust background fluid, $\gamma_b = 1$ and a dS vacuum with $\zeta = 0.3$. We run two large simulations: `FP-A` and `FP-G`. For simulation `FP-A`, we evolve 562500 models, each chosen to begin near fixed point **A** with $\Omega_{\rm b}(\text{initial}) = 0.99$. We scan $\{C, \beta\}$ evenly in logarithmic space on a 25×25 grid, and at each point we use our initial condition algorithm to evenly sample the space of $\{z_i, r_i, s_i\}$ over $\mathcal{M}$. For `FP-G`, we evolve 506100 models, each chosen to begin near to fixed point **G**. Unlike simulation `FP-A`, we are not free to independently vary the initial conditions and C since in fixed point **G**,

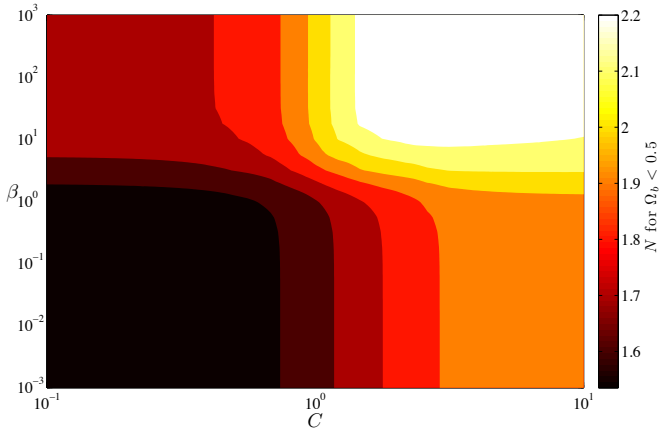

Figure 3.12 Contour plot of the number of e–folds, $N_{\rm efd}$, when $\Omega_b < 0.5$ for a scan over parameter space of all models beginning near fixed point **A** with $\Omega_b = 0.99$ (the `FP-A` simulation). Each point in $\{C, \beta\}$ represents an average over the initial condition manifold $\mathcal{M}$.

$\Omega_{\rm b} = 1 - 3/C^2$. Furthermore, $y_{\rm c} = \sqrt{\frac{3}{2}\frac{1}{C}}$ and so $y_i \neq 0$. Hence, every time C and y_i are changed, the shape of the initial condition manifold also changes. Therefore we absorb y_i and $\Omega_{\rm b}$ into the parameter p of Eq. (3.34): $p = \frac{3}{C^2} - y_i^2$. We then vary C logarithmically and y_i linearly across a 10×15 grid and use our initial condition algorithm to evenly sample the space of $\{z_i, r_i, s_i\}$ over $\mathcal{M}$ for each point, $\{C, y_i\}$, where $\mathcal{M}$ has a different shape. β is varied 15 times on a logarithmic scale.

In both simulations, individual models are terminated under two conditions: either they have settled into fixed point **M** for more than 5 e–folds, or, they have ran for a total of more than 500 e–folds. The results are presented so that at each point in $\{C, \beta\}$ space, the average over all trajectories on $\mathcal{M}$ is taken, or alternatively for each point in $\{z_i, r_i\}$ space we could average over parameters $\{C, \beta\}$, i.e. repeated points in any plane have their contour value averaged over the other parameters.

3.3.3.1 *The End of Fluid Domination*

In Fig. 3.12 we plot in the $\{C, \beta\}$ plane, for models from the `FP-A` simulation, the number of e–folds, $N_{\rm efd}$, from the beginning of the evolution until the end of fluid domination when $\Omega_b < 0.5$.

Before analysing the figure in more detail, it is first worth thinking about what

we should expect from such a number. The maximum across all models occurred for $N_{\rm efd} \approx 5.3$ while the minimum occurred for $N_{\rm efd} \approx 1.5$. It is simple to show from the Friedmann equation that a ΛCDM cosmology beginning with $\Omega_{\rm m}(\text{initial}) = 0.9$ will reach $\Omega_m = \Omega_\Lambda = 0.5$ after $N_{\rm efd} \approx 1.5$ e–folds. In the absence of energy input, a cosmological constant maximally decreases $(1 - \Omega_m)$: this should be the limiting case of our model when the fields are frozen, which indeed it is. On the other hand, a model beginning at matter-radiation equality at $a_{\rm eq} \approx 10^{-3}$ has $(1 - \Omega_{\rm m}(\text{initial})) \sim \mathcal{O}(10^{-9})$, and depending on $\Omega_{m,0}$ has $6 \lesssim N_{\rm efd} \lesssim 7$.

In our model $N_{\rm efd}$ can be increased and approach this limiting case in three ways. The fields can oscillate before they overtake the fluid density, they will then scale like matter, always remaining sub-dominant and the end of fluid domination will be caused by the cosmological constant. Secondly, they could enter a scaling solution, where they also remain a fixed sub-dominant fraction of the energy density. Thirdly, they could roll to the minimum of the potential, reducing the vev due to the negative energy term in the modulus only part of the potential. We see that our maximum of $N_{\rm efd}$ approaches the limiting case, being slightly below it as some time is taken for these dynamics to occur.

In Fig. 3.12 there is a clear correlation of $N_{\rm efd}$ with the parameters. Smaller average $N_{\rm efd}$ occurs for low β, where the axion mass is small preventing oscillations, and low C where the scalar field energy density in scaling solutions is large. Larger average $N_{\rm efd}$ occurs for large β and C where oscillations can occur earlier and the energy density in scaling solutions is smaller.

When considering models from `FP-G` (not shown) we imposed a cut for all $C < \sqrt{3}$, where **G** is unphysical (the initial conditions correspond to negative Ω_b). The first difference observed from fixed point **A** was a vertical line giving very low $N_{\rm efd}$ at small C. These models had initially very small Ω_b: the minimum of $N_{\rm efd}$ output from the code is $N_{\rm efd} = 0.005$ which is our numerical step size in N, i.e. the models began out of fluid domination. Since C sets the initial Ω_b for models beginning in **G**, the general trend of increasing $N_{\rm efd}$ with C continued and was dominant, until at large C and β it gave way to the effects described above in the case of **A**. Axion oscillations lead to a decrease in ϕ to $\phi < \tilde{\phi}$ and therefore spoiled **G** after some short time, decreasing the

overall scalar field density. In the case of an AdS negative potential minimum, these regions where **G** is spoiled would be those that eventually collapse.

3.3.3.2 *Multiple Periods of Accelerated Expansion*

Motivated by the fact that spiralling trajectories in phase space may generate multiple periods of accelerated expansion, we scan the model parameter space for this feature. We compute the number of periods of accelerated expansion, $\mathcal{N}_{\rm ae}$, by counting the number of times $w_{\rm total} = \sum_i w_i \Omega_i < -\frac{1}{3}$ along the model trajectory. Here, i labels the axion and modulus fields, the dust fluid and ρ_Λ. If one, or both scalar fields are oscillating about their minima, the *averaged* equations of state, $\bar{w}_\phi$ and $\bar{w}_\chi$ are used in the calculation of $w_{\rm total}$. The average taken is a moving average and is re–calculated every 0.005 e–folds as the trajectory advances in time. We define the onset of coherent oscillations as the time when the field velocity ($\dot{\phi}$ or $\dot{\chi}$) changes sign for the *third* time. This ensures that we do not average any heavily or critically damped oscillations. This definition is somewhat arbitrary and so we should expect that $\mathcal{N}_{\rm ae}$ may be sensitive to the definition of the averaging process. Furthermore, for regions of parameter space where the fields are highly oscillatory (large C and β), sampling the trajectory every 0.005 e–folds may not be frequent enough to accurately average a single oscillation. We also note that this sampling rate is one tenth of the length of a period of accelerated expansion allowed by observation. Hence, computing $\mathcal{N}_{\rm ae}$ by taking the moving average of w_ϕ and w_χ on such a time scale is not always the observationally relevant procedure.

With these limitations acknowledged, we consistently apply our definition of $\mathcal{N}_{\rm ae}$ to every single model in our simulations. From the `FP-A` simulation we found that of our 562500 models, 17668 had $\mathcal{N}_{\rm ae} > 1$. Of these, 676 models were terminated after 500 e–folds for not reaching fixed point **M**, so that the multiple $\mathcal{N}_{\rm ae}$ can be said to have definitely occurred near to a fixed point or the local minimum. We also found 54 models with the largest $\mathcal{N}_{\rm ae} = 8$. Of the remaining models with $\mathcal{N}_{\rm ae} = 1$, 176599 were terminated for not reaching **M** after 500 e–folds, and were thus still on the potential plateau trapped in **B**. $\mathcal{N}_{\rm ae}$ may increase in future for these models, but the time scale

is immense: situating them today, 500 e–folds gives $\Delta t = \Delta N / H_0 \sim 10^{12-13}$ years[6]. We stress that we are not proposing any measure or figure of merit for fine tuning in this model, and as such the specific number of models pertaining to each case does not have any (clear) meaning.

When considering the the distribution of $\mathcal{N}_{\rm ae}$ against $\{C, \beta\}$ we took all models with $\mathcal{N}_{\rm ae} > 1$ and averaged over $\mathcal{M}$ as described above. We found some large regions of parameter space with $\mathcal{N}_{\rm ae} = 1$ over all of $\mathcal{M}$. We also saw that there was a high density of large $\mathcal{N}_{\rm ae}$ at larger values of C and intermediate values of β, with one clear peak. We show these locations schematically in Fig. 3.13

Our results also showed an interesting correlation between three dependent (output) variables where it was noticed that trajectories with large $\mathcal{N}_{\rm ae}$ occurred in those cosmologies that at the exit from fluid domination (entering the current epoch) contained only small values of Ω_ϕ and $|\Omega_\chi|$ (it is consistent in this model to have $\Omega_\chi < 0$ since it does not contain ρ_Λ: the total energy density remains always positive). This, combined with the larger values of C in these regions, as we will discuss below, suggests that these models were likely in or near to **G** (or **B**) at this time (again, see the schematic Fig. 3.13). Small values of $|\Omega_\chi|$ and Ω_ϕ for light axions are those allowed by current data (we discuss some bounds in Section 3.4), but is also potentially detectable with next generation experiments (see Chapter 5 and [144]). Our scan suggests that such a cosmology could reasonably expect to undergo multiple periods of accelerated expansion in the future, and may have in its past. We re-state the bound from above: [206] showed that an intermediate epoch of accelerated expansion in the matter era must have lasted less than 0.05 e–folds.

Finally, our results showed that that almost all models with $\mathcal{N}_{\rm ae} > 2$ had begun on trajectories with $\phi > \tilde{\phi}$, i.e. with a destabilised modulus, and thus access to **G** (see below). We reiterate that we have only analysed the dS case in this example: such allowable cosmologies may undergo a different cycle of $\mathcal{N}_{\rm ae}$ before collapse in the AdS case.

[6]The time scale for collapse out of **B** or **G** for similar trajectories with an AdS minimum would be similar.

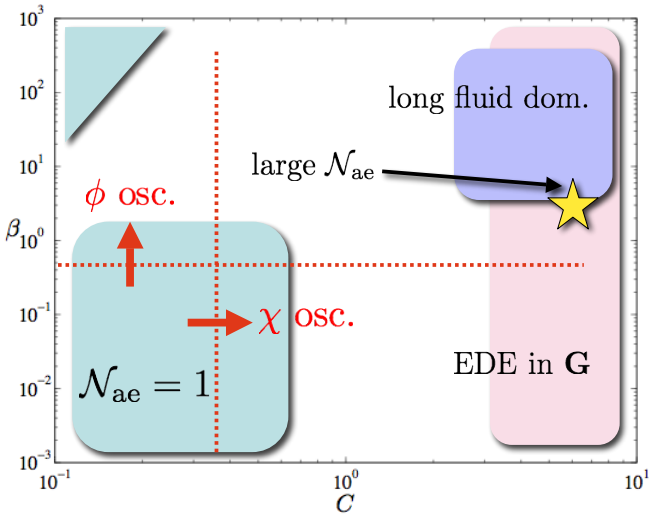

Figure 3.13 Schematic summary of findings in $\{C, \beta\}$ space. C is the exponent in the modulus potential, and gives the coupling between axion and modulus. β is defined in Eq. (3.9) and represents a ratio of scales between the axion and modulus terms in the potential. They are the only two parameters that appear in the dynamical system, Eqs. (3.16). The vertical and horizontal lines for field oscillations are the conditions of Eq. (32) of [235] that determine axion and modulus oscillations about **M** from the stability of the fixed point, and are shown for $\zeta \approx 0.3$ dS vacuum (see Eqs. (3.20), (3.21)). They move in the directions shown for increasing ζ. The regions with $\mathcal{N}_{\rm ae} = 1$ periods of accelerated expansion over all initial conditions only occurred for models from the `FP-A` simulation.

3.4 DISCUSSION

3.4.1 *Phenomenology of Fixed Points*

The analysis in Section 3.3 showed the existence of many fixed points, with various degrees of stability. Discussing the possible phenomenological implications of all of these would be a long and tedious process that we choose not to engage in. However, we will find it illuminating to discuss some properties of fixed point **G**, both by way of example, and since we will find them to be particularly interesting.

The first thing to note about the fixed points is whether or not they occur in the bowl of the potential or on the plateau. We have that $s/r = \phi/\tilde{\phi}$, so that if $s/r > 1$ the fixed point is on the plateau where the modulus is destabilised. For points **G** and **F** it is clear that they are on the plateau. Fixed point **B** has $s = r = 0$, so the ratio is undefined, and is technically at infinite modulus value. Hence in Chapter 2 temporary trapping was observed with large initial field values and a destabilised modulus, with

exit from the fixed point occurring as the axion field value decayed.

G is the only fixed point that allows for scaling solutions where both axion and modulus track the dominant fluid component. This was the tracking behaviour observed in Chapter 2. This can be of particular use in *alleviating fine tuning of axion initial misalignment angles* in the following way. Heavy axions require fine tuning of their initial misalignment angle if they are not to 'overclose' the universe by causing matter-radiation equality to occur at too high a redshift: they are outside the 'anthropic window' (see Chapter 4 and [104, 202, 203]). However, by allowing for tracking in the radiation era, the axion energy density will scale as $1/a^4$, instead of remaining a constant. Eventually oscillations will set in, since **G** is a saddle point, and the axion dark matter will scale as $1/a^3$, however this will begin from a lower energy density. The energy density is dumped into modulus kinetic energy of overdamped motion, and reduces the axion mass. This scaling will manifest as EDE, which we discuss in the next subsection. The difference to more standard tracking models is that the saddle point nature of **G** caused by the axion mass provides a natural mechanism for exit from tracking. Also in this model the tracking EDE field is not required to be the same as the field responsible for late time accelerated expansion, i.e. we have the additional ρ_Λ.

3.4.2 *Early Dark Energy*

Temporary trapping in **G** during the radiation era is phenomenologically attractive because, as also pointed out in Chapter 2, it has the possibility of leaving observable, and therefore constrainable, consequences as EDE. When is this situation possible? First, the modulus must be destabilised by axion initial misalignment, given by the bounds of Eqs. (3.10) and (3.11). The modulus will roll out towards $\chi \to \infty$ until Hubble friction stops it (if in additon $C < \sqrt{6}$ then a temporary axion-modulus domination in **F** will occur). Later, if the bound of Eq. (3.32) is satisfied, tracking will begin. The effects of this will further bound C.

The axion-modulus EDE energy density contributes an amount $\Omega_e = \Omega_\phi + \Omega_\chi = 3\gamma_b/C^2$ during any period of tracking. EDE phenomenology places upper bounds on

Ω_e that translate simply to bounds on C; in the radiation era this is:

$$C > 2\Omega_e^{-1/2}\,. \tag{3.35}$$

During the radiation era the scaling EDE will behave as an extra effective relativistic species, $\Delta N_{\rm eff}$, contributing to the background expansion. The density contribution can then be constrained by BBN and CMB bounds on $N_{\rm eff}$. For example, the BBN constraints of [255] allow for $N_{\rm eff} = 3.85 \pm 0.26$, consistent with no change between BBN and the CMB. Taking the central value, parameterising the energy density as [256, 257], and assuming all the additional energy density to be in the form of EDE allows for $\Omega_e \lesssim 0.1$:

$$C \gtrsim 6.2 \quad \text{BBN } \Delta N_{\rm eff} \text{ only, [255].} \tag{3.36}$$

This large value of Ω_e would, however, be in conflict with the CMB (the agreement in [255] was for $N_{\rm eff}$ only, and neutrinos behave differently in perturbations than EDE due to, for example, anisotropic stress). One of the main effects of the presence a sizeable Ω_e on the CMB is to change the location and amplitude of the acoustic peaks. The location of the first peak is related to the size of the sound horizon at decoupling which is given by

$$r_s(a) = \int_0^a \mathrm{d}a \frac{\mathrm{d}\tau}{\mathrm{d}a} c_s\,. \tag{3.37}$$

Here, $c_s^{-2} = 3(1+R)$ is the sound speed of the photon–baryon fluid and $R(a) = \frac{3}{4}\frac{\rho_b}{\rho_\gamma}$ is the photon to baryon ratio. Using the Friedmann equation today (subscript 0) and at an epoch during the radiation era when the universe has evolved to point **G** yields:

$$\left(\frac{\mathrm{d}a}{\mathrm{d}\tau}\right)^2 = H_0^2\left[\frac{\Omega_{m,0}a + \Omega_{\gamma,0}}{1-\Omega_e}\right]\,. \tag{3.38}$$

In order to estimate the effect, we will assume a constant $\Omega_e = \frac{3\gamma_b}{C^2}$ despite the presence of *two* background components, radiation, subscript γ, *and* matter (dark and baryonic), subscript m. This amounts to assuming that the change in Ω_e between equality and last scattering will not significantly affect the time variation of the Hubble parameter, i.e. the EDE is very sub dominant.

Performing the integral in Eq. (3.37) (similarly to [258]) labeling the last scattering surface (ls) and the epoch of matter radiation equality (eq) gives:

$$r_s = \frac{4}{3H_0}\sqrt{1-\frac{3\gamma_b}{C^2}}\sqrt{\frac{\Omega_{\gamma,0}}{\Omega_{m,0}\Omega_{b,0}}} \times \ln\left[\frac{\sqrt{1+R_{\rm ls}}+\sqrt{R_{\rm ls}+R_{\rm eq}}}{1+\sqrt{R_{\rm eq}}}\right] = \sqrt{1-\frac{4}{C^2}}r_{s0}\,, \tag{3.39}$$

where r_{s0} is the standard sound horizon, we have *assumed* that last scattering is unaffected by the EDE, and we have *defined* equality using matter and radiation only. The location of the first peak multipole is then:

$$l_{\rm peak} \approx \frac{2\pi}{r_s H_0} = \frac{C}{\sqrt{C^2-3\gamma_b}}l_0\,, \tag{3.40}$$

where the standard peak multipole is:

$$l_0 = \frac{2\pi}{r_{s0}H_0} \approx 200\,. \tag{3.41}$$

The qualitative behaviour is clear: for smaller C, i.e., for larger Ω_e, the first peak occurs at a higher multipole. Ref. [259] performed simultaneous fits for Ω_e and neutrino species along with other extended cosmological parameter sets, and found maximum values for Ω_e at the 95% confidence level of a few percent, with the absolute limit being dependent on priors about the DE ($w > -1$: no crossing of the phantom divide) or the neutrinos ($N_{\rm eff} > 3$ from the standard model). The central value for $N_{\rm eff}$ in these fits was around $N_{\rm eff} \sim 3.6 \pm 0.6$. Taking the most generous upper limit of $\Omega_e < 0.042$ gives:

$$C \gtrsim 9.8 \quad \text{CMB and } \Delta N_{\rm eff}\text{, [259].} \tag{3.42}$$

Currently, there is no detection of Ω_e, but it will be possible to detect with current and future CMB experiments of Planck and CMBPol [144]. Ref. [144] reports, for a fiducial Planck central value of $\Omega_e = 0.03$ and marginalising over their other extended DE parameters, an error of $\sigma_{\Omega_e} = 0.003$. A 3σ measurement of Ω_e at the fiducial value translates to a bound:

$$10.1 \lesssim C \lesssim 13.8 \quad \text{Planck forecast, [144].} \tag{3.43}$$

It is worth noting finally that the CMB and BBN bounds need not both apply, since the fields do not have to have entered the scaling solution at any particular era, and

can leave it. Of course there is also the caveat that these bounds only apply to the extent that motion in and near **G** is accurately described by the parameterisations used to derive them ([259] used a modified version of the parameterisation of [260]), and that approximately stable evolution in **G** can be maintained for long enough.

In Fig. 3.13 we show a schematic for the phenomenology in different regions of $\{C, \beta\}$ parameter space that the results of this discussion and Section 3.3.3 have led us to.

3.4.3 *The Assumption of Fixed f_a, and Uplifting the Potential*

Throughout this Chapter, and Chapter 2, as we have mentioned, we have assumed that f_a can be taken fixed and that the modulus only effects the axion through exponentially scaling the mass. This had the simplifying property of providing a trivial metric on field space, with no change to the canonical kinetic terms. We can look at the validity of this assumption by computing what the change in f_a would be along any particular trajectory. The assumption will be approximately valid if:

$$|\Delta f_a| / f_{a,0} \lesssim 1 \,, \tag{3.44}$$

where $f_{a,0}$ is the point on the trajectory deemed to be 'today' and the difference is calculated from the last relevant epoch. In the axiverse the scale of f_a is fixed around 10^{16} GeV by fixing the product $S = C\chi \sim 200$. This does not appear in our dynamical systems analysis, since the scale of χ only comes in via ω, which the system does not depend on.

As mentioned in Section 3.2, and computed in Eq. 3.12, the change in f_a will most likely be large for any trajectories that begin on the plateau of the potential and end in the bowl. This would require us to compute corrections in moving, for example, *between* fixed points **G**, **B** and the global minimum **M**. In the vicinity of the fixed points, checking that f_a remains roughly fixed would require specifying ω and checking on a case-by-case basis.

It is possible that trapping in **G**, or any fixed point with non-zero y, for an extended period of time could lead to large $\Delta f_a / f_a$. We can estimate this effect as follows. For a trapping of ΔN e–folds in **G** and setting $C\chi_i = 200$ to get the correct f_a for the

axiverse in the early universe, factors of C cancel and we have:

$$\frac{\Delta\chi}{\chi_i} = -\frac{\Delta f_a}{f_{a,0}} = \frac{3\gamma_b}{200}\Delta N = \mathcal{O}(10^{-2})\Delta N\,. \tag{3.45}$$

This will always be small for any scenarios of interest, since ΔN could only be large if **G** were driving inflation but we have seen that **G** itself cannot be accelerated and hence this is impossible. f_a today will be only ΔN% away from its initial value for small ΔN, and therefore predictions based on trapping in **G** in any particular epoch should be unaffected by our assumption of fixed f_a. However, in predicting the fate of the universe, we emphasise again that **G** is unstable and moving into **M** in the future (or in the current epoch, as in [244]) may entail large changes in f_a.

While the dynamical effect of changing the kinetic terms is hard to predict, it is simple to compute the change in the potential caused by identifying $f_a = \frac{1}{C\chi}$. The coupling term in the potential becomes:

$$U(\phi,\chi) = \frac{\mu^4}{2}C^2 e^{-C\chi}\chi^2\phi^2\,. \tag{3.46}$$

This has one very interesting property: the emergence of a new, meta-stable (in the sense that it has a small barrier that can be tunnelled through, like the potentials of [219]) modulus minimum in the region of large ϕ. This meta-stable minimum can have *positive cosmological constant, with no need for additional uplifting*, i.e. with $\rho_\Lambda = 0$. However, it is unstable in the axion direction, and could only usefully drive current accelerated expansion with an ultra-light axion of mass $m_a \lesssim 10^{-33}$ eV. The emergence of the new minimum at large ϕ can be traced to the extra term in $\partial_\chi U$ with opposite sign.

For the new minimum to emerge one requires $\chi < 2/C$ which makes $S \sim \mathcal{O}(1)$ and pushes $f_a \to M_{pl}$. This leads to more fine tuning if this minimum is to provide late time acceleration since the small axion mass necessary for stability then needs to be put in by hand from the non-perturbative side, ruining the naturalness of the axiverse scenario for light axions. We leave further study of the properties of this $f_a(\chi)$ scenario, particularly its possibility of giving an alternative axion inflationary model, to a future work.

3.5 CONCLUSIONS

In this Chapter we have studied a rich model of the dark sector involving axions and moduli, with many possible observational signatures as DM and DE, that extends and builds on well known work and tries to bring it into a broader theoretical context. Some of our findings are summarised in the schematic of Fig. 3.13.

Axions and moduli are intimately linked to the problem of the cosmological constant. Polchinski argued some time ago [261], and indeed it has been known since the earliest days of string theory [192, 262] that the lightness and profusion of axions is a natural consequence of the theory, and is related to the anthropic demand for a small cosmological constant. Ultra-light axion fields with the hierarchy of masses generated by exponential dependence on the internal geometry of the compact space are observationally relevant as a distinct form of dark matter. We have studied the cosmological evolution of axions when the energy scale of the potential is allowed to be dynamically controlled by a modulus of this geometry, instead of remaining fixed. If both the potential of the axion and the modulus arise from non-pertrubative physics at similar energy scales, then we have shown that axion initial misalignment can leave the modulus destabilised in the early universe and when the axion is allowed to be cosmologically light this can lead to significant evolution of the modulus throughout cosmic history. This evolution allows for the possibility that the vacuum energy can change sign through the course of cosmic evolution, with today's quasi de-Sitter expansion being only temporary and the future evolution of the universe is a Big Crunch cosmic doomsday. We have demonstrated the topological change in the allowed phase space that such a possibility creates in two separate coordinate systems.

By looking for fixed points of the dynamical system we have shown that a modulus destabilised by a large axion initial misalignment gives rise to a scaling solution where excess energy density in the axion field is redshifted away during the radiation era. One can always argue that a valid model must cut off the fine tuning on axion fields to values where there is a stable modulus, and we have shown the ratios of scales necessary for this. Alternatively, if destabilisation does occur and such a tracking behaviour ensues during cosmic evolution, then fine tuning on the axion dark matter

is alleviated and in addition observational limits on EDE place constraints on the couplings of the model.

We have not discussed the possibility of fitting this model to be cosmologically viable, which would require fixing H_0 and $w(z)$, among other things. Fits of this kind would allow comparison to current and projected constraints on $w(z)$ and distance measurements (see, e.g. [67, 68, 142]), and in the context of this model trapped in **B** or **G** would allow predictions for future vacuum decay to dS in **M** [244] or collapse [234, 263]. It is worth noting, however, that even small uncertainties in the curvature, Ω_k, can produce significant degeneracies and misestimations of $w(z)$ from distance measurements alone [71, 72], which highlights the need for more complete models, and use of more experimental estimators, when discussing non-standard models of DE. We have also not discussed perturbations, which would be necessary to compare this model properly to LSS or CMB measurements.

If the modulus in this model controlled a coupling of the standard model, then predictivity of any model building will demand for it to be stabilised, and observational constraints will demand variations caused by axion evolution to be small, although potentially observable (see, e.g., [264, 265])[7]. Our analysis showed that this would lead to a tuning on axion initial misalignment, in addition to any related to dark matter density, if $\phi_i < \tilde{\phi}$. If this bound is violated and the modulus is destabilised, any low energy constants that depend on it will be stabilised by Hubble friction and eventually scale according to the dynamics of a fixed point. We have shown that trapping in such a fixed point can reasonably maintain the axion decay constant, f_a, and so may also be expected to naturally maintain any other constant with similar modular dependence. Anthropically, the meta-stability of this state of affairs is only as unnatural as a generic model allowing for a future Big Crunch.

The future singularity allowed in the parameter space of this model changes the asymptotic structure of spacetime and may be relevant to holographic models, or 'Cosmology/CFT' [266–269], although a rolling rather than tunnelling to an AdS state in our model may trivialise any specific holographic mapping. Allowing for long

[7]Many analyses of this kind, however, fail to account for the huge effect that variation in α would have on the standard model contribution to the vacuum energy through vacuum bubbles, at best greatly worsening fine tuning, and at worst ruining most anthropic explanations for the smallness of Λ.

lived unstable scalar potentials muddies the waters somewhat in the question of fine tuning in the landscape. The axiverse and supergravity [249, 263, 270, 271] naturally allow for scalar masses around H_0, but string quintessence models run up against many problems [272], although for axions successful models do exist [230, 273, 274][8]. However, if the landscape favours instabilities [276] and they appear to be a necessary feature in eternal inflation [268], it certainly seems pertinent to study their cosmology.

Could it be that the seemingly unlikely situation of many light axions pulling the moduli hither and thither in ultimately collapsing universes in fact opens up a whole new part of the 'wasteland', or that axion friction can favour a large number of destabilised moduli and a natural route to non-trivial quintessence? What types of universe dominate the (admittedly controversially-defined) landscape volume: unstable, cosmological constant, cyclic or quintessence? We have also seen that a coupling of axions and moduli can allow for large variations of the cosmological constant in the future, making multiple epochs of accelerated expansion possible during the matter dominated epoch in our past (observationally tightly constrained by [206]), or in the future evolution of the universe. Does this, too, effect our perception of fine tuning in relation to DE?

In closing, we like to hope that the study of this model will motivate string theorists to further consider late time effects that the existence of ultra-light axions can have on diverse aspects of string cosmology, and demonstrate the detailed study of a rich model of the dark sector to cosmologists.

[8]During the final stages of preparation of this manuscript a very interesting model for natural, and indeed coupled, quintessence in string theory was proposed in [275]. In particular, this involved a modulus controlling the size of a four-cycle, which in Type IIB theory in which this model is constructed can have a C_4 axion associated to it. The mass of this axion will depend on the quintessence field, realising our model. In that work, the important constraints of fifth-force experiments and predictions for SUSY breaking are also addressed.

4

ULTRA-LIGHT AXIONS AND STRUCTURE FORMATION

"The body of reality is infinite; its substance neither increases nor decreases. It can be great or small, square or round; it manifests visible forms in accordance with things and beings, like the moon reflected in water."

Ma Tsu (709 – 788), in *Classics of Zen and Buddhism, T. Cleary*

PREFACE

This Chapter begins our formal study of the cosmology of ultra-light axions with perturbations about homogeneity. We take the quadratic potential and both numerically and analytically solve the equations of motion for the background and perturbations. This allows us to see exactly how the axions suppress the formation of structure, at what scales, and by how much. The work in this Chapter is based on Ref. [233].

4.1 THE FORMALISM: EQUATIONS OF MOTION

The axion Lagrangian is given by:

$$\mathcal{L} = -\frac{1}{2}(\partial\phi)^2 - \frac{1}{2}m_a^2\phi^2 \,. \tag{4.1}$$

We work in first order cosmological perturbation theory of the FLRW metric, in

the synchronous gauge, as presented in [40]. The line element is:

$$ds^2 = a^2(\tau)[-d\tau^2 + (\delta_{ij} + h_{ij})dx^i dx^j]\,, \tag{4.2}$$

where $a(\tau)$ is the scale factor, and τ is conformal time. The scalar modes of h_{ij} can be written as a Fourier integral in terms of the two fields $h(\vec{k},\tau)$ and $\eta(\vec{k},\tau)$:

$$h_{ij}(\vec{x},\tau) = \int d^3k e^{i\vec{k}\vec{x}}[\hat{k}_i\hat{k}_j h(\vec{k},\tau) + (\hat{k}_i\hat{k}_j - \frac{1}{3}\delta_{ij})6\eta(\vec{k},\tau)]\,, \tag{4.3}$$

where $\hat{k}_i$ is a unit vector in the i^{th} direction.

For a perfect fluid of energy density ρ and pressure P the energy momentum tensor is given by:

$$\begin{aligned} T^0{}_0 &= -(\rho + \delta\rho)\,, \\ T^0{}_i &= (\rho + P)v_i\,, \\ T^i{}_j &= (P + \delta P)\delta^i_j\,, \end{aligned} \tag{4.4}$$

where ρ and P are the average density and pressure, and $\delta\rho$ and δP represent first order perturbations about homogeneity and isotropy. To zeroth order, the Einstein equations give the Friedmann:

$$\mathcal{H}^2 = \left(\frac{\dot{a}}{a}\right)^2 = \frac{8\pi G}{3}a^2\rho\,, \tag{4.5}$$

where an overdot denotes a derivative with respect to conformal time τ. There are four first order equations, of which we will use two:

$$k^2\eta - \frac{1}{2}\mathcal{H}\dot{h} = 4\pi G a^2 \delta T^0{}_0\,, \tag{4.6}$$

$$\ddot{h} + 2\mathcal{H}\dot{h} - 2k^2\eta = -8\pi G a^2 \delta T^i{}_i\,, \tag{4.7}$$

from which η can be eliminated, leaving us with a second order equation for h:

$$\ddot{h} + \mathcal{H}\dot{h} = 8\pi G a^2[\delta T^0{}_0 - \delta T^i{}_i]\,. \tag{4.8}$$

To couple a scalar field to these equations we compute the energy momentum tensor from the variation of the action, the invariant integral of Eq.(4.1), with respect to the metric in the usual way:

$$T^\mu{}_\nu = \phi^{,\mu}\phi_{,\nu} - \frac{1}{2}(\phi^{,\alpha}\phi_{,\alpha} + 2V)\delta^\mu_\nu\,. \tag{4.9}$$

Working to first order in perturbations about a homogeneous field:

$$\phi(\vec{k},\tau) = \phi_0(\tau) + \phi_1(\vec{k},\tau)\,, \tag{4.10}$$

we have, for a quadratic potential $V(\phi) = (1/2)m^2\phi^2$:

$$\rho_a = \frac{a^{-2}}{2}\dot{\phi}_0^2 + \frac{m^2}{2}\phi_0^2\,, \tag{4.11}$$

$$\delta\rho_a = a^{-2}\dot{\phi}_0\dot{\phi}_1 + m^2\phi_0\phi_1\,, \tag{4.12}$$

$$P_a = \frac{a^{-2}}{2}\dot{\phi}_0^2 - \frac{m^2}{2}\phi_0^2\,, \tag{4.13}$$

$$\delta P_a = a^{-2}\dot{\phi}_0\dot{\phi}_1 - m^2\phi_0\phi_1\,, \tag{4.14}$$

$$(\rho + P)\theta_a = a^{-2}k^2\dot{\phi}_0\phi_1\,. \tag{4.15}$$

The advantage of the synchronous gauge is that all of these quantities are independent of the metric perturbations.

Next we require the equations of motion for ϕ_0 and ϕ_1, which are found from the Lagrangian, Eq. (4.1) in curved space:

$$\ddot{\phi}_0 + 2\mathcal{H}\dot{\phi}_o + m^2a^2\phi_0 = 0\,, \tag{4.16}$$

$$\ddot{\phi}_1 + 2\mathcal{H}\dot{\phi}_1 + (m^2a^2 + k^2)\phi_1 = -\frac{1}{2}\dot{\phi}_0\dot{h}\,. \tag{4.17}$$

To obtain the evolution equations for perturbations in the dust CDM and the radiation we use conservation of energy momentum, $T^{\mu\nu}{}_{;\mu} = 0$, in k-space to obtain the first order conservation equations:

$$\dot{\delta} = -(1+w)\left(\theta + \frac{\dot{h}}{2}\right) - 3\mathcal{H}\left(\frac{\delta P}{\delta\rho} - w\right)\delta\,, \tag{4.18}$$

$$\dot{\theta} = -\mathcal{H}(1-3w)\theta - \frac{\dot{w}}{1+w}\theta + \frac{\delta P/\delta\rho}{1+w}k^2\delta - k^2\sigma\,. \tag{4.19}$$

The variables θ and σ are defined as:

$$(\rho + P)\theta \equiv ik^j\delta T^0{}_j\,, \tag{4.20}$$

$$(\rho + P)\sigma \equiv -(\hat{k}_i\hat{k}_j - \frac{1}{3}\delta_{ij})\Sigma^{ij}\,. \tag{4.21}$$

$\Sigma^i{}_j$ is the traceless component of $T^i{}_j$, a perturbation we henceforth ignore; $w = P/\rho$ is the equation of state, and $\delta = \delta\rho/\rho$ is the overdensity (we could also use this formalism with the fluid dynamical variables of Eqs. (4.11, 4.12, 4.13, 4.14) to treat

the scalar field [115]. This provides considerable simplification if assumptions can be made about the axion sound speed and equation of state. We will make use of this description extensively in Chapter 6).

We work with no baryons coupled to the photon fluid. The equations of state are $w_\gamma = (P/\rho)_\gamma = (\delta P/\delta\rho)_\gamma = 1/3$, and $w_c = (P/\rho)_c = (\delta P/\delta\rho)_c = 0$. Therefore for CDM there is no growing mode for the velocity perturbation ($\sim \theta$) and so the synchronous gauge defines a frame comoving with the CDM, i.e. $\theta_c = 0$. The EOMs are:

$$\dot{\delta}_c = -\frac{1}{2}\dot{h}\,, \tag{4.22}$$

$$\dot{\delta}_\gamma = -\frac{4}{3}\left(\theta_\gamma + \frac{\dot{h}}{2}\right)\,, \tag{4.23}$$

$$\dot{\theta}_\gamma = \frac{1}{4}k^2\delta_\gamma\,. \tag{4.24}$$

4.2 BACKGROUND EVOLUTION AND PRODUCTION OF ALPS IN THE EARLY UNIVERSE

We are interested in scenarios containing a fraction of the total energy density today in an ultra-light scalar field, therefore we would like to be able to specify Ω_a in terms of the initial displacement of the field, ϕ_i, or equivalently the initial misalignment angle, θ_i (not to be confused with the fluid-dynamical variable θ). To do this we look for an analytic solution to the equation of motion, Eq. (4.16). This is most easily done in physical time, defined by $dt = a(\tau)d\tau$. In this subsection, overdots will denote derivatives with respect to t, so that the Hubble parameter is given by $H(t) = \dot{a}/a$.

We work in reduced Planck units $1/m_{pl}^2 = 8\pi G = 1$. Next we rescale to use dimensionless variables $t \to H_0 t$, $H \to H/H_0$, $\phi \to \phi/m_{pl}$, $m \to m/H_0$, where H_0 is Hubble today, and remain in these variables until we discuss the matter power spectrum in Section 4.5. The equations governing the background become:

$$\ddot{\phi}_0 + 3H\dot{\phi}_0 + m^2\phi_0 = 0\,, \tag{4.25}$$

$$H^2 = \frac{\rho_a(t)}{3} + \frac{\Omega_c}{a^3} + \frac{\Omega_\gamma}{a^4} + \Omega_\Lambda\,, \tag{4.26}$$

where the density in ALPs is now given by:

$$\rho_a(t) = \frac{1}{2}\dot{\phi}_0^2 + \frac{1}{2}m^2\phi_0^2 \,. \tag{4.27}$$

Eq. (4.25) can be solved in terms of Bessel functions if we take the ansatz $a(t) \propto t^p$, which is true in both radiation dominated (early time), and matter dominated (late time) eras, giving:

$$\phi_0(t) = a(t)^{-3/2}(mt)^{1/2}(AJ_n(mt) + BY_n(mt)) \,, \tag{4.28}$$

with $n = (1/2)\sqrt{9p^2 - 6p + 1}$. We ignore the Y_n solution since it is singular at early times where we know that ϕ_0 should take its value from the misalignment angle. The asymptotic forms of J_n tell us how the energy density in a scalar field redshifts at early and late times and exhibits a well know feature of scalar field evolution in an expanding universe. For $mt \ll 1$:

$$J_n(mt) \approx \frac{1}{\Gamma(n+1)}\left(\frac{mt}{2}\right)^n \,. \tag{4.29}$$

Substituting into Eq. (4.28), along with $a \propto t^p$ yields:

$$\phi_0(t) \propto t^{-\frac{3}{2}p} t^{\frac{1}{2}} t^n \,, \tag{4.30}$$

which gives $\phi_0 = \textbf{const}$. for both the radiation dominated era ($p = 1/2$, $n = 1/4$) and the matter dominated era ($p = 2/3$, $n = 1/2$). This in turn shows that the energy density remains a constant in this regime: at early times the energy density in ALPs redshifts like a cosmological constant.

Later, such that $mt \gg 1$, we have that:

$$J_n(mt) \approx \left(\frac{2}{\pi mt}\right)^{1/2} \cos\left(mt - \frac{n\pi}{2} - \frac{\pi}{4}\right) \,. \tag{4.31}$$

Substituting $H = p/t$, and $\delta = \frac{n\pi}{2} - \frac{\pi}{4}$ now gives:

$$\begin{aligned} \rho_a(t) &= \frac{A^2m^2}{\pi}\frac{1}{a^3}\left(1 + \frac{3p}{mt}\cos(mt-\delta)\sin(mt-\delta) + \frac{9}{4}\frac{p^2}{(mt)^2}\cos^2(mt-\delta)\right) \,, \\ &\propto \frac{1}{a^3} + \mathcal{O}((mt)^{-1}) \,. \end{aligned} \tag{4.32}$$

for all values of p. We see that at late times the energy density in axions redshifts like ordinary matter regardless of the background expansion.

What these simple observations do not tell us about is the transition in the axion behaviour, and how this transition can affect the expansion rate and age of the universe if it contains a significant fraction of DM in ALPs. As we will see later there are novel effects even here in the background.

For now we will continue to work analytically and delineate two important scales in the evolution, an important region of ALP parameter space, and set the initial condition on ϕ_0 for a given Ω_a.

The axion field starts oscillating in the crossover between the two asymptotic expressions for the Bessel function, when $mt_{\rm osc} \approx 1$, which is the same order as the time when the mass overcomes the Hubble drag, $m \approx 3H(t_{\rm osc}) = 3p/t_{\rm osc}$. This defines one scale in the problem. The background evolution will depend on whether this occurs in the radiation or matter dominated era, defined by $\rho_m(a_{\rm eq}) = \rho_\gamma(a_{\rm eq})$, where $\rho_m = \rho_c + \rho_a$, the total density in matter. If the field has begun oscillations in the radiation dominated era then it will be redshifting like matter and contribute as usual when deriving $a_{\rm eq} = \Omega_\gamma/\Omega_m$. However, if the ALPs begin oscillating in the matter dominated era, they will be redshifting as a cosmological constant at equality and will contribute negligibly to ρ_m (as long as they are subdominant to CDM today). In particular, we can ignore $\rho_a(t)a^4/\rho_c(t_0)$, so that if the ALPs make up a fraction, f_{ax}, of the total density in matter today, we obtain the modified formula for the scale factor at equality:

$$a_{\rm eq} = \frac{\Omega_\gamma}{\Omega_m}\frac{1}{(1-f_{ax})}\,, \tag{4.33}$$

with $\Omega_m = \Omega_c + \Omega_a$. For ALPs that begin oscillations in the matter era, this change to the redshift of equality will have knock-on effects for the estimation of other cosmological parameters via degeneracies.

The temperature of the CMB fixes $\Omega_\gamma \approx 8 \times 10^{-5}$. Then using $\Omega_m \sim \Omega_c \sim 10^4\Omega_\gamma$, simple substitution gives that $(m/H_0) \sim \mathcal{O}(10^6)$ separates fields that begin oscillations during the radiation and matter dominated eras.

We can estimate the contribution to the critical density today coming from ALPs

by assuming an instantaneous transition from Λ to DM behaviour and redshifting the initial constant energy density from $a(t_{\rm osc})$ to $a(t_0) = 1$ as if it were ordinary CDM. We have that:

$$\begin{aligned} a_{\rm osc} &= \left(\frac{t_{\rm eq}}{t_0}\right)^{1/6} \left(\frac{1}{m t_0}\right)^{1/2}; \qquad m \gtrsim 10^6\,, \\ a_{\rm osc} &= \left(\frac{1}{m t_0}\right)^{2/3}; \qquad m \lesssim 10^6\,, \end{aligned} \tag{4.34}$$

which leads to (noting that we are using units where $H_0 = 1$):

$$\Omega_a = \left(\frac{t_{\rm eq}}{t_0}\right)^{1/2} \left(\frac{1}{t_0}\right)^{3/2} \frac{m^{1/2}}{6} \phi_0(t_i)^2; \qquad m \gtrsim 10^6\,, \tag{4.35}$$

$$\Omega_a = \frac{1}{6}\left(\frac{1}{t_0}\right)^2 \phi_0(t_i)^2; \qquad m \lesssim 10^6\,. \tag{4.36}$$

These expressions can be easily inverted to find an expression for the initial condition $\phi_0(t_i, \Omega_a)$. In our numerical analysis we supplement these with an iteratively improved constant to take into account the ALP effects on t_0, and $t_{\rm eq}$.

There are two remaining quantities to be determined, if we take the initial scale factor, a_i, as an input parameter: t_i and t_0. We begin in the radiation dominated era, so that:

$$t_i = \left(\frac{t_{\rm eq}}{t_0}\right)^{-1/3} a_i^2 t_0\,. \tag{4.37}$$

We know t_0 for a matter dominated universe from the Hubble time: $t_0 = 2/3$. Neglecting effects of the ALPs (we will address this in more detail in Section 4.4) then we can include the effect of Λ on our initial conditions by integrating Eq. (4.26). The calculation can be found in e.g. [29]:

$$t_0 = \frac{2}{3}\Omega_\Lambda^{-1/2} \sinh^{-1}\left(\left(\frac{\Omega_\Lambda}{\Omega_m}\right)^{1/2}\right), \tag{4.38}$$

which is a monotonically increasing function of Ω_Λ- a cosmological constant makes the universe older.

The difference in our approach here for computing Ω_a from works that have been mainly concerned with the QCD axion, e.g. [172, 174], is that we assume no temperature variation to the axion mass. Or rather, we assume that it has reached its

zero temperature value quickly, and crucially before oscillations of the field begin, which since the fields are so light will be at a low temperature any how. We consider this a reasonable simplification because we do not in general know the temperature dependence of the mass for a string axion since we do not know what non-perturbative physics will make the dominant contribution to the potential.

If we wanted to restrict our analysis to true axions, rather than the more general case of ultra-light scalar field ALPs, there is an important region of axion parameter space, known as the "anthropic boundary", which is instructive to locate. True axions are periodic in $\theta = \phi/f_a$ and so the initial misalignment angle has a "maximum" at $\theta_i = \pi$. Eq. (4.35) shows that Ω_a depends on the axion mass for axions that begin oscillating in the radiation era. The result is that for masses $m \lesssim 10^{12}$ it is impossible, without taking account of anharmonic terms in the potential and tuning the initial misalignment arbitrarily close to π [172], for these axions to produce $\Omega_a > 1$ and overclose the universe. This somewhat alleviates fine tuning problems for these light, high-f_a ALPs that lead, in the usual case, to one having to tune θ_i arbitrarily close to zero to prevent overclosure of the universe and other cosmological problems [170, 176]. Therefore with ultra-light ALPs the fine tuning arguments of Mack and Steinhardt [202, 203] lose some of their power.

The flip side to this is that without tuning the initial misalignment arbitrarily close to π and including anharmonic effects in the potential it is impossible for axions with masses much below the anthropic boundary to constitute an order one fraction of the dark matter. For example, axions that begin oscillating in the matter dominated era, such that Ω_a is independent of the mass (Eq. (4.36)), the maximum possible contribution to the energy budget is $\Omega_a \sim 4 \times 10^{-4}$. This observation seems to cause problems for the arguments in [201] that any axion should contribute an order one fraction of the dark matter.

These conflicting observations on fine tuning for axions below the anthropic boundary give some reason for the decision made in Chapter 1 to generalise to ultra-light scalar fields with a quadratic potential that do not respect the shift symmetry of axions when considering such low masses as are relevant for the FCDM scenario. We simply allow ourselves to look at a larger range of Ω_a with disregard for fine tuning.

4.3 EVOLUTION OF THE PERTRUBATIONS

4.3.1 *Initial Conditions*

To solve for the evolution of the density perturbations and compute the resulting matter power spectrum we need to find the appropriate initial conditions for the perturbations in the various fluid components. We will derive these in detail for the adiabatic and axion isocurvature modes in Chapter 6, for now we will simply state the adiabatic modes necessary for the current example. Working to lowest order in $k\tau$ the coupled equations Eqs. (4.8, 4.23), and (4.24) can be solved analytically and the dominant late time growing mode solution is [40]:

$$h = C(k)(k\tau)^2\,, \tag{4.39}$$

$$\delta_c = -\frac{1}{2}C(k)(k\tau)^2\,, \tag{4.40}$$

$$\delta_\gamma = -\frac{2}{3}C(k)(k\tau)^2\,, \tag{4.41}$$

$$\theta_\gamma = -\frac{1}{18}C(k)(k^4\tau^3)\,, \tag{4.42}$$

where $C(k)$ is fixed by the primordial power spectrum. In this Chapter we assume scale invariance, which requires $\delta \sim k^{1/2}$ and so $C(k) = Ck^{-3/2}$. With these initial conditions, Eq. (4.22) can easily be integrated to give $\delta_c = -\frac{1}{2}h$, so that the evolution of the CDM becomes trivial and we need only work with h.

To find the initial condition on ϕ_1 we use the condition of zero entropy relating adiabatic perturbations in two fluids a and b:

$$S_{ab} = \frac{\delta_a}{1+w_a} - \frac{\delta_b}{1+w_b}\,, \tag{4.43}$$

$$S_{ab} = \dot{S}_{ab} = 0\,. \tag{4.44}$$

From this one finds that the initial values of ϕ_1 and $\dot{\phi}_1$ both depend on $\phi_{0,t}(0)$, the initial value of the derivative of ϕ_0 with respect to physical time [277]. For ultra-light scalar fields that are the PGBs of a spontaneously broken symmetry this derivative is zero, since the field is frozen at the initial misalignment by Hubble drag, and there is no initial velocity, i.e. at early times $w_a = P_a/\rho_a = -1$. Therefore the perturbed axion

initial conditions in the adiabatic mode are simply:

$$\phi_1 = 0\,, \tag{4.45}$$

$$\dot{\phi}_1 = 0\,. \tag{4.46}$$

The initial conditions derived in [40] are for a numerical integration beginning in the radiation dominated era, which we also adopt. We can analytically integrate the background expansion, Eq. (4.5), and find:

$$\tau_i = \frac{1}{\sqrt{\Omega_\gamma}} a_i\,, \tag{4.47}$$

which is the final input required to fix the initial conditions completely, up to the constant C that sets the primordial fluctuation amplitude, which in this Chapter we need not specify since we will only be considering ratios of power spectra.

4.3.2 *Suppression of Structure Formation*

Once the scalar field is deep into its oscillatory phase and the background evolution is well described by pure matter or radiation domination it is possible to solve the equations of motion with a WKB approximation. This gives:

$$\phi_0(\tau) = A_0 \left(\frac{a(\tau_{\rm osc})}{a(\tau)}\right)^{3/2} \cos\left[m\int_{\tau_{\rm osc}}^{\tau} {\rm d}\tau a(\tau)\right]\,, \tag{4.48}$$

$$\phi_1(\tau) = A_1 \left(\frac{a(\tau_{\rm osc})}{a(\tau)}\right)^{3/2} \cos\left[\int_{\tau_{\rm osc}}^{\tau} {\rm d}\tau (m^2 a(\tau)^2 + k^2)^{1/2}\right]\,. \tag{4.49}$$

Eq. (1.32) showing the asymptotic limits of the scale dependent sound speed, $c_s^2 = \delta P_a/\delta\rho_a$, can be derived by substituting these solutions into Eqs. (4.14, 4.12) and averaging over the rapid oscillations [115, 117]. We restate the result:

$$\begin{aligned} c_s^2 &= \frac{k^2}{4m^2a^2}; \quad k < 2ma\,, \\ c_s^2 &= 1; \quad k > 2ma\,. \end{aligned} \tag{4.50}$$

This momentum dependent sound speed leads to the emergence of a new scale in the scalar field evolution: $k_R = 2ma$. For $k < k_R$ the sound speed in the density perturbations is small and the scalar field behaves as ordinary dust CDM. For $k >$

k_R the sound speed in the density perturbations goes relativistic and the axion overdensities cannot cluster: this is analogous to neutrino free-streaming, but is non-thermal. This similarly defines a time τ_R after which a given mode ceases to behave relativistically.

A mode of wavenumber k crosses the horizon when $k \approx Ha$, or equivalently $k\tau \approx 1$. For a given k this defines a time of horizon crossing τ_c. Whether the free-streaming scale leads to a suppression of structure, and corresponding step-like feature in the matter power spectrum depends on the ordering of the times τ_c and τ_R. If a given mode enters the horizon once it has already become non-relativistic, $\tau_R < \tau_c$, then the density perturbations in that mode will behave as ordinary CDM and there will be no suppression of structure relative to the standard model. However if a mode is relativistic when it enters the horizon, so that $\tau_c < \tau_R$ then structure will be suppressed on that scale. For a field of a given mass, m, at a given redshift, z, we estimate the wavenumber, k_m, above which structure formation is suppressed.

Smaller and smaller k values are entering the horizon at all times. The mode that entered the horizon at matter-radiation equality corresponds to $k_{\rm eq} \equiv k_c(z_{\rm eq}) \approx 0.03h\,{\rm Mpc}^{-1}$. As the scale factor increases so does the boundary value for relativistic modes, k_R. We require $k_R < k_c$, for suppression of structure at a given redshift z. The large scales that we are interested in for the FCDM scenario suppress structure formation in modes that entered during matter domination. During matter domination $a \sim \tau^2$, which leads to a prediction for the mass dependence of the scale k_m:

$$k_m \sim m^{1/3}\,. \tag{4.51}$$

For heavier scalar fields that suppress structure formation in modes that entered during the radiation dominated era we have:

$$k_m \sim m^{1/2}\,, \tag{4.52}$$

so that masses in the range $10^4 \lesssim m \lesssim 10^6$ separate the regions. However we also know that only masses $m \gtrsim 10^6$ were oscillating in the radiation era, and therefore it is only for these masses that the derivation of k_R holds. Therefore in addition we expect some numerical corrections and z dependence to be introduced into the expressions

above by the transitionary dynamics of the background expansion between matter and radiation domination, which will effect the expansion rate used to derive k_m, and also due to the background scalar field transition between DM and Λ behaviour. This will be most severe for fields that are still undergoing their transition at the redshift of observation, $z_{\rm obs} \sim z_{\rm osc}$.

How much suppression of structure do we expect relative to ordinary CDM? The matter power spectrum is given by $P(k) = \delta_m^2$, where δ_m is the total overdensity in matter: $\delta_m = (\delta\rho_c + \delta\rho_a)/\rho_m$. After matter radiation equality, density perturbations in ordinary CDM grow like $\delta \sim a$. It is a well known result [278] that if a fraction $f(z)$ of the matter is unable to cluster then perturbations grow as $\delta \sim a^q$, where $q = 1/4(-1 + \sqrt{25 - 24f(z)})$. The deviation from $q = 1$ at a given redshift will therefore start at the scale k_m and saturate at the Jeans scale $k_J = a\sqrt{Hm}$: this is why we expect to see the emergence of "steps" in the power spectrum relative to ordinary CDM [104, 205].

We can estimate the suppression of power, S, in a step using a parameterisation found in [205], by taking the ratio of the two different growth rates of the density perturbations:

$$S(a) = \left(\frac{a_s}{a}\right)^{2(1-q)}, \tag{4.53}$$

where $a_s = max(a_{\rm osc}, a_{\rm eq})$. The size of a step is then given by $1 - S$.

An important difference between this work and the work in [205] is that we make no approximations for the evolution of the scalar field when actually computing $P(k)$.

4.3.3 *The Scales Involved*

Here we summarise the previous sections by restating the important scales to consider when thinking about the effects of ultra-light scalar fields on structure formation.

- A scalar field receives an initial value after symmetry breaking and at early times it remains frozen at this value by the Hubble drag. A frozen scalar field behaves as a cosmological constant; once it begins oscillating it will behave as matter. A field begins oscillating when:

$$H(t) \lesssim m$$

- Do oscillations begin in the radiation or matter dominated era? We will mostly be interested in ultra-light fields that begin oscillations in the matter dominated era:

$$m \lesssim 10^{-27}\,\mathrm{eV}$$

- The energy density today in such an ultra-light field depends on its initial value as:

$$\Omega_a = \frac{1}{6}\left(\frac{1}{t_0}\right)^2 \phi_0(t_i)^2$$

- Perturbations in the scalar field have a scale dependent sound speed, so we can ask: are the perturbations, on a given scale, at a given time, relativistic? The scale $k_R = ma(t)$ separates the two regimes. On small scales:

$$k > k_R$$

the sound speed is relativistic so that overdensities cannot cluster, suppressing structure formation. This is the analogue for the cold axion condensate of neutrino free streaming.

- Time dependence of the scale k_m and the finite size of the horizon mean that suppression of structure formation will accumulate on scales smaller than this. For the ultra-light fields under consideration, suppression of structure begins at a scale:

$$k_m \sim \left(\frac{m}{10^{-33}\,\mathrm{eV}}\right)^{1/3}\left(\frac{100\,\mathrm{km\,s^{-1}}}{c}\right) h\,\mathrm{Mpc}^{-1}$$

- The steps in the power spectrum caused by this suppression of structure depend on the fraction, f_{ax}, of matter in ultra-light fields. The amount of suppression can be estimated as:

$$S(a) = \left(\frac{a_{\mathrm{osc}}}{a}\right)^{2(1-1/4(-1+\sqrt{25-24f_{ax}}))}$$

As one would expect, a larger f_{ax} gives rise to greater suppression of structure, as do lighter fields that suppress structure on larger scales.

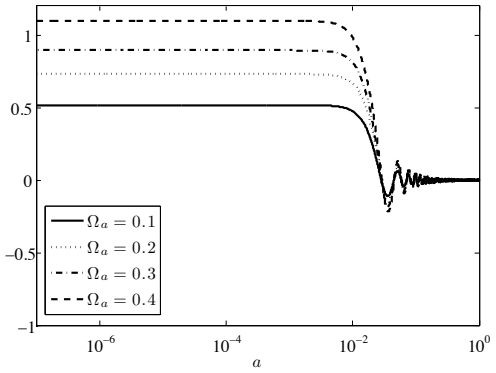

Figure 4.1 ϕ_0 versus a for $m = 10^3$, various Ω_c, $\Omega_\Lambda = 0$

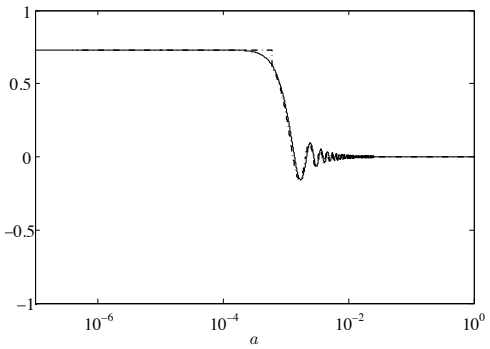

Figure 4.2 A fit for ϕ_0 versus a for $m = 10^5$, $\Omega_c = 0.8$, $\Omega_\Lambda = 0$. The solid line is the result of numerically integrating the equations of motion, whilst the dotted line is the analytic fit of Eq. (4.28).

4.4 RESULTS IN THE BACKGROUND

Firstly we show a representative figure, Fig. 4.1, for the evolution of the field ϕ_0. This shows how the initial misalignment depends on Ω_a.

In Fig. 4.2 we show a representative fit to the numerical solutions using the analytic results obtained in Section 4.2. The fit is made by fixing the field to its initial value before $a_{\rm osc}$, and then applying the analytic solution of Eq. (4.28) after $a_{\rm osc}$. The analytic solution captures the decay envelope and transition well, and the estimate for $a_{\rm osc}$ is also a good one. There is not a fit for the whole evolution of ϕ because the Bessel function solution assumes a single background fluid.

There are two important scales in the background evolution: the redshift of matter radiation equality, $z_{\rm eq}$, and the redshift at which axion oscillations begin, $z_{\rm osc}$. Both of these can be identified on a plot of $\log a$ versus $\log \rho$, Fig. 4.3, and agree well with

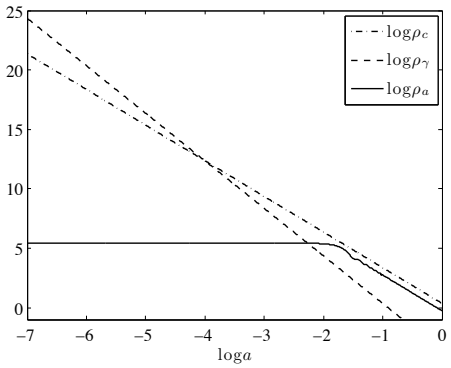

Figure 4.3 $\log\rho$ versus $\log a$ for $m = 10^3$, $\Omega_c = 0.8$, $\Omega_\Lambda = 0$

the expected values, so that for example with $m = 10^3$ the oscillations begin in the matter dominated era. Fig. 4.3 again demonstrates the main features of the scalar field evolution, this time through the redshifting of the energy density: there is a period of constant energy density, and a period where the energy density redshifts with the matter. However there is also a significant region between $a \sim 10^{-2}$ and $a \sim 10^{-1}$ where the scalar field undergoes a transition in its behaviour.

One way of looking at the length and significance of this transition is to see how it effects the expansion rate. In a pure matter, or pure radiation dominated era the scale factor evolves as $a \sim \tau^p$, with a slow, smooth transition between the two regimes (see Fig. 4.4). Therefore plotting $\mathcal{H}\tau$ versus scale factor will extract the time evolution of p. When the scalar field begins oscillation there is a more rapid time dependence introduced to p, however one can demonstrate that for the ultra-light scalar fields of interest here, where oscillations begin around $\tau \sim \mathcal{O}(1)$, that the product $\dot{p}\tau \ln \tau$ remains small compared to p and therefore the expansion is still well described by plotting $\mathcal{H}\tau$ versus scale factor.

A plot of the exponent p during the transition in the scalar field behaviour estimated in this way is also shown in Fig. 4.4. The relative change in the numerical value of p is small during this transition. The transition here begins well into the matter epoch, and lasts for approximately one order of magnitude in scale factor growth, much shorter than the transition from pure radiation to pure matter expansion, which lasts over four orders of magnitude for the case at hand. Results for different masses of scalar field show that the length of the transition as one order of magnitude in scale

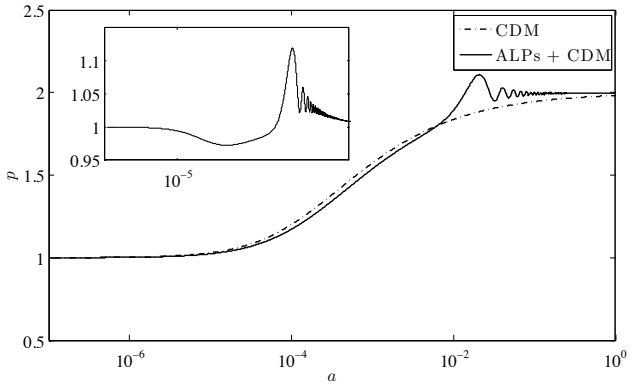

Figure 4.4 p versus a for $m = 10^3$, $\Omega_c = 0.8$, $\Omega_\Lambda = 0$. Insert: ALPs + CDM divided by standard CDM alone

factor is approximately mass independent. These two observations of a relatively short and small effect on the expansion rate due to the presence of an ultra-light scalar field lead to the prediction that such a dark matter component will have a correspondingly small effect on the age of the universe, and this intuition is indeed borne out in the numerical results.

When a non-zero cosmological constant is included the effect on the evolution of the background field is minimal. An accelerated expansion rate at late times is included simply by altering $\phi_0(t_i)$ through the effect on t_0 as discussed in Section 4.2; a larger t_0 simply increases the required initial misalignment for a fixed fraction in ALPs: the accelerated expansion dilutes the ALP density. Furthermore, the mass range of ALPs that will contribute to the matter fraction, Ω_m, today must be deep in their oscillatory regime. Those ALPs light enough that we would expect oscillations to begin in a Λ dominated era cannot fulfil this requirement and are overdamped by the increased expansion rate, as such we will not be interested in them since they will not be contributing to the matter power spectrum and will simply be adding on to increase the effective value of Λ: the lightest fields we will consider in this Chapter are of mass $m \gtrsim 10^2$. We conclude that the overall effect of Λ is exactly as for standard ΛCDM and is unaltered by the presence of an ALP component in the dark matter, as it should be since there is no direct interaction.

4.5 THE MATTER POWER SPECTRUM

In this section we return to using physical, dimensionful variables.

In this Chapter, in order to have the smallest and simplest set of fits to make to our results that will be most useful for comparison with observations, we will simply fit for $\bar{k}_m$ at the centre of any step in the power spectrum, and take the saturation at k_J as given. We will be interested in the function:

$$T^2_{ax}(k) = \frac{P(k)_{\text{ALPs + CDM}}}{P(k)_{\text{CDM}}}\,, \tag{4.54}$$

from which we can define the step size:

$$S = T^2_{ax}(k_{max} \gg k_m)\,, \tag{4.55}$$

where k_{max} is the smallest scale of interest in the numerical or observational situation at hand. The dependence on m, Ω_a, and z is implicit. Later we will consider the effect of non-zero Ω_Λ.

In Fig. 4.5 we show $T^2_{ax}(k)$ for $m = 10^{-29}$eV for various values of Ω_a at $z = 0$. To fit for S we use the parameterisation of Eq. (4.53) for $T^2_{ax}(k)$ taken at the largest $k = 3 \times 10^2\ h\text{Mpc}^{-1}$ in our numerical results, modified with the addition of two exponents, β_1 and β_2:

$$S(z) = \left(\frac{(1+z)^{1+\beta_1}}{(1+z_{\text{osc}})^{1+\beta_2}}\right)^{2(1-q)}\,. \tag{4.56}$$

This fit applies when $z_{\text{osc}} < z_{\text{eq}}$ and when $z < z_J$, where z_J is the redshift at which $k_J(z) = 3 \times 10^2\ h\text{Mpc}^{-1}$. The factor of q contains the dependence on $f_{ax}(z)$, and z_{osc} contains the dependence on the mass. The parameters β_1 and β_2 are chosen by trial and error, and take into consideration the approximations in the scale $\bar{k}_m$ and oscillation scale used to derive the fit. For those fields still far from matter-like behaviour at a given z, we expect a poorer fit. We also expect a poorer fit for those fields where $z_{\text{osc}} \sim z_{\text{eq}}$.

In Fig. 4.6 we show $S(f_{ax})$ at $z = 0$ for three masses of scalar field. The fits are used to determine β_2, and a reasonable match to within a few percent is obtained using the value $\beta_2 = 0.6$. Next, Fig. 4.7 shows $S(f_{ax}(z))$ for $m = 10^{-29}$ eV with three values of z. The fits are again reasonable for a value of $\beta_1 = 0$, across two orders of

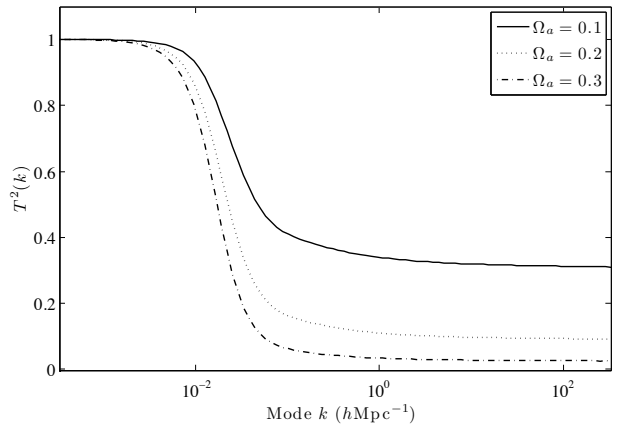

Figure 4.5 $T^2(k)$ for $m = 10^{-29}$ eV, $\Omega_\Lambda = 0$

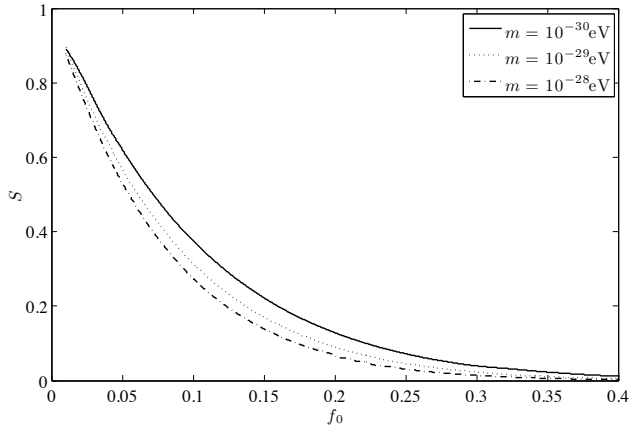

Figure 4.6 S versus $f_{ax}(z = 0) = f_0$ for $m = 10^{-30}$eV, 10^{-29}eV, 10^{-28}eV, $\Omega_\Lambda = 0$.

magnitude in mass. Particularly, for $m = 10^{-29}$ eV the fit is good up to $z \sim 100$, but breaks down at $z \sim 200$, which is what we expect since at such high redshift the field is still very early in its transitionary regime and has yet to complete a full oscillation.

The final quantity we fit for is $\bar{k}_m$, which we define by:

$$T^2_{ax}(\bar{k}_m) = \frac{1+S}{2}\,. \tag{4.57}$$

The fit should be well described by Eq. (4.51) and only depend weakly on z and Ω_a outside of the transition regime in the scalar field behaviour. For sufficiently small z such that the field in question has completed its transition we use the fit:

$$\bar{k}_m = A f_0^{\alpha_1}(1+z)^{\alpha_2} m^{1/3}\,, \tag{4.58}$$

where f_0 is the fraction in ALPs at $z = 0$, A is a constant of proportionality, and α_1, α_2 are exponents to be fit for.

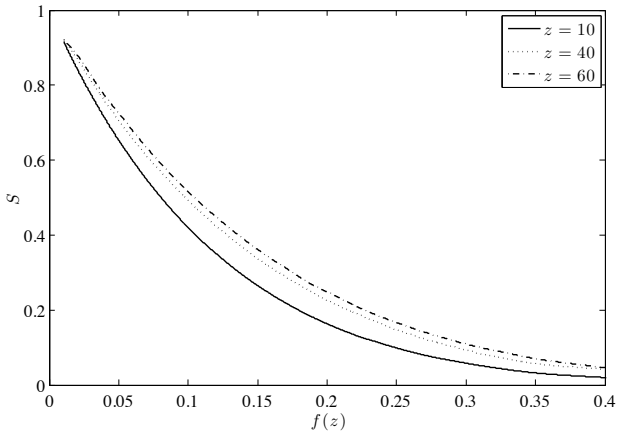

Figure 4.7 S versus $f_{ax}(z)$ at $z = 10$, 40, 60 for $m = 10^{-29}$eV, $\Omega_\Lambda = 0$.

Fig. 4.8 shows the shape of $\bar{k}_m$ as a function of m at $z = 0$ for three values of Ω_a. At $z = 0$ all the masses of scalar field under consideration have, for the best part, undergone their full transition to matter like behaviour, and the shape is well fit by Eq. (4.58) with $A = 1.25$, $\alpha_1 = -0.5$. With these values essentially normalising each curve, the shape follows $m^{1/3}$ well, until $m \gtrsim 10^{-28}$eV. The discussion surrounding Eqs. (4.51) and (4.52) tells us that these masses suppress structure formation in modes that entered when the background expansion rate was transitioning from pure radiation to pure matter dominated behaviour. In addition, at the time when the associated modes entered the horizon the masses in question were still undergoing their own transition from cosmological constant to dark matter behaviour, which will not only effect the background expansion rate but also the growth of scalar field overdensities so that neither Eq. (4.51) nor Eq. (4.52) will hold exactly for the mass dependence of k_m. This departure from the naive picture underlines the importance of numerical solutions to determine the effect of ultra-light scalar fields on the matter power spectrum.

Fig. 4.9 shows the shape of $\bar{k}_m$ as a function of m at three different z values. When a scalar field is transitioning in behaviour from cosmological constant to CDM, or indeed when it is still behaving as pure cosmological constant, then the sound speed of Eq. (4.50) no longer applies and the steps in the power spectrum cannot be simply described by Eq. (4.51). At high redshift the lower mass scalar fields cause the curve to peel away from the $m^{1/3}$ shape. The fit of Eq. (4.58) does not attempt to capture the

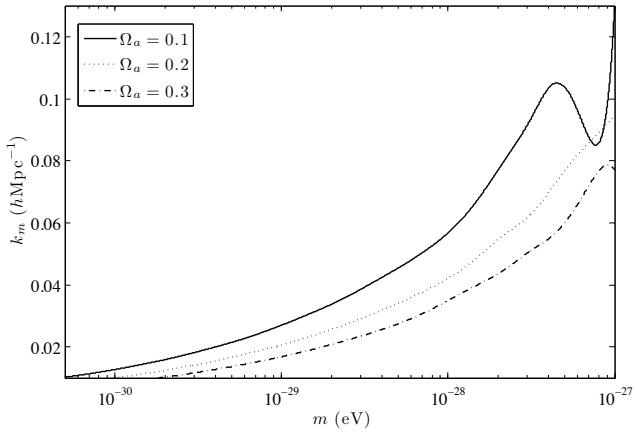

Figure 4.8 $\bar{k}_m$ versus m at $z = 0$ for $\Omega_a = 0.1$, $\Omega_a = 0.2$, $\Omega_a = 0.3$, $\Omega_\Lambda = 0$.

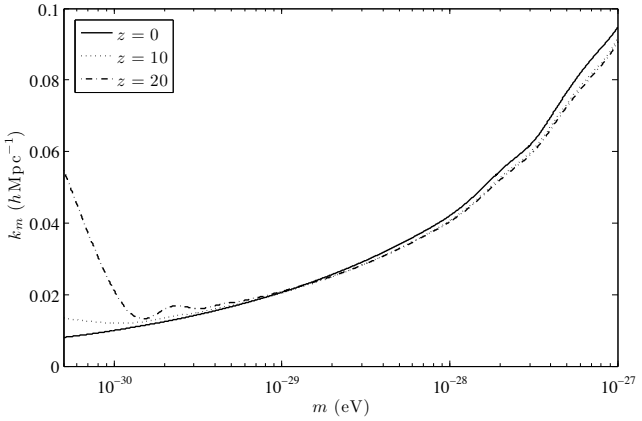

Figure 4.9 $\bar{k}_m$ versus m at $z = 0$, 10, 20 for $\Omega_c = 0.8$, $\Omega_\Lambda = 0$.

transitionary behaviour, and we only note that for fields with a larger mass that have completed the transition to CDM there is no remaining z dependence in the location of the step, i.e. $\alpha_2 = 0$.

Given the step size, and the location of the centre of the step it is simple to fit the shape of $T^2_{ax}(k)$:

$$T^2_{ax}(k) = \frac{1 + S(k/\bar{k}_m)^\gamma}{1 + (k/\bar{k}_m)^\gamma}\,. \tag{4.59}$$

The difference plot for this fit against the steps shown in Fig. 4.5 with $\gamma = 2$ is shown in Fig. 4.10, and is good within around 5% of the total step size, $1 - S$. The fit is worst around $\bar{k}_m$, where we expect the most uncertainty in this treatment, both from the discussion of the fit to Eq. (4.58), and from our choice to fit for the centre of the step only, ignoring the distinct scales k_m and k_J. Just a small misestimation of k_m leads to a much poorer fit for T^2_{ax} because it is at k_m where T^2_{ax} has a large gradient.

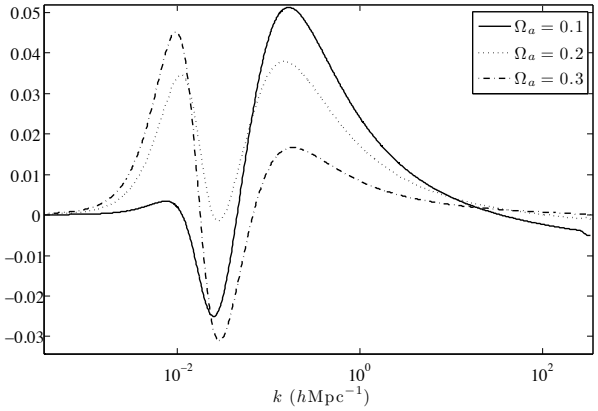

Figure 4.10 Difference plot for the analytic fit of Eq. (4.59) with $\gamma = 2$ to the numerical results shown in Fig. 4.5

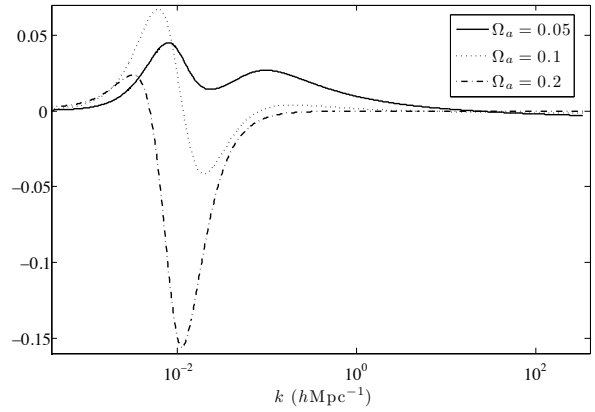

Figure 4.11 Difference plot for the analytic fit of Eq. (4.59) with $\gamma = 2$, using Eq. (4.60) with $\alpha_3 = 0.75$ to fit $\bar{k}_m$, to numerically generated power spectra for $m = 10^{-29}$eV and $\Omega_\Lambda = 0.7$ at $z = 0$.

When a non-zero cosmological constant is included corresponding to $\Omega_\Lambda = 0.7$, with no change to the fits, they remain good at large k and so we conclude that S has little or no dependence on Ω_Λ. The fit is very poor for $k \sim \bar{k}_m$ so we modify Eq. (4.58) to include one more exponent, α_3:

$$\bar{k}_m = A f_0^{\alpha_1} (1+z)^{\alpha_2} (1-\Omega_\Lambda)^{\alpha_3} m^{1/3}\,. \tag{4.60}$$

With $\alpha_3 = 0.4$ we return to fits good to around $5-15\%$ of the total step size, as shown in Fig. 4.11.

We have not considered power spectra for fields with $m > 10^{-27}$ eV that begin oscillating in the radiation era, and suppress structure formation in modes that entered during this era, since their behaviour will be much simpler: scalar fields with these

masses will be much better fit by the approximations of [205] and Chapter 6, and of our fits, in almost all observational situations for LSS at low z. They will not effect the epoch of equality, and will only effect the expansion rate beyond $z_{\rm eq}$. Furthermore, because they will be well transitioned to DM behaviour at all redshifts of interest then the scale k_m will be extremely well fit by $m^{1/2}$.

4.6 DISCUSSION

In this Chapter we have explored the cosmological behaviour of ultra-light scalar fields and found that they can have a significant effect on the growth of structure at late times. This is not surprising given that we are essentially studying the clustering of very light axions, i.e. axions whose mass scale is close to the current cosmological horizon.

Ultra-light axions have, until now, been difficult to motivate theoretically. Most of the focus of previous research has been on QCD or QCD-like axions for which there are well defined production mechanisms in the early Universe. There have been some studies of what has been dubbed Fuzzy Cold Dark Matter [117], albeit in a slightly different mass regime. But with the rise of the string axiverse [104, 195] it makes sense to loosen our usual assumptions that tie the axion fractional energy, Ω_a, to the mass scale, m. This means that we have been generous with what we deem allowable for the misalignment angle– to consider appreciable Ω_a we must allow large misalignment angles, pushing the dynamics of the axion field towards the anharmonic part of the axion potential, or even beyond the maximum set by the shift symmetry for a given sub-Planckian f_a.

We have studied scalar fields whose evolution is such that the length scale for oscillations and clustering is greater than that set by the horizon size at radiation-matter equality. Hence, the transition from 'frozen' (cosmological constant) to oscillatory behaviour occurs after radiation-matter equality. Two interesting features arise. First of all, the energy density of the scalar field behaves as a DE at early times and then transits to dust-like DM behaviour at late times- this transition happens after equality. Second, and as result of the previous point, the redshift of equality is shifted by a

factor $(1 - f_{ax})$. If f_{ax} is substantial, the affect can be appreciable. This transition between DE and DM-like behaviour will affect the expansion rate and, unlike the standard axion picture, it will not be purely dust dominated. As a guide, this effect is of order 10% for $f_{ax} \simeq 0.3$.

When we look at the evolution of perturbations and their effect on clustering we find that, as was expected, there is suppression of power on the smaller scales. The transition wave number $k_m \sim m^{1/3}$: a mass dependence which is specific to these ultra-light fields, i.e. with a transition after radiation-matter equality. We have refined the dependence of the scale at which the suppression kicks in as well as the amount of the damping on small scales, giving us a better handle on how this effect depends on the parameters m and Ω_a.

The next obvious step is to see if these various effects can be picked out in cosmological observables. These ultra-light fields affect the growth rate of perturbations and should be detectable by the standard selection of methods: the Integrated Sachs-Wolfe effect in the CMB, weak-lensing of the large scale structure and galaxy, cluster and Lyman-α surveys. An intriguing possibility is that these effects may contaminate and bias characteristic scales in large scale structure such as the BAO.

5

FORECASTING FOR OBSERVATIONS

"Shakyamuni Buddha said: 'It is like someone with cataracts seeing flowers in the sky: when the affliction of cataracts is removed, the flowers perish in the sky.'

... Do not ignorantly consider cataracts *to be delusive factors and this study as if there were something else which is real – that would be a small view."*

Dōgen Zenji (1200 – 1253), in *Shōbōgenzō*

PREFACE

In this chapter we take the basic intuition for the effects of ultra-light axions on the power spectrum developed in Chapter 4 and look at many more cosmological observables. These observables are then used to forecast for the detectability of axions. The work in this Chapter is based on Ref. [279].

5.1 RELATIVISTIC SPECIES

Observations of the CMB and LSS in recent years have consistently found the need for excess relativistic energy density [5, 54, 280–282] [1]. This excess radiation is parameterised in terms of the effective number of relativistic neutrino species, $N_{\rm eff,rel}$

[1] However, the authors of [283] suggest that this may be due to priors.

[256, 257, 284], as:

$$\rho_R = \left[1 + \frac{7}{8}\left(\frac{4}{11}\right)^{4/3} N_{\rm eff,rel}\right]\rho_\gamma\,, \tag{5.1}$$

where ρ_γ is the energy density in photons fixed by the CMB temeperature. Even within the SM, with no neutrino masses, $N_{\rm eff,rel}$ can be non-integer and greater than three if neutrino decoupling is non-instantaneous and the thermal neutrinos are partially reheated by electron positron annihilation [101]. It is often stated that three massless standard model neutrinos are best described by $N_{\rm eff,rel} \approx 3.04$, which is the assumption we mentioned in Chapter 1. Any increase from this is thought of as 'extra'.

The radiation density at BBN is constrained by the light element abundances, but bounds vary depending on the treatment of astrophysical uncertainties, new physics scenarios and improved measurements. For example, [285] has $N_{\rm eff,rel} = 2.5^{+1.1}_{-0.9}$, while [286] allow up to $\Delta N_{\rm eff,rel} = N_{\rm eff,rel} - 3.04 = 1.39$ at 95% credible interval. However, the BBN limits need not apply at the CMB or LSS scales, since late decaying particles may increase the neutrino abundance after BBN, but before or after CMB formation. Accordingly, $N_{\rm eff,rel}$ is taken as a free parameter in most cosmological parameter estimations, with best fit values from WMAP7 $N_{\rm eff,rel} = 4.34^{+0.86}_{-0.88}$ [5][2], ACT $N_{\rm eff,rel} = 4.6 \pm 0.8$ [54], SDSS-DR7 $N_{\rm eff,rel} = 4.78^{+1.86}_{-1.79}$ [281]. Motivation for such extra radiation density is lacking in the SM and concordance models, however many theoretical extensions of these models provide clues. Such a situation is indeed expected in the 'Freeze-in' mechanism of producing asymmetric dark matter, if the relic particles decay to neutrinos [113, 114].

The observation of neutrino oscillations requires the introduction of neutrino masses, which constitutes a hot dark matter (HDM) component (for a review of massive neutrinos in cosmology, see [287], and for a historical review of HDM see [288]). The situation is further complicated due to the degeneracy, on certain scales and for certain observables, between massive neutrinos and other extended sets of cosmological parameters [289].

The situation with regards the measurement of massive neutrino parameters using

[2]Note that this is not the value quoted in Table 1.1: this value uses data other than the CMB to get a detection, while the value in Table 1.1 uses the CMB alone.

terrestrial experiments is summarised in some recent fits by Giunti [98]. These fits seem to favour not only massive standard model neutrinos, the absolute mass scale of which can only currently be determined by cosmology, but also the inclusion of one or two species of massive 'sterile' neutrinos, which have a large mass splitting from the standard model neutrinos. The fits to this model and cosmology favour the standard model neutrinos being approximately massless, and the sterile neutrinos to have masses in the eV range. Sterile neutrinos are even more ambiguous cosmologically, since incomplete thermalisation allows the effective number of massive neutrinos, $N_{\rm eff,mass}$, to also take non-integer values. Cosmological fits for sterile neutrinos are given in [286], and forecasts are made in [290], while forecasts for the cosmological measurement of standard model neutrino mass splittings are made in [291]. It is also well known that cosmology can potentially resolve the neutrino mass hierarchy as being the 'normal' hierarchy if the sum of neutrino masses, $\Sigma m_\nu < 95\,\mathrm{meV}$, an accuracy within reach if many cosmological probes are combined [145].

The existence of neutrino masses, while in some views of the history of particle physics strictly BSM, is at least well established enough, both experimentally and theoretically, that many would not class them as BSM at all. Their effects, as we have seen, are included in many cosmological analyses, too. Their known existence, combined with the fact that HDM cannot account for all the dark matter, is definitive evidence that the dark sector is multi-component.

5.2 ULTRA-LIGHT AXIONS VS MASSIVE NEUTRINOS

Light species of particles, such as massive neutrinos with $m_\nu \lesssim 1\,\mathrm{eV}$, can act as hot dark matter and suppress formation of large scale structure via free-streaming [278]. On scales smaller than the free streaming scale, i.e. for wavenumbers $k > k_{FS}$, this Hot Dark Matter (HDM) cannot cluster. This is determined by the temperature at which the species becomes non-relativistic, and therefore by the mass of the species. During matter or Λ domination [287]:

$$k_{FS} = 0.82 \frac{\sqrt{\Omega_\Lambda + \Omega_m (1+z)^3}}{(1+z)^2} \left(\frac{m_\nu}{1\,\mathrm{eV}}\right) h\,\mathrm{Mpc}^{-1}\,. \tag{5.2}$$

If there is a fraction of matter, f, in such a non-clustering species then the overdensities in matter grow as $\delta \sim a^q$, with $q = 1/4(-1 + \sqrt{25 - 24f})$ for $k > k_{FS}$. This behaviour leads to the formation of 'steps' in the matter power spectrum [205]. The size of these steps was first estimated in [289] to be $\Delta P(k)/P(k) \approx -8\tilde{f}_\nu$ ($\tilde{f}_\nu = \Omega_\nu/\Omega_m$). Fits for the steps can be found in [292] and [293].

As discussed in Chapter 4, a qualitatively similar feature occurs in the presence of ultra-light scalar fields with $m_a \lesssim 10^{-18}$ eV, such as string axions, but the physics behind this process is quite different to the case of neutrinos or any other eV mass particles, such as the QCD axion [104, 117, 205, 233].

Recall that there is a scale, k_m, analogous to the neutrino free streaming scale, for ultra-light scalars. Modes with $k > k_m$ enter the horizon whilst the sound speed is relativistic and will display a suppression of power, while modes with $k < k_m$ enter the horizon as the sound speed is decaying to zero and cluster as ordinary CDM. In this Chapter we will express this as:

$$\begin{aligned} \frac{k_m}{H_0} &= (2\Omega_m)^{1/3}\left(\frac{m_a}{H_0}\right)^{1/3}; \quad k_m < k_{\rm eq}\,, \\ \frac{k_m}{H_0} &= \left(\frac{4\Omega_m}{1+z_{\rm eq}}\right)^{1/4}\left(\frac{m_a}{H_0}\right)^{1/2}; \quad k_m > k_{\rm eq}\,, \end{aligned} \tag{5.3}$$

where Ω_m is the total fraction of the critical density in baryons, CDM, axions, and massive neutrinos (if they are non-relativistic at these scales), and H_0 is the Hubble scale today. We note that this definition of k_m reproduces the same scaling with mass as the definition used in [205] where k_m is defined as the scalar field Jeans scale during matter domination evaluated at the redshift when scalar field oscillations begin. We further note that in our fits for the matter power spectrum made in subsequent sections we will only be considering $k_m < k_{\rm eq}$, since massive neutrinos corresponding to those allowed by WMAP have k_{FS} in this region, and we are interested in the degeneracy. How much degeneracy there is between axions and neutrinos will clearly depend on exactly how close k_m and k_{FS} are and how sensitive a particular observable in a particular survey is to physics on these scales.

As in Chapter 4 our fits use $\bar{k}_m$, where we add a bar to distinguish this value,

which fits the *middle* of the step, from the value derived above, which fits the start. The two differ by an order of magnitude for our fiducial cosmologies, which reflects the scale over which the transition in axion clustering behaviour occurs. The fit is given by Eq. (4.60). Note that the fitted value of $\alpha_3 = 0.4$ is close to the expected value of $\alpha_3 = 1/3$.

Finally we note that k_m enters the horizon when $H \approx m_a$ ($\mathcal{H} = aH$), at exactly the same time when scalar field oscillations are expected to begin. This is again consistent with the definitions given in [205]. However since Eq. (4.50) only holds once the fields have already begun oscillations we should take this as a warning that the expressions for k_m given by Eq. (5.3) will only be approximate.

Here we see the physical difference between suppression of structure by ultra-light scalars and the free-streaming of neutrinos. Free-streaming is related to a change in temperature causing the *particles* to become non-relativistic when the temperature drops below the mass. Ultra-light scalars, if treated as *thermal* particles, would still be relativistic today and their 'free-streaming' scale would be larger than the horizon. However, ultra-light scalars form a *cold condensate* (see, for example, [122] and references therein), and we treat them as a classical field. As such it is the sound speed of perturbations in this condensate, which depends only on the mass and scale factor, not the temperature, which determines whether overdensities can form and grow. This leads to an interesting coincidence of scales: an ultra-light scalar with a mass in the range of 10^{-30} eV will suppress structure on approximately the same scale as a neutrino with a mass $\mathcal{O}(10^{30})$ times greater, which will make up about 1% of the total energy density. However, there is an extra parameter to consider for ultra-light scalars that comes from the production mechanism of their relic density and leads to an extra degree of freedom when considering their effects on the matter power spectrum.

The relic density of massive neutrinos is fixed by the mass of each neutrino species, assuming standard model interactions (see [35] for more discussion on this point). For one massive neutrino this is approximately given by:

$$\Omega_\nu \approx \frac{m_\nu}{93.14h^2\,\mathrm{eV}}\,, \tag{5.4}$$

where h is the Hubble parameter defined as usual by $H_0 = 100h\,\mathrm{kms}^{-1}\,\mathrm{Mpc}^{-1}$ (rather than the scalar metric perturbation). We see that both k_{FS} (Eq. (5.2)) and Ω_ν are fixed by the neutrino mass, m_ν. However, as mentioned in Section 5.1, for the case of sterile neutrinos this is not necessarily true. Sterile neutrinos are thermalised with active neutrinos via the mixing process, but the degree of thermalization depends strongly on the masses and mixing parameters [294] and therefore, just like the case of $N_{\mathrm{eff,rel}}$, $N_{\mathrm{eff,mass}}$ can be given non-integer values to parameterise this. For thermalised standard neutrinos, since Ω_ν is fixed by the mass alone, we have $k_{FS} = k_{FS}(\Omega_\nu)$. However for a sterile neutrino this is no longer true, since $\Omega_\nu = \Omega_\nu(m_\nu, N_{\mathrm{eff,mass}})$, while k_{FS} remains fixed by only the mass [286].

Axions have two contributions to their relic density. First of all there is standard thermal production due to axion couplings to the standard model. However, just like the self interaction terms in the potential, all of these couplings appear in the Lagrangian suppressed by powers of f_a. For large, stringy values of $f_a \sim 10^{16}\,\mathrm{GeV}$ these couplings are very small and the thermal relic density of ultra-light axions due to them is negligible.

There is also a second, non-thermal production known as the vacuum realignment mechanism. The axion arises from the spontaneous breaking of the Peccei-Quinn symmetry at the energy scale f_a. At this scale the parent scalar field acquires a vacuum expectation value and the Goldstone boson, which is the axion, acquires a *random* initial value: the initial misalignment, ϕ_i. Later, the field acquires its potential, $V(\phi)$, due to non-perturbative physics and once the mass of this potential overcomes Hubble friction, $H(z_{\mathrm{osc}}) \approx m_a$, the field will roll and generate a relic density that depends on the initial misalignment.

Until z_{osc} the axion contributes negligibly to the energy density as a cosmological constant, in contrast to a massive neutrino, which scales as radiation before becoming non-relativistic. The effects on the redshift of equality by axions and neutrinos are thus not the same in our parameterisation. Axions reduce the amount of matter only and do not affect the expansion rate while frozen; once rolling they have but a transitory effect on the background expansion away from ΛCDM as they go through their first few oscillations (see Chapter 4). Massive neutrinos, or extra relativistic species, in our

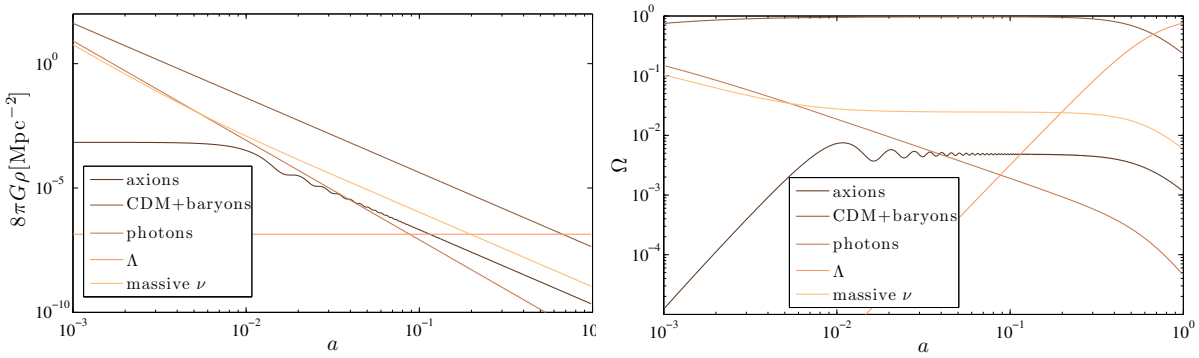

Figure 5.1 Ultra-light axion and massive neutrino evolution in the background. $m_a = 10^{-30}\,\mathrm{eV}$, $\Omega_a = 0.1\Omega_d$, $N_{\mathrm{eff,mass}} = 3$, $m_\nu = 0.1\,\mathrm{eV}$. Left panel: evolution of the energy densities in massive neutrinos and axions compared to vanilla cosmological components. Right Panel: Contributions to the critical density, $\Omega_i \equiv \rho_i/3H^2$.

parameterisation reduce Ω_Λ compared to redshift zero, but also increase the amount of radiation at early times. This has a non-negligible effect on the expansion rate and leads to a markedly different effect in small scale CMB anisotropies between axions and neutrinos, as we discuss in Section 5.3.5. Fig. 5.1 shows the evolution of the energy density in various components.

Using that $z_{\mathrm{eq}} = 2.5 \times 10^4 \Omega_m h^2 \Theta_{2.7}^{-4}$, where $\Theta_{2.7} = T_{CMB}/2.7$, and the neutrino sector consists of three standard massless neutrinos, we can express the relic density from vacuum misalignment as:

$$\Omega_a = 8.4 \times 10^{-5} h^{-3/2} \Theta_{2.7}^3 \left(\frac{m_a}{H_0}\right)^{1/2} \phi_i^2; \quad z_{\mathrm{osc}} > z_{\mathrm{eq}}\,, \tag{5.5}$$

$$\Omega_a = \frac{1}{6}\Omega_m \phi_i^2; \quad z_{\mathrm{osc}} < z_{\mathrm{eq}}\,, \tag{5.6}$$

where ϕ is dimensionlessly given in Planck units.

For a quadratic potential, where we have explicitly broken the axion shift symmetry and are strictly working with generalised ultra-light scalars (ALPs), we are essentially free to choose ϕ_i to give us the desired relic density, be it large or small, for any axion mass. Therefore for axions the scale for suppression of power and the relic density are separately under control via the two parameters m_a and ϕ_i, in contrast to standard massive neutrinos where both are fixed by the mass, m_ν. It is, however, pertinent to consider questions of fine tuning for this production mechanism. We direct the reader to the discussions of [201–203], and other Chapters in this thesis.

Another feature of vacuum realignment affecting the axion relic density comes from the periodicity of the axion potential. The periodicity, if the shift symmetry remains unbroken, leads to the axion field having a maximum value given by $\phi_{max} = \pi \frac{f_a}{M_{pl}}$. Therefore it is clear that for axions below a certain mass it is impossible, barring anharmonic effects in the potential, to produce $\mathcal{O}(1)$ values for Ω_a, which leads to the existence of what the authors of [104] call 'the anthropic window', and which we identified in Chapter 4. However, in the spirit of cosmological parameterisation, this need not worry us. If our model requires a larger amount of axion energy density at a certain mass than we can produce with $\phi_i \leq \phi_{max}$ then we can view this in the same way as $N_{\rm eff}$: it may be telling us that there are many species of axion in that mass range, where the masses cannot be resolved. This may, however, require additional fine tuning within the axiverse. For the fiducial models considered for forecasts in this work, however, we do not saturate this bound, and so the shift symmetry is preserved with $f_a < M_{pl}$.

Standard model neutrinos come in three species, and each species should be massive, with some hierarchy and degeneracy structure between them. The cosmological detection of this degeneracy using weak lensing was discussed in [291]. In the axiverse scenario we have multiple species of axion, with their own mass splittings. Naively, then, because of the qualitative similarity in their effects on cosmology, we may expect to account for any discrepancy between terrestrial measurements of N_ν, m_ν and mass splittings with the values determined by cosmology via the introduction of ultra-light scalars. In contrast, the possible existence of sterile neutrinos and other relativistic relics may obscure the possible cosmological effects of axions and close this observational window on them. It is one of the principle aims of this Chapter to go some way towards addressing these potential degeneracies, and indeed we expect many of them to be broken by considering multiple cosmological probes in the CMB and LSS, in the same way as degeneracies between neutrinos, dark energy and initial conditions can be broken in this way [145, 289, 295]. However, due to complications in forecasting for the effects of a varying axion mass and of the effect of a neutrino hierarchy splitting, we will leave the analysis of this particular degeneracy for a future work, and here focus in our forecasts purely on the density for a single species of

m_a (eV)	$k_m(h\text{Mpc}^{-1})$	$\bar{k}_m(h\text{Mpc}^{-1})$	z_{osc}
10^{-29}	0.0058	0.0575	350
10^{-30}	0.0027	0.0267	74
10^{-31}	0.0012	0.0124	15
10^{-32}	0.0006	0.0057	2.4

$$k_{\text{eq}}(f_{ax} = 0) = 0.0136h\,\text{Mpc}^{-1}$$
$$k_{\text{eq}}(f_{ax} = 0.01) = 0.0135h\,\text{Mpc}^{-1}$$
$$k_{FS}(m_\nu = 0.055\,\text{eV}, z = 0) = 0.0451h\,\text{Mpc}^{-1}$$

Table 5.1 Relevant scales for our fiducial cosmologies with $f_{ax} = 0.01$. k_m is the scale at which structure suppression begins, given by Eq. (5.3). $\bar{k}_m$ is the location of the middle of the induced feature in $P(k)$, fit for in [233]. z_{osc} is the redshift at which axion oscillations begin, which has an $\mathcal{O}(1)$ multiplicative uncertainty.

axion, and on degenerate massive neutrinos.

We summarise in Table 5.1 the relevant scales of z_{osc}, k_m, and $\bar{k}_m$ for the axions used in our fiducial cosmologies. We also quote $k_{\text{eq}}(f_{ax} = 0)$, $k_{\text{eq}}(f_{ax})$ (where $f_{ax} = \frac{\Omega_a}{\Omega_d}$), and $k_{FS}(m_\nu, z = 0)$ for comparison. Note that although we always have $k_m < k_{\text{eq}}$, this is not always the case for $\bar{k}_m$. We also note that one's definition of z_{osc} is somewhat ambiguous: does one define it from when $m_a = H$ or when $m_a = 3H$, or somewhere in between; when slow roll is broken, or when the oscillations have settled down to CDM behaviour? This leads to an $\mathcal{O}(1)$ multiplicative factor of uncertainty. In particular, this makes z_{osc} with $m_a = 10^{-29}$ eV potentially very close to recombination, $z_{rec} \sim 1100$.

5.3 THE AXIVERSE AND COSMOLOGICAL OBSERVABLES

As discussed in Chapter 4, ultra-light axions give rise to steps in the matter power spectrum, $P(k)$. Fig. 5.2 shows this effect on the cosmology of WMAP7 [5], with the introduction of a single axion species with fraction f_{ax}. Large axion fractions, disallowing variation of other parameters, can easily be ruled out at current sensitivity, while a small fraction of around 1% is indistinguishable from ΛCDM using the power spectrum of SDSS alone [66], c.f. Fig. 1 of [289]. Fig. 5.2 also shows power spectrum constraints coming from the ACT measurement of the primordial power spectrum [147]. This appears to be able to rule out a 10% fraction in axions easily using the CMB

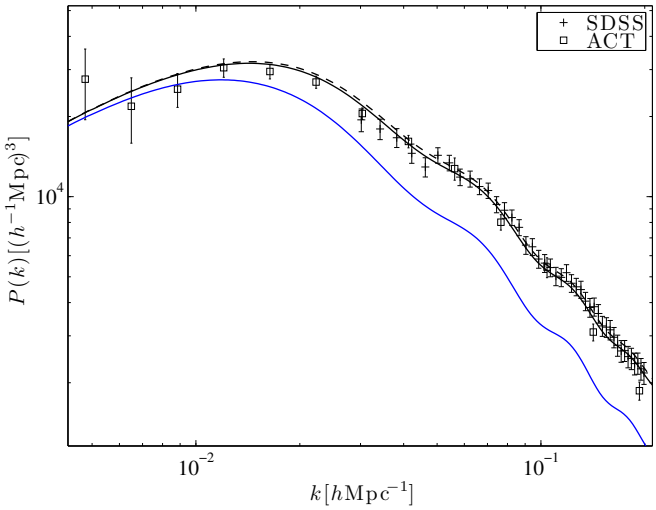

Figure 5.2 The matter power spectrum for three cosmologies shown with current measurements from SDSS [66], and ACT [147]. We show first the WMAP7 cosmology (dashed black line). We also show two axion cosmologies, both with $m_a = 10^{-29}$ eV: $f_{ax} = 0.1$ (solid blue line), and $f_{ax} = 0.01$ (solid black line), with all other parameters held fixed at their WMAP7 values. Both axion cosmologies have only a small effect on the CMB power spectrum, but are clearly distinguished in their effect on $P(k)$, with $f_{ax} = 0.1$ clearly ruled out by the data.

alone, which we will see is not the case for Planck (see Section 5.4.1). The reason being that these data points are evolved from the primordial power *assuming pure CDM* in the transfer function. This is just one example, of which we will see others later, of the way in which we might naively misinterpret data if we do not assume the correct underlying cosmology. We will see that the even smaller fractions of axions in our fiducial models, while still indistinguishable from ΛCDM with a single observable at a single redshift, can be distinguished using redshift information and/or a combination of observables.

In this Section we discuss in detail the theoretical effects of ultra-light axions on the various cosmological observables. The effects are explored both analytically, using the fits of Chapter 4 and [296], and through numerical solution of the Boltzmann equations obtained from a modified version of the publicly available code `CAMB` [45, 48, 49]. Our modification introduces a module to deal with scalar fields having a quadratic potential with mass large compared to the Hubble rate, the bulk of which involves accurately fixing the initial conditions and background evolution in the presence of rapid oscillations, and integrating such oscillations accurately. The

addition of galaxy lensing into the code was made by Maxime Trebitsch.

We exactly numerically solve the evolution of the axion field, ϕ, the difficulty of which stops us exploring the region of parameter space with $m_a \gtrsim 10^{-28}$ eV, suggested by [104] to be the most interesting region to look for unique step-like features in the power spectrum with a high precision galaxy survey or 21cm tomography survey. We are also limited to studying a single axion field, however our results will show that in fact, since constraints from some observables are mass independent, this is not a practical limitation. Our technique makes no use of the approximate treatments of axion sound speed and averaging used in the analysis of [205]. In addition, the mass range that we study is the one found in [205] to have the most tightly constrained axion fraction, but also the range in which the approximations used are least sound. Future observations will bound this regime even more tightly; making reliable predictions for high precision measurements in this important regime requires an exact treatment such as ours.

Throughout this section we will use our physical intuition about the suppression of power caused by ultra-light axions, and the similarities and differences with respect to neutrino free-streaming, to try and understand our numerical results. Where possible, we will be guided by analytic fits, but stress that these are meant for qualitative purposes only, and have some limited applicability, which we discuss. Analytic fits are not used in our forecasts. We emphasise that the figures and discussion of parameter variation in this section are meant only for illustrative purposes, and are not meant in any way as parameter estimation from existing data, nor do they necessarily reflect the fiducial models of our forecasts. An MCMC analysis for parameter estimation in this model will be the subject of a future work, and is discussed briefly in Chapter 6.

5.3.1 *The Matter Power Spectrum*

In Chapter 4 we derived fits, $T_{ax}(k, z, f_{ax})$, for the shape of the steps in $P(k)$ in a flat universe containing radiation, axions, CDM, and a cosmological constant, Λ, but no

baryons:

$$\begin{aligned}\tilde{f}_d T_d(k,z,\tilde{f}_{ax}) &= \tilde{f}_c T_c(k,\tilde{f}_{ax}) + \tilde{f}_{ax} T_a(k,z,\tilde{f}_{ax}) \\ &= \tilde{f}_d T_{ax}(k,z,\tilde{f}_{ax}) T_c(k,\tilde{f}_{ax}=0)\,. \end{aligned} \tag{5.7}$$

Here, and throughout this Chapter, $f_i = \Omega_i/\Omega_d$, $\tilde{f}_i = \Omega_i/\Omega_m$ so that $\tilde{f}_i = f_i \tilde{f}_d$. In Chapter 4, these quantities were equal since $\tilde{f}_d = 1$ in the absence of baryons. The difference between f_{ax}, $\tilde{f}_{ax}$ is important in the functional form of T_{ax}, as we will see below. We explicitly show the redshift dependence of T_d arising from T_{ax}, which corresponds to scale dependent growth. Whenever we drop redshift dependence, it is assumed that $z = 0$.

The matter power spectrum is related to the transfer function by: $P(k,z) = \mathcal{P}(k) T_m^2(k) D_1^2(z)$, where $D_1(z)$ is the growing mode, given for example in [292], and $\mathcal{P}(k)$ is the primordial power. Therefore, the step in the matter power spectrum in Chapter 4 was given by:

$$T_{ax}^2(k,z,f_{ax}) = \frac{P(k,z,f_{ax})}{P(k,f_{ax}=0)}\,. \tag{5.8}$$

In our numerical studies using `CAMB` the cosmology contains, in addition to CDM, axions and Λ considered in Chapter 4, the other standard ingredients of baryons, and their coupling to photons, massless and massive neutrinos. In the presence of baryons we model the full matter transfer function according to [296] as:

$$T_m(k) = \tilde{f}_d T_d(k) + \tilde{f}_b T_b(k)\,, \tag{5.9}$$

$T_d(k)$ is the total dark matter transfer function, including CDM, axions and massive neutrinos, if present, and $T_b(k)$ is the baryon transfer function. The fitted baryon transfer function contains the gravitational effects of the coupling to dark matter through its dependence on the matter fraction $\Omega_m = \Omega_d + \Omega_b$, the sound horizon s, the drag epoch z_d, the epoch of equality $z_{\rm eq}$, the scale of equality $k_{\rm eq}$, and the Silk damping scale k_{Silk}. There is also a dependence on these scales incorporated into the dark matter transfer function. In the case of ultra-light axions that do not begin their oscillations until the matter dominated era, these scales should all be altered to account for the change in matter content during these epochs in our parameterisation.

For example, $z_{\rm eq} \to \tilde{f}_{c+b} z_{\rm eq}$. Since the gravitational effect of the DM has thus already been accounted for in the baryon transfer function, the step feature modelled by $T_{ax}(k, z, f_{ax})$ should only multiply the DM transfer function, but with the weighting for axion effects coming in as $\tilde{f}_{ax} = \Omega_a/\Omega_m$ that is $T_d(k) \to T_d(k, z, \tilde{f}_{ax})$. The total matter transfer function is thus given by:

$$T_m(k, z, \tilde{f}_{ax}) = \tilde{f}_d T_{ax}(k, z, \tilde{f}_{ax}) T_c(k, \tilde{f}_{ax} = 0) + \tilde{f}_b T_b(k, \tilde{f}_{ax}) \,, \tag{5.10}$$

where $T_c(k, \tilde{f}_{ax})$ and $T_b(k, \tilde{f}_{ax})$ are fit by the formulae of [296], with relevant scales modified by the presence of the ultra-light component. The distinction between f_{ax} and $\tilde{f}_{ax}$ is especially important in the explicit form of T_{ax} from Chapter 4.

Therefore the step in the power spectrum caused by an axion component in the presence of baryons is given by:

$$\tilde{T}^2_{ax}(k, z, \tilde{f}_{ax}) = \frac{T^2_m(k, z, \tilde{f}_{ax})}{T^2_m(k, \tilde{f}_{ax} = 0)} \,, \tag{5.11}$$

where $T_m(k, z, f_{ax})$ is given by Eq. (5.10). Note that this fit is related to the fit of [293] used to investigate the effects of massive neutrinos by $\Delta P(k)/P(k) = \tilde{T}^2_{ax}(k, \tilde{f}_{ax}) - 1$. In particular, the step size is defined by:

$$\tilde{S}(\tilde{f}_{ax}) = \lim_{k \to \infty} \tilde{T}^2_{ax}(k, \tilde{f}_{ax}) \,. \tag{5.12}$$

Given that the baryon transfer function goes to zero faster than the CDM transfer function as k goes to infinity, we have:

$$\tilde{S}(\tilde{f}_{ax}) = S(\tilde{f}_{ax}) \,, \tag{5.13}$$

where S is defined in Chapter 4, which produces a *smaller* step than the case with no baryons, $S(\tilde{f}_{ax}) > S(f_{ax})$. This is caused by axions making up a smaller fraction of the total matter than of the dark matter alone, i.e. $\tilde{f}_{ax} < f_{ax}$.

The "naive" fit: $\tilde{T}_{ax}(k, \tilde{f}_{ax}) = T_{ax}(k, \tilde{f}_{ax})$, corresponds to axions suppressing growth on CDM and baryons evenly, with no account made for axion effects on the sound horizon, drag epoch etc. This, as expected, reproduces the small scale limit. The modified fit for $\tilde{T}_{ax}(k, \tilde{f}_{ax})$ incorporates changes to the sound horizon, Silk damping scale and drag epoch using the fits of [296] and thus qualitatively captures the

deviations from the smooth fit due to distortions of the BAO, which are seen in the full numerical solution. However, the fits presented here end up overestimating the total amount of power suppression by a few percent.

A step in the power spectrum corresponds to a change in the ratio of small to large scale power, which can naively be mimicked by changes in other cosmological parameters, such as the tilt of the primordial power spectrum, n_s. If measurements at large scales are poor, the effect can be compensated by adding more CDM, which shifts the power spectrum over to larger k, by moving the turnover, $k_{\rm eq}$. Isolating the unique effect of a structure suppressing species requires precise observations at the relevant scale, k_{FS} or k_m [289]. We are considering axion species varying in mass over many orders of magnitude, so have a correspondingly large variation of the scale k_m. Power spectrum measurements have varying precision over this range of k_m, and so we expect different constraints on the axion fraction, and possibly different degeneracies with other cosmological parameters, for the axions of different masses if k_m for the different species falls into regions of different accuracy in the survey. In particular, we should expect stronger constraints from galaxy redshift surveys alone on heavier axions with larger k_m. However, since all the axions we consider have $k_m < k_{\rm eq}$, where survey accuracy is at its lowest, this effect should not be significant.

5.3.2 *Baryon Acoustic Oscillations*

The theory behind BAO and their effect on the matter power spectrum has been known since at least 1998 in the work of Eisenstein and Hu [296], and they are an important cosmological tool used in the distance ladder (see for example [62, 297–303], and most recently [304], and for a review see [59]). Measuring the BAO to high precision is thus a key goal in modern cosmology. Here we briefly discuss a method of extracting, and hence working definition of, BAO from the matter transfer function.

We define the linear BAO as in e.g. [297]:

$$B_{lin} = \frac{T^2_{m,\rm full}(k)}{T^2_{m,\text{no osc}}(k)}\,, \tag{5.14}$$

where $T_{m,\rm full}(k)$ is the matter transfer function for a certain cosmology, either numerical or analytical, and $T_{m,\text{no osc}}(k)$ is defined as the oscillation free, smooth transfer

function taken as an $n-$node cubic spline of $T_{m,\mathrm{full}}(k)$ at points k_i, $i = 1, \ldots, n$ chosen empirically to get the best smooth fit.

There is a small distortion of $\tilde{T}_{ax}(k, \tilde{f}_{ax})$ in a cosmology with baryons, away from its smooth form in the region of the BAO. We now aim to give some analytic understanding of the reason for this, and therefore predict how large we can expect any BAO distortions due to light axions to be.

Since the gravitational effect of the dark matter has already been accounted for in the baryon transfer function, the step feature modelled by $T_{ax}(k, z, f_{ax})$ should only multiply the DM transfer function, but with the weighting for axion effects coming in as $\tilde{f}_{ax} = \Omega_a/\Omega_m$ that is $T_d(k) \to T_d(k, z, \tilde{f}_{ax})$. We fit $T_c(k, \tilde{f}_{ax})$ and $T_b(k, \tilde{f}_{ax})$ using the formulae of [296], with relevant scales modified by the presence of the ultra-light component. We see that while T_{ax} is smooth and should thus be captured by the spline in B_{lin}; we have also introduced a dependence on axion fraction into the baryon transfer function, which is oscillatory.

In Eq. (21) of [296] it is clear that the amplitude of the oscillations in the baryon transfer function has a detailed dependence on all the cosmological scales: the Silk damping scale, the scale of equality, the redshift of the drag epoch, and the sound horizon at the drag epoch. All of these scales depend on the matter content at the time when they are relevant, and at all such scales the lightest axions were frozen and not contributing as matter. The dependence of the sound horizon on the redshifts of drag and equality further implies that varying these redshifts by including an exotic species will cause a variation in the period of the BAO, as we can see again from Eq. (21) of [296], or from the fit used in [297].

If we hold the total amount of dark matter fixed and introduce ultra-light axions with $z_{\mathrm{osc}} < z_{\mathrm{eq}}$ then all these scales are shifted relative to where they would be if the dark matter were pure CDM. The shift is simple to compute: we simply alter the matter content in the equations for calculating these scales by a factor $(1 - \tilde{f}_{ax})$ to account for the frozen axions. The distortions in this case can be easily understood from [296]. We effectively change $\Omega_m(z)$ during specific epochs (Ω_0 in the notation of [296]) while keeping the fraction Ω_b/Ω_m (at $z = 0$) constant. In a cosmology with massive neutrinos we must further shift these quantities by increasing the density in

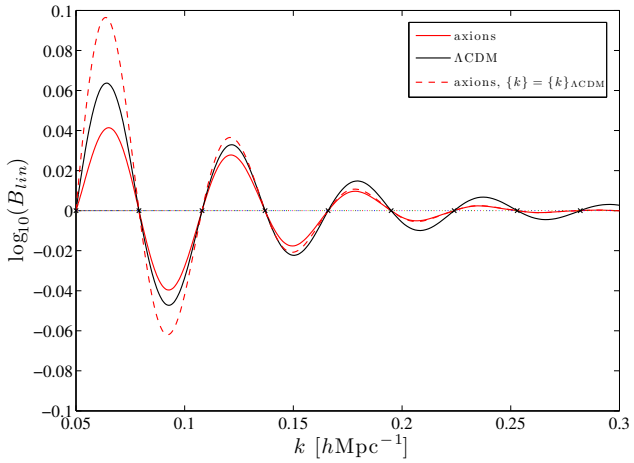

Figure 5.3 The BAO (at $z = 0$) for two models: a fiducial ΛCDM model, and a model with axions having $m_a = 10^{-30}$ eV, $f_{ax} = 0.1$. We also show the BAO for the same axion model, but where the smooth transfer function is splined assuming ΛCDM.

relativistic species at the relevant epochs appropriately for the mass of the neutrino species: a more complicated effect. Note that such distortions in the case of massive neutrinos are not modelled in either [292] or [293], where BAO are not present: it is only the scale dependent growth due to massive neutrinos that is considered there (see Section 5.3.3).

In Fig. 5.3 we show the BAO calculated numerically including the effects of ultra-light axions with $m = 10^{-30}$ eV, such that $k_m < k_{\rm eq}$, keeping Ω_d constant, and fitting a smooth $T_{\rm no\ osc}(k)$ using a cubic spline. We see an overall *suppression* of BAO amplitude caused by the presence of axions, despite an increased ratio Ω_b/Ω_d in the radiation dominated era.

Some model dependence enters in our definition of $T_{\rm no\ osc}(k)$. For our ΛCDM model, we find empirically the best k points for our cubic spline are $k = 0.001$ and $0.029 \leq k \leq 0.369$ with $\Delta k = 0.05$[3]. The step in the transfer function caused by axions is a smooth feature, and is best captured by introducing two extra points into the spline at $k = 0.0081, 0.02$, where the first is our estimate for k_m in this cosmology. The frequency of the BAO is fixed by the choice of the set $\{0.029 \leq k \leq 0.369, \Delta k = 0.05\}$, since the spline anchors $B_{lin} = 1$ at these values, therefore we cannot see any change in the frequency in the figure. That the same set and spacing of these values fits $T_{\rm no\ osc}(k)$

[3]This is slightly different from the values chosen in [298].

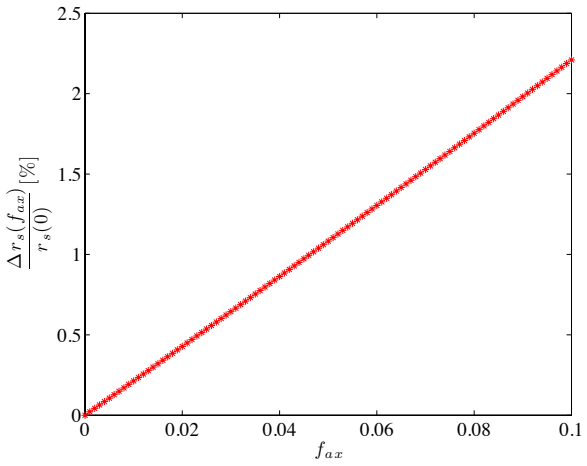

Figure 5.4 Change in the sound horizon at recombination as function of axion fraction as a percentage of its zero axion value, calculated using the formulae of [296].

(by eye) both with and without axions tells us that any change in frequency is small. To quantify this, we note that the frequency of the BAO is set by the sound horizon as $\sin(r_s k)$ [297]. In Fig. 5.4 we plot the change in the sound horizon calculated using the formulae of [296] as a function of f_{ax} as a percentage of its zero axion value. Axions always increase the size of the sound horizon, but even for large fractions the change is only by a few percent. The increase is linear, a fact not at all obvious from the relevant formulae.

We may ask whether the BAO can be biased by our choice of $T_{\text{no osc}}(k)$, effectively the underlying cosmology that we assume. In Fig. 5.3 we show an example of such bias by choosing to instead fit a smooth transfer function using the k points necessary for a ΛCDM cosmology, with no extra points to fit the step. This leads to an increase in the apparent BAO amplitude on large scales in the first few oscillations.

There is, according to our fits, a significant degeneracy between f_{ax} and $\Omega_c h^2$. We can introduce more CDM to fix the epoch of equality while ultra-light axions are present. Fixing a flat universe, this will reduce Ω_Λ by some small amount, the effect on the power spectrum being only through the normalisation [296], and invisible in ratios such as the BAO and $\tilde{T}_{ax}$. Restoring equality also restores the Silk damping scale and the drag epoch to their axion-free values, and this restoring effect dwarfs any small changes to the BAO through the alteration of the matter fractions $\tilde{f}_d$, $\tilde{f}_b$. In this case the BAO distortions can be removed, and the overall suppression of power

due to axions, $\tilde{T}_{ax}$, is also reduced as the increase in CDM shifts the power spectrum over to larger k. Avoiding such an alteration to the BAO may have effects on the CMB, and will need further compensation for example in fitting the Hubble expansion rate by lowering the DE equation of state, $w < -1$ [4]. We discuss some of these issues in Sections 5.3.4 and 5.3.5.

Real BAO measurements depend on redshift and can measure the expansion rate as a function of z [304], which can break some of the simple degeneracies discussed here, for the $z = 0$ BAO. In addition, their measurement in models including axions will therefore be complicated by the scale dependent growth introduced by the z dependence of T_{ax}, which we now discuss.

5.3.3 *The Growth Rate*

The growth rate is another useful cosmological observable, which has been measured by [306–310], and is used particularly in studies of modified gravity [138]. It is defined as:

$$f = \frac{d\ln\delta}{d\ln a} = \frac{\dot{\delta}}{\mathcal{H}\delta}\,. \tag{5.15}$$

In standard ΛCDM it is known to be approximately scale invariant and behave with redshift as $f = \Omega_m(z)^{\gamma_g}$ (this is a useful approximation, but see for example [311] for a recent discussion). We expect the growth rate for cosmologies including axions or massive neutrinos to pick up some additional scale dependence related to the appearance of steps in the matter power spectrum, and the corresponding non-factorisation of δ_m[5].

In Fig. 5.5 we plot the growth rate as function of z for a standard ΛCDM cosmology, and for a cosmology with a fraction of axions $f_{ax} = 0.01$. The growth rate with axions is plotted at two different k-values: the highest and lowest from $P(k)$ being $k_{min} \approx 10^{-5}h\,\mathrm{Mpc}^{-1}$, $k_{max} \approx 0.3h\,\mathrm{Mpc}^{-1}$. The true growth rate with axions (insert of Fig. 5.5) is seen to contain rapid oscillations that obscure the details of any step in $f(k)$ at a given redshift. These oscillations are not observable, and should be averaged

[4] see e.g. [305] for a model where it is possible to see an effective $w < -1$ if dark sector interactions are present but unaccounted for

[5] For a discussion on scale-dependent growth, see [312] and references therein.

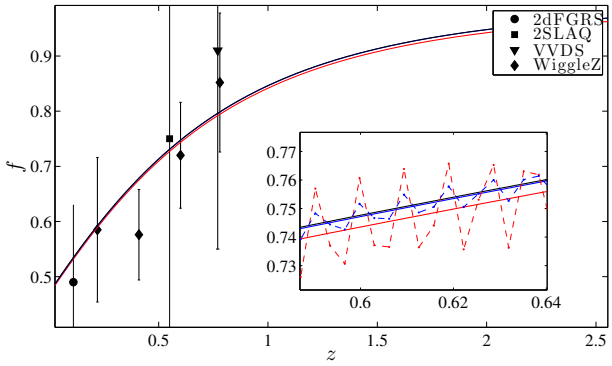

Figure 5.5 The (reduced) growth rate (Eq. (5.16)), $f(z)$, for $m_a = 10^{-30}$ eV, $f_{ax} = 0.01$, with current measurements of [306–309]. Red: $f_{(c+b)}(k = k_{max})$; blue: $f_{(c+b)}(k = k_{min})$; black: ΛCDM. Insert: zoom in to an arbitrary region of z showing oscillations in the true growth rate (dashed lines) about the reduced growth rate. The reduced growth rate is seen to be a good qualitative tracer of the average, following the shape in z and demonstrating scale dependence in its amplitude.

over to be consistent with the interpretation of scalar fields behaving as dark matter in the background, which is also only true on average as seen from the WKB solution to Eq. (4.16). To account for this easily we present an approximation scheme that is valid for both axion and massive neutrino effects on the growth rate when the fraction in these species is small, as is true for all of our fiducial models.

We split the density into two pieces: ρ_{c+b} in the dominant CDM and baryon components, and $\rho_{a+\nu}$ in the sub-dominant axion and massive neutrino components, and do the same for the perturbations. Using that $\rho_{a+\nu}$ is of order a few percent of ρ_{c+b} we expand the expression for f and drop terms of order $\rho_{a+\nu}^2$ and $\rho_{a+\nu}\delta\rho$ as being second order. Next we note that the overdensities will also be predominantly made up of CDM and baryons and so further expand in powers of $\delta\rho_{a+\nu}/\delta\rho_{c+b}$ and take terms of order $(\delta\rho_{a+\nu}/\delta\rho_{c+b})^2$, $\rho_{a+\nu}(\delta\rho_{a+\nu}/\delta\rho_{c+b})$ and $\delta\rho_{a+\nu}/\delta\rho_{c+b}^2$ as second order. The resulting expression for the growth rate is given by:

$$f = f_{(c+b)} - \left(\frac{\delta\rho_{a+\nu}}{\delta\rho_{c+b}}\right)(3 + f_{(c+b)}) + \frac{1}{\mathcal{H}}\frac{d}{d\tau}\left(\frac{\delta\rho_{a+\nu}}{\delta\rho_{c+b}}\right) + \text{h. o. t.}, \tag{5.16}$$

where $f_{(c+b)}$ is the growth rate in only the CDM and baryon components, but *calculated in the cosmology including the exotics*. We will call this the *reduced growth rate*. The true growth rate is a small perturbation about this, with all potentially oscillatory contributions isolated. The effects of the axions and neutrinos contribute to the

reduced growth rate only through the gravitational couplings via the potential h, and through the background expansion coming from $\mathcal{H}$.

It is this reduced growth rate that is shown in Fig. 5.5. In the blow up insert, we see that as expected it traces somewhat the average of the oscillations in the true growth rate, and shows scale dependence.

To more clearly show the scale dependence, in Fig. 5.6 we plot the reduced growth rate, $f_{(c+b)}$ as a function of k, normalised to unity on the largest scales so that z-dependence and normalisation to ΛCDM are absent . There is a clear step occurring at $k \approx \bar{k}_m$, the same scale as the suppression of power in $P(k)$.

We have checked that the same growth rate is recovered in both the case where massive neutrinos are included exactly[6], and where an averaging is taken over the oscillations present with an axion component. The accuracy of the approximation is to within a few percent of the total step size, which is itself only a few percent of the total value of the growth rate in a pure ΛCDM cosmology. It is thus this reduced growth rate that we will use in our forecasts for galaxy redshift surveys (GRS), which require the growth as a function of k in a redshift bin, and is output for them from our modified version of `CAMB`. In these forecasts we therefore make no use of the fitting $f = \Omega_m(z)^{\gamma_g}$.

Now we turn our attention to understanding the size, shape and position of this scale dependent growth in more detail. We have already described the effect of axions on the matter power spectrum using the transfer function $\tilde{T}_{ax}$. We use the same transfer function for the overdensities, i.e. $\delta_m = \tilde{T}_{ax}(k)\delta_{\Lambda\mathrm{CDM}}$. Note that this is smooth as a function of z: T_{ax} is already an on-average fitting. Note also that this is an alternative to parameterisations of scale dependent growth used in discussing massive neutrinos in [145, 292]. Substitution into Eq. (5.15) immediately yields:

$$\begin{aligned} f &= f_{(\Lambda\mathrm{CDM})} + \frac{1}{\mathcal{H}}\frac{\dot{\tilde{T}}_{ax}}{\tilde{T}_{ax}} \\ &= f_{(\Lambda\mathrm{CDM})} - \Delta f(k,z)\,. \end{aligned} \tag{5.17}$$

[6] In this case the growth rate contains no visible-by-eye oscillations, and is computed exactly using a numerical derivative of δ.

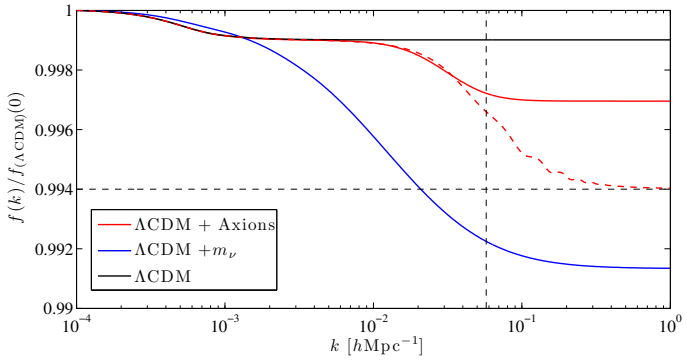

Figure 5.6 The reduced growth rate, $f_{(c+b)}(k)$, for three fiducial cosmologies: ΛCDM; ΛCDM with axions: $m_a = 10^{-29}\,\mathrm{eV}$, $f_{ax} = 0.01$; ΛCDM with massive neutrinos, $m_\nu = 0.055\,\mathrm{eV}$, $N_{\mathrm{eff,mass}} = 3.04$. We normalise all growth rates to one on the largest scales to account for normalisation by ΛCDM on the largest scales at arbitrary redshift. The results shown in solid are numerical, and the dashed line is that predicted by our fit for Δf in the presence of axions, Eq. (5.17). The vertical dashed line on the plot shows the expected value of $\bar{k}_m$, Eq. (4.60), while the horizontal dashed line shows the expectation of Eq. (5.18).

Using our fitting formulae we can calculate Δf. We work in the regime where $\tilde{f}_{ax}$ is fixed as a function of time, i.e. the axions have completed their transition to matter like behaviour, which will always be true for our fiducial models in the redshifts of interest, and in any case the fitting formulae break down where this condition is not satisfied.

In the redshifts of interest, the z dependence of the additional term is mild relative to $f_{(\Lambda\mathrm{CDM})}$, and so the shape of the growth rate as a function of z, modulo the oscillations, is largely unaltered by the presence of axions. In Fig. 5.5 we have already shown the reduced growth rate as a function of z, and see that this is indeed the case. In Fig. 5.6 we also show the fit of Eq. (5.17). Notably, since the fit gives us the total growth, f, rather than the reduced growth, the fit overestimates the size of the step. This can be taken as an indication of the amount by which the reduced growth is perhaps an underestimate of the true step.

We estimate the change in growth rate amplitude at scales below $\bar{k}_m$ to be:

$$\Delta f(k > \bar{k}_m, z = 0) = (1 - q) \approx \frac{3}{5} f_{ax}\,, \tag{5.18}$$

for small f_{ax}.

The most important feature of this analysis has been the identification of smooth,

step-like, scale dependent growth occurring in models containing an ultra-light scalar field caused by the same physics as causes the suppression of power in the matter power spectrum, and also mimicking the corresponding effect due to massive neutrinos, though to a lesser degree, as seen in Fig. 5.6. While the size of this effect is not accurately estimated analytically, it's location in k-space can be predicted with reasonable accuracy. The location of the step depends only on the axion mass, while the size depends only on the density fraction. Measurements of the growth rate amplitude will therefore measure the fraction in axions, but be insensitive to the mass unless scale dependent growth can be resolved at $\bar{k}_m$. Suppression of the growth rate, if measured in a non-scale dependent way, is clearly degenerate with the total total matter content, evident from the simple fitting in ΛCDM of $f = \Omega_m(z)^{\gamma_g}$, and suggesting further positive correlation between f_{ax} and $\Omega_c h^2$. Again, using a single observable, precise scale dependent measurements are required to isolate a unique signal.

Weak lensing tomography also measures the growth rate, and we can use this to put tight constraints on the existence of smooth components, such as axions at wavenumbers larger than k_m, or massive neutrinos at wavenumbers larger than k_{FS}, from the amplitude change relative to ΛCDM [313]. In the case of weak lensing, which measures the growth rate more accurately and via different means, no approximation is made at all and the full numerical evolution of the overdensity is used, i.e. we will not use the reduced growth in lensing. In this case, the oscillations are naturally smoothed by the redshift integral (see below).

5.3.4 Galaxy Weak Lensing

Galaxy weak lensing was first observed in 2000 by [314–317]. The measurement of the weak lensing power spectrum is a direct probe of the dark matter. Through tomography, made possible by measuring galaxy photometric redshifts, we also gain information in the radial or temporal direction, and probe the growth rate and distance-redshift relation. This measurement of the growth rate gives constraining power for the presence of ultra-light axions.

We first review some weak lensing basics. The effect of weak gravitational lensing

is usually split into two components: the complex shear (γ_1, γ_2) and the convergence κ, with the shear being derivable from the convergence (see [318] for a complete review). Let us denote χ the comoving distance:

$$\chi(z) = \int_0^z \frac{dz'}{H(z')}\,, \tag{5.19}$$

and $r(\chi)$ the coordinate distance, defined by $r(\chi) = K^{-1/2}\sin\left(K^{1/2}\chi\right)$ for a closed universe, $r(\chi) = \chi$ for a flat universe, and $r(\chi) = (-K)^{1/2}\sinh\left((-K)^{1/2}\chi\right)$ for an open universe, where K is the curvature.

The convergence in a given direction $\hat{\boldsymbol{n}}$ of the sky is given by an integral along the line-of-sight [319]

$$\kappa(\hat{\boldsymbol{n}}, \chi) = \int_0^\chi W(\chi')\delta(\chi')\mathrm{d}\chi'\,, \tag{5.20}$$

where δ is the overdensity and

$$W(\chi) = \frac{3}{2}\Omega_m H_0^2 g(\chi)(1+z)\,, \tag{5.21}$$

is a weighting function. $g(\chi)$ is given by

$$g(\chi) = r(\chi)\int_\chi^\infty \mathrm{d}\chi' n(\chi')\frac{r(\chi'-\chi)}{r(\chi')}\,, \tag{5.22}$$

where $n(\chi)$ is the source distribution:

$$n(z) = \frac{3}{2z_0}\left(\frac{z}{z_0}\right)^2 e^{-(z/z_0)^{3/2}}\,. \tag{5.23}$$

We can now expand the convergence in multipoles κ_{lm}, and define the convergence power spectrum by the relation

$$\langle \kappa_{lm}\kappa_{l'm'}\rangle = \delta_{ll'}\delta_{mm'}P_l^\kappa\,, \tag{5.24}$$

and using Eq. (5.20) under Limber's approximation, we have the following expression:

$$\begin{aligned} P_l^\kappa &= \int_0^{\chi_\infty} \mathrm{d}\chi \frac{W^2(\chi)}{r^2(\chi)} P(l/r(\chi), z)\,, \\ &= \frac{9}{4}\Omega_m^2 H_0^4 \int_0^{\chi_\infty} d\chi \left(\frac{g(\chi)}{r(\chi)}\right)^2 (1+z)^2 P(l/r(\chi), z)\,, \end{aligned} \tag{5.25}$$

where χ_∞ stands for $\chi(z\to\infty)$, and P is the matter power spectrum evaluated at $k = \ell/r$.

In this way, the convergence power spectrum depends directly on the matter power spectrum at redshift z, and thus tomographic information will measure the growth rate. The scale at which the growth rate is measured depends on the pixel size, and for our purposes this will measure *below* either k_m or k_{FS} for *all* axion and neutrino masses considered. Therefore, the constraint on these species will be independent of this scale and will depend only on the density fraction, i.e. for the case of ultra-light axions where the density fraction depends only on the initial misalignment angle *constraints on f_{ax} from weak lensing are expected to be independent of axion mass*, but due to their similar effects will be degenerate with the neutrino density fraction, and the dark energy equation of state, w (not forecast), the strongest constraint being from the amplitude of the growth rate [313]. In addition, our method for calculating the weak lensing tomography comes directly from integrating the density parameters inside `CAMB`, and so is not limited by the approximation of the reduced growth rate used for GRS, as mentioned already above.

Note that this effect in the growth rate is distinguishable from many DE effects, which occur predominantly through modifying the distance-redshift relation via changes in the expansion rate, $H(z)$, in Eq. (5.19). As we have already seen, axion and neutrino effects on the expansion rate during the matter era are small to non-existent. Establishing the distance-redshift relation in addition to the growth rate using lensing tomography serves to break degeneracies occurring between axion/neutrino components and DE. For example, as discussed earlier one can change the DE contribution to restore $k_{\rm eq}$ and the canonical shape of $P(k > k_{\rm eq})$. However this then demands a change in w if we are also to restore the Hubble expansion H_0, leading to an apparent degeneracy between w and m_ν or f_{ax}, which can be broken by lensing tomography or BAO measurements that pin down the expansion as a function of redshift [295].

Because of the dependence on $P(k, z)$, all of our intuition of the similarity of axion and neutrino effects on the matter power spectrum should carry over into galaxy weak lensing. However, only our Fisher matrix analysis will show what degeneracies really exist in the fiducial models we investigate under the precision of the observations in question.

In Fig. 5.7 we show the effect in the convergence power spectrum of adding an

axion fraction $f_{ax} = 0.01$ in a species of mass $m_a = 10^{-29}\,\mathrm{eV}$ in various different redshift bins. The unclustered species causes a suppression of power on small scales, which increases with increasing fraction in that species, as one would expect from the structure suppression in $P(k)$. The errors on the convergence power spectrum expected form a large future survey are also shown (see Appendix A of [279] for survey parameters). In some single redshift bins, these are not strong enough to distinguish a ΛCDM model from a model with axions at 1σ, while in others they just are. The amplitude of suppression of power is independent of axion mass, and like effects in the growth rate is smaller than the same effect due to massive neutrinos.

A possible uncertainty on constraints from weak lensing lies in the treatment of the non-linear regime, necessary for weak lensing calculations. Inside `CAMB` we use a standard version of halofit [320], which is optimised from simulations to standard CDM and may not accurately describe the non-linear effects of axions or massive neutrinos. However, mistreatment of non-linear effects likely leads to an underestimate of the suppression of power on small scales [145], and so our projected weak lensing constraints should be conservative. Hannestad et al [295] estimate that the effect of assuming no non-linear effects in neutrinos leads to an uncertainty in lensing observables of around 0.1%. For a discussion of the non-linear effects of neutrinos see [321], and for an N-body simulation with ultra-light scalars, see [124].

5.3.5 *The CMB*

5.3.5.1 *Temperature Power Spectrum*

Here we discuss axion effects on the CMB temperature-temperature auto correlation power spectrum, C_ℓ^{TT}, the TT power spectrum (for a review of CMB anisotropies, see [42], and for specific applications to HDM and neutrinos see [322, 323]).

In Fig. 5.8 we show the effects of various axion fractions and masses on C_ℓ^{TT}. Axions have the effect of shifting the acoustic peaks by changing the epoch of equality. The changes in equality in these models, $\Delta z_{\rm eq}(f_{ax}) = z_{\rm eq}(0) - z_{\rm eq}(f_{ax})$, are $\Delta z_{\rm eq}(0.1) = 328$ and $\Delta z_{\rm eq}(0.01) = 32.2$ respectively.

The most pronounced effect for heavier axions occurs in the Integrated Sachs-

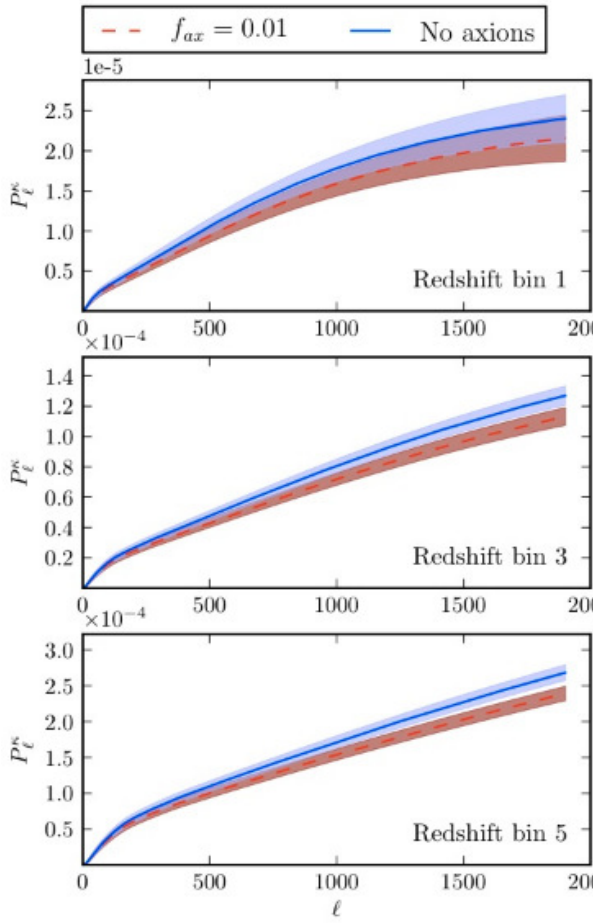

Figure 5.7 The convergence power spectrum for three redshift bins, with expected 1σ errors from a large future weak lensing survey, defined in Appendix A of [279]. Overlapping regions of error are shown in purple. The models compared are ΛCDM, and ΛCDM+f_{ax}, with $m_a = 10^{-29}$ eV, $f_{ax} = 0.01$. This plot was made by using a further modification of `CAMB` to include weak lensing as well as axions, which was written by Maxime Trebitsch.

Wolfe (ISW) region at very low ℓ, as pointed out in [205]. As also pointed out in [205], this ISW effect is maximal for masses at the larger end of those we study, suggesting stronger CMB constraints at larger masses. These heavier axions, as discussed earlier, are making their transition from cosmological constant to CDM behaviour very close to CMB formation. As such, they are contributing a significant fraction to the energy density while in a non-standard stage of evolution, and thus causing large variations in the potential on the largest scales where this transition is beginning. At high ℓ there is no difference in the effect of axions of different mass, so small scale CMB measurements will constrain the total fraction possible in ultra-light

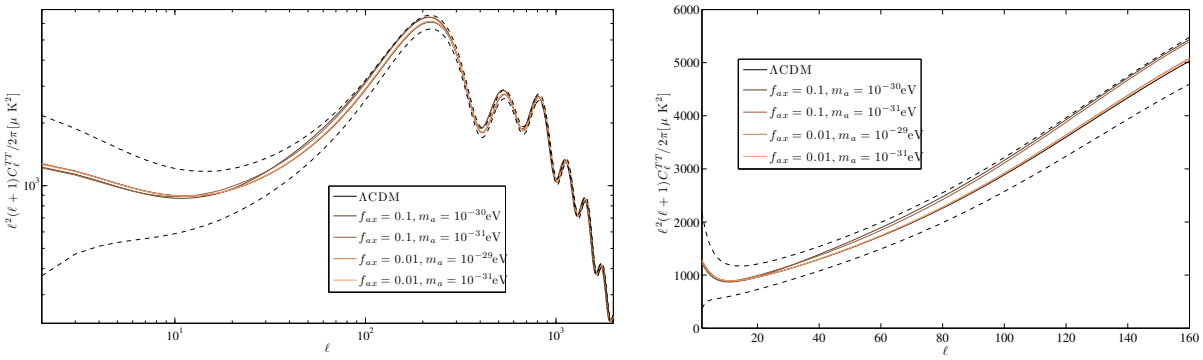

Figure 5.8 Effect of axions on the CMB power spectrum. Left panel: TT power spectrum. Right Panel: magnified low ℓ region showing the ISW effect. Expected error bands from Planck are shown as dotted lines, see [279] for details.

axions independent of mass. Heavier axions than those we consider here that have completed their transition to CDM in the radiation dominated era should be expected to have no effect at all on the (unlensed) CMB temperature power spectrum, as they are gravitationally indistinguishable from CDM in the background (however, see Chapter 6).

In addition, the low-ℓ ISW effect distinguishes axions from massive neutrinos. It is in the high-ℓ region of the TT power spectrum that evidence from the CMB for extra relativistic energy density comes, due to the effect of this energy density on the pre-recombination expansion rate and corresponding increase in the amount of Silk damping leading to the required lower fluctuation amplitude [54, 324]. The best way to explore the effect of extra relativistic species on the TT power spectrum is to hold fixed a number of quantities and isolate the extra effects at high-ℓ. We can apply the same logic to further understand the effect of ultra-light axions since they affect the epoch of equality in the same way as extra relativistic energy density: increasing $N_{\mathrm{eff,rel}}$ means more radiation, making equality later, while introducing axions with $z_{\mathrm{osc}} < z_{\mathrm{eq}}$ reduces the amount of dark matter at equality, giving the same effect [323]. The amount of baryons, ρ_b, should be fixed to keep the even and odd acoustic peaks in the correct ratio of amplitude. The epoch of equality, z_{eq}, being tightly constrained by the position of the first peak should then be fixed by changing ρ_d. The angular size of the sound horizon, $\theta_s = r_s/D_A$, should be fixed by changing H_0. Finally, the height of the first peak, which isolates the low and high-ℓ effects, should be fixed by

changing the scalar amplitude, A_s.

When all of these changes are made, the result is to completely remove the effect of axions from the CMB, while the same changes made in a cosmology $\Delta N_{\rm eff} > 0$ leave the expected effect in the Silk damping tail This is because the extra relativistic energy density has left an imprint in altering the expansion rate during the radiation era. In an axion cosmology, restoring equality, as mentioned above in our discussion of the BAO, also restores the Silk damping scale. Axions in the CMB are degenerate with a combination of changing ρ_d and H_0, while neutrinos are not. These observations are important, since they will apply also to massive neutrinos: *the CMB breaks the degeneracy between axions and neutrinos due to neutrino effects on the expansion rate in the radiation era, and axion ISW effects in the matter era*.

E-mode CMB polarisation auto-correlation power spectra , C_ℓ^{EE}, and temperature-polarisation cross-correlations, C_ℓ^{TE}, the EE and TE power spectra, are also useful cosmological probes, and they too are used in our forecasts. Polarisation will also be particularly important if ultra-light axions have the model dependent coupling to $\vec{E} \cdot \vec{B}$. In this case the polarisation angle can be rotated by $\Delta\beta \approx 10^{-3}$, an effect within reach of Planck and CMBPol [104]. If an observation of this rotation were combined with other axion observations as described above, this would provide very strong evidence for the existence of axions with this coupling, but since the coupling is model dependent, polarisation rotation need not accompany other axion effects. Observation of polarisation effects without other axion effects would, however, rule out axions as a cause of the rotation. We do not include the possibility for such a rotation in our models.

The CMB is an important constraint on another effect of axions, which we do not consider in this Chapter: axion isocurvature perturbations. These will be discussed in detail Chapter 6.

5.3.5.2 CMB Lensing

CMB lensing has recently been detected and measured by ACT [129, 325], and its measurement by Planck and other future surveys will be a powerful cosmological

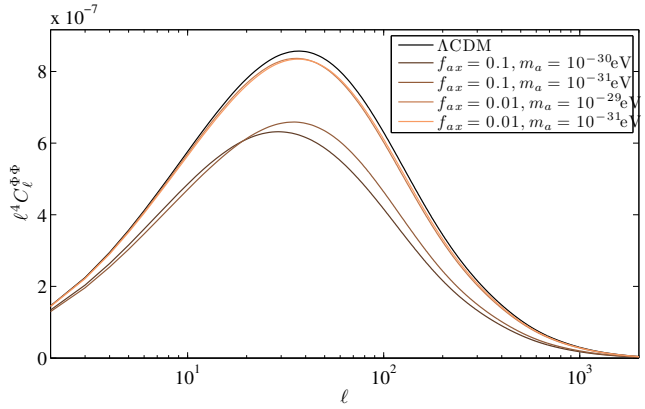

Figure 5.9 The CMB lensing power spectrum, calculated using CAMB for ΛCDM and axion cosmologies.

probe.

CMB lensing, like galaxy weak lensing, is a direct probe of the DM density and expansion history between the surface of last scattering and us. Hence, in terms of CMB observables, the EDE fraction and Σm_ν are most strongly constrained by CMB lensing [145]. However for our purposes, we cannot include CMB lensing and galaxy weak lensing together since addressing correlations between these observables is beyond the scope of this thesis. We do not use CMB lensing in our forecasts, but we show the power spectrum here and make some comments for the sake of completeness.

We show the lensing power spectrum in Fig. 5.9. A large fraction in axions produces a noticeable effect in reducing the lensing power. However, if as above we fix $z_{\rm eq}$ and θ_S again the effect can be totally removed. This occurs due to the degeneracy of axions with other parameters in their effects on the matter power spectrum, as already discussed.

5.4 COSMOLOGICAL OBSERVABLES: FORECASTS

In this section we consider the potential to identify traces of axion dark matter with some of the cosmological probes of the upcoming decade. We adopt a Fisher matrix (FM) approach to forecast results achievable with a next generation galaxy redshift and weak lensing survey. There are many large weak lensing and galaxy

redshift surveys proposed for the coming years: we choose to model our surveys to be similar to the proposed Euclid mission [67, 68]. We combine these results with Fisher forecasts for an all sky CMB survey based on the Planck mission [14]. The Fisher matrix provides the lowest possible intrinsic statistical uncertainty, thus results from Fisher forecasts tend to be optimistic when compared to real results.

The forecasts made in this Chapter for Galaxy Redshift Surveys (GRS) and Weak Lensing Tomography (WLT) are described in [279]. They were made using Fisher matrix codes written by Edward Macaulay and Maxime Trebitsch. These codes utilised the version of `CAMB` written by me. For the CMB forecasts, we used "FisherCodes" by Sudeep Das [326], suitably modified by me to include the axion component.

5.4.1 *Results: CMB, Galaxy Redshift Survey and Weak Lensing Forecasts*

We first consider a cosmology with massive neutrinos and a fraction of CDM in axions. We assume a fiducial model with parameters $w = -1$, $\Omega_b h^2 = 0.02258$, $\Omega_d h^2 = 0.1109$, $n_s = 0.963$, $A_s = 2.3 \times 10^{-9}$, $m_\nu = 0.055$eV, $N_{\rm eff} = 3.04$ and $f_{ax} = 0.01$. We use a fixed value of $H_0 = 71.9$km s^{-1}Mpc^{-1}. Following [327], we also include the optical depth to reinozation $\tau = 0.166$ and helium fraction $Y_{He} = 0.24$ as free parameters in the CMB FM. Similarly, galaxy bias $b = 1.7$ and non-linear velocity dispersion $\sigma_v = 350$ kms^{-1} were included as free parameters in the GRS FM. These parameters were marginalized over before the matrices were combined. CMB, GRS and WL Fisher matrices were calculated for this fiducial cosmology for $m_a = 10^{-29}, 10^{-30}, 10^{-31}$ and 10^{-32} eV. As an example, Fisher ellipses for the $m_a = 10^{-30}$ eV case are plotted in Fig. 5.10 for axion and neutrino parameters. We see the expected negative correlation between f_{ax} and m_ν, but a small positive correlation between f_{ax} and $N_{\rm eff}$ in GRS, since in the case of massive neutrinos increasing $N_{\rm eff}$ adds more matter at late times and indeed boosts the power [323].

With the different sets of forecasts over a range of axion mass, we can compare how the fully marginalised uncertainty on our parameters varies with axion mass. We can see in Fig. 5.11 that the uncertainty in f_{ax} from galaxy redshift surveys does not change appreciably with axion mass, as expected for the masses under consideration, and providing a good test that any numerical uncertainties, for example in the background

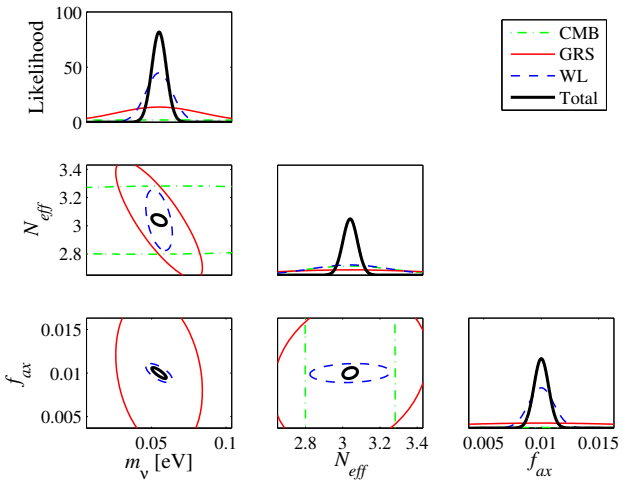

Figure 5.10 One standard deviation Fisher ellipses for m_ν, $N_{\rm eff}$ and f_{ax}. The full combined set of parameters also includes w, $\Omega_b h^2$, $\Omega_c h^2$, n_s and A_s, which have been marginalized over in this plot. Here the weak lensing forecast (blue dashed line) provides the best constraints. These forecasts are for an axion mass of $m_a = 10^{-30}$ eV. Figure made by Edward Macaulay.

evolution, which would vary with mass, do not affect the constraints. However, we do see some unexpected variation in the weak lensing constraints with mass, of $\mathcal{O}(1)$ of the total uncertainty. We believe this is due to numerical uncertainty in the complex calculation for lensing with an oscillating background, and so our results here can only be considered reliable to within this extra uncertainty.

The CMB becomes more sensitive to f_{ax} for higher mass: this we believe to be physical. It is caused by the increased ISW effect for axions that begin oscillations at redshifts closer to the surface of last scattering, as expected. The trend to slightly better constraints at higher mass has been tested and seen to be stable: stability requires calculations to be made at extremely high numerical accuracy. The required level of accuracy is computationally very expensive, and ensuring its stability has been the main limitation on models we have been able to forecast for. The constraining power of the CMB alone allows $f_{ax} \approx 0.1$ to be detected, which is consistent with the results of [205] and Chapter 6.

The improvement in the CMB measurement of f_{ax} is shown again in Fig. 5.12 for the range of fiducial m_a, where we show the Fisher ellipse with $\Omega_d h^2$. These results show the expected positive correlation between f_{ax} and $\Omega_d h^2$ caused by the effects on

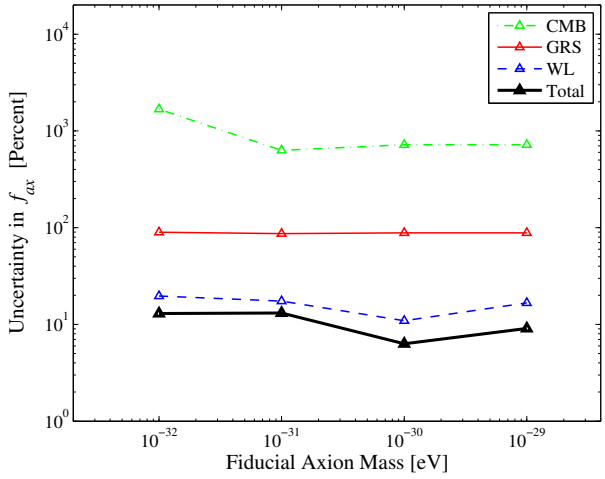

Figure 5.11 Marginalized uncertainty in f_{ax} for our three observables, evaluated for four different fiducial axion masses, for the cosmology ΛCDM+f_{ax} + m_ν. The uncertainty from the GRS and WLT surveys does not change appreciably across the range of axion mass, whereas the uncertainty from the CMB survey decreases for higher axion masses. We cannot be sure if the small decrement in uncertainty in the WLT survey at $m_a = 10^{-30}$ is significant. Figure made by Edward Macaulay.

equality already discussed. The increase in CMB constraining power at high masses does not reach a sufficient level to break this degeneracy.

In Fig. 5.13 we show the effect of having redshift information on the constraints from a galaxy survey. Although a measurement of the power spectrum at a single redshift cannot distinguish $f_{ax} = 0.01$ from $f_{ax} = 0$ at 1σ, this becomes possible when all z bins are combined. We reiterate that this constraint is independent of axion mass.

Fig. 5.14 shows the expected mild positive correlation between constraints on f_{ax} and constraints on n_s from GRS. The constraints on $\Omega_b h^2$ and f_{ax} are shown in Fig. 5.15 and show a negative correlation in GRS, and small positive correlation in WLT. Both figures show no visible correlation in the CMB on the scale of the plot. The strong constraining power of the CMB on $\Omega_b h^2$ and n_s relative to f_{ax} breaks the expected degeneracies at this level.

For comparison, we also considered a cosmology as before, but with massless neutrinos. The constraints on f_{ax} from all observables, along with the mass dependence, was approximately the same as with massive neutrinos.

We finally consider an axion-free cosmology ($f_{ax} = 0$), with massive neutrinos. The Fisher ellipse for $N_{\rm eff}$ and m_ν is shown in Fig. 5.16 for our different observables.

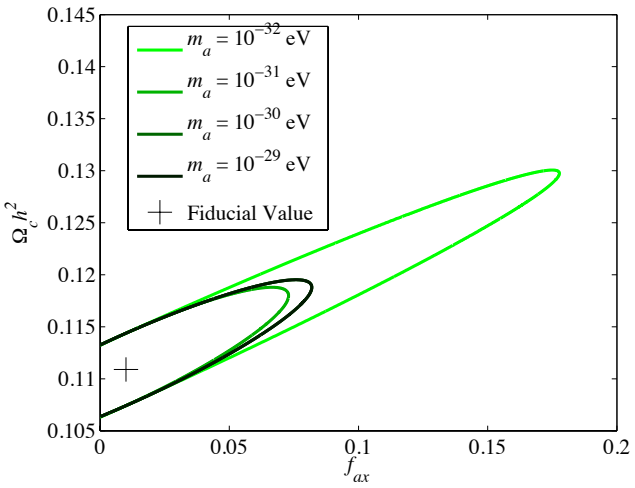

Figure 5.12 Fisher ellipses for our forecast CMB survey for parameters $\Omega_c h^2$ and f_{ax} for a range of axion mass. The ellipses for $m_a = 10^{-29}$ eV and $m_a = 10^{-30}$ eV lie directly on top of each other with the thickness of line in the plot. Note that if we fix f_{ax}, we obtain the same uncertainty on $\Omega_d h^2$ for all the different masses. This plot was made by Edward Macaulay.

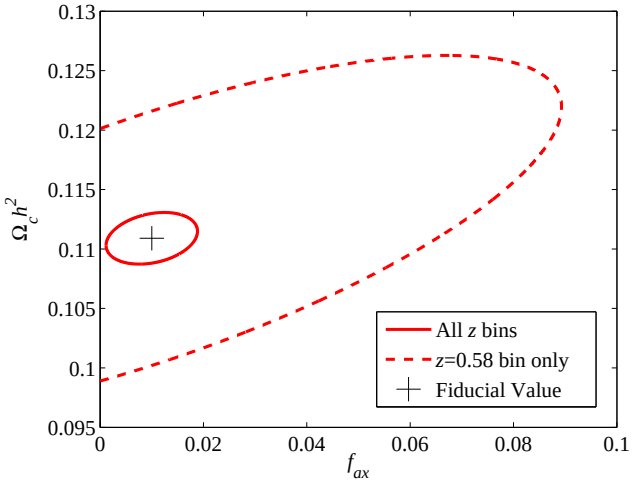

Figure 5.13 Forecasts on $\Omega_d h^2$ and f_{ax}, for the galaxy redshift survey. With one redshift bin of the survey (dashed line), the survey cannot discriminate between a cosmology with or without axions, and can only rule out $f_{ax} \lesssim 10\%$. When constraints from all 15 redshift bins are combined, detecting $f_{ax} > 0$ is just possible to 1σ. The constraints are the same for all axion masses. Figure made by Edward Macaulay.

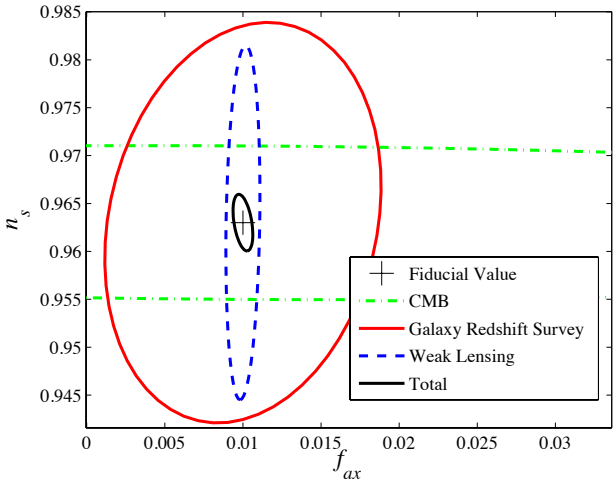

Figure 5.14 Constraints on n_s and f_{ax}, for $m_a = 10^{-30}$ eV, showing the expected positive correlation from galaxy redshift surveys. At this level of constraint, no correlation is visible in the CMB. Figure made by Edward Macaulay.

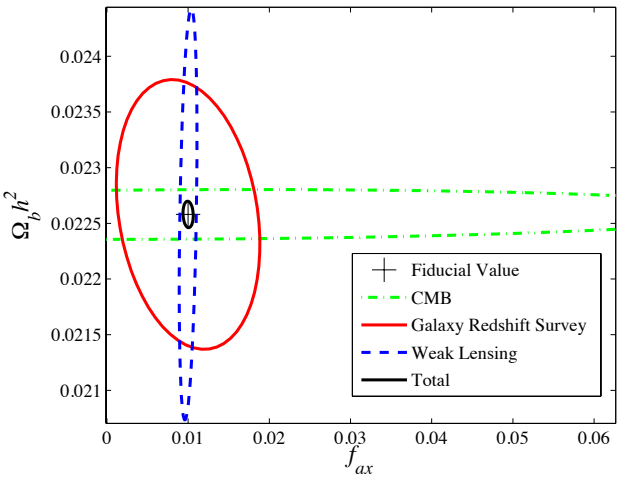

Figure 5.15 Constraints on $\Omega_b h^2$ and f_{ax}, for $m_a = 10^{-30}$ eV. We note a negative correlation from galaxy redshift surveys, whereas at this level of constraint, no correlation is visible in the CMB. Figure made by Edward Macaulay.

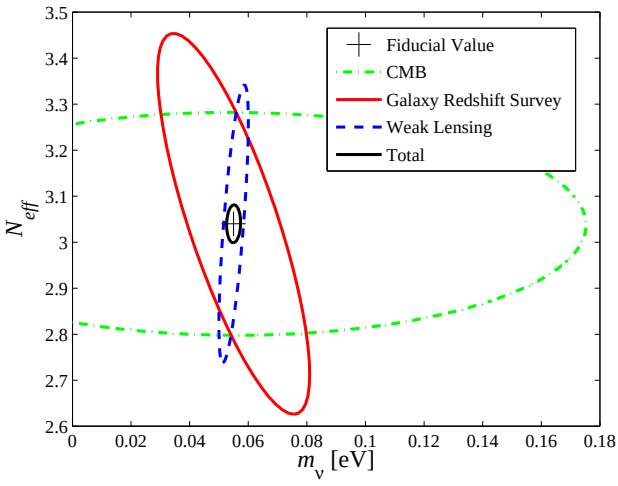

Figure 5.16 Constraints on $N_{\rm eff}$ and m_ν for the axion-free cosmology. This plot was made by Edward Macaulay.

5.5 DISCUSSION AND CONCLUSIONS

Ultra-light axions and sub eV mass neutrinos are on the face of it very similar, when viewed in their effects on the matter power spectrum, and we seem hard pressed to distinguish them from ΛCDM, never mind one another, within the limits of current or future observations of galaxy clustering alone. There are in addition many other cosmological ingredients that can mimic various parts of such a signal and display degeneracies with axions and neutrinos. Despite this, we have seen that in fact quite tight bounds could be placed on the axiverse by combining many precision cosmological observations, in particular weak lensing tomography.

All the effects of an ultra-light species stem from two main sources: the effective removal of some dark matter from the background expansion while the field is frozen at redshifts greater than $z_{\rm osc}$ (or, in an alternative parameterisation, the addition of extra matter after this time), and the suppression of structure due to the quantum pressure of the field below the scale k_m, an effect very similar to neutrino free streaming. This is because the axions are having purely gravitational effects. The effects of quantum pressure on the matter power spectrum, growth rate, and galaxy weak lensing can all be qualitatively understood in terms of the simple step picture provided by the fitting of T_{ax}. The effects on the CMB, and additional effects in the BAO can be

understood simply from the transition in scalar field behaviour at $z_{\rm osc}$.

An important positive correlation exists between the fraction in axions, f_{ax}, and the total content in DM, $\Omega_d h^2$, since in this parameterisation these ingredients have opposite effects in moving cosmological time scales, such as equality and Silk damping. However, f_{ax} can still be quite tightly constrained and this degeneracy broken. In the case of GRS observables alone, a fraction in axions of 1% can be distinguished from zero at 1σ, independent of mass. Redshift information breaks the degeneracy with CDM by resolving growth rate effects that compliment those obtained from the power spectrum alone. Axions cause a distinctive scale dependent suppression of the growth rate at the scale k_m, in a manner which can be understood in order of magnitude as being due to the step in the power spectrum, T_{ax}. $\Omega_d h^2$ also controls the magnitude of the growth rate, so that measurements of growth and clustering together can constrain CDM and axions independently.

We have checked for dependence of our results when varying k_{max} and the bias. A change in k_{max} from $0.156h\,\mathrm{Mpc}^{-1}$ to $0.146h\,\mathrm{Mpc}^{-1}$ has very little effect on the GRS uncertainties on f_{ax}, as expected due to the axion effects occurring predominantly at much smaller k's. However, introducing a redshift dependent bias of $b = 0.6(1+z)$ has a slightly larger effect, pushing the 1σ error to be *just* larger than $f_{ax} = 0.01$ from GRS alone. The constraint is slightly worse when massive neutrinos are not present. The small dependence on neutrinos can be understood since neutrino mass adds more radiation at early times, and consequently moves the relevant scales, in this case making the axion effects slightly harder to resolve in the surveys considered.

The *mass independence* of axion constraints from galaxy redshift surveys and weak lensing can be important for the axiverse scenario, since a measurement will consequently constrain the existence of any and all species in the mass range we have investigated, where axions begin oscillating in the matter dominated era, $m_a \lesssim 10^{-28}\,\mathrm{eV}$.

The correlation of axions with baryon content is more subtle, in that it is observable dependent. We expected a positive correlation in CMB observables: increasing f_{ax} delays equality, while increasing $\Omega_b h^2$ adds more matter, making it earlier. However, the vastly different constraining power of the CMB between these observables broke

this degeneracy. On the other hand, we found a negative correlation in GRS, where baryons have the competing effect of also suppressing structure formation. Similarly, we see a positive correlation between axions and the number of effective neutrino species. One normally thinks of extra relativistic energy density causing suppression of power in the CMB, but this is only true if all other parameters are altered so as to preserve equality and the angular horizon size. A simple increase in $N_{\rm eff}$ actually boosts CMB power, and competes in an opposite manner to axions. If equality and horizon size are fixed in the presence of these ultra-light axions, the CMB is left unchanged: axions effect the CMB purely through the expansion rate, the change to which is only slight near $z_{\rm osc}$, making the unlensed CMB a poor observable to look for axions.

Constraints on axions from the CMB are subtly dependent on axion mass. Although the axions effect the CMB purely gravitationally via the expansion rate, they do not simply "switch on" to DM behaviour out of nowhere, but contribute as a DE term prior to this. If the DE contribution is significant near to the surface of last scattering, then the CMB becomes more sensitive to these axions. This is true for the heaviest axions we have considered, since their masses cause slow roll to occur near to last scattering, and the axions transition through this while contributing of order $f_{ax}\Omega_d h^2$ to the energy density. The constraints on this axion mass range coming from the CMB are thus related to well known CMB constraining power on EDE [144]. This result is also consistent with the results of [205], where it is this mass range that is most strongly constrained by the CMB, with a sharp rise in uncertainty outside of this range when axions are either pure CDM or pure cosmological constant as far as the background expansion post recombination, and hence the CMB, is concerned. However, axions are distinct from EDE in that they exit slow roll shortly after this, whilst EDE does not: it remains in a scaling solution. An investigation into correlations between such axions and popular models of EDE would be interesting to pursue.

In all cases, we have seen the tightest constraints on f_{ax} coming from weak lensing, and just like GRS the strength of this constraint depends on the photometric redshift measurement i.e. on tomography. Lensing tomography allows another measurement of the growth rate, and the redshift evolution of the axion suppression of small scale

convergence power can be resolved. We have checked that varying ℓ_{max} from 1900 to 1500 has very little effect on the uncertainty. This is, just as the case with GRS, expected since axions have their effects predominantly at much smaller ℓ (larger scales) than this.

Our major result has been to show that with current and next generation galaxy surveys alone it should be possible to unambiguously detect a fraction of dark matter in axions of the order of a few percent of the total.

In conclusion, we have seen that even such a simple ingredient as a light, non-interacting scalar field, such as the axion, can lead to interesting cosmology. The effects are sometimes subtle, and minor, making such an ingredient hard to spot. When these constraints are independent of the mass of the scalar field, they will be important to bound a large range of parameter space in the string axiverse. However, we have shown there is the potential to determine ultra-light axions as a distinct dark matter ingredient to high precision using future observations, in particular via weak lensing tomography.

6

ISOCURVATURE PERTURBATIONS AND THE ENERGY SCALE OF INFLATION

"The primordial cosmic Buddha is infinitely boundless, independent in all circumstances, in a thousand different daily affairs – why do you not see it?

It is because you still have calculation in your mind and your views are limited to effect and cause: you are note yet able to transcend religious sentiments and get beyond the shadows and traces."

Huang-lung Hui-nan, in *Classics of Zen and Buddhism, T. Cleary*

PREFACE

This Chapter presents a short introduction to isocurvature perturbations in axion cosmologies. We will derive the appropriate initial conditions and state the relation between the isocurvature amplitude and the energy scale of inflation. Numerical results on the various power spectra and observables are presented under an approximate formulation that differs from the exact treatment in Chapters 4 and 5. This will allow us to explore a wider region of parameter space, and is also appropriate for use in an MCMC analysis that is necessary to constrain this model, and of which brief results are presented. This represents an ongoing project of as-yet unpublished work.

6.1 THE FLUID APPROXIMATION FOR AXIONS

The equations of motion (EOMs) for a perturbed scalar field on a cosmological background (see Section 4.1) can be re-written in terms of those for a perfect fluid [115] with an equation of state $w_a = \frac{P_a}{\rho_a}$ and sound speed $c_s^2 = \frac{\delta P_a}{\delta \rho_a}$ (see Chapter 1). We will fix the background evolution by approximating that w_a makes an instantaneous transition from cosmological constant to matter like behaviour at some value of the scale factor, $a_{\rm osc}$:

$$w_a(a) = -\theta(a_{\rm osc} - a)\,. \tag{6.1}$$

where $\theta(x)$ is the Heaviside function.

The evolution of the perturbations, δ_a and θ_a, will be fixed by approximating the evolution of c_s^2. Since in Section 6.2 we will be interested in very early times, we must append to Eq. 4.50 the behaviour when $a < a_{\rm osc}$:

$$\begin{aligned} c_s^2 &= -1; \quad \forall a < a_{\rm osc}\,, \\ c_s^2 &= \frac{k^2}{4m_a^2 a^2}; \quad k < 2m_a a\,, \\ c_s^2 &= 1; \quad k > 2m_a a\,. \end{aligned} \tag{6.2}$$

The approximations on the sound speed and equation of state for $a < a_{\rm osc}$ sets the evolution of the overdensity to $\dot{\delta}_a = 0$. They apply when $\dot{\phi}_0 = 0$ strictly. This is only consistent for adiabatic initial conditions where $\delta_a = 0$, and we must be much more careful when we are discussing isocurvature initial conditions. We will have much more to say about this in the forthcoming paper, for now we direct the reader to the discussion in [115]. The inconsistency in the isocurvature case only shows up strongly for axions with $a_{\rm osc} > a_{\rm eq}$, which we will not consider yet in this Chapter.

It is also useful to restate the equations of motion:

$$\dot{\rho}_a = -3\mathcal{H}\rho(1 + w_a)\,, \tag{6.3}$$

$$\dot{\delta}_a = 3\mathcal{H}[(1 + w_a) - (1 + c_s^2)]\delta_a - (1 + w_a)\left(\theta_a + \frac{1}{2}\dot{h}\right)\,, \tag{6.4}$$

$$\dot{\theta}_a = -\mathcal{H}(1 - 3w_a)\theta_a - \frac{\dot{w}_a}{1 + w_a}\theta_a + \frac{k^2 c_s^2}{(1 + w_a)}\delta_a\,, \tag{6.5}$$

where dots denote derivatives with respect to conformal time, ∂_τ.

We will use this approximate description of the axion fluid to study the adiabatic and isocurvature perturbations numerically, after carefully deriving the appropriate initial conditons. We will use as our parameters Ω_a and $a_{\rm osc}$. The relationship $m_a(a_{\rm osc}, \Omega_a)$ necessary to apply Eq. (6.2) from specifying $a_{\rm osc}$ for the background evolution is trivial to find in closed form, while the inverse, $a_{\rm osc}(m_a, \Omega_a)$ required to specify the background evolution form the mass is not, and depends on assumptions about the background evolution and H_0. The approximations given in Chapter 4 are not enough when we wish to scan wide ranges of parameter space where axions can be dominant over CDM, particularly with $a_{\rm osc} \sim a_{\rm eq}$ and with $a_{\rm eq}$ being free, or including Ω_Λ. We find $m_a(a_{\rm osc}, \Omega_a)$ simply from the Friedmann equation evaluated for $m_a = 3H(a_{\rm osc})$, with massless neutrinos only:

$$\frac{m_a}{H_0} = 3\left(\frac{\Omega_\gamma + \Omega_\nu}{a_{\rm osc}^4} + \frac{\Omega_c + \Omega_b + \Omega_a}{a_{\rm osc}^3} + \Omega_\Lambda\right)^{1/2} . \tag{6.6}$$

Note that for $a < a_{\rm osc}$ when $w_a = c_s^2 = -1$ we trivially have $\dot{\delta}_a = 0$. One must be more careful with $\dot{\theta}_a$, as this appears to diverge in this limit. To resolve this we must go back to the scalar field equations, and return to the conditions under which Eq. (6.1) holds. The physical quantity appearing in the energy momentum tensor is:

$$(\rho_a + P_a)\theta_a = a^{-2}k^2\dot{\phi}_0\phi_1 \,. \tag{6.7}$$

Taking the derivative with respect to conformal time and substituting the EOMs (Eqs. 4.16 and 4.17) gives:

$$\partial_\tau[(\rho_a + P_a)\theta_a] = a^{-2}k^2[-\phi_1(4\mathcal{H}\dot{\phi}_0 + m_a^2 a^2\phi_0) + \dot{\phi}_0\dot{\phi}_1] \,. \tag{6.8}$$

To resolve the apparent divergence of $\dot{\theta}_a$, we must not drop $\dot{\phi}_0$ terms immediately (setting $\dot{\phi}_0 = 0$ gives $w_a = -1$), but first recognise that this comes from the motion being overdamped, which is the *physical mechanism* (in the scalar field EOMs) for no/slow roll. Overdamped motion means that in the EOMs $\mathcal{H}\dot{\phi}_0 \gg m^2a^2\phi_0$, i.e. $H \gg m$. Therefore we drop the potential term relative to the friction term and obtain:

$$\partial_\tau[(\rho_a + P_a)\theta_a] = a^{-2}k^2[-4\mathcal{H}\phi_1 + \dot{\phi}_1]\dot{\phi}_0 \,. \tag{6.9}$$

Imposing no roll at this point sets $\dot{\phi}_0 = 0$ and hence $\partial_\tau[(\rho + P)\theta] = 0$. So really we are keeping $\dot{\phi}_0 \neq 0$ all the way through, and at the end setting it to be very small. The apparent inconsistency is resolved because, when the field is totally stationary, then there is no friction so $\ddot{\phi}_0 = -\partial_\phi V$, but as soon as even the tiniest $\dot{\phi}_0$ appears, the overdamped condition keeps this from growing.

Re-arranging:

$$\partial_\tau[\rho_a(1+w_a)\theta_a] = \left[-4\mathcal{H} + \frac{\dot{\phi}_1}{\phi_1}\right]\rho_a(1+w_a)\theta_a\,. \tag{6.10}$$

We see that the divergence of $\dot{\theta}_a$ arose from trying to divide both sides of this equation by a quantity that is zero under the $w_a = -1$ approximation, when ρ_a and w_a are constant. What we can be sure of is that at early times ($a < a_{\rm osc}$) the physical quantity $\rho_a(1+w_a)\theta_a = 0$ and remains so until $a > a_{\rm osc}$ when $w_a = 0$, Eq. 6.5 applies and it is consistent to think of θ_a as the variable. This state of affairs must be carefully implemented in the numerical analysis.

The utility of approximating the axion evolution as that of a perfect fluid governed by Eqs. (6.1) and (6.2) and the two parameters Ω_a and $a_{\rm osc}$ (and later the isocurvature amplitude), is that unlike the evolution of the scalar fields ϕ_0 and ϕ_1 this evolution does not involve oscillations in the same way. The background does not oscillate as this approximation takes the average of the rapid oscillations as given, and oscillations in δ_a do not have an ever increasing frequency in conformal time. This considerably speeds up the running of `CAMB` with this fluid compared to the scalar field, allowing an efficient and inexpensive MCMC to determine constraints on the model. We also find that describing the cosmology by the parameters Ω_a and $a_{\rm osc}$ is most physical in terms of the observables, while the priors on Ω_a and $a_{\rm osc}$ confine both to the range $[0, 1]$. We leave discussion of prior distributions and their potential effects on the constraints to the forthcoming paper.

6.2 INITIAL CONDITIONS

The evolution of cosmological fluids cannot begin at time $\tau = 0$. Instead we must derive the approximate early time, super-horizon, evolution of each mode as

a power series expansion [40]. We choose to work in the simplest possible situation for the axion field, where we impose $\tau_i \ll \tau_{\rm osc}$ for all modes so that we may take $w_a = -1$, $\dot{\delta}_a = 0$ and ignore θ_a. We have already stated the adiabatic initial conditions in Section 4.3.1 and they are:

$$\delta_a = \theta_a = 0; \quad \text{adiabatic initial conditions.} \tag{6.11}$$

We will explain the physical origin of axion isocurvature initial conditions in Section 6.3. For the purposes of this Section it is enough to know that this gives an initial non-zero amplitude to δ_a (which will be the parameter of interest), the power spectrum of which is the same as the adiabatic mode, but is uncorrelated with it. Our task now is to derive the early time behaviour of the other cosmological fluids sourced by this mode.

Deriving the complete set of initial conditions, including neutrino velocities, anisotropic stress, and higher order corrections, for example due to the non-trivial presence of matter during the radiation era, requires the use of a matrix ODE formalism, expanded order by order in $k\tau$ to obtain the super-horizon solutions. Such a formalism identifies all the relevant modes, adiabatic and isocurvature in all species, and eliminates the gauge modes. This is systematically implemented in the forthcoming paper to accompany this Chapter, and makes use of the computer algebra in *Mathematica*. The initial conditions on the metric perturbation h, and the fluid overdensities, δ_i, are simple to derive by hand to lowest order, and give a feel for the computer-aided calculation.

In this derivation we follow the normalisation of [277] for the scale factor, since it matches the usual definition with $a_0 = 1$. The solution at early times in a universe containing only matter and radiation is given by:

$$a(\kappa) = \kappa + \frac{1}{4}\frac{\Omega_m}{\Omega_r}\kappa^2\,, \tag{6.12}$$

where $\kappa = (\sqrt{8\pi G\rho_{\rm crit}\Omega_r/3})\tau$.

For our solutions to be consistent with this we must ensure that not only does the numerical integration begin at a time when the axion field is frozen, $\tau_i < \tau_{\rm osc}$, but also that the axion density at this time is sub-dominant to both the radiation *and* the matter.

Since we will be concerned with cosmologies where axions can account for all of the DM, this final condition on what we mean by 'early times' must be implemented with respect to the baryons. It is possible that this will push the initial conditions into the BBN or post-inflationary epoch, $T \gtrsim$ MeV. In terms of the density condition, this will not effect us: the relevant species make up a higher density at early times than cold baryons. However, if the early time condition were to push us beyond reheating and the hot big bang, all of our results would have to be reassessed, with new initial conditions (see e.g. [328]), and indeed densities (in the low temperature reheating scenario, density scalings of heavy axions are modified, see e.g. [329]). This interesting problem is left to a future work. The light axions we work with in this Chapter should not encounter it.

One now takes the first order perturbed Einstein equations Eqs. (4.6) and (4.7) with matter, radiation, and axion source terms. It is important to note here that although the matter and radiation are *initially* zero for an isocurvature perturbation their super-horizon evolution makes them non-zero at early times. They cannot simply be dropped from the Einstein equations and must be retained consistently at each order in the expansion. In particular, we will see that the radiation term in Eq. (4.6) is of the same order as the axion term, and neglecting it leads to an inconsistent solution for h that does not solve Eq. (4.7). Making this mistake leads to the manifestly wrong initial conditions of [277], which differ from ours by an $\mathcal{O}(1)$ multiplicative factor. It is inconsistent to take the lowest order solution for the background sourced by radiation, $a = \kappa$, and not perturb the corresponding fluid density, i.e. GR tells us that any fluid with $w \neq -1$ must cluster. The confusion in [277] seemed to arrive by analogy to CDM isocurvature, where one can really take, at lowest order, δ_c as the only initial non-zero quantity to source h with $\dot{\delta}_c \neq 0$ and very different resultant scaling with τ of the various components.

We begin with a sufficient condition for isocurvature, from the gauge invariant curvature perturbation in the synchronous gauge:

$$h + 6\eta = 0\,, \tag{6.13}$$

from which it is manifest that in the super-horizon expansion in powers of $k\tau$ that

$h \sim \eta$. At lowest order in τ we also have that $\mathcal{H} = 1/\tau$. Therefore in Eq. (4.6) we have that $k^2\eta$ is higher order than $\mathcal{H}\dot{h}$, and so can be neglected. At lowest order we also drop the matter contribution in $\delta\rho$ relative to the radiation, since from the EOMs (Eqs. (4.22), (4.23) and (4.24)) $\delta_r \sim \delta_m$, while the background densities go as $1/a^4$ and $1/a^3$ respectively. With $' = \partial_\kappa$ we now have:

$$\frac{1}{\kappa}h' = 3\kappa^2\left(\frac{\rho_{a,0}\delta_{a,i}}{a_{\rm osc}^3\rho_{r,0}}\right) + \frac{3}{\kappa^2}\delta_r\,. \tag{6.14}$$

This equation now only depends on κ, so this must be our expansion parameter for isocurvature perturbations. Taking ∂_κ, substituting the EOM for δ_r, and noting that this gives θ_r as higher order than δ_r we obtain:

$$\frac{1}{\kappa}h'' + \frac{3}{\kappa^2}h' = 12\kappa\left(\frac{\rho_{a,0}\delta_{a,i}}{a_{\rm osc}^3}\rho_{r,0}\right)\,. \tag{6.15}$$

This is solved by the ansatz $h = K\kappa^n$ with $n = 4$, $K = \frac{1}{2}\left(\frac{\rho_{a,0}\delta_{a,i}}{a_{\rm osc}^3\rho_{r,0}}\right)$, which is a factor of $2/3$ different from the incorrect solution of [277].

Rearranging, the solution for h is:

$$h = \frac{1}{2}\delta_{a,i}\left(\frac{(H_0^2\Omega_a\Omega_r)^2}{a_{\rm osc}^3}\right)\tau^4 = \frac{1}{2}\delta_{a,i}\left(\frac{\rho_{a,0}}{a_{\rm osc}^3}\frac{a^4}{\rho_{r,0}}\right)\,. \tag{6.16}$$

One can easily check that this solution also solves Eq. (4.7). This solution grows like the ratio of axion density to radiation density in the early universe as the radiation redshifts away–in the same way as in CDM isocurvature h grows as the ratio of CDM to radiation [330]–with amplitude and power spectrum given by $\delta_{a,i}/2$.

The leading order behaviour of the overdensities are trivially given by:

$$\delta_\gamma = \delta_\nu = \frac{4}{3}\delta_c = \frac{4}{3}\delta_b = -\frac{2}{3}h\,. \tag{6.17}$$

The full solution for all the relevant fluid components including higher order terms has been derived and will be given in the forthcoming paper. The complete solutions are used in the version of `CAMB` for this Chapter.

6.3 THE INFLATIONARY ENERGY SCALE AND GRAVITATIONAL WAVES IN THE CMB

Ordinarily, perturbations in the various cosmological fluids are seeded from the *curvature* fluctuations laid down during inflation (see e.g. [331]), and these fluctuations

are adiabatic or *isentropic*, effecting all fluids equally. One alternative source for primordial density fluctuations is inflationary *isocurvature*, or *entropy perturbations* that occur when there are other (scalar) fields present during inflation. In fact, any field that is present during inflation but not taking part in inflation, i.e. is orthogonal to the inflationary trajectory in field space, undergoes such fluctuations [332].

As long as the PQ symmetry giving us the axion field is broken prior to inflation, $T_I < f_a$, and the axions we are interested in do not take part in inflation (which is certainly the case for ultra-light axions), then the de Sitter space quantum fluctuations of the axion field give a non-zero value to the perturbed field initial condition [112] with magnitude:

$$\phi_1 = \frac{H_I}{2\pi}\,. \tag{6.18}$$

If inflation were pure de Sitter expansion, then the power spectrum of these fluctuations would be scale invariant. In reality, the expansion differs from de Sitter due to slow roll of the inflaton, leading to the tilted spectrum with $n_s \neq 1$, which is entirely due to the background inflaton evolution of $H(a)$ [148]: *the power spectrum of axion isocurvature fluctuations is the same as the adiabatic inflationary power spectrum*. However, the amplitudes of the two power spectra differ, the amplitude of the axion power spectrum being set by Eq. (6.18), rather than A_s. Since the axion field is an independent quantum field from the inflaton, then these fluctuations are realised in our universe by an independent Gaussian random field, and hence the axion has *totally uncorrelated isocurvature perturbations*.

The axion isocurvature fluctuations generated in this manner are totally unavoidable in any standard inflationary scenario with the large, stringy, values of $f_a \sim 10^{16}\,\text{GeV}$. The robust criterion for their existence is [200]:

$$f_a > \text{Max}\{T_{\text{GH}}, T_{\text{max}}\}\,, \tag{6.19}$$

where T_{GH} is the Gibbons-Hawking temperature of de Sitter space, $T_{\text{GH}} = H_I/2\pi$ [333] and T_{max} is the maximum thermalisation temperature after inflation, $T_{\text{max}} = \epsilon_{\text{eff}} E_I$ (ϵ_{eff} is an efficiency parameter), i.e. neither the quantum fluctuations of ϕ_1 nor reheating should restore the PQ symmetry. The condition Eq. (6.19) is always respected whenever we want inflation to save us from topological relics of the PQ phase transition [112].

Isocurvature fluctuations lead to a new mode of fluctuations in the CMB power spectrum, which are *out of phase* with the dominant adiabatic mode. They are also constrained by the resulting addition of extra power on large scales. Although the initial conditions Eq. (6.16) are very different from CDM isocurvature [330] in their early time evolution, for sufficiently heavy axions the resulting CMB power spectra are the same, as we will see in Section 6.4, so that in some mass range axion isocurvature can be considered as CDM isocurvature observationally. There are constraints (e.g. WMAP7 [5]) on the relative amplitude, α, of CDM isocurvature fluctuations defined by:

$$\frac{\alpha(k_0)}{1-\alpha(k_0)} \equiv \frac{\mathcal{P}_{\mathcal{S}}(k_0)}{\mathcal{P}_{\mathcal{R}}(k_0)}\,, \tag{6.20}$$

where $\mathcal{P}_{\mathcal{S}(\mathcal{R})}$ is the isocuravture (adiabatic) primordial power spectrum evaluated at pivot wavenumber k_0. We will review the observational constraints shortly.

These constraints translate into *constraints on the energy scale of inflation*, via Eq. (6.18) in the following way. We begin with the definition of the adiabatic curvature power spectrum:

$$\frac{k^3}{2\pi^2}\mathcal{P}_{\mathcal{R}}(k) = A_s\left(\frac{k}{k_0}\right)^{n_s-1} = \frac{1}{2\epsilon}\left(\frac{H_I/M_{pl}}{2\pi}\right)^2\left(\frac{k}{k_0}\right)^{n_s-1}\,, \tag{6.21}$$

where A_s is the scalar amplitude, n_s is the tilt, and ϵ is an inflationary slow roll parameter which we need not define. Now, the power spectrum of the axion isocurvature perturbations has the same k-dependence as this, while the amplitude is given by:

$$\delta_{a,i}^2 = 4\left(\frac{\phi_1}{\phi_0}\right)^2 = \frac{(H_I/M_{pl})^2}{\pi^2(\phi_{0,i}/M_{pl})^2}\,, \tag{6.22}$$

$$\left(\frac{\phi_{0,i}}{M_{pl}}\right)^2 = \frac{2\rho_{\rm crit}\Omega_a}{m_a^2 a_{\rm osc}^3}\,. \tag{6.23}$$

This gives:

$$\frac{\alpha}{1-\alpha} = \frac{8\epsilon}{(\phi_{0,i}/M_{pl})^2}\,. \tag{6.24}$$

Note that for the ultra-light axions there is no factor of $(\Omega_a/\Omega_c)^2$ in this ratio, as there is in the standard treatment of e.g. [174, 334]. This is because the ultra-light axion must be treated as a separate component from the CDM, and Ω_a will be separately constrained, rather than only scaling the isocurvature amplitude. We do not know *a priori* what mass ($a_{\rm osc}$) range will be observationally distinct from CDM

for a given combination of datasets: our treatment makes no assumptions about this. The overdensity amplitude parameterised in this way *increases* as Ω_a decreases, but there is no inconsistency since the physical density, $\delta\rho_a = \rho_a\delta_a$ still decreases. The isocurvature amplitude, however, which is the parameter we constrain, does not care about this interpretation and has the well defined prior range $\alpha \in [0, 1]$.

The isocurvature amplitude is directly related to the tensor-to-scalar-ratio, r, by $r = 16\epsilon$. This results simply because both the isocurvature amplitude and the amplitude of tensor modes, $\mathcal{P}_h$, scale in the same way with H_I/M_{pl}:

$$\mathcal{P}_h = 8\left(\frac{H_I/M_{pl}}{2\pi}\right)^2. \tag{6.25}$$

Therefore a small amplitude of axion isocurvature fluctuations implies a small amplitude of primordial tensor modes, and both imply bounds on the energy scale of inflation. A conflict between the measurements can only arise under confirmation of the source of one of these ingredients. In the case of ultra-light axions, this confirmation can be gained, for example, from their measurable effect on the LSS discussed earlier in this thesis.

This connection, between axion isocurvature perturbations and the energy scale of inflation, and hence amplitude of primordial gravitational waves in the CMB, has been studied by many authors, and dates back to [112, 335, 336]. Axion isocurvature constraints with WMAP were given in detail in the 5 year data release [334], and were updated for the 7 year release [5]. These results concluded that in almost all situations $r \lesssim 0.01$ is required: barely detectable in the foreseeable future (it is of order the Planck forecasted 1σ errors [14]). These results, however, do depend on some details specific to the QCD axion, in particular the relation between Ω_a, $\phi_{0,i}$, and f_a. The situation was reinterpreted by the authors of [200] in terms of the energy scale of inflation: axion dark matter in the large f_a regime prefers low-scale inflation, and a detection of isocurvature perturbations would serve as strong evidence for axions, and also serve as a probe of low-scale inflation, inaccessible via the tensor modes. The strongest claim made in this regard was made by the authors of [174] who stated that any observation of gravitational waves interpreted as arising from high scale inflation rules out a string/M-theory QCD axion from solving the strong *CP*

problem itself, and that any large f_a string axion would comprise only a small fraction of the CDM. Considerations of fine tuning on both axion initial misalignment and the inflationary parameters necessary for multiple string axions to respect these bounds led the authors of [202, 203] to conclude that the fine tuning is so severe, much worse than the strong *CP* problem, as to place light string axions at odds with inflationary cosmology [1]. However, we reiterate that these conclusions were drawn from standard axion CDM isocurvature constraints such as [5], and do not take into account the differences when one considers the axions to be ultra-light.

The aim of the ongoing work that this Chapter forms a part of is to extend these arguments into the regime of ultra-light axions, with equation of state and sound speed given by Eqs. (6.1) and (6.2). Firstly, primarily from LSS constraints coming from the 'fuzziness' of these components [205], it is already known that these axions are constrained to be sub-dominant components of the DM from the adiabatic mode alone. Our first goal is to update these constraints to contemporary data such as WMAP7. Secondly, the phase structure of the power spectra in both adiabatic and isocurvature will surely be altered by the axion sound speed, effecting the correlations with other cosmological parameters in a manner distinct from from CDM axions that simply scale their isocurvature amplitude by Ω_a. It will be important to understand how the standard constraints are altered when the axions are ultra-light and therefore what probes are most powerful for making statements about the link between axion DM and the energy scale of inflation. Ultimately we wish to be able to extend the statements of [174] precisely into the ultra-light regime, such that the implications for the axiverse of future bounds on, or indeed measurements of, r can be properly understood.

It is finally worth noting in this regard that in the model of [337] large amplitude, observable, tensor modes can be produced even with a low inflationary energy scale. In such a scenario, a measurement of r need not constrain the existence of high f_a axions, and in fact would leave the measurement of isocurvature fluctuations interpreted as sourced by such an axion as one of the only remaining probes of the

[1] This conclusion of [202, 203] allowed one to define fine tuning on the inflationary parameter ϵ: it is not clear without embedding in a definite high energy theory that small ϵ implies any degree of fine tuning.

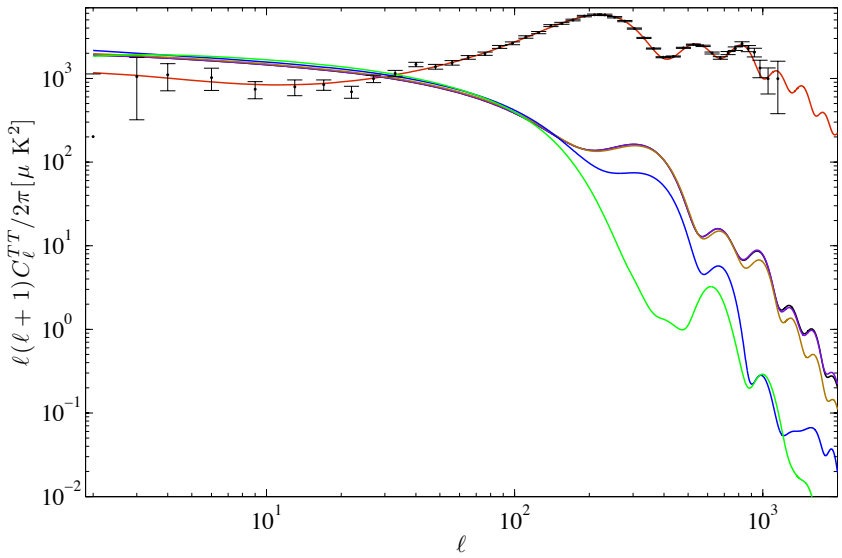

Figure 6.1 Isocurvature with ultra-light axions, with amplitude $\alpha = 1$. Red: ΛCDM adiabatic power spectrum with WMAP7 data [44]. Black: CDM isocurvature. Axion models have $\Omega_a h^2 = 0.112$, so that axions comprise all the DM. Purple: $a_{\rm osc} = 1 \times 10^{-7}$, which lies almost exactly on top of Black. Brown: $a_{\rm osc} = 2 \times 10^{-5}$, the spectrum has extra damping at large multipoles. Blue: $a_{\rm osc} = 1 \times 10^{-4}$, damping moves to lower multipoles. Green: $a_{\rm osc} = 3 \times 10^{-4}$, new peak structure interpreted as beats.

inflationary energy scale, sensitive down to very low energies.

6.4 SPECTRA AND CONSTRAINTS ON THE MODES

In Fig. 6.1 we show the isocurvature TT power spectra (with arbitrary amplitude) for a variety of models, with the ΛCDM adiabatic power spectrum with WMAP7 data for reference. Note that many of these isocurvature models are unrealistic: to amplify the visible effects we allow ultra-light axions to comprise all the DM.

When all the DM is taken to be in an ultra-light component with $a_{\rm osc} \gtrsim 1 \times 10^{-7}$ then the isocurvature power spectrum is virtually indistinguishable from CDM isocurvature. This is a dynamical phenomenon: the initial conditions on e.g. h are very different for CDM isocuvature. However, as long as $a_{\rm osc}$ is early enough and the sound speed is effectively zero on all relevant scales, then the evolution of these differing initial conditions becomes the same and they 'catch up' to one another, producing the same power spectrum.

As $a_{\rm osc}$ is increased and the scales where the axion sound speed is non-zero start to correspond to observationally relevant multipoles, we see a damping of the isocurvature power spectrum, which moves to lower multipoles as $a_{\rm osc}$ is increased further. This is a novel feature to our isocurvature model. However, this damping makes the isocurvature have less of a contribution with the spectral index locked to that of the adiabatic mode. The folklore that, since the isocurvature mode is out of phase with the adiabatic, isocurvature is constrained by the ratio of the amplitudes of odd versus even peaks in the CMB power spectrum is only really powerful when the isocurvature mode has large spectral index. For example in [338] when the constraint $n_s = n_{\rm iso}$ is lifted, the constraints on α loosen from $\alpha < 0.15$ to $\alpha < 0.68$. It is the first peak position and height that tells us that the primordial spectrum is predominantly adiabatic.

Furthermore, with higher values of $a_{\rm osc}$ we see new forms of peak structure appear in the isocurvature power spectrum. These resemble beats, coming from the interference of two separate waves with different frequencies. The frequency of waves in the baryon-photon fluid is set by the sound speed, giving the baryon acoustic oscillations, and is sourced by radiation pressure. When an axion fluid with non-zero sound speed is present on some scale, it also acts as a pressure source, and introduces a new frequency to the dynamics. An analytic model for this will be presented in the paper.

We show constraints on the model in the adiabatic mode in Fig. 6.2 obtained from an MCMC using WMAP7 data [44] and the publicly available code `cosmomc` [57, 58] performed by Renée Hlozek. In addition to the axion parameters $a_{\rm osc}$ and $\Omega_a h^2$ we also included the standard parameters $\{\Omega_b h^2, \Omega_c h^2, \tau, n_s, A_s, \theta_A\}$ (θ_A is the angular size of the sound horizon at last scattering, and is the standard parameter more suitable for MCMC than Ω_Λ). A full description of our results will be given in the forthcoming paper. We note that the shape of the constraints is in agreement with those obtained by [205]: a one-to-one degeneracy between Ω_a and Ω_Λ for $a_{\rm osc} \gtrsim 1 \times 10^{-1}$, a one-to-one degeneracy between $\Omega_a h^2$ and $\Omega_c h^2$ for $a_{\rm osc} \lesssim 1 \times 10^{-8}$, and $f_{ax} \equiv \Omega_a h^2 / (\Omega_a h^2 + \Omega_c h^2) \lesssim 0.5$ between these values.

In Chapter 5 we noted that all axion effects on observables can be understood

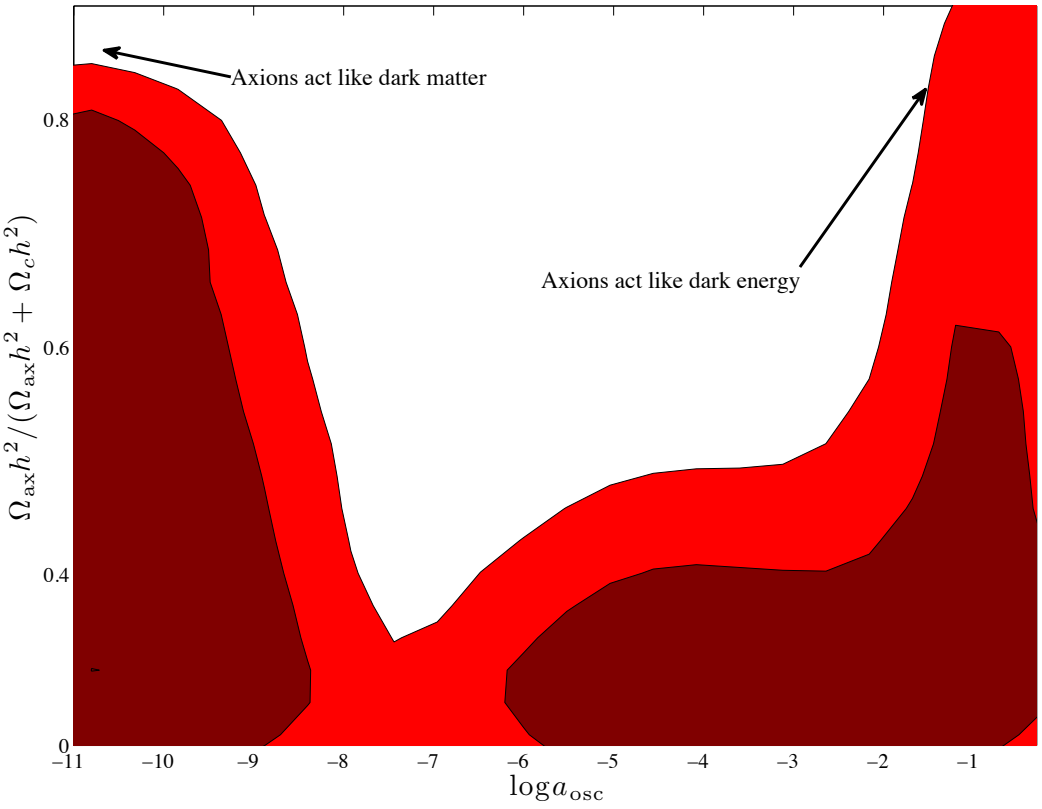

Figure 6.2 PRELIMINARY: Constraints on ultra-light axions under the fluid approximation of Eqs. (6.1) and (6.2) using WMAP7 data [44]. For $a_{\rm osc} \gtrsim 10^{-1}$ the axion behaves as DE, while for $a_{\rm osc} \lesssim 10^{-8}$ it behaves as CDM: in both these regimes a large fractional density relative to the pure CDM is allowed. In the intermediate range, the fraction is constrained to be $f_{ax} \lesssim 0.5$. Figure made by Renée Hlozek.

as emerging from two physical processes: the background evolution giving a shift in equality when $a_{\rm osc} > a_{\rm eq}$ and the structure suppression caused by the non-zero sound speed. In the context of the CMB, the non-zero sound speed also gives the beat phenomenon highlighted above. To quantify which of these phenomena is giving constraints in the CMB, and how strong these are, we will in future perform a separate run where we impose the equation of state Eq. (6.1) on the axion fluid while fixing the sound speed to zero, and compare the CMB constraints to those of Fig. 6.2.

The full constraints on this model, including LSS, cluster number counts, H_0 and BAO data, and the isocurvature perturbations and their implication on the inferred energy scale of inflation, are still under preparation, and will appear in full in the forthcoming paper. We hope to find that are interesting changes to the standard interpretation of isocurvature bounds interpreted as emerging from

inflationary perturbations in an ultra-light axion field when they are combined with other constraints on such a species. Forthcoming LSS data in the next few years e.g. BOSS Lyman-alpha, well prior to any Euclid-like mission considered in Chapter 5, has the potential to detect axions in the intermediate mass range, where fuzzy effects make axions similar in their clustering to warm, rather than hot, DM. Planck has the potential to not only tighten CMB constraints on isocurvature by breaking degeneracies with other parameters, but also probe inflation with much higher accuracy and potentially detect the tensor modes. The combination of these two observables will have very important consequences for the axiverse and inflation if *either* makes a positive detection. The machinery and understanding developed in this Chapter will be vital to apply as new data becomes available.

7

CONCLUSIONS

"The worthwhile problems are the ones you can really solve or help solve, the ones you can really contribute something to. ... No problem is too small or too trivial if we can really do something about it."

Richard Feynman, letter to Koichi Ano (1966) in *Perfectly Reasonable Deviations from the Beaten Track : The Letters of Richard P. Feynman*

In this thesis, we have begun the systematic study of *Axiverse Cosmology*, we have learned many things about it and the observational implications it may have, but there is still a wide open set of problems and questions to be addressed.

Firstly, what have we learned? If axions are sufficiently decoupled from all other cosmological components, which is naturally achieved by their perturbative shift symmetry, pseudoscalar nature, and large decay constant in string theory models, then all production of axions in the universe proceeds via the vacuum misalignment production. Therefore, this abundance is governed by the mass of the field, and its initial conditions. The mass and the densities of the other components therefore specify entirely the background cosmological evolution. Depending on the mass, axions contribute as either matter or a cosmological constant at different epochs, with only small deviations from this.

However, the mass should be controlled by the value of some modulus field of the extra dimensions. The combined evolution of the axion-modulus system can lead to new DE phases and attractor solutions in the evolution allowing considerable

departure from the usual expansion history of the universe by introducing multiple epochs of accelerated expansion and other effects in the equation of state. Such effects may signal that we are living away from the true scalar vacuum, and that cosmological collapse might be our fate. The effect of axions on the moduli can be large if misalignment is large. If the masses of axions and moduli are of the same order in any construction, then their combined evolution must be followed, but even if the modulus is much heavier than the axion then its vev will still evolve with the axion and induce an effective potential for it.

When an axion field is perturbed about the homogeneous background evolution, coherent oscillations lead to a scale dependent sound speed. This in turn induces scale dependent growth, and suppression of structure formation on scales governed by the inverse axion mass. The ultra-light axions we have been studying manifest this scale in LSS.

Due to this effect, by combining probes of GRS, WLT, and CMB temperature and polarisation anisotropies it should be possible with near future observations to measure an ultra-light axion component at the percent level. This sensitivity in the most extreme cases of very low mass can depend in some ways on the scalar field evolution before oscillations have become sufficiently fast that averaging allows one to consistently treat axions as DM with a sound speed. Making such an approximation, however, allowed us to look at a large range of axion masses, and place constraints on the allowed density of axions using current data.

Since axions are a fundamental scalar field that exists in the very early universe, then inflation induces isocurvature perturbations in their density that cannot be ignored. These perturbations have a significant effect on the CMB, and since their amplitude is also related to the amplitude of primordial tensor perturbations then the T and B modes of the CMB combined with LSS constraints on the axion density can squeeze the parameter space significantly in the most naive models. It is an ongoing project to see how this picture is changed in the case where the axions are ultra-light, as is expected in the axiverse. In doing this, one will be able to, and indeed should, make new statements about the fine tuning of axiverse cosmology.

What other open problems are there in axiverse cosmology? The most obvious

open direction is the inclusion of many light axion fields that have dynamics relevant to late time cosmological observables. In terms of LSS one should expect to be able to linearly superpose many steps in the power spectrum, however the backreaction on the expansion rate may complicate this picture, or resonances may come into play as they do in inflation and reheating. Combining more features into the power spectrum, one would wish to construct specialised statistics for their detection.

Another crucial direction for study of ultra-light axions is the effects of the sound speed on non-linear structure formation. One of the original motivations for studying such a component was its potential to resolve problems in the current models of structure formation with CDM, but a hunch alone is not good enough. N-body simulations with scalar fields in these regimes will need to be performed, but they may be complicated by the relativistic nature of the effect, and of course the major limiting factors in any simulation are baryonic effects and feedback.

The major open question in the modulus sector, besides an explicit construction of the model in string theory and confronting the parameter space with cosmological constraints on the equation of state, is the effect of the modulus dynamics on the axion decay constant, and if this will lead to yet more new phenomenology. This additional coupling may be particularly interesting in a model of axion-modulus inflation, and the non-Gaussian effects it may induce in the primordial power spectrum. Also, the evolution of the decay constant may introduce new fine tunings in axiverse cosmology, particularly altering the axion density and the PQ phase transition in an inflationary context.

It is assumed in the post inflationary universe that if coherent scalar energy density is present then this energy density decays to SM particles and contributes non-thermally to their relic densities, changing reheating dynamics. In the axion-modulus model, one should investigate the effects of such a coupling for the modulus, both at early and late times.

One should also include the coupling of the modulus non-minimally to gravity, the plague of most quintessence models, and investigate the fifth force constraints. The anharmonic and coupled axion-modulus potential should be investigated for containing chameleon-like features due to the dynamical mass. If such phenomena

are present, then they will even further enrich the observational implications and validity of the model, while if they are not, then via the modulus sector the axiverse will face new constraints both from observation and model-building.

The most simple extension to make to the axion-modulus model, that is indeed necessary for any consistent treatment, is to introduce modulus perturbations. The new background dynamics in this model will in many regions of parameter space effect the scaling of the axion sound speed. Similar phenomena in the modulus direction will also exist. Couplings in the dark sector have long been motivated as ingredients to help DM structure formation match up more elegantly with observations of galaxies, here we have both ingredients of sound speed and coupling and the implications are unknown.

Then there are the other directions for axiverse phenomenology originally suggested in [104]: namely black hole superradiance and rotation of CMB polarisation. Combining polarisation rotation into the parameter estimation in the axiverse will be model dependent, but will have significant effects for the lightest axions if included. Black hole superradiance should have significant effects on the modulus sector as the growing axion amplitude could lead to vacuum destabilisation. The gravitational wave signature of a superradiance event has not been calculated to our knowledge, but may be detectable in the near future. If unique, it will be the closest thing to direct detection that ultra-light axions can exhibit.

And finally, all of our studies have ignored cosmic curvature. It is standard practice in cosmology to say "all of our results can be trivially generalised to the case with curvature", but this generalisation should be made, especially when degeneracies with curvature will strongly effect constraints on DE features and therefore possibly statements about fine tuning.

REFERENCES

[1] G. F. Smoot, J. Aymon, G. D. Amici, L. Tenorio, C. Bennett, et al. (1991).

[2] G. F. Smoot, C. Bennett, A. Kogut, E. Wright, J. Aymon, et al., Astrophys.J. **396**, L1 (1992).

[3] J. C. Mather, E. Cheng, D. Cottingham, R. Eplee, D. Fixsen, et al., Astrophys.J. **420**, 439 (1994).

[4] C. L. Bennett, M. Halpern, G. Hinshaw, N. Jarosik, A. Kogut, M. Limon, S. S. Meyer, L. Page, D. N. Spergel, G. S. Tucker, et al., The Astrophysical Journal Supplement Series pp. 1+ (2003), URL `http://dx.doi.org/10.1086/377253`.

[5] E. Komatsu, K. M. Smith, J. Dunkley, C. L. Bennett, B. Gold, G. Hinshaw, N. Jarosik, D. Larson, M. R. Nolta, L. Page, et al., The Astrophysical Journal Supplement Series **192**, 18+ (2011), ISSN 0067-0049, `1001.4538`, URL `http://dx.doi.org/10.1088/0067-0049/192/2/18`.

[6] *http://lambda.gsfc.nasa.gov/*.

[7] C. Stoughton et al. (SDSS Collaboration), Astron.J. **123**, 485 (2002).

[8] H. Aihara, C. Allende Prieto, D. An, S. F. Anderson, É. Aubourg, E. Balbinot, T. C. Beers, A. A. Berlind, S. J. Bickerton, D. Bizyaev, et al., ApJS **193**, 29 (2011), `1101.1559`.

[9] A. G. Sanchez, C. G. Scoccola, A. J. Ross, W. Percival, M. Manera, F. Montesano, X. Mazzalay, A. J. Cuesta, D. J. Eisenstein, E. Kazin, et al. (2012), `1203.6616`, URL `http://arxiv.org/abs/1203.6616`.

[10] B. A. Reid, L. Samushia, M. White, W. J. Percival, M. Manera, N. Padmanabhan, A. J. Ross, A. G. Sánchez, S. Bailey, D. Bizyaev, et al. (2012), 1203.6641, URL http://arxiv.org/abs/1203.6641.

[11] *http://www.sdss.org/*.

[12] *http://www.sdss3.org/index.php*.

[13] P. Collaboration, P. A. R. Ade, N. Aghanim, M. Arnaud, M. Ashdown, J. Aumont, C. Baccigalupi, M. Baker, A. Balbi, A. J. Banday, et al. (2011), 1101.2022, URL http://arxiv.org/abs/1101.2022.

[14] *http://www.rssd.esa.int/SA/PLANCK/docs/Bluebook-ESA-SCI(2005)1_V2.pdf*.

[15] A. Einstein, Annalen Phys. **17**, 891 (1905).

[16] A. Einstein, Sitzungsber.Preuss.Akad.Wiss.Berlin (Math.Phys.) **1914**, 1030 (1914).

[17] A. Einstein, Sitzungsber.Preuss.Akad.Wiss.Berlin (Math.Phys.) **1915**, 778 (1915).

[18] I. Newton, *PhilosophiæNaturalis Principia Mathematica* (1687).

[19] R. Descartes, *La Géométrie* (1637).

[20] A. Friedmann, Z.Phys. **21**, 326 (1924).

[21] G. Lemaitre, Mon.Not.Roy.Astron.Soc. **91**, 490 (1931).

[22] A. Einstein, Sitzungsber.Preuss.Akad.Wiss.Berlin (Math.Phys.) **1917**, 142 (1917).

[23] E. Hubble, Proc.Nat.Acad.Sci. **15**, 168 (1929).

[24] M. Planck, Verhandl. Dtsch. phys. Ges. **2**, 237 (1901).

[25] G. Lemaître, General Relativity and Gravitation **43**, 2929 (2011), ISSN 0001-7701, URL http://dx.doi.org/10.1007/s10714-011-1214-6.

[26] K. R. Popper, *Logik der Forschung* (1934).

[27] K. R. Popper, *The Logic of Scientific Discovery* (Hutchinson of London, 1959).

[28] R. M. Wald, *General Relativity* (University Of Chicago Press, 1984), 1st ed., ISBN 0226870332, URL http://www.worldcat.org/isbn/0226870332.

[29] S. Dodelson, *Modern Cosmology* (Academic Press, 2003), 1st ed., ISBN 0122191412, URL http://www.worldcat.org/isbn/0122191412.

[30] W. de Sitter, Mon.Not.Roy.Astron.Soc. **78**, 3 (1917).

[31] G. Gamow, Physical Review Online Archive (Prola) **70**, 572 (1946), URL http://dx.doi.org/10.1103/PhysRev.70.572.2.

[32] R. A. Alpher, H. Bethe, and G. Gamow, Physical Review Online Archive (Prola) **73**, 803 (1948), URL http://dx.doi.org/10.1103/PhysRev.73.803.

[33] A. G. Riess, A. V. Filippenko, P. Challis, A. Clocchiatti, A. Diercks, P. M. Garnavich, R. L. Gilliland, C. J. Hogan, S. Jha, R. P. Kirshner, et al., Astron. J. **116**, 1009 (1998), astro-ph/9805201, URL http://dx.doi.org/10.1086/300499.

[34] S. Perlmutter, G. Aldering, G. Goldhaber, R. A. Knop, P. Nugent, P. G. Castro, S. Deustua, S. Fabbro, A. Goobar, D. E. Groom, et al., Astrophys. J. **517**, 565 (1999), astro-ph/9812133, URL http://dx.doi.org/10.1086/307221.

[35] J. A. Peacock, *Cosmological Physics (Cambridge Astrophysics)* (Cambridge University Press, 1998), 1st ed., ISBN 0521422701, URL http://www.worldcat.org/isbn/0521422701.

[36] S. Weinberg, Reviews of Modern Physics **61**, 1 (1989), URL http://dx.doi.org/10.1103/RevModPhys.61.1.

[37] A. Raychaudhuri, Phys.Rev. **98**, 1123 (1955).

[38] L. D. Landau and E. M. Lifshitz, *The Classical Theory of Fields, Fourth Edition: Volume 2 (Course of Theoretical Physics Series)* (Butterworth-Heinemann, 1980), 4th ed., ISBN 0750627689, URL http://www.worldcat.org/isbn/0750627689.

[39] H. Kodama and M. Sasaki, Prog.Theor.Phys.Suppl. **78**, 1 (1984).

[40] C. Ma and E. Bertschinger, Astrophys. J. **455** (1995), astro-ph/9506072, URL http://dx.doi.org/10.1086/176550.

[41] A. A. Penzias and R. W. Wilson, Astrophys. J. **142**, 419 (1965).

[42] W. Hu and S. Dodelson, Annual Review of Astronomy and Astrophysics **40**, 171 (2002), URL http://dx.doi.org/10.1146/annurev.astro.40.060401.093926.

[43] J. Bond and G. Efstathiou, Mon.Not.Roy.Astron.Soc. **226**, 655 (1987).

[44] D. Larson, J. Dunkley, G. Hinshaw, E. Komatsu, M. R. Nolta, C. L. Bennett, B. Gold, M. Halpern, R. S. Hill, N. Jarosik, et al., The Astrophysical Journal Supplement Series **192**, 16+ (2011), ISSN 0067-0049, URL http://dx.doi.org/10.1088/0067-0049/192/2/16.

[45] *http://camb.info/*.

[46] U. Seljak, Astrophysical Journal Letters **435**, L87 (1994), astro-ph/9406050, URL http://dx.doi.org/10.1086/187601.

[47] U. Seljak and M. Zaldarriaga (1996), astro-ph/9603033, URL http://dx.doi.org/10.1086/177793.

[48] A. Lewis, A. Challinor, and A. Lasenby, The Astrophysical Journal pp. 473+ (2000), astro-ph/9911177, URL http://dx.doi.org/10.1086/309179.

[49] A. Lewis and A. Challinor (2002), astro-ph/0203507, URL http://arxiv.org/abs/astro-ph/0203507.

[50] A. D. Miller, R. Caldwell, M. J. Devlin, W. B. Dorwart, T. Herbig, M. R. Nolta, L. A. Page, J. Puchalla, E. Torbet, and H. T. Tran, The Astrophysical Journal Letters **524**, L1+ (1999), URL http://dx.doi.org/10.1086/312293.

[51] P. de Bernardis, P. A. R. Ade, J. J. Bock, J. R. Bond, J. Borrill, A. Boscaleri, K. Coble, B. P. Crill, G. De Gasperis, P. C. Farese, et al., Nature **404**, 955 (2000), ISSN 0028-0836, URL http://dx.doi.org/10.1038/35010035.

[52] S. Hanany, P. Ade, A. Balbi, J. Bock, J. Borrill, A. Boscaleri, P. de Bernardis, P. G. Ferreira, V. V. Hristov, A. H. Jaffe, et al., The Astrophysical Journal Letters **545**, L5+ (2000), URL http://dx.doi.org/10.1086/317322.

[53] J. W. Fowler, V. Acquaviva, P. A. R. Ade, P. Aguirre, M. Amiri, J. W. Appel, L. F. Barrientos, E. S. Battistelli, J. R. Bond, B. Brown, et al., The Astrophysical Journal **722**, 1148+ (2010), ISSN 0004-637X, URL http://dx.doi.org/10.1088/0004-637X/722/2/1148.

[54] J. Dunkley, R. Hlozek, J. Sievers, V. Acquaviva, P. A. R. Ade, P. Aguirre, M. Amiri, J. W. Appel, L. F. Barrientos, E. S. Battistelli, et al. (2010), 1009.0866, URL http://arxiv.org/abs/1009.0866.

[55] K. K. Schaffer, T. M. Crawford, K. A. Aird, B. A. Benson, L. E. Bleem, J. E. Carlstrom, C. L. Chang, H. M. Cho, A. T. Crites, T. de Haan, et al., The Astrophysical Journal **743**, 90+ (2011), ISSN 0004-637X, URL http://dx.doi.org/10.1088/0004-637X/743/1/90.

[56] R. Keisler, C. L. Reichardt, K. A. Aird, B. A. Benson, L. E. Bleem, J. E. Carlstrom, C. L. Chang, H. M. Cho, T. M. Crawford, A. T. Crites, et al., The Astrophysical Journal **743**, 28+ (2011), ISSN 0004-637X, URL http://dx.doi.org/10.1088/0004-637X/743/1/28.

[57] A. Lewis and S. Bridle, Physical Review D **66**, 103511+ (2002), URL http://dx.doi.org/10.1103/PhysRevD.66.103511.

[58] *http://cosmologist.info/cosmomc/*.

[59] B. A. Bassett, Y. Fantaye, R. Hlozek, and J. Kotze, International Journal of Modern Physics D **20**, 2559+ (2011), 0906.0993, URL http://arxiv.org/abs/0906.0993.

[60] M. Colless, Philosophical Transactions of the Royal Society of London. Series A: Mathematical, Physical and Engineering Sciences **357**, 105 (1999), ISSN 1471-2962, URL http://dx.doi.org/10.1098/rsta.1999.0317.

[61] M. Colless, G. B. Dalton, S. J. Maddox, W. J. Sutherland, P. Norberg, S. Cole, J. Bland-Hawthorn, T. J. Bridges, R. D. Cannon, C. A. Collins, et al., Monthly Notices of the Royal Astronomical Society **328** (2001), astro-ph/0106498, URL http://arxiv.org/abs/astro-ph/0106498.

[62] W. J. Percival, C. M. Baugh, J. Bland-Hawthorn, T. Bridges, R. Cannon, S. Cole, M. Colless, C. Collins, W. Couch, G. Dalton, et al., Monthly Notices of the Royal Astronomical Society **327**, 1297 (2001), URL http://dx.doi.org/10.1046/j.1365-8711.2001.04827.x.

[63] *http://www.mso.anu.edu.au/2dFGRS/*.

[64] V. Springel, S. D. M. White, A. Jenkins, C. S. Frenk, N. Yoshida, L. Gao, J. Navarro, R. Thacker, D. Croton, J. Helly, et al., Nature **435**, 629 (2005), ISSN 0028-0836, astro-ph/0504097, URL http://dx.doi.org/10.1038/nature03597.

[65] P. G. Ferreira and C. Skordis, Physical Review D **81**, 104020+ (2010), URL http://dx.doi.org/10.1103/PhysRevD.81.104020.

[66] B. A. Reid, W. J. Percival, D. J. Eisenstein, L. Verde, D. N. Spergel, R. A. Skibba, N. A. Bahcall, T. Budavari, J. A. Frieman, M. Fukugita, et al., Monthly Notices of the Royal Astronomical Society **404**, 60 (2010), ISSN 0035-8711, URL http://dx.doi.org/10.1111/j.1365-2966.2010.16276.x.

[67] R. Laureijs, J. Amiaux, S. Arduini, J. L. Augueres, J. Brinchmann, R. Cole, M. Cropper, C. Dabin, L. Duvet, A. Ealet, et al. (2011), 1110.3193, URL http://arxiv.org/abs/1110.3193.

[68] *http://www.euclid-ec.org*.

[69] R. Penrose, General Relativity and Gravitation **43**, 901 (2011), ISSN 0001-7701, URL http://dx.doi.org/10.1007/s10714-010-1110-5.

[70] R. Amanullah, C. Lidman, D. Rubin, G. Aldering, P. Astier, K. Barbary, M. S. Burns, A. Conley, K. S. Dawson, S. E. Deustua, et al., The Astrophysical Journal **716**, 712+ (2010), ISSN 0004-637X, URL http://dx.doi.org/10.1088/0004-637X/716/1/712.

[71] C. Clarkson, M. Cortês, and B. Bassett, Journal of Cosmology and Astroparticle Physics **2007**, 011 (2007), ISSN 1475-7516, astro-ph/0702670, URL http://dx.doi.org/10.1088/1475-7516/2007/08/011.

[72] R. Hlozek, M. Cortês, C. Clarkson, and B. Bassett, General Relativity and Gravitation **40**, 285 (2008), ISSN 0001-7701, URL http://dx.doi.org/10.1007/s10714-007-0548-6.

[73] K. Nakamura and P. D. Group, Journal of Physics G: Nuclear and Particle Physics **37**, 075021+ (2010), ISSN 0954-3899, URL http://dx.doi.org/10.1088/0954-3899/37/7A/075021.

[74] P. Dirac, Proc.Roy.Soc.Lond. **A118**, 351 (1928).

[75] R. P. Feynman, Physical Review Online Archive (Prola) **76**, 769 (1949), URL http://dx.doi.org/10.1103/PhysRev.76.769.

[76] J. Schwinger, Physical Review Online Archive (Prola) **74**, 1439 (1948), URL http://dx.doi.org/10.1103/PhysRev.74.1439.

[77] S. Tomonaga, Progress of Theoretical Physics **1**, 27 (1946), URL http://dx.doi.org/10.1143/PTP.1.27.

[78] F. J. Dyson, Physical Review Online Archive (Prola) **75**, 486 (1949), URL http://dx.doi.org/10.1103/PhysRev.75.486.

[79] P. W. Higgs, Physical Review Letters **13**, 508 (1964), URL http://dx.doi.org/10.1103/PhysRevLett.13.508.

[80] F. Englert and R. Brout, Phys. Rev. Lett. **13**, 321 (1964), URL http://link.aps.org/doi/10.1103/PhysRevLett.13.321.

[81] G. S. Guralnik, C. R. Hagen, and T. W. B. Kibble, Physical Review Letters **13**, 585 (1964), URL http://dx.doi.org/10.1103/PhysRevLett.13.585.

[82] S. L. Glashow, Nuclear Physics **22**, 579 (1961), ISSN 00295582, URL http://dx.doi.org/10.1016/0029-5582(61)90469-2.

[83] S. Weinberg, Physical Review Letters **19**, 1264 (1967), URL http://dx.doi.org/10.1103/PhysRevLett.19.1264.

[84] A. Salam, Conf.Proc. **C680519**, 367 (1968).

[85] N. Cabibbo, Physical Review Letters **10**, 531 (1963), URL http://dx.doi.org/10.1103/PhysRevLett.10.531.

[86] M. Kobayashi and T. Maskawa, Progress of Theoretical Physics **49**, 652 (1973), URL http://dx.doi.org/10.1143/PTP.49.652.

[87] M. Gell-Mann (1961).

[88] S. Weinberg, Phys.Rev.Lett. **31**, 494 (1973).

[89] G. 'tHooft, Nuclear Physics B **33**, 173 (1971), ISSN 05503213, URL http://dx.doi.org/10.1016/0550-3213(71)90395-6.

[90] Hooft, Nuclear Physics B **35**, 167 (1971), ISSN 05503213, URL http://dx.doi.org/10.1016/0550-3213(71)90139-8.

[91] G. 't Hooft and M. Veltman, Nuclear Physics B **44**, 189 (1972), ISSN 05503213, URL http://dx.doi.org/10.1016/0550-3213(72)90279-9.

[92] D. Gross and F. Wilczek, Phys.Rev. **D8**, 3633 (1973).

[93] D. Gross and F. Wilczek, Phys.Rev. **D9**, 980 (1974).

[94] H. D. Politzer, Phys.Rev.Lett. **30**, 1346 (1973).

[95] H. D. Politzer, Phys.Rept. **14**, 129 (1974).

[96] (2012), URL http://cdsweb.cern.ch/record/1459565.

[97] S. Weinberg, *The First Three Minutes: A Modern View Of The Origin Of The Universe* (Basic Books, 1993), 2nd ed., ISBN 0465024378, URL http://www.worldcat.org/isbn/0465024378.

[98] C. Giunti (2011), 1106.4479, URL http://arxiv.org/abs/1106.4479.

[99] B. Pontecorvo, Soviet Journal of Experimental and Theoretical Physics **26**, 984 (1968).

[100] Z. Maki, M. Nakagawa, and S. Sakata, Progress of Theoretical Physics **28**, 870 (1962), URL http://dx.doi.org/10.1143/PTP.28.870.

[101] A. D. Dolgov, Physics Reports **370**, 333 (2002), ISSN 03701573, hep-ph/0202122, URL http://dx.doi.org/10.1016/S0370-1573(02)00139-4.

[102] S. Coleman, *Aspects of Symmetry: Selected Erice Lectures* (Cambridge University Press, 1988), ISBN 0521318270, URL http://www.worldcat.org/isbn/0521318270.

[103] C. A. Baker, D. D. Doyle, P. Geltenbort, K. Green, M. G. D. van der Grinten, P. G. Harris, P. Iaydjiev, S. N. Ivanov, D. J. R. May, J. M. Pendlebury, et al., Physical Review Letters **97**, 131801+ (2006), URL http://dx.doi.org/10.1103/PhysRevLett.97.131801.

[104] A. Arvanitaki, S. Dimopoulos, S. Dubovsky, N. Kaloper, and J. March-Russell, Physical Review D **81**, 123530+ (2010), URL http://dx.doi.org/10.1103/PhysRevD.81.123530.

[105] A. Nelson, Physics Letters B **136**, 387 (1984), ISSN 03702693, URL http://dx.doi.org/10.1016/0370-2693(84)92025-2.

[106] S. M. Barr, Physical Review Letters **53**, 329 (1984), URL http://dx.doi.org/10.1103/PhysRevLett.53.329.

[107] R. D. Peccei and H. R. Quinn, Physical Review Letters **38**, 1440 (1977), URL http://dx.doi.org/10.1103/PhysRevLett.38.1440.

[108] S. Weinberg, Physical Review Letters **40**, 223 (1978), URL http://dx.doi.org/10.1103/PhysRevLett.40.223.

[109] F. Wilczek, Physical Review Letters **40**, 279 (1978), URL http://dx.doi.org/10.1103/PhysRevLett.40.279.

[110] S. Dimopoulos and H. Georgi, Nuclear Physics B **193**, 150 (1981), ISSN 05503213, URL http://dx.doi.org/10.1016/0550-3213(81)90522-8.

[111] E. Noether, Gott.Nachr. **1918**, 235 (1918), physics/0503066.

[112] E. W. Kolb and M. S. Turner, *The early universe* (Westview Press, 1994), ISBN 0201626748, URL http://www.worldcat.org/isbn/0201626748.

[113] L. J. Hall, K. Jedamzik, J. March-Russell, and S. M. West (2009), 0911.1120, URL http://arxiv.org/abs/0911.1120.

[114] L. J. Hall, J. March-Russell, and S. M. West (2010), 1010.0245, URL http://arxiv.org/abs/1010.0245.

[115] W. Hu, The Astrophysical Journal **506**, 485 (1998), astro-ph/9801234, URL http://dx.doi.org/10.1086/306274.

[116] D. N. Spergel and P. J. Steinhardt, Physical Review Letters **84**, 3760 (2000), URL http://dx.doi.org/10.1103/PhysRevLett.84.3760.

[117] W. Hu, R. Barkana, and A. Gruzinov, Physical Review Letters **85**, 1158 (2000), astro-ph/0003365, URL http://dx.doi.org/10.1103/PhysRevLett.85.1158.

[118] P. Sikivie (2010), 1003.2426, URL http://arxiv.org/abs/1003.2426.

[119] M. P. Silverman and R. L. Mallett, General Relativity and Gravitation **34**, 633 (2002), ISSN 00017701, URL http://dx.doi.org/10.1023/A:1015934027224.

[120] T. Fukuyama, M. Morikawa, and T. Tatekawa, Journal of Cosmology and Astroparticle Physics **2008**, 033+ (2008), ISSN 1475-7516, URL http://dx.doi.org/10.1088/1475-7516/2008/06/033.

[121] T. Rindler-Daller and P. R. Shapiro (2011), 1106.1256, URL http://arxiv.org/abs/1106.1256.

[122] P. Sikivie and Q. Yang (2009), 0901.1106, URL http://dx.doi.org/10.1103/PhysRevLett.103.111301.

[123] P. Sikivie (2010), 1012.1553, URL http://arxiv.org/abs/1012.1553.

[124] T.-P. Woo and T. Chiueh, The Astrophysical Journal **697**, 850+ (2009), ISSN 0004-637X, URL http://dx.doi.org/10.1088/0004-637X/697/1/850.

[125] A. Pontzen and F. Governato (2012), 1106.0499, URL http://arxiv.org/abs/1106.0499.

[126] B. Kain and H. Y. Ling (2010), 1004.4692, URL http://arxiv.org/abs/1004.4692.

[127] A. Arvanitaki and S. Dubovsky, Physical Review D **83**, 044026+ (2011), 1004.3558, URL http://arxiv.org/abs/1004.3558.

[128] J. G. Rosa (2010), 0912.1780, URL http://arxiv.org/abs/0912.1780.

[129] B. D. Sherwin, J. Dunkley, S. Das, J. W. Appel, J. R. Bond, C. S. Carvalho, M. J. Devlin, R. Dünner, T. E. Hileman, J. W. Fowler, et al., Physical Review Letters **107**, 021302+ (2011), URL http://dx.doi.org/10.1103/PhysRevLett.107.021302.

[130] H. Casimir, Indag.Math. **10**, 261 (1948).

[131] M. J. Sparnaay, Nature **180**, 334 (1957), URL http://dx.doi.org/10.1038/180334b0.

[132] S. Weinberg, Physical Review Letters **59**, 2607 (1987), URL http://dx.doi.org/10.1103/PhysRevLett.59.2607.

[133] S. Coleman and F. De Luccia, Physical Review D **21**, 3305 (1980), URL http://dx.doi.org/10.1103/PhysRevD.21.3305.

[134] R. Bousso and J. Polchinski, Journal of High Energy Physics **2000**, 006+ (2000), ISSN 1126-6708, URL http://dx.doi.org/10.1088/1126-6708/2000/06/006.

[135] T. Banks (1996), hep-th/9601151, URL http://arxiv.org/abs/hep-th/9601151.

[136] N. Arkani-Hamed, L. J. Hall, C. Kolda, and H. Murayama (2000), astro-ph/0005111, URL http://arxiv.org/abs/astro-ph/0005111.

[137] A. Aguirre and M. Tegmark (2004), hep-th/0409072, URL http://arxiv.org/abs/hep-th/0409072.

[138] T. Clifton, P. G. Ferreira, A. Padilla, and C. Skordis (2011), 1106.2476v1, URL http://arxiv.org/abs/1106.2476v1.

[139] C. Wetterich, Nuclear Physics B **302**, 668 (1988), ISSN 05503213, URL http://dx.doi.org/10.1016/0550-3213(88)90193-9.

[140] P. J. E. Peebles and B. Ratra, Astrophys. J. Lett. **325**, L17 (1988), URL http://dx.doi.org/10.1086/185100.

[141] B. Ratra and P. J. E. Peebles, Physical Review D **37**, 3406 (1988), URL http://dx.doi.org/10.1103/PhysRevD.37.3406.

[142] E. J. Copeland, M. Sami, and S. Tsujikawa, International Journal of Modern Physics D **15**, 1753 (2006), hep-th/0603057, URL http://dx.doi.org/10.1142/S021827180600942X.

[143] R. de Putter, O. Zahn, and E. V. Linder, Physical Review D **79**, 065033+ (2009), URL http://dx.doi.org/10.1103/PhysRevD.79.065033.

[144] E. Calabrese, R. de Putter, D. Huterer, E. V. Linder, and A. Melchiorri, Physical Review D **83**, 023011+ (2011), URL http://dx.doi.org/10.1103/PhysRevD.83.023011.

[145] S. Joudaki and M. Kaplinghat (2011), 1106.0299, URL http://arxiv.org/abs/1106.0299.

[146] P. Hunt and S. Sarkar, Monthly Notices of the Royal Astronomical Society **401**, 547 (2010), ISSN 1365-2966, URL http://dx.doi.org/10.1111/j.1365-2966.2009.15670.x.

[147] R. Hlozek, J. Dunkley, G. Addison, J. W. Appel, J. R. Bond, C. S. Carvalho, S. Das, M. Devlin, R. Dünner, T. Essinger-Hileman, et al. (2011), 1105.4887, URL http://arxiv.org/abs/1105.4887.

[148] D. H. Lyth and A. R. Liddle, *The Primordial Density Perturbation: Cosmology, Inflation and the Origin of Structure* (Cambridge University Press, 2009), revised ed., ISBN 052182849X, URL http://www.worldcat.org/isbn/052182849X.

[149] A. H. Guth, Physical Review D **23**, 347 (1981), URL http://dx.doi.org/10.1103/PhysRevD.23.347.

[150] A. D. Linde, Physics Letters B **108**, 389 (1982), ISSN 03702693, URL http://dx.doi.org/10.1016/0370-2693(82)91219-9.

[151] A. Albrecht and P. J. Steinhardt, Physical Review Letters **48**, 1220 (1982), URL http://dx.doi.org/10.1103/PhysRevLett.48.1220.

[152] P. J. Steinhardt, *Natural Inflation* (Cambridge University Press, 1983), proceedings of the Nuffield Workshop, Cambridge, 21 June – 9 July, 1982.

[153] A. Vilenkin, Physical Review D **27**, 2848 (1983), URL http://dx.doi.org/10.1103/PhysRevD.27.2848.

[154] A. H. Guth, Journal of Physics A: Mathematical and Theoretical **40**, 6811+ (2007), ISSN 1751-8113, hep-th/0702178, URL http://dx.doi.org/10.1088/1751-8113/40/25/S25.

[155] A. A. Starobinsky, Physics Letters B **91**, 99 (1980), ISSN 03702693, URL http://dx.doi.org/10.1016/0370-2693(80)90670-X.

[156] M. B. Green, J. H. Schwarz, and E. Witten, *Superstring Theory: Volume 1, Introduction* (Cambridge University Press, 1988), ISBN 0521357527, URL http://www.worldcat.org/isbn/0521357527.

[157] M. B. Green, J. H. Schwarz, and E. Witten, *Superstring Theory: Volume 2, Loop Amplitudes, Anomalies and Phenomenology* (Cambridge University Press, 1988), first edition ed., ISBN 0521357535, URL http://www.worldcat.org/isbn/0521357535.

[158] L. Smolin, *The Trouble With Physics: The Rise of String Theory, the Fall of a Science, and What Comes Next* (Houghton Mifflin Harcourt, 2006), ISBN 0618551050, URL http://www.worldcat.org/isbn/0618551050.

[159] M. R. Douglas and S. Kachru, Reviews of Modern Physics **79**, 733 (2007), hep-th/0610102, URL http://dx.doi.org/10.1103/RevModPhys.79.733.

[160] B. S. Acharya, G. Kane, and P. Kumar (2012), 1204.2795, URL http://arxiv.org/abs/1204.2795.

[161] G. T. Hooft, Physical Review Letters **37**, 8+ (1976), URL http://dx.doi.org/10.1103/PhysRevLett.37.8.

[162] G. T. Hooft, Physical Review D **14**, 3432 (1976), URL http://dx.doi.org/10.1103/PhysRevD.14.3432.

[163] J. E. Kim, Physical Review Letters **43**, 103 (1979), URL http://dx.doi.org/10.1103/PhysRevLett.43.103.

[164] M. Dine, W. Fischler, and M. Srednicki, Physics Letters B **104**, 199 (1981), ISSN 03702693, URL http://dx.doi.org/10.1016/0370-2693(81)90590-6.

[165] M. B. Wise, H. Georgi, and S. L. Glashow, Physical Review Letters **47**, 402 (1981), URL http://dx.doi.org/10.1103/PhysRevLett.47.402.

[166] J. Preskill, M. Wise, and F. Wilczek, Physics Letters B **120**, 127 (1983), ISSN 03702693, URL http://dx.doi.org/10.1016/0370-2693(83)90637-8.

[167] P. Steinhardt and M. Turner, Physics Letters B **129**, 51 (1983), ISSN 03702693, URL http://dx.doi.org/10.1016/0370-2693(83)90727-X.

[168] M. Turner, F. Wilczek, and A. Zee, Physics Letters B **125**, 35 (1983), ISSN 03702693, URL http://dx.doi.org/10.1016/0370-2693(83)91229-7.

[169] L. Abbott and P. Sikivie, Physics Letters B **120**, 133 (1983), ISSN 03702693, URL http://dx.doi.org/10.1016/0370-2693(83)90638-X.

[170] M. Dine and W. Fischler, Physics Letters B **120**, 137 (1983), ISSN 03702693, URL http://dx.doi.org/10.1016/0370-2693(83)90639-1.

[171] J. Ipser and P. Sikivie, Physical Review Letters **50**, 925 (1983), URL http://dx.doi.org/10.1103/PhysRevLett.50.925.

[172] M. S. Turner, Physical Review D **33**, 889 (1986), URL http://dx.doi.org/10.1103/PhysRevD.33.889.

[173] Z. G. Berezhiani, A. S. Sakharov, and M. Y. Khlopov, Soviet Journal of Nuclear Physics **55**, 1063 (1992), URL http://adsabs.harvard.edu/cgi-bin/nph-bib_query?bibcode=1992SvJNP..55.1063B.

[174] P. Fox, A. Pierce, and S. Thomas (2004), hep-th/0409059, URL http://arxiv.org/abs/hep-th/0409059.

[175] S. Hannestad, A. Mirizzi, and G. Raffelt, Journal of Cosmology and Astroparticle Physics **2005**, 002+ (2005), ISSN 1475-7516, URL http://dx.doi.org/10.1088/1475-7516/2005/07/002.

[176] L. Visinelli and P. Gondolo, Physical Review D **80**, 035024+ (2009), 0903.4377, URL http://dx.doi.org/10.1103/PhysRevD.80.035024.

[177] S. Hannestad, A. Mirizzi, G. G. Raffelt, and Y. Y. Y. Wong (2010), 1004.0695, URL http://arxiv.org/abs/1004.0695.

[178] P. Sikivie, in *Axions*, edited by M. Kuster, G. Raffelt, and B. Beltrán (Springer Berlin Heidelberg, Berlin, Heidelberg, 2008), vol. 741 of *Lecture Notes in Physics*, chap. 2, pp. 19–50, ISBN 978-3-540-73517-5, URL http://dx.doi.org/10.1007/978-3-540-73518-2_2.

[179] A. Zee, *Quantum Field Theory in a Nutshell* (Princeton University Press, 2010), 2nd ed., ISBN 0691140340, URL http://www.worldcat.org/isbn/0691140340.

[180] D. J. Gross, R. D. Pisarski, and L. G. Yaffe, Reviews of Modern Physics **53**, 43 (1981), URL http://dx.doi.org/10.1103/RevModPhys.53.43.

[181] C. Hill and G. Ross, Nuclear Physics B **311**, 253 (1988), ISSN 05503213, URL http://dx.doi.org/10.1016/0550-3213(88)90062-4.

[182] L. J. Hall, Y. Nomura, and S. J. Oliver, Physical Review Letters **95**, 141302+ (2005), URL http://dx.doi.org/10.1103/PhysRevLett.95.141302.

[183] E. Mörtsell and A. Goobar, Journal of Cosmology and Astroparticle Physics **2003**, 003+ (2003), ISSN 1475-7516, URL http://dx.doi.org/10.1088/1475-7516/2003/04/003.

[184] D. Cadamuro, S. Hannestad, G. Raffelt, and J. Redondo (2011), 1011.3694, URL http://arxiv.org/abs/1011.3694.

[185] L. Amendola, Physical Review D **62**, 043511+ (2000), URL http://dx.doi.org/10.1103/PhysRevD.62.043511.

[186] J. Khoury and A. Weltman, Physical Review D **69**, 044026+ (2004), URL http://dx.doi.org/10.1103/PhysRevD.69.044026.

[187] P. Brax, C. van de Bruck, and A. C. Davis, Journal of Cosmology and Astroparticle Physics **2004**, 004+ (2004), ISSN 1475-7516, URL http://dx.doi.org/10.1088/1475-7516/2004/11/004.

[188] P. Brax, C. van de Bruck, and A. C. Davis, Physical Review Letters **99**, 121103+ (2007), URL http://dx.doi.org/10.1103/PhysRevLett.99.121103.

[189] J. P. Conlon and F. G. Pedro (2010), 1010.2665, URL http://arxiv.org/abs/1010.2665.

[190] J. Cao, Z. Heng, J. Yang, Y. Zhang, and J. Zhu, Journal of High Energy Physics **2012**, 1 (2012), URL http://dx.doi.org/10.1007/JHEP03.

[191] T. Banks, M. Berkooz, and P. J. Steinhardt, Physical Review D **52**, 705 (1995), URL http://dx.doi.org/10.1103/PhysRevD.52.705.

[192] E. Witten, Physics Letters B **149**, 351 (1984), ISSN 03702693, URL http://dx.doi.org/10.1016/0370-2693(84)90422-2.

[193] P. Svrcek and E. Witten, Journal of High Energy Physics **2006**, 051+ (2006), ISSN 1126-6708, hep-th/0605206, URL http://dx.doi.org/10.1088/1126-6708/2006/06/051.

[194] P. Candelas, G. T. Horowitz, A. Strominger, and E. Witten, Nuclear Physics B **258**, 46 (1985), ISSN 05503213, URL http://dx.doi.org/10.1016/0550-3213(85)90602-9.

[195] B. S. Acharya, K. Bobkov, and P. Kumar (2010), 1004.5138, URL http://arxiv.org/abs/1004.5138.

[196] B. S. Acharya, G. Kane, and E. Kuflik (2010), 1006.3272, URL http://arxiv.org/abs/1006.3272.

[197] T. Higaki and T. Kobayashi (2011), 1106.1293v1, URL http://arxiv.org/abs/1106.1293v1.

[198] J. A. Frieman, C. T. Hill, A. Stebbins, and I. Waga, Physical Review Letters **75**, 2077 (1995), URL http://dx.doi.org/10.1103/PhysRevLett.75.2077.

[199] A. Linde, Physics Letters B **259**, 38 (1991), ISSN 03702693, URL http://dx.doi.org/10.1016/0370-2693(91)90130-I.

[200] M. P. Hertzberg, M. Tegmark, and F. Wilczek, Physical Review D **78**, 083507+ (2008), 0807.1726, URL http://dx.doi.org/10.1103/PhysRevD.78.083507.

[201] M. Tegmark, A. Aguirre, M. J. Rees, and F. Wilczek, Physical Review D **73**, 023505+ (2006), URL http://dx.doi.org/10.1103/PhysRevD.73.023505.

[202] K. J. Mack, Journal of Cosmology and Astroparticle Physics **2011**, 021+ (2011), ISSN 1475-7516, URL http://dx.doi.org/10.1088/1475-7516/2011/07/021.

[203] K. J. Mack and P. J. Steinhardt, Journal of Cosmology and Astroparticle Physics **2011**, 001+ (2011), ISSN 1475-7516, URL http://dx.doi.org/10.1088/1475-7516/2011/05/001.

[204] A. Linde and M. Noorbala (2010), 1006.2170, URL http://arxiv.org/abs/1006.2170.

[205] L. Amendola and R. Barbieri, Physics Letters B **642**, 192 (2006), ISSN 03702693, hep-ph/0509257, URL http://dx.doi.org/10.1016/j.physletb.2006.08.069.

[206] E. V. Linder (2010), 1006.4632, URL http://arxiv.org/abs/1006.4632.

[207] V. Balasubramanian, P. Berglund, J. P. Conlon, and F. Quevedo, Journal of High Energy Physics **2005**, 007+ (2005), ISSN 1126-6708, URL http://dx.doi.org/10.1088/1126-6708/2005/03/007.

[208] P. Brax, C. van de Bruck, A.-C. Davis, and D. J. Shaw (2010), 1005.3735, URL http://arxiv.org/abs/1005.3735.

[209] J. P. Conlon and F. Quevedo (2007), 0705.3460, URL http://arxiv.org/abs/0705.3460.

[210] V. Balasubramanian, P. Berglund, R. Jimenez, J. Simon, and L. Verde (2008), 0712.1815, URL http://arxiv.org/abs/0712.1815.

[211] L. McAllister and E. Silverstein (2008), 0710.2951, URL http://dx.doi.org/10.1007/s10714-007-0556-6.

[212] M. Cicoli and F. Quevedo (2011), 1108.2659, URL http://arxiv.org/abs/1108.2659.

[213] J. Redondo and A. Ringwald (2010), 1011.3741, URL http://arxiv.org/abs/1011.3741.

[214] L. Ostman and E. Mortsell (2005), astro-ph/0410501, URL http://arxiv.org/abs/astro-ph/0410501.

[215] M. Dine, G. Festuccia, J. Kehayias, and W. Wu (2010), 1010.4803, URL http://arxiv.org/abs/1010.4803.

[216] J. P. Conlon (2006), hep-th/0611039, URL http://arxiv.org/abs/hep-th/0611039.

[217] D. J. E. Marsh, Physical Review D **83**, 123526+ (2011), 1102.4851, URL http://arxiv.org/abs/1102.4851.

[218] K. Becker, M. Becker, and J. H. Schwarz, *String Theory and M-Theory: A Modern Introduction* (Cambridge University Press, 2007), 1st ed., ISBN 0521860695, URL http://www.worldcat.org/isbn/0521860695.

[219] S. Kachru, R. Kallosh, A. Linde, and S. P. Trivedi, Physical Review D **68**, 046005+ (2003), hep-th/0301240, URL http://dx.doi.org/10.1103/PhysRevD.68.046005.

[220] M. Cicoli, C. P. Burgess, and F. Quevedo (2011), 1105.2107, URL http://arxiv.org/abs/1105.2107.

[221] A. R. Liddle, A. Mazumdar, and F. E. Schunck, Physical Review D **58**, 061301+ (1998), URL http://dx.doi.org/10.1103/PhysRevD.58.061301.

[222] E. J. Copeland, A. Mazumdar, and N. J. Nunes, Physical Review D **60**, 083506+ (1999), URL http://dx.doi.org/10.1103/PhysRevD.60.083506.

[223] J. Hartong, A. Ploegh, T. Van Riet, and D. B. Westra, Classical and Quantum Gravity **23**, 4593 (2006), ISSN 0264-9381, URL http://dx.doi.org/10.1088/0264-9381/23/14/003.

[224] M. Cicoli, F. G. Pedro, and G. Tasinato (2011), 1110.6182, URL http://arxiv.org/abs/1110.6182.

[225] J. Beyer, S. Nurmi, and C. Wetterich (2011), 1012.1175, URL http://arxiv.org/abs/1012.1175.

[226] J. L. Cervantes-Cota, R. de Putter, and E. V. Linder (2010), 1010.2237, URL http://arxiv.org/abs/1010.2237.

[227] R. Catena and J. Möller (2007), 0709.1931, URL http://arxiv.org/abs/0709.1931.

[228] V. Pettorino and C. Baccigalupi (2008), 0802.1086, URL http://arxiv.org/abs/0802.1086.

[229] J. Sonner and P. K. Townsend, Physical Review D **74**, 103508+ (2006), URL http://dx.doi.org/10.1103/PhysRevD.74.103508.

[230] S. Panda, Y. Sumitomo, and S. P. Trivedi (2010), 1011.5877, URL http://arxiv.org/abs/1011.5877.

[231] E. J. Copeland, A. R. Liddle, and D. Wands, Physical Review D **57**, 4686 (1998), URL http://dx.doi.org/10.1103/PhysRevD.57.4686.

[232] G. Felder, A. Frolov, L. Kofman, and A. Linde (2002), hep-th/0202017, URL http://arxiv.org/abs/hep-th/0202017.

[233] D. J. E. Marsh and P. G. Ferreira, Physical Review D **82**, 103528+ (2010), ISSN 1550-2368, 1009.3501, URL http://arxiv.org/abs/1009.3501.

[234] Y. Wang, J. M. Kratochvil, A. Linde, and M. Shmakova (2004), astro-ph/0409264, URL http://arxiv.org/abs/astro-ph/0409264.

[235] D. J. E. Marsh, E. R. M. Tarrant, E. J. Copeland, and P. G. Ferreira, Physical Review D **86**, 023508+ (2012), URL http://dx.doi.org/10.1103/PhysRevD.86.023508.

[236] M. Kunz (2007), astro-ph/0702615, URL http://arxiv.org/abs/astro-ph/0702615.

[237] J. P. Conlon, R. Kallosh, A. Linde, and F. Quevedo, Journal of Cosmology and Astroparticle Physics **2008**, 011+ (2008), ISSN 1475-7516, URL http://dx.doi.org/10.1088/1475-7516/2008/09/011.

[238] R. Brustein and P. Steinhardt, Physics Letters B **302**, 196 (1993), ISSN 03702693, URL http://dx.doi.org/10.1016/0370-2693(93)90384-T.

[239] D. Skinner, Physical Review D **67**, 103506+ (2003), URL http://dx.doi.org/10.1103/PhysRevD.67.103506.

[240] B. S. Acharya, P. Kumar, G. Kane, and S. Watson (2009), 0908.2430, URL http://arxiv.org/abs/0908.2430.

[241] R. Bousso (2006), hep-th/0610211, URL http://arxiv.org/abs/hep-th/0610211.

[242] T. Banks (2003), hep-th/0211160, URL http://arxiv.org/abs/hep-th/0211160.

[243] P. J. Steinhardt and N. Turok, Physical Review D **65**, 126003+ (2002), URL http://dx.doi.org/10.1103/PhysRevD.65.126003.

[244] M. A. Amin, P. Zukin, and E. Bertschinger (2011), 1108.1793, URL http://arxiv.org/abs/1108.1793.

[245] E. Silverstein and A. Westphal, Physical Review D **78**, 106003+ (2008), URL http://dx.doi.org/10.1103/PhysRevD.78.106003.

[246] A. Achúcarro, J.-O. Gong, S. Hardeman, G. A. Palma, and S. P. Patil (2011), 1010.3693, URL http://arxiv.org/abs/1010.3693.

[247] S. Cespedes, V. Atal, and G. A. Palma (2012), 1201.4848, URL http://arxiv.org/abs/1201.4848.

[248] S. Dubovsky and V. Gorbenko (2010), 1012.2893, URL http://arxiv.org/abs/1012.2893.

[249] R. Kallosh and A. Linde, Journal of Cosmology and Astroparticle Physics **2003**, 002+ (2003), ISSN 1475-7516, URL http://dx.doi.org/10.1088/1475-7516/2003/02/002.

[250] C. Wetterich, Physics Letters B **594**, 17 (2004), ISSN 03702693, URL http://dx.doi.org/10.1016/j.physletb.2004.05.008.

[251] A. Coley and M. Goliath (2000), gr-qc/0004060, URL http://dx.doi.org/10.1103/PhysRevD.62.043526.

[252] M. Gasperini and G. Veneziano (1993), hep-th/9309023, URL http://dx.doi.org/10.1142/S0217732393003433.

[253] J. E. Lidsey, D. Wands, and E. J. Copeland (2000), hep-th/9909061, URL http://arxiv.org/abs/hep-th/9909061.

[254] S. B. Giddings and R. C. Myers, Physical Review D **70**, 046005+ (2004), URL http://dx.doi.org/10.1103/PhysRevD.70.046005.

[255] K. M. Nollett and G. P. Holder (2011), 1112.2683, URL http://arxiv.org/abs/1112.2683.

[256] V. F. Shvartsman, JETP Lett **9**, 184+ (1969), URL http://www.jetpletters.ac.ru/ps/1661/article_25352.shtml.

[257] G. Steigman, D. N. Schramm, and J. E. Gunn, Physics Letters B **66**, 202 (1977), ISSN 03702693, URL http://dx.doi.org/10.1016/0370-2693(77)90176-9.

[258] W. Hu and N. Sugiyama, Astrophys. J. **444**, 489 (1994), astro-ph/9407093, URL http://dx.doi.org/10.1086/175624.

[259] S. Joudaki (2012), 1202.0005, URL http://arxiv.org/abs/1202.0005.

[260] M. Doran and G. Robbers, Journal of Cosmology and Astroparticle Physics **2006**, 026+ (2006), ISSN 1475-7516, URL http://dx.doi.org/10.1088/1475-7516/2006/06/026.

[261] J. Polchinski (2006), hep-th/0603249, URL http://arxiv.org/abs/hep-th/0603249.

[262] J. H. Schwarz (1992), hep-th/9209125, URL http://arxiv.org/abs/hep-th/9209125.

[263] R. Kallosh, J. Kratochvil, A. Linde, E. V. Linder, and M. Shmakova, Journal of Cosmology and Astroparticle Physics **2003**, 015+ (2003), ISSN 1475-7516, URL http://dx.doi.org/10.1088/1475-7516/2003/10/015.

[264] S. Lee, K. A. Olive, and M. Pospelov, Physical Review D **70**, 083503+ (2004), URL http://dx.doi.org/10.1103/PhysRevD.70.083503.

[265] E. Calabrese, E. Menegoni, C. J. A. P. Martins, A. Melchiorri, and G. Rocha (2011), 1104.0760, URL http://arxiv.org/abs/1104.0760.

[266] A. Strominger, Journal of High Energy Physics **10**, 034+ (2001), ISSN 1126-6708, URL http://dx.doi.org/10.1088/1126-6708/2001/10/034.

[267] J. Maldacena (2011), 1012.0274, URL http://arxiv.org/abs/1012.0274.

[268] D. Harlow and L. Susskind (2010), 1012.5302, URL http://arxiv.org/abs/1012.5302.

[269] S. Kanno, M. Sasaki, and J. Soda (2011), 1107.1491, URL http://arxiv.org/abs/1107.1491.

[270] R. Kallosh, A. Linde, S. Prokushkin, and M. Shmakova, Physical Review D **66**, 123503+ (2002), URL http://dx.doi.org/10.1103/PhysRevD.66.123503.

[271] R. Kallosh (2002), hep-th/0205315, URL http://arxiv.org/abs/hep-th/0205315.

[272] N. Kaloper and L. Sorbo, Physical Review D **79**, 043528+ (2009), URL http://dx.doi.org/10.1103/PhysRevD.79.043528.

[273] J. E. Kim and H.-P. Nilles, Physics Letters B **553**, 1 (2003), ISSN 03702693, URL http://dx.doi.org/10.1016/S0370-2693(02)03148-9.

[274] J. E. Kim and H. P. Nilles, Journal of Cosmology and Astroparticle Physics **2009**, 010+ (2009), ISSN 1475-7516, URL http://dx.doi.org/10.1088/1475-7516/2009/05/010.

[275] M. Cicoli, F. G. Pedro, and G. Tasinato (2012), 1203.6655, URL http://arxiv.org/abs/1203.6655.

[276] D. Marsh, L. McAllister, and T. Wrase (2012), 1112.3034, URL http://arxiv.org/abs/1112.3034.

[277] F. Perrotta and C. Baccigalupi, Physical Review D **59**, 123508+ (1999), URL http://dx.doi.org/10.1103/PhysRevD.59.123508.

[278] J. R. Bond, G. Efstathiou, and J. Silk, Physical Review Letters **45**, 1980 (1980), URL http://dx.doi.org/10.1103/PhysRevLett.45.1980.

[279] D. J. E. Marsh, E. Macaulay, M. Trebitsch, and P. G. Ferreira (2011), 1110.0502, URL http://arxiv.org/abs/1110.0502.

[280] J. Hamann, S. Hannestad, G. G. Raffelt, and Y. Y. Y. Wong, Journal of Cosmology and Astroparticle Physics **2007**, 021+ (2007), ISSN 1475-7516, URL http://dx.doi.org/10.1088/1475-7516/2007/08/021.

[281] J. Hamann, S. Hannestad, J. Lesgourgues, C. Rampf, and Y. Y. Y. Wong, Journal of Cosmology and Astroparticle Physics **2010**, 022+ (2010), ISSN 1475-7516, URL http://dx.doi.org/10.1088/1475-7516/2010/07/022.

[282] M. C. Gonzalez-Garcia, M. Maltoni, and J. Salvado, JHEP **1008**, 117 (2010), URL http://dx.doi.org/10.1007/JHEP08(2010)117.

[283] A. X. Gonzalez-Morales, R. Poltis, B. D. Sherwin, and L. Verde (2011), 1106.5052, URL http://arxiv.org/abs/1106.5052.

[284] A. Linde, Physics Letters B **83**, 311 (1979), ISSN 03702693, URL http://dx.doi.org/10.1016/0370-2693(79)91115-8.

[285] A. Cuoco, F. Iocco, G. Mangano, G. Miele, O. Pisanti, and P. D. Serpico, International Journal of Modern Physics A **19**, 4431+ (2004), astro-ph/0307213, URL http://arxiv.org/abs/astro-ph/0307213.

[286] J. Hamann, S. Hannestad, G. G. Raffelt, I. Tamborra, and Y. Y. Y. Wong (2010), 1006.5276, URL http://arxiv.org/abs/1006.5276.

[287] J. Lesgourgues and S. Pastor, Physics Reports **429**, 307 (2006), ISSN 03701573, astro-ph/0603494, URL http://dx.doi.org/10.1016/j.physrep.2006.04.001.

[288] J. R. Primack (2001), astro-ph/0112336, URL http://arxiv.org/abs/astro-ph/0112336.

[289] W. Hu, D. J. Eisenstein, and M. Tegmark, Physical Review Letters **80**, 5255 (1998), URL http://dx.doi.org/10.1103/PhysRevLett.80.5255.

[290] E. Giusarma, M. Corsi, M. Archidiacono, R. de Putter, A. Melchiorri, O. Mena, and S. Pandolfi, Physical Review D **83**, 115023+ (2011), URL http://dx.doi.org/10.1103/PhysRevD.83.115023.

[291] F. De Bernardis, T. D. Kitching, A. Heavens, and A. Melchiorri, Physical Review D **80**, 123509+ (2009), URL http://dx.doi.org/10.1103/PhysRevD.80.123509.

[292] D. J. Eisenstein and W. Hu, The Astrophysical Journal pp. 5+ (1999), URL http://dx.doi.org/10.1086/306640.

[293] A. Kiakotou, Ø. Elgarøy, and O. Lahav, Physical Review D **77**, 063005+ (2008), URL http://dx.doi.org/10.1103/PhysRevD.77.063005.

[294] A. Melchiorri, O. Mena, S. Palomares-Ruiz, S. Pascoli, A. Slosar, and M. Sorel, Journal of Cosmology and Astroparticle Physics **2009**, 036+ (2009), ISSN 1475-7516, URL http://dx.doi.org/10.1088/1475-7516/2009/01/036.

[295] S. Hannestad, H. Tu, and Y. Y. Y. Wong (2006), astro-ph/0603019, URL http://arxiv.org/abs/astro-ph/0603019.

[296] D. J. Eisenstein and W. Hu, The Astrophysical Journal **496**, 605+ (1997), astro-ph/9709112, URL http://dx.doi.org/10.1086/305424.

[297] W. J. Percival, S. Cole, D. J. Eisenstein, R. C. Nichol, J. A. Peacock, A. C. Pope, and A. S. Szalay (2007), 0705.3323, URL http://arxiv.org/abs/0705.3323.

[298] W. J. Percival, B. A. Reid, D. J. Eisenstein, N. A. Bahcall, T. Budavari, J. A. Frieman, M. Fukugita, J. E. Gunn, Z. Ivezic, G. R. Knapp, et al. (2009), 0907.1660, URL http://arxiv.org/abs/0907.1660.

[299] H. Seo and D. J. Eisenstein, ApJ **598**, 720 (2003), arXiv:astro-ph/0307460.

[300] D. J. Eisenstein, I. Zehavi, D. W. Hogg, R. Scoccimarro, M. R. Blanton, R. C. Nichol, R. Scranton, H.-J. Seo, M. Tegmark, Z. Zheng, et al., ApJ **633**, 560 (2005), arXiv:astro-ph/0501171.

[301] W. J. Percival, B. A. Reid, D. J. Eisenstein, N. A. Bahcall, T. Budavari, J. A. Frieman, M. Fukugita, J. E. Gunn, v. Ivezić, G. R. Knapp, et al., Monthly Notices of the Royal Astronomical Society **401**, 2148 (2010), ISSN 0035-8711, URL http://dx.doi.org/10.1111/j.1365-2966.2009.15812.x.

[302] F. Beutler, C. Blake, M. Colless, D. H. Jones, L. Staveley-Smith, L. Campbell, Q. Parker, W. Saunders, and F. Watson, Mon. Not. Roy. Astron. Soc. **416**, 3017 (2011), 1106.3366, URL http://dx.doi.org/10.1111/j.1365-2966.2011.19250.x.

[303] C. Blake, E. Kazin, F. Beutler, T. Davis, D. Parkinson, S. Brough, M. Colless, C. Contreras, W. Couch, S. Croom, et al. (2011), 1108.2635, URL http://arxiv.org/abs/1108.2635.

[304] K. T. Mehta, A. J. Cuesta, X. Xu, D. J. Eisenstein, and N. Padmanabhan (2012), 1202.0092, URL http://arxiv.org/abs/1202.0092.

[305] S. Das, P. S. Corasaniti, and J. Khoury (2005), astro-ph/0510628, URL http://arxiv.org/abs/astro-ph/0510628.

[306] J. Peacock, S. Cole, P. Norberg, C. Baugh, J. Bland-Hawthorn, T. Bridges, R. Cannon, M. Colless, C. Collins, W. Couch, et al., Arxiv preprint astro-ph/0103143 (2001).

[307] N. Ross, J. da Angela, T. Shanks, D. Wake, R. Cannon, A. Edge, R. Nichol, P. Outram, M. Colless, W. Couch, et al., Monthly Notices of the Royal Astronomical Society: Letters **381**, 573 (2007).

[308] L. Guzzo, M. Pierleoni, B. Meneux, E. Branchini, O. Le Fèvre, C. Marinoni, B. Garilli, J. Blaizot, G. De Lucia, A. Pollo, et al., Nature **451**, 541 (2008).

[309] C. Blake, S. Brough, M. Colless, C. Contreras, W. Couch, S. Croom, T. Davis, M. J. Drinkwater, K. Forster, D. Gilbank, et al., Monthly Notices of the Royal Astronomical Society **415**, 2876 (2011), URL http://dx.doi.org/10.1111/j.1365-2966.2011.18903.x.

[310] C. Blake, S. Brough, M. Colless, C. Contreras, W. Couch, S. Croom, D. Croton, T. Davis, M. J. Drinkwater, K. Forster, et al. (2012), 1204.3674, URL http://arxiv.org/abs/1204.3674.

[311] M. Giovannini (2011), 1106.5043, URL http://arxiv.org/abs/1106.5043.

[312] V. Acquaviva and E. Gawiser (2010), 1008.3392, URL http://arxiv.org/abs/1008.3392.

[313] W. Hu, Physical Review D **66**, 083515+ (2002), URL http://dx.doi.org/10.1103/PhysRevD.66.083515.

[314] L. Van Waerbeke, Y. Mellier, T. Erben, J. C. Cuillandre, F. Bernardeau, R. Maoli, E. Bertin, H. J. M. Cracken, O. Le Fevre, B. Fort, et al. (2000), astro-ph/0002500, URL http://arxiv.org/abs/astro-ph/0002500.

[315] N. Kaiser, G. Wilson, and G. A. Luppino (2000), astro-ph/0003338, URL http://arxiv.org/abs/astro-ph/0003338.

[316] D. Bacon, A. Refregier, and R. Ellis (2000), astro-ph/0003008, URL http://arxiv.org/abs/astro-ph/0003008.

[317] D. M. Wittman, J. A. Tyson, D. Kirkman, I. Dell'Antonio, and G. Bernstein (2000), astro-ph/0003014, URL http://arxiv.org/abs/astro-ph/0003014.

[318] M. Bartelmann and P. Schneider, Phys. Rept. **340**, 291 (2001), astro-ph/9912508.

[319] D. Huterer, Phys. Rev. **D65**, 063001 (2002), astro-ph/0106399.

[320] R. E. Smith, J. A. Peacock, A. Jenkins, S. D. M. White, C. S. Frenk, F. R. Pearce, P. A. Thomas, G. Efstathiou, H. M. P. Couchmann, and V. Consortium, Mon. Not. Roy. Astron. Soc. **341**, 1311 (2003), astro-ph/0207664, URL http://dx.doi.org/10.1046/j.1365-8711.2003.06503.x.

[321] S. Saito, M. Takada, and A. Taruya (2008), 0801.0607, URL http://arxiv.org/abs/0801.0607.

[322] S. Dodelson, E. Gates, and A. Stebbins (1995), astro-ph/9509147, URL http://arxiv.org/abs/astro-ph/9509147.

[323] S. Bashinsky and U. Seljak (2004), astro-ph/0310198, URL http://arxiv.org/abs/astro-ph/0310198.

[324] Z. Hou, R. Keisler, L. Knox, M. Millea, and C. Reichardt (2011), 1104.2333, URL http://arxiv.org/abs/1104.2333.

[325] S. Das, B. D. Sherwin, P. Aguirre, J. W. Appel, J. R. Bond, C. S. Carvalho, M. J. Devlin, J. Dunkley, R. Dünner, T. E. Hileman, et al., Physical Review Letters **107**, 021301+ (2011), URL http://dx.doi.org/10.1103/PhysRevLett.107.021301.

[326] *http://www.astro.princeton.edu/~sudeep/fisherCodesDoc/*.

[327] A. Albrecht, G. Bernstein, R. Cahn, W. L. Freedman, J. Hewitt, W. Hu, J. Huth, M. Kamionkowski, E. W. Kolb, L. Knox, et al., ArXiv Astrophysics e-prints (2006), arXiv:astro-ph/0609591.

[328] A. L. Erickcek and K. Sigurdson (2011), 1106.0536, URL http://arxiv.org/abs/1106.0536.

[329] K. R. Dienes and B. Thomas (2012), 1203.1923, URL http://arxiv.org/abs/1203.1923.

[330] M. Bucher, K. Moodley, and N. Turok, Physical Review D **62**, 083508+ (2000), URL http://dx.doi.org/10.1103/PhysRevD.62.083508.

[331] J. Maldacena (2005), astro-ph/0210603, URL http://arxiv.org/abs/astro-ph/0210603.

[332] C. Gordon, D. Wands, B. A. Bassett, and R. Maartens (2000), astro-ph/0009131, URL http://arxiv.org/abs/astro-ph/0009131.

[333] T. S. Bunch and P. C. W. Davies, Proceedings of the Royal Society of London. A. Mathematical and Physical Sciences **360**, 117 (1978), URL http://dx.doi.org/10.1098/rspa.1978.0060.

[334] E. Komatsu, J. Dunkley, M. R. Nolta, C. L. Bennett, B. Gold, G. Hinshaw, N. Jarosik, D. Larson, M. Limon, L. Page, et al., The Astrophysical Journal Supplement Series **180**, 330 (2009), ISSN 0067-0049, 0803.0547, URL http://dx.doi.org/10.1088/0067-0049/180/2/330.

[335] D. Seckel and M. S. Turner, Physical Review D **32**, 3178 (1985), URL http://dx.doi.org/10.1103/PhysRevD.32.3178.

[336] A. D. Linde, Physics Letters B **158**, 375 (1985), ISSN 03702693, URL http://dx.doi.org/10.1016/0370-2693(85)90436-8.

[337] L. Senatore, E. Silverstein, and M. Zaldarriaga (2011), 1109.0542, URL http://arxiv.org/abs/1109.0542.

[338] R. Bean, J. Dunkley, and E. Pierpaoli, Physical Review D **74**, 063503+ (2006), URL http://dx.doi.org/10.1103/PhysRevD.74.063503.